Naval Research Laboratory
Washington, DC 20375-5320 NRL/PU/5230--95-274 May 1995

1995 NRL Review

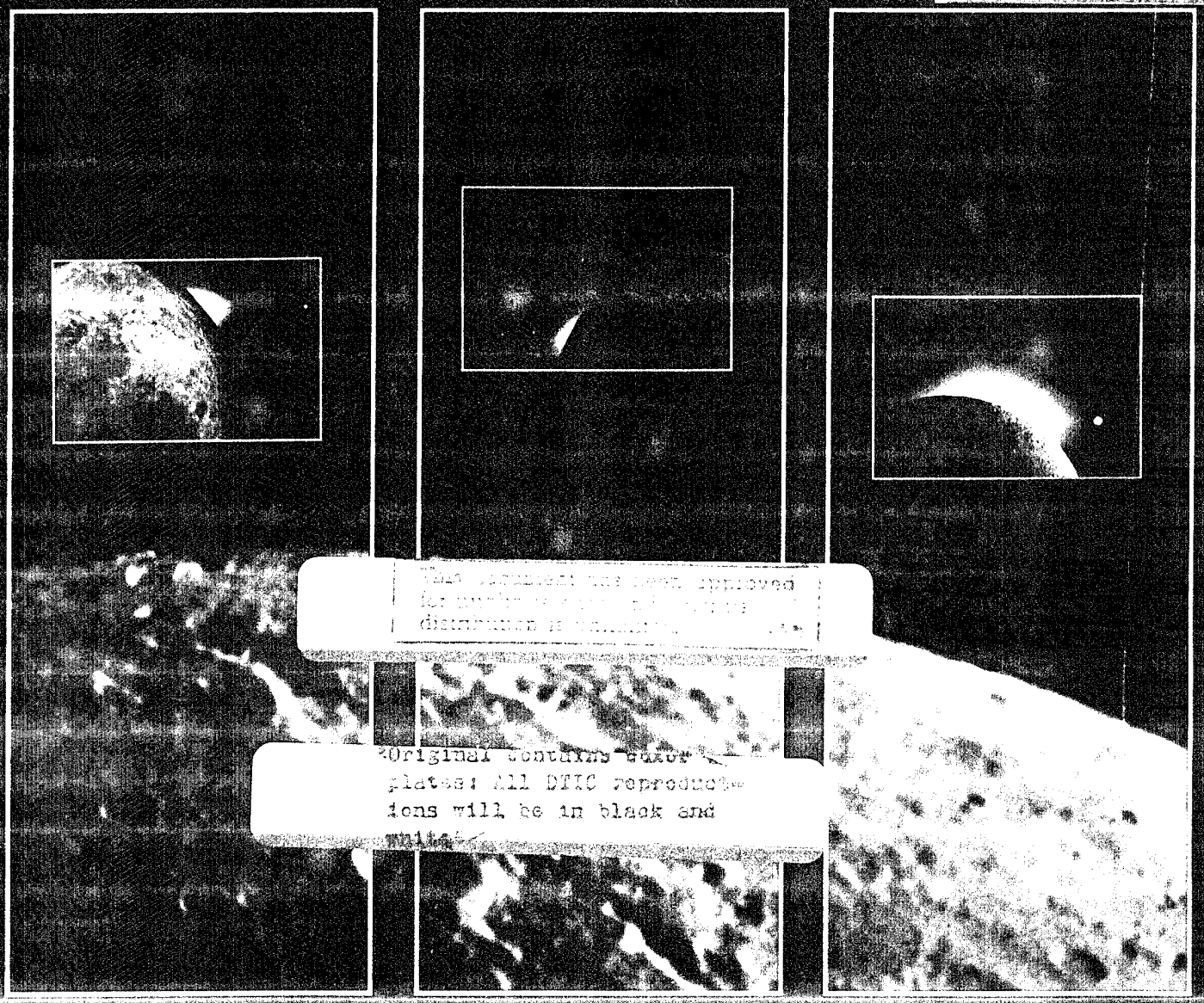

This *1995 NRL Review* introduces you to the Naval Research Laboratory—the Navy's Corporate Laboratory—and focuses on research highlights from fiscal year 1994. In addition, it presents the special honors awarded to NRL employees and describes the programs available to NRL and non-NRL employees. This publication offers an exchange of information among scientists, engineers, scholars, and managers, and it is used as a recruiting tool.

As you read the *NRL Review*, you will become even more aware that the Naval Research Laboratory comprises a dynamic team of scientists, engineers, and support personnel working together to promote the programs that will continue to foster discoveries and scientific advances for the Navy of the future.

Photo Captions: The photos are color-enhanced images of the Moon taken by the Startracker camera aboard the *Clementine* spacecraft.

Cover: (left panel) (from left to right) the Earth-lit Moon, the Sun's corona, and—to the far right—Venus; (center panel) (from right to left) the Moon lit by the Earth, the terminator—or boundary between light and dark—into the dark side with the solar corona just rising over the limb, and the bright planets Saturn, Mars, and Mercury; (right panel) an image of Venus, the Solar corona, and the Moon and its terminator.

Title Page: This is a color-enhanced image of Venus, the solar corona, and the Moon. The terminator between the dark side of the Moon and the Earth-lit side can also be seen.

Mission Page: This colorized image shows the full Earth over the lunar north pole as *Clementine* completes mapping orbit 102 on March 13, 1994. It is a clear day over Africa and the Arabian Peninsula. The angular separation between lunar horizon and Earth has been reduced for illustration purposes. The large crater at the bottom of the image is Plaskett at 180° West, 82° North.

1995 NRL Review

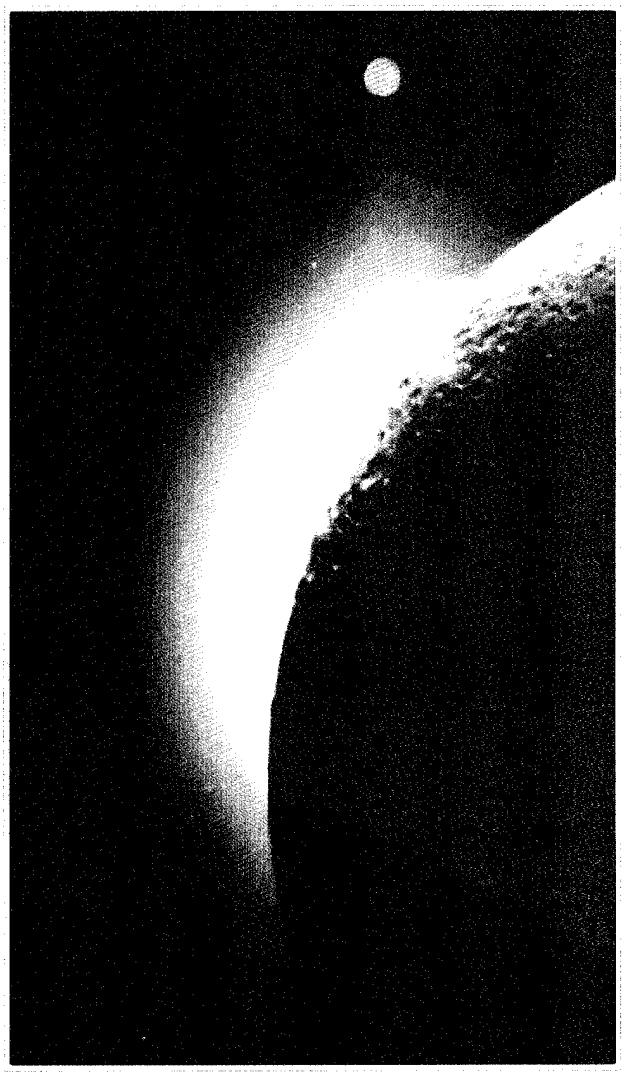

Naval Research Laboratory
Washington, DC 20375-5320

DISCLAIMER NOTICE

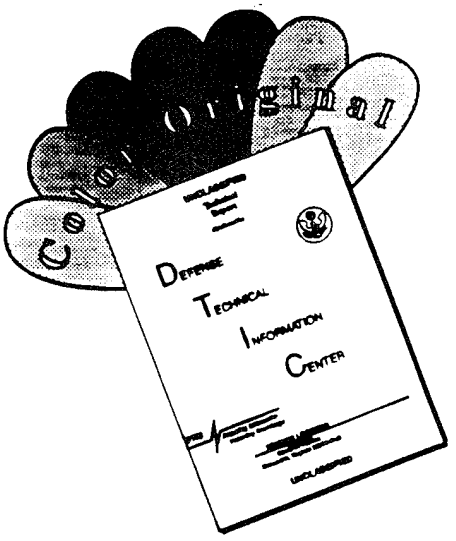

THIS DOCUMENT IS BEST QUALITY AVAILABLE. THE COPY FURNISHED TO DTIC CONTAINED A SIGNIFICANT NUMBER OF COLOR PAGES WHICH DO NOT REPRODUCE LEGIBLY ON BLACK AND WHITE MICROFICHE.

Electronics and Electromagnetics

Energetic Particles, Plasmas, and Beams

Information Technology and Communication

Materials Science and Technology

Numerical Simulating, Computing, and Modeling

Ocean and Atmospheric Science and Technology

Optical Science

Space Research and Satellite Technology

Awards and Recognition

Professional Development

General Information

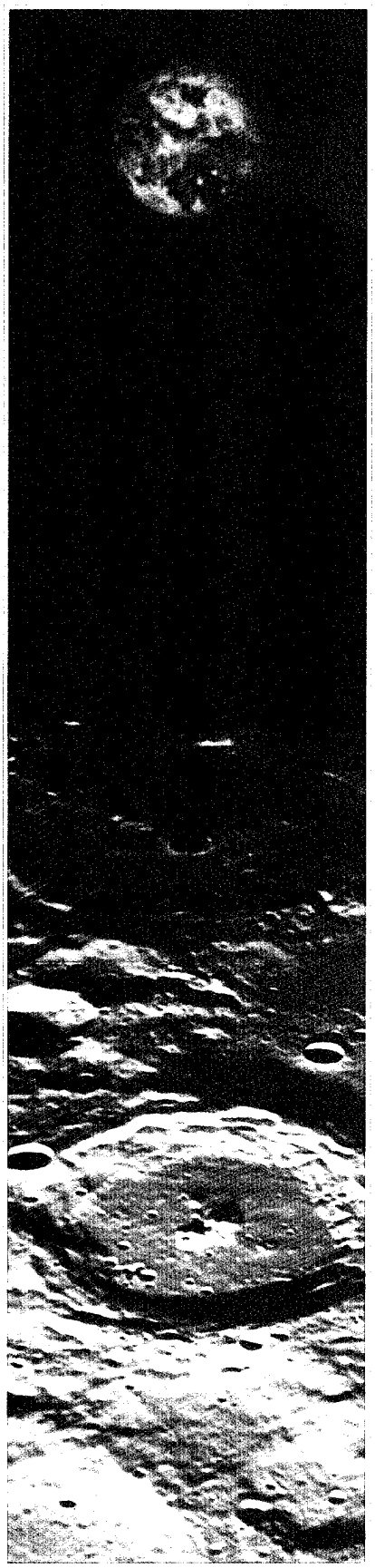

Mission

To conduct a broadly based multidisciplinary program of scientific research and advanced technological development directed toward maritime applications of new and improved materials, techniques, equipment, systems, and ocean, atmospheric, and space sciences and related technologies.

The Naval Research Laboratory provides

- primary in-house research for the physical, engineering, space, and environmental sciences;
- broadly based exploratory and advanced development programs in response to identified and anticipated Navy needs;
- broad multidisciplinary support to the Naval Warfare Centers;
- space and space systems technology development and support.

Reflections
...FROM THE CHIEF OF NAVAL RESEARCH

Today is an exciting and challenging time for the Department of the Navy, and in particular, its research and development community. We are rapidly transforming the Navy and Marine Corps from Cold War organizations into ones that will fulfill the missions of the 21st century, the demands of which will stretch from potential interventions in guerilla-style, low-intensity conflicts to abrupt and rapid engagements in electronic warfare. Along the way, we are also right-sizing the Department by positioning personnel levels and existing infrastructure to meet the challenges ahead in the most efficient and practical ways possible.

Our current naval recapitalization initiatives are based on fielding technologically superior forces. Because tomorrow's manpower will be greatly reduced, the naval research and development community has the responsibility of ensuring that our Sailors and Marines have the force-multiplying weaponry and supporting secure and reliable systems needed to win in combat and capably defend American interests and policies.

RADM MARC YE PELAEZ USN

During my visits to the Naval Research Laboratory (NRL) this year, I saw again and again the kind of scientific and technological breakthroughs that will ensure the safety of our troops. When it comes to developing affordable, innovative, and superior military technologies from concept through demonstration, NRL has always been a leader. In fact, NRL's investments in clock technology, space technology, biomolecular engineering, acoustics, radar, and electronic warfare—to name but a few of the areas represented—have resulted in the Laboratory claiming more than 3500 patents, each one representing a significant advancement in the development of naval technology. Of these militarily significant accomplishments, many also have had a profound impact on civilian and consumer life. NRL developed the principle that led to the Global Positioning System, a space-based system that in peacetime provides enormous benefits to commercial navigation. NRL programs also have led to the development of a world-class firefighting doctrine. In addition, because of the Fleet's interest in atmospheric phenomenon and how they may affect certain kinds of communications, the Laboratory has become a leader in the observation of global environmental change.

Still, let me remind you: NRL is a military institution. Whatever the "dual use" applications may be for whatever the Laboratory produces, its first priority is to support Fleet operations. My visits have shown me that it does that job exceedingly well. Because the long-term strategic objective is to produce a Navy and Marine Corps team that is able to wage and win wars any time and in any place, and because the Laboratory has been meeting those objectives for more than 70 years, I believe the NRL mission will remain broad and robust well into the 21st century.

Imagine a time when the U.S.'s main enemy is in defeat, its economy in disarray, with poverty and hyperinflation rampant, an enemy whose armed forces have been reduced to a mere shadow of the threat that led to the most intense military buildup in the country's history, an enemy whose decline had led to a massive drawdown in defense spending. You could be describing today's situation very accurately. But if you substituted Germany for the USSR and 1923 for 1995, you would also be describing the international condition at the time of the founding of NRL. As you read the history of the Laboratory described later in this publication, you will see that NRL evolved to its current size and role in response to the country's and the Navy's needs through both World War II and the Cold War. These historical antecedents are important in charting the future role of NRL since today's research will influence the Navy's direction for the next several decades. Predicting that history is as difficult today as it was in 1923.

Today we stand peering into the darkness of a great unknown. We have never faced times such as these—there is no threat to the continental United States, our existing Armed Forces are far superior to any others in the world, and our economy is globally interlocked by ubiquitous communications systems and instantaneous information. Explaining our investment in defense during "normal" times is contentious at best. Today, explaining the level of investment in defense—particularly defense science and technology—becomes even more abstract in a Navy concerned with meeting near-term Fleet operating budgets.

The solution is to demonstrate our direct contribution to the operating forces, but these contributions rarely transition overnight. The outcome of today's scientific discovery may take close to 20 years to reach fruition in the Fleet—as did the discovery of radar, or it might take weeks—as did many of NRL inventions in Desert Storm and other recent conflicts. In a world in flux, it also becomes important to retain the excellence of in-house research for which NRL has become noted. The pressures to close, realign, consolidate, reengineer, and right-size are clear and present. As we have in the past, we must match NRL to the needs of the operating forces while continuing to retain a long view and a world-class operation. We know full well that a great research institution, like a great Navy, is not easily regained once lost.

The research programs reflected in this *1995 NRL Review* represent an attempt to address both the realities and the uncertainties by maintaining an in-house expertise in areas currently not in vogue in academia or industry but which have the clear potential to resurface in the decades ahead. These research programs also reflect the true strengths of NRL—broad multidisciplinary programs of research concentrated in a single location and programs that represent a rational mix between the advancement of science and the high risk search for breakthroughs that could revolutionize Naval warfare.

The research papers, the listing of the prestigious national and international awards presented to our people, and the technology available to transfer to the Navy and the nation that are presented in the *1995 NRL Review* are clear indicators of the Laboratory's health and show that we are headed fair for the next century.

One reads much in the press today about the changing environment in which the Nation's science and technology (S&T) are conducted. Many assumptions that the S&T community have taken for granted are being challenged. For example, the role of academic research within the Department of Defense, the role of the federal laboratories, and the relationship among all of the players in the national S&T infrastructure are being examined. While questioning the status quo can be very disruptive, it does, in fact, need to be done periodically. At some point, of course, the reevaluation must be brought to closure; otherwise, one becomes lost in the evaluation process, and the process itself becomes the objective.

The purposes of federal S&T funding are to conduct research and to develop technology that are believed to be in the National interest and require federal funding if they are to be pursued. The reevaluation of what the National interest requires and who should satisfy those requirements is prudent. One common theme among the numerous ongoing studies is that merely conducting good science and technology in the abstract is not a justification for federally funded research. It seems clear that future endeavors will have to include a clear definition of where the efforts are leading; likewise, this definition will have to provide enough information for the broader community (Congress, Administration decision-makers, the public) to understand and endorse the directions.

For a mission-oriented institution like the Naval Research Laboratory (NRL), this should not be a great problem. The Laboratory has traditionally articulated its programs within the context of items to be delivered to or needed by the Department of the Navy, the Department of Defense, or other government agencies. In the future, however, we, too, will have to spend more time and effort in articulating the expected outcome of NRL's S&T programs in a vernacular that is more easily understood by both key decision-makers and the American people. Efforts in this regard are already well under way. For example, much of the recent reorganization of the Office of Naval Research (ONR) was motivated by the necessity to deal with these issues. The initiatives by ONR to view, formulate, and fund the Navy's S&T program as an integrated program rather than as a separate science program and a separate technology program is a significant step in this direction.

NRL must proceed in partnership with ONR as the integrated S&T program develops. We are the Navy's corporate laboratory, and the pursuit of science and technology in support of naval needs is our principal mission. We, therefore, have an enormous stake in the successful outcome of the integrated Navy's S&T program. The developments that are now under way will have significant long-term effects on the NRL program. Fortunately, there is a clear recognition in the Department of the Navy of the contributions that the Laboratory has made over the years, as well as the key role that the Laboratory will play in enhancing the technological supremacy of the Navy of the future. In this regard, we have a unique opportunity to develop even stronger working relationships between NRL and ONR. These new relationships should serve the Navy and the nation well in the coming years.

The Naval Research Laboratory

NRL—Our Heritage

Today, when government and science seem inextricably linked, when virtually no one questions the dependence of national defense on the excellence of national technical capabilities, it is noteworthy that in-house defense research is relatively new in our Nation's history. The Naval Research Laboratory (NRL), the first modern research institution created within the United States Navy, began operations in 1923.

Thomas Edison's Vision—The first step came in May 1915, a time when Americans were deeply worried about the great European war. Thomas Edison, when asked by a *New York Times* correspondent to comment on the conflict, argued that the Nation should look to science. "The Government," he proposed in a published interview, "should maintain a great research laboratory....In this could be developed...all the technique of military and naval progression without any vast expense." Secretary of the Navy Josephus Daniels seized the opportunity created by Edison's public comments to enlist Edison's support. He agreed to serve as the head of a new body of civilian experts—the Naval Consulting Board—to advise the Navy on science and technology. The Board's most ambitious plan was the creation of a modern research facility for the Navy. Congress allocated $1.5 million for the institution in 1916, but wartime delays and disagreements within the Naval Consulting Board postponed construction until 1920.

The Laboratory's two original divisions, Radio and Sound, pioneered in the fields of high-frequency radio and underwater sound propagation. They produced communications equipment, direction-finding devices, sonar sets, and perhaps most significant of all, the first practical radar equipment built in this country. They also performed basic research, participating, for example, in the discovery and early exploration of the ionosphere. Moreover, the Laboratory was able to work gradually toward its goal of becoming a broadly based research facility. By the beginning of World War II, five new divisions had been added: Physical Optics, Chemistry, Metallurgy, Mechanics and Electricity, and Internal Communications.

The War Years and Growth—Total employment at the Laboratory jumped from 396 in 1941 to 4400 in 1946, expenditures from $1.7 million to $13.7 million, the number of buildings from 23 to 67, and the number of projects from 200 to about 900. During WWII, scientific activities necessarily were concentrated almost entirely on applied research. New electronics equipment—radio, radar, sonar—was developed. Countermeasures were devised. New lubricants were produced, as were antifouling paints, luminous identification tapes, and a sea marker to help save survivors of disasters at sea. A thermal diffusion process was conceived and used to supply some of the ^{235}U isotope needed for one of the first atomic bombs. Also many new devices that developed from booming wartime industry were type tested and then certified as reliable for the Fleet.

NRL Reorganizes for Peace—Because of the major scientific accomplishments of the war years, the United States emerged into the postwar era determined to consolidate its wartime gains in science and technology and to preserve the working relationship between its armed forces and the scientific community. While the Navy was establishing its Office of Naval Research (ONR) as a liaison with and supporter of basic applied scientific research, it was also encouraging NRL to broaden its scope and become, in effect, its corporate research laboratory. There was a transfer of NRL to the administrative oversight of ONR and a parallel

shift of the Laboratory's research emphasis to one of long-range basic and applied investigation in a broad range of the physical sciences.

However, rapid expansion during the war had left NRL improperly structured to address long-term Navy requirements. One major task—neither easily nor rapidly accomplished—was that of reshaping and coordinating research. This was achieved by transforming a group of largely autonomous scientific divisions into a unified institution with a clear mission and a fully coordinated research program. The first attempt at reorganization vested power in an executive committee composed of all the division superintendents. This committee was impracticably large, so in 1949 a civilian director of research was named and given full authority over the program. Positions for associate directors were added in 1954.

The Breadth of NRL—During the years since the war, the areas of study at the Laboratory have included basic research concerning the Navy's environments of Earth, sea, sky, and space. Investigations have ranged widely from monitoring the Sun's behavior to analyzing marine atmospheric conditions to measuring parameters of the deep oceans. Detection and communication capabilities have benefited by research that has exploited new portions of the electromagnetic spectrum, extended ranges to outer space, and provided means of transferring information reliably and securely, even through massive jamming. Submarine habitability, lubricants, shipbuilding materials, fire fighting, and the study of sound in the sea have also been steadfast concerns.

The Laboratory has pioneered naval research into space from atmospheric probes with captured V-2 rockets through direction of the *Vanguard* project—America's first satellite program—to involvement in such projects as the Navy's Global Positioning System. As part of the SDI program, the Low-Power Atmospheric Compensation Experiment (LACE) satellite was designed and built by NRL. Today NRL is the Navy's lead laboratory in space systems research, fire research, tactical electronic warfare, microelectronic devices, and artificial intelligence. NRL has also evaluated new issues,

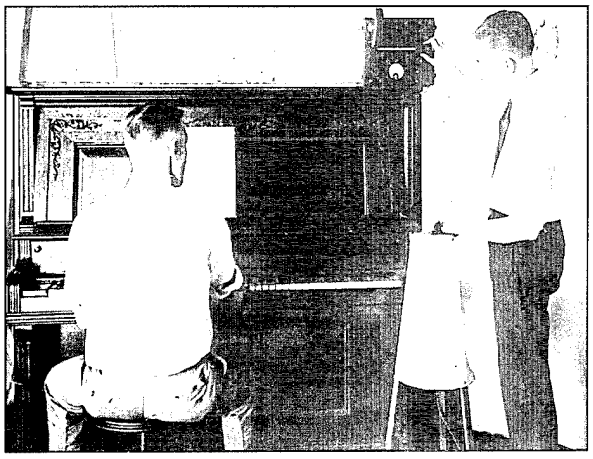

NRL of yesteryear—shown is the first regularly scheduled radio broadcast, with R.B. Meyer at the piano and Leo Young at the controls. Music was first broadcast from the Anacostia Naval Air Station (later incorporated into the Naval Research Laboratory) in 1920.

such as the effects of intense radiation and various forms of shock and vibration on aircraft, ships, and satellites.

The consolidation of NRL and the Naval Oceanic and Atmospheric Laboratory, with centers at Bay St. Louis, Mississippi, and Monterey, California, has added new strengths to the Laboratory. NRL now serves as the lead Navy laboratory for research in ocean and atmospheric sciences with special strengths in physical oceanography, marine geosciences, ocean acoustics, marine meteorology, and remote oceanic and atmospheric sensing. The expanded Laboratory is focusing its research efforts on new Navy strategic interests and needs in the post-Cold War world. Although not abandoning its interests in blue-water operations and research, the Navy is also focusing on defending American interests in the world's littoral regions. NRL scientists and engineers are working to give the Navy the special knowledge and capabilities it needs to operate in these waters.

The last year proved to be a productive one for NRL scientists and engineers. The *Clementine* spacecraft, built by Laboratory engineers for the Department of Defense's Ballistic Missile Defense Organization, was launched on January 25, 1994 and placed into lunar orbit on February 19. *Clementine* was the first American spacecraft to visit the moon since the *Apollo* moon missions. During 71 days of lunar orbit,

On April 28, 1994, CAPT Richard M. Cassidy, Jr. (right) relieved RADM (Sel.) Paul G. Gaffney II as Commanding Officer of NRL. Here they are shown cutting the ceremonial cake. CAPT Cassidy became the 31st Naval officer to head NRL.

the spacecraft mapped the moon's 38 million square kilometers in seven colors in the visible and near infrared spectrum, collected thousands of high-resolution and thermal images, charted the lunar topography with a laser-ranging experiment, improved understanding of the surface gravity field through radio tracking, and carried a charged-particle telescope to characterize the solar and magnetospheric particle environment. Over 1.8 million images were collected, making the moon the most completely mapped of any celestial body.

Elsewhere in the heavens, scientists from NRL, in collaboration with colleagues from the Jet Propulsion Laboratory in Pasadena, California, studied changes in Jupiter's magnetosphere as a result of the spectacular collision of Comet Shoemaker-Levy 9 with the planet. By studying the daily variations of emitted radiation over time, the researchers sought to increase their understanding of emission sources and the production of high-energy electrons in the magnetosphere. Other Laboratory space scientists reported the first detection of a millisecond pulsar in the extreme ultraviolet region, Pulsar J0437-4715, and the first observation of radio waves from Supernova 19941, in the Messier 51 galaxy.

In the upper atmosphere, NRL scientists have been studying ozone depletion in the polar regions. A new space-based sensor, the Polar Ozone and Aerosol Measurement experiment, was launched in 1993 and is now collecting information on the temperature and abundance of ozone, water vapor, nitrogen dioxide, and aerosols from between 50 to 30 miles above the surface. Another NRL experiment, the Middle Atmosphere High-Resolution Spectrograph Investigation (MAHRSI), also began work measuring trace elements in the atmosphere. MAHRSI is a remote-sensing ultraviolet mapping instrument dedicated to making the first global measurements of nitric oxide (NO) and the hydroxyl radical (OH) in the middle atmosphere.

In other work, Laboratory scientists developed a method to deposit biocompatible ceramic coatings using a pulsed-laser-deposition technique. The process directs the beam from a KrF excimer laser onto a target of calcium hydroxylapatite. The interaction of the laser energy with the target creates a plume of evaporated material that is directed at a substrate, such as a metal, ceramic, semiconductor, or polymer. In research on a different form of lining, NRL scientists have developed a new fluoropolymer lining for use in petroleum tanks. The lining will prevent corrosion in steel tanks, help keep the fuel clean, and seal minor leaks.

Within the past year, NRL scientists concluded the design and assemblage of a microwave monolithic integrated circuit electronic warfare (EW) receiver. The new receiver represents a significant improvement in the performance, weight, size, power, and cost of current EW receivers. In the world of artificial intelligence, computer scientists at NRL have used evolutionary computational methods to control the behaviors of computer-simulated autonomous vehicles. They have now demonstrated that these behaviors perform well in "real-world" environments. A robot at NRL's Navy Center for Applied Research in Artificial Intelligence, when directed to navigate through a room containing randomly placed obstacles, exhibited the same behaviors in laboratory tests as it had under simulation.

At the Laboratory's Center for Bio/Molecular Science and Engineering, scientists collaborated with colleagues at the National Institutes of Health and the University of California in the formation of networks using living neural cells. The researchers have placed embryonic brain

cells from laboratory rats in desired spots on silicon or glass chips and have induced the cells to grow in desired geometries. They soon expect to get the cells to grow defined connections between axons and dendrites, crudely mimicking the circuitry that neurons form in the brain.

NRL was active last year in transferring technology developed at the Laboratory to private industries for production and marketing. While the majority of Cooperative Research and Development Agreements (CRADAs) are with industrial firms, several are also with universities and nonprofit organizations. To date, NRL has signed over 70 CRADAs and patent license agreements. One of the licensees, Quantum Magnetics—the R&D subsidiary of Quantum Design, Inc. of San Diego, California—demonstrated a new, sensitive explosives detector at NRL on August 26, 1994. The explosives detector is based on a technology known as quadrupole resonance (QR). QR improves the selectivity and sensitivity over conventional detection systems and, as a result, subkilogram quantities of explosives can be detected quickly and accurately within such items as envelopes, packages, boxes, and baggage. Although Quantum Magnetics' system was developed to detect explosives, QR has the demonstrated ability to also detect narcotics. In addition, in February 1994, NRL signed a patent licensing agreement with JohnCo. Rental Inc. (JRI), of Gowanda, New York, a Seneca Nation Indian company, granting JRI a partial right to manufacture and market an NRL-developed portable, hand-held sensor that can be used to identify drugs of abuse hidden in confiscated packages or solid material. The licensed technology, known as the Microassay on a Card (MAC), also has applications for police departments, customs operations, and schools.

NRL's Technology Transfer Office signed a patent licensing agreement with JohnCo Rental Inc. to manufacture and market Microassay on a Card (MAC), which is used to identify drugs of abuse hidden in confiscated packages and solid materials.

NRL Today

ORGANIZATION AND ADMINISTRATION

The position of NRL within the Navy is that of a field command under the Chief of Naval Research.

Heading the Laboratory with joint responsibilities are the naval commanding officer, CAPT Richard M. Cassidy, USN, and the civilian director of research, Dr. Timothy Coffey. Line authority passes from the commanding officer and the director of research to four associate directors of research, an associate director for strategic planning, a director of the Naval Center for Space Technology, and an associate director for business operations. Research is performed in the following areas:

- General Science and Technology
- Warfare Systems and Sensors Research
- Materials Science and Component Technology
- Ocean and Atmospheric Science and Technology
- Naval Center for Space Technology.

Through FY 94, NRL operated as a Defense Business Operating Fund (DBOF) activity. As a DBOF activity, all costs, including overhead, were charged to various research projects. Funding in FY 94 came from the Chief of Naval Research, the Naval Systems Commands, other Navy sources; government agencies, such as the U.S. Air Force, Advanced Research Projects Agency, the Department of Energy, and the National Aeronautics and Space Administration; and several nongovernment activities.

PERSONNEL DEVELOPMENT

At the end of FY 94, NRL employed 3858 personnel—51 officers, 92 enlisted, and 3715 civilians. In the research staff, there are 883 employees with doctorate degrees, 465 with masters degrees, and 653 with bachelors degrees. The support staff assists the research staff by providing administrative, computer-aided design, machining, fabrication, electronic

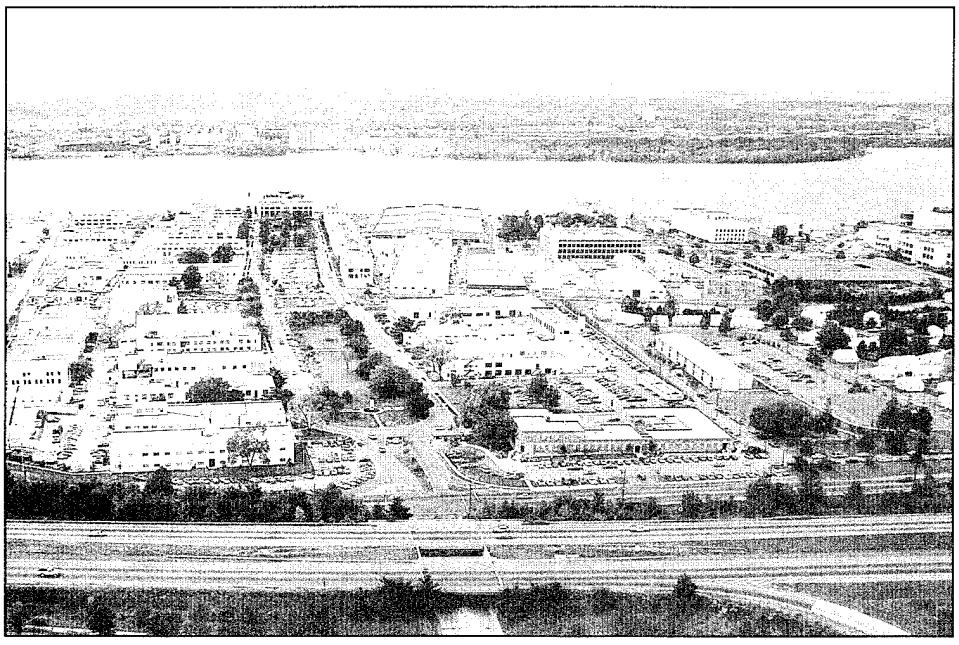

NRL headquarters in Washington as viewed from the east.

construction, publication, personnel development, information retrieval, large mainframe computer support, and contracting and supply management services.

Opportunities for higher education and other professional training for NRL employees are available through several programs offered by the Employee Development Branch. These programs provide for graduate work leading to advanced degrees, advanced training, college course work, short courses, continuing education, and career counseling. Graduate students, in certain cases, may use their NRL research for thesis material.

For non-NRL employees, several post-doctoral research programs exist. There are also cooperative education agreements with several universities, summer and part-time employment programs, and various summer and interchange programs for college faculty members, professional consultants, and employees of other government agencies.

NRL has active chapters of Women in Science and Engineering, Sigma Xi, Toastmasters International, Federally Employed Women, and the Federal Executive and Professional Association. Three computer clubs meet regularly—NRL Microcomputer User's Group, NeXT, and Sun NRL Users Group. An amateur radio club, a drama group (the Showboaters), and several sports clubs are also active. NRL has a recreation club that provides basketball and softball leagues and swim, sauna, whirlpool bath, gymnasium, and weight-room facilities. The recreation club also offers classes in martial arts, aerobics, swimming, and water walking.

The Community Outreach Program traditionally has used its extensive resources to foster programs that provide benefits to students and other community citizens. Volunteer employees assist with and judge science fairs, give lectures, tutor, mentor, coach, and serve as classroom resource teachers. The program also sponsors Black History Month art and essay contests for local schools, student tours of NRL, a student Toastmasters Youth Leadership Program, an annual holiday party for neighborhood children in December, an equipment loan program that provides surplus equipment to partnership schools, a book donation program for both students and teachers, and an annual collection for Children's Hospital. Through the Community Outreach Program, NRL has active partnerships with four District of Columbia public schools.

NRL has an active, growing Credit Union, with assets over $155 million and a membership numbering over 19,500. The NRL Federal Credit Union offers competitive and innovative financial services.

Public transportation to NRL is provided by Metrobus.

For more information, see the *NRL Review* chapter entitled, "Programs for Professional Development."

SCIENTIFIC FACILITIES

In addition to its Washington, D.C. campus of about 130 acres and 102 main buildings, NRL maintains 14 other research sites, including a vessel for fire research and a Flight Support Detachment. The many diverse scientific and technological research and support facilities are described in the following paragraphs.

Research Facilities

Radar

NRL has gained worldwide renown as the "birthplace of radar" and, for a half-century, has maintained its reputation as a leading center for radar-related research and development. An impressive array of facilities managed by NRL's Radar Division continues to contribute to this reputation.

In connection with airborne radar, the division uses a Radar Imaging Facility, consisting of an inverse synthetic aperture radar (ISAR) that can be deployed to collect radar-imaging data from the air in a P-3 or a trailer for ground or ship installation. New technology associated with aircraft early warning (AEW) radar uses a rooftop space-time adaptive processing (STAP) array and associated processors. In connection with ship-based radar, the division operates a Radar Test Bed Facility at the Chesapeake Bay Detachment (CBD), Randle Cliffs, Maryland. Represented are test bed radars and related data

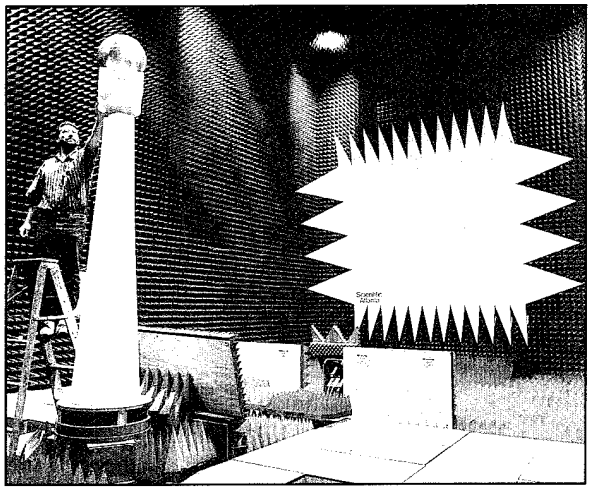

The Radar Division uses a Compact Range Facility to measure antenna properties and radar cross sections of various targets. The targets are then used to verify and optimize the designs for new systems to improve existing systems. Instrumented for measurements from 2 to 60 GHz, it provides a quiet zone approximately 7 ft in diameter and 8 ft in length. The range is jointly operated and shared by Radar Division and the Space Systems Development Department.

processing facilities for long-range air search, point defense, and surface search. Concepts and engineering developments in connection with target identification are explored by using an experimental Cooperative Aircraft Identification (CAI) System. Other installations operated by the division include an Electromagnetic Interference (EMI) Facility, a Radar Signature Calculation Facility for complex electromagnetic radar target modeling, a Compact Antenna Range (operated jointly with the Space Systems Development Department) for antenna design and development, and a Computer-aided Engineering (CAE) Facility.

Information Technology

The Information Technology Division (ITD) is at the forefront of DoD research and development in artificial intelligence, telecommunications, computer networking, human-computer interaction, information security, parallel computation, and computer science.

The division maintains local area computer networks to support its research and hosts testbeds for advanced high-performance fiber-optic network research. The networks are made available to local and remote users' hundreds of high-performance computers (more than 500 Macintoshes, PCs, and other workstations). The ITD research networks are part of NRL's internal network and also connect via T1 lines to the regional SURAnet, to DISnet, and via ATM/SONET links to ATDnet, an experimental wide-area network connecting a number of research organizations in the metropolitan area.

Major shared resources include the systems and networks available in the division's Center for Computational Science, including a 256-processor CM5, 16-K processor CM200 equipped with a 10-Gigabyte data vault, dual processor Cray Y-MP EL, 1.5-Terabyte file server/archiver, and Scientific Visualization Lab. The center manages and operates the NRL local area network (NICEnet), which includes a new FDDI network. NICEnet provides external connections to networks worldwide.

The division facilities also include a Certification and Information Security Engineering Laboratory and an experimental facility with special displays, eye and gesture trackers, and speech I/O devices for research in human computer interaction.

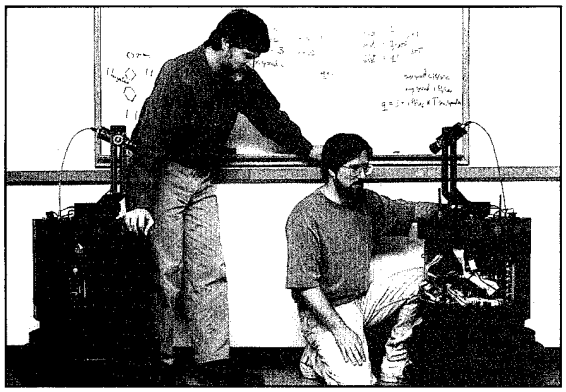

Computer scientists at NRL's Navy Center for Applied Research in Artificial Intelligence use evolutionary computation methods to control the behaviors of computer-simulated autonomous vehicles. The scientists have demonstrated that these behaviors perform well in real-world environments. Here a robot navigates through a room while avoiding randomly placed obstacles. The robot exhibited the same behaviors in laboratory tests as it had under simulation.

Optical Sciences

The Optical Sciences Division has a broad program of basic and applied research in optics and electro-optics. Areas of concentration in electro-optics include fiber optics, integrated optical devices, fiber-optic sensors, high-power diode lasers, and diode-pumped solid-state lasers. Modern electro-optic sensors such as infrared focal plane arrays are developed by NRL as well as signal processors, digital processors, computer algorithms, and digitized background scene imagery to allow computer-augmented sensor design for Naval applications. The division also maintains a capability to perform optical field measurements from ground-based, water-based, or air-based platforms at appropriate sites away from NRL. The Optical Sciences Division has recently occupied the newly constructed Electro-Optics Research Facility (Buildings 215-216). These two buildings together provide 87,000-ft^2 of modern office and laboratory spaces. Together with recently renovated spaces in Buildings A-12 and A-50, the division now occupies some of the most modern optical facilities in the country. These facilities allow work to be performed in the areas of fiber optics, integrated optics, optical information processing, infrared sensors and modeling and testing of sensors, optical components, and signal processing. Facilities include the following:

Ultralow-Loss, Fiber-Optic Waveguides—NRL has developed record-setting ultrahigh transparency infrared waveguides. These fluoride glass materials offer the promise of long-distance communications without the need of signal amplification or repeaters. The high temperature IR glass technology is also useful for bulk optical materials and as a host for laser ions or other species in devices such as chemical detectors.

Focal Plane Evaluation Facility—This facility has extensive capabilities to measure the optical and electrical characteristics of infrared focal plane arrays being developed for advanced Navy sensors.

IR Missile-Seeker Evaluation Facility—This facility performs open-loop measurements of the susceptibilities of infrared tracking sensors to optical countermeasures.

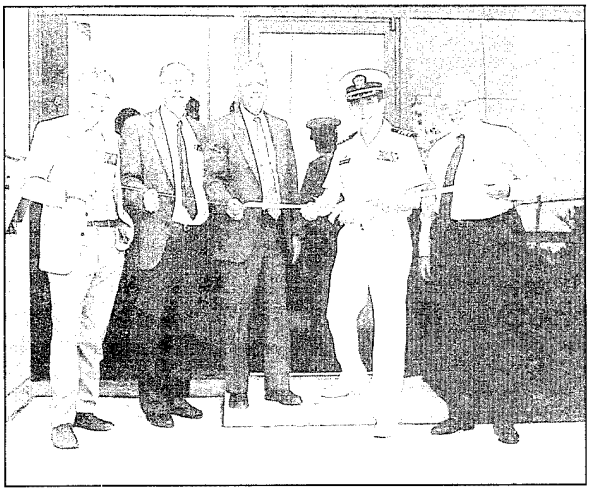

A ribbon-cutting ceremony was held on September 24, 1993, to dedicate the new state-of-art Electro-Optics Laboratory for NRL's Optical Sciences Division.

Large Optic, High-Precision Tracker—NRL has developed a tracker system with an 80-cm primary mirror for atmospheric transmission and target signature measurements. By using a quadrant detector, the servo system has demonstrated a 12-mrad tracking accuracy. An optical correlation tracker system tracks objects without a beacon.

High-Energy Pulsed Hydrogen Fluoride, Deuterium Fluoride Laser—NRL has constructed a pair of pulsed chemical lasers, each capable of producing up to 30 J of laser energy at 2.7 to 3.2 mm and 3.8 to 4.5 mm in a 2-ms pulse. This facility is used to investigate a variety of research areas, including stimulated Brillouin scattering, optical phase conjugation, pulsed laser amplification, propagation, and beam combining.

Fiber-Optics Sensors—The development and fabrication of fiber-optic sensor concepts, including acoustic, magnetic, and rate-of-rotation sensors, are conducted in several facilities within the Laboratory's Optical Sciences and Acoustics Divisions. Equipment includes facilities for evaluating optical fiber coatings, fiber splicers, an acoustic test cell, a three-axis magnetic sensor test cell, a rate table, and various computers for concept analysis.

Digital Processing Facility—This facility is used to collect, process, analyze, and manipulate infrared data and imagery from several sources.

Emittance Measurements Facility—NRL routinely performs measurements of directional hemispherical reflectance from 2 to 16 mm in the infrared by using a diffuse gold-integrating sphere and a Fourier transform spectrophotometer (FTS). Sample temperatures can be varied from room temperature to 250°C and incidence angles from 0° to 60°.

Diode Pumped Solid-State Lasers—Two micrometer lasers operate in an eye-safe region of the optical spectrum, an important issue for laser use in industry or in cases where eye damage to the public could be a safety and liability issue. Research at NRL in the 1980s had a major role in demonstrating room temperature flashlamp and diode pumped lasers. The lamp pumped lasers have found wide usage in laser surgery while diode pumped lasers appear to be leading candidates for eye-safe laser radars for aircraft and for laser sources to counter IR missile seekers. Newer lasers have been found that operate from 0.400 μm in the near UV to beyond 5 μm in the IR.

Electronic Warfare

The scope of research and development at NRL in the field of electronic warfare covers the entire electromagnetic spectrum—from basic technology research, component, and subsystem development—to system design and effectiveness evaluation. Major emphasis is placed on providing the methods and means to counter enemy hostile actions in all battle phases, from the beginning—when enemy forces are mobilized for an attack—through the final engagement stages. For this purpose, NRL has constructed special research and development laboratories, anechoic chambers, and facilities for modeling and simulation. NRL has also added extensive new facilities where scientists can focus on the coordinated use of all organic defensive and offensive resources now present in the Fleet.

Structure of Matter

The laboratory investigates the atomic arrangements in materials to improve them or facilitate the development of new substances. Various diffraction methodologies are used to make these investigations. Subjects of interest include the structural and functional aspects of energy conversion, ion transport, device materials, and physiologically active substances such as drugs, antibiotics, and antiviral agents. Theoretical chemistry calculations are used to complement the structural research. A real-time graphics system aids in modeling and molecular dynamics studies.

Chemistry

NRL has been a major center for chemical research in support of naval operational requirements since the late 1920s. The Chemistry Division continues its tradition with a broad spectrum of basic and applied research programs concerned with controlled energy release (fuels, fire, combustion, countermeasure decoys, explosives), surface chemistry (corrosion, adhesion, tribology, adsorbents, film growth/etch), advanced polymeric materials (high-strength/low-weight structures, drag reduction, damping,

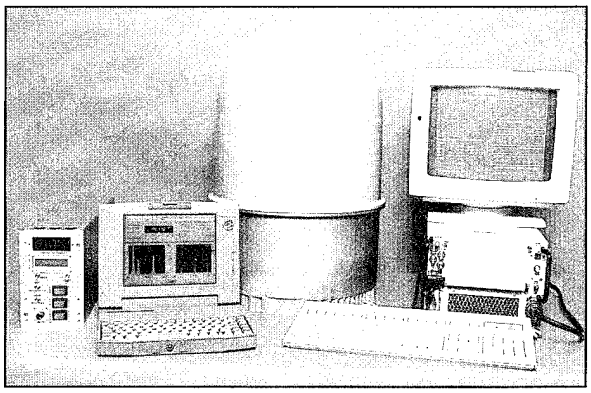

By using the latest composite, MMIC (microwave monolithic-integrated circuit), and processing technologies, the Tactical Electronic Warfare Division has developed a small, lightweight, and inexpensive electronic support measures receiving system for use on frigates, Coast Guard vessels, and various patrol aircraft.

special function), and advanced detection techniques (environment, chemical/biological, surveillance). Facilities for research include a wide range of the modern photon/electron, magnetic and ion-based spectroscopic/microscopic techniques for bulk and surface analysis; multiple facilities for materials synthesis and physical/chemical characterization; a 325-M^3 (11,400 ft^3) fire research chamber (Fire I), and a 475-ft ex-USS *Shadwell* (LSD-15) advanced fire research ship.

Materials

NRL has capabilities for X-ray and electron diffraction analyses and for electron and Auger spectroscopy. Scanning, transmission, and combined scanning-transmission electron microscopes are used to study surface and/or internal microstructures. The division has a secondary ion mass spectrometer for surface analysis that significantly extends the diagnostic capability of the technique. A high-resolution, reverse-geometry mass spectrometer is used to probe reactions between ions and molecules. The Laboratory has a fully equipped fatigue and fracture laboratory, a modern vacuum arc melting furnace for reactive metals, an ultrasonic gas atomization system for making metal powders, and hot isostatic press facilities. The Laboratory's cryogenic facilities include dilution refrigerators and superconducting magnetic sensors for measuring ultrasmall magnetic fields. Also available are two molecular beam epitaxy devices for growing thin films.

Laboratory for Computational Physics and Fluid Dynamics

The Laboratory for Computational Physics and Fluid Dynamics is in round-the-clock production for computational studies in the fields of compressible and incompressible fluid dynamics, reactive flows, fluid-structure interaction (including submarine, ship, and aerospace applications), atmospheric and solar magnetoplasma dynamics, and for application of parallel processing to large-scale problems such as unstructured grid generation for complex flows, for target tracking and correlations for battle management, and other disciplines of continuum and quantum computational physics. The system is used to develop and maintain state-of-the-art analytical and computational capabilities in fluid dynamics and related fields of physics, to establish in-house expertise in parallel processing and on-line graphical rendering for large-scale scientific computing, to perform analyses and computational experiments on specific relevant problems, and to transfer this technology to new and ongoing projects through cooperative programs.

The Parallel High Performance Computer/ Graphics Facility is a heterogeneous high-performance computer system composed of a number of autonomous computers with a composite peak speed equivalent to about 10 Cray YMP processors. The system is coupled directly to the advanced video recording center described below. The main computational engine is an Intel iPSC/860 Touchstone Gamma parallel supercomputer supported by the hardware and

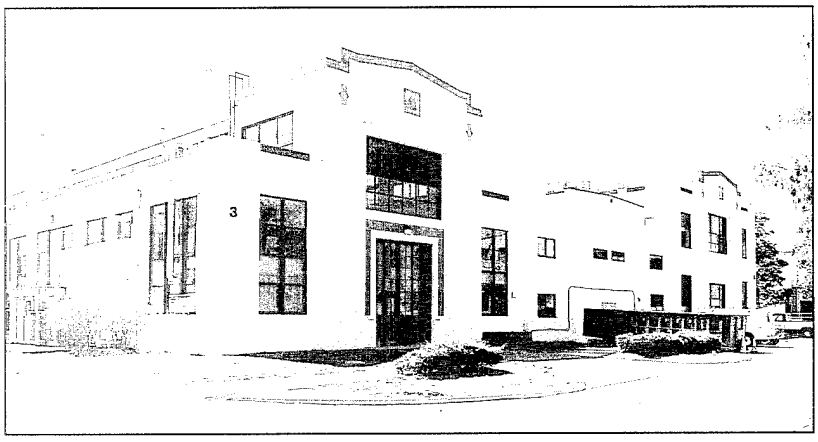

On April 26, 1994, Building 3 at NRL Washington, D.C., was dedicated as a historical landmark by the American Society of Metals International. The building has been devoted to materials research since the inception of the Laboratory's Physical Metallurgy Division in 1927, 4 years after NRL's official opening.

software environment necessary to develop, debug, and benchmark parallel simulations. With multi-MFLOP processors as building blocks, the Intel iPSC/860 is a MIMD-distributed memory machine configured as a hypercube. This 32-node parallel supercomputer has a peak computational speed of several GFLOPS with a cross-connected disk farm file system and network connections.

The facility's disk farm also supports three IBM RS/6000 and three DEC AXP high capacity compute-server computers, providing the facility with medium-to-large-scale memory and computational power enabling heterogeneous simulations with a significant scalar component, algorithm development, and diagnostic and postprocessing for large simulations. Special software allows simultaneous use of these computers on a single problem. A 64-million word Convex C210 currently provides this facility with medium performance scalar and vector capability for jobs that require large amounts of memory. Access to various other HPCC capabilities around the U.S. is accomplished through this system by using the new DoD high-bandwidth communication networks. A four-processor, five-Gigabyte SGI Onyx provides the division with state-of-the-art high performance visualization.

A high-quality video studio has been created around a Sony D2 digital recording system with a coupled Lyon-Lamb animation controller and a large memory Silicon Graphics ONYX workstation. Through the network, other graphics stations, including the extensive resources of NRL's Visualization Laboratory, can create and record high-quality graphical images of simulation data for analysis and presentation by using digital recording techniques.

Condensed Matter and Radiation Sciences

The Condensed Matter and Radiation Sciences Division is the primary Navy center studying the effects of radiation on material items, including electronic equipment, satellites, etc., and the condensation of materials (thin films) on other objects through the use of charged-particle radiation. The division approaches these activities from both the theoretical and applied aspects, including application to environmental as well as military situations. The facilities for production and employment of photons, electrons, ions, and hypervelocity projectiles available to the division include:

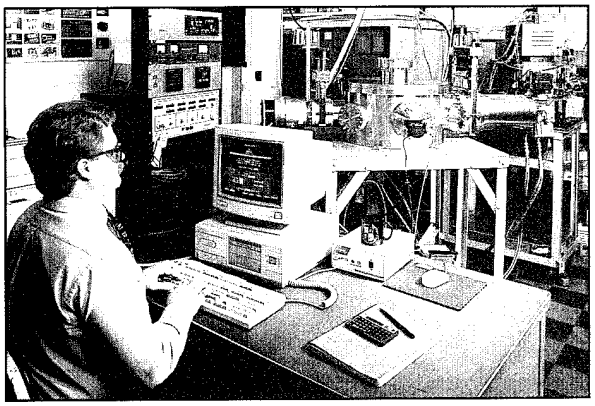

Shown here is the Condensed Matter and Radiation Sciences Division's computer-automated pulsed-laser deposition system. The chamber is designed to deposit epitaxial multilayers and superlattices of multicomponent materials such as the high-temperature superconductors and other electronic ceramics.

High-Power Microwave (HPM) Facility—This facility is used to investigate the response of systems and components to pulsed high-power microwave radiation. Effects, susceptibility, and survivability are the major research areas of interest. The large anechoic chamber (4.9 m × 4.9 m × 9.8 m) can be used at frequencies ranging from 0.5 to 94 GHz.

Laser Facilities—The ultrafast lasers provide a broad range of capabilities by bringing together an extensive array of laser sources for the study of condensed matter interactions. Pulses of up to several joules are available from one system, while time resolutions down to 100 femtoseconds are produced by another. Synchronized Q-switched oscillators are configured for pump-probe experiments. A range of optical, laser, and soft X-ray spectroscopes are used to study nonlinear optical effects, time responses, and laser-target interactions.

Thin-Film Preparation Facilities—The division has several major capabilities for preparation of thin films of advanced materials, such as high-temperature superconductors and active dielectrics. These include ion-assisted evaporation (which produces dense, adherent films),

various dc plasma sources (which can etch as well as deposit films), and pulsed laser deposition (for production of chemically complex films).

X-ray Facility—Laboratory X-ray sources, monochromators, detectors, and related equipment are available for X-ray energies from 0.7 to 25 keV and dose rates up to 10^5 rads/s.

Synchrotron Radiation Facility—Intense, monochromatic X-ray photon beams tunable from 10 eV to 12 keV are available from the three beam lines developed by NRL at the National Synchrotron Light Source at the Brookhaven National Laboratory. Standard measurements include X-ray diffraction, absorption, reflectance, and photo-electron emission. Environmental target chambers can span a pressure range from 10^{-12} to 10^5 atmospheres and temperatures from 10 to 1500 K.

Ion Implantation Facility—The facility consists of a 200-keV ion implanter with specialized ultrahigh vacuum chambers and associated in situ specimen analysis instrumentation. The facility is used to develop advanced surface treatments of materials to modify their properties and improve corrosion and wear resistance.

3-MeV Tandem Van de Graaff—This facility is used to study charged-particle radiation damage effects such as occur in space, to perform Rutherford backscattering spectroscopy, elastic recoil detection, ion channeling and nuclear reaction analysis, to provide high-sensitivity composition depth profiles, and to perform MeV energy implants in materials.

Hypervelocity Impact Facilities—Three facilities are used for ballistics research at speeds exceeding 6 km/s with toxic and explosive targets while measuring projectile velocity, orientation, and dynamic projectile-target interaction.

Plasma Physics

The Plasma Physics Division is the major center for in-house Navy and DoD plasma physics research. The division conducts a broad experimental and theoretical program in basic and applied research in plasma physics, which includes laboratory and space plasmas, pulsed-power sources, electric mass launchers, intense

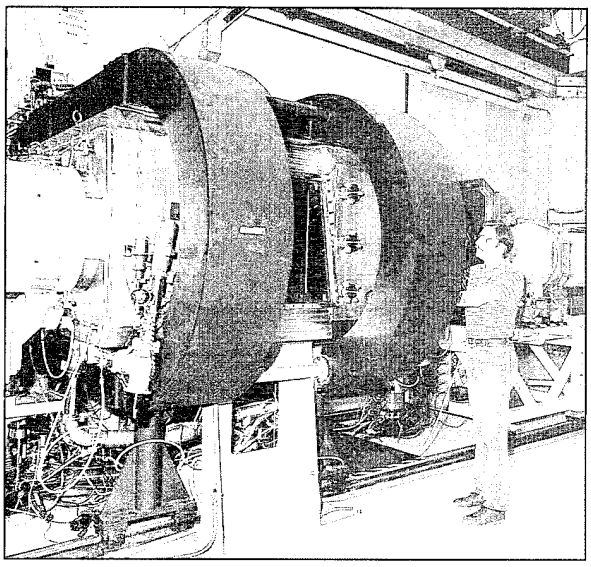

The Nike 60-cm amplifier, Plasma Physics Division's new facility, is the final and largest amplifier in the Nike krypton fluoride laser. It increases the laser beam energy from 150 J to over 5000 J. The laser beam enters the gas-filled laser cell through the window and is amplified by two opposing 670,000 V electron beams. The electron beams are guided by the two large black electromagnets.

electron and ion beams, atomic physics, laser physics, and numerical simulations. The facilities include an extremely high-power laser—Pharos III—for the laboratory simulation of space plasmas and high-altitude nuclear explosion effects studies, a short pulse, high intensity Table-Top Terawatt (T^3) laser to study intense laser beam and laser interactions, and the electric mass launcher laboratory to study railgun physics. The division has developed a variety of pulsed-power sources to generate electron and ion beams, powerful discharges, and various types of radiation. The largest of these pulsers—GAMBLE II—is used to study the production of megampere electron beams and for producing very hot, high-density plasmas. Other generators are used to produce particle beams that are injected into magnetic fields and/or cavities to generate intense microwave pulses. A charged-particle-beam (CPB) propagation facility exists for testing advanced CPB propagation (both endo- and exoatmospheric) concepts. A 5-MV generator injects pulses of electron current into preheated ionization channels to study the effectiveness of propagation under various conditions.

Electronics Science

In addition to specific equipment and facilities to support individual science and technology programs, NRL operates the Nanoelectronics Processing Facility (NPF), the Laboratory for Advanced Material Synthesis (LAMS), and the EPICENTER. The NPF's mission is to provide service to both NRL and external organizations requiring micro- and nanofabrication processing support. Lithography is a particular strength of the NPF, with feature sizes down to 150 Å possible with an e-beam nanowriter. The NPF can supply items ranging from individual discrete structures and devices to circuits with very large scale integration complexity. The LAMS' mission is to support NRL programs that require thin film III-V semiconductor technology. The LAMS employs organometallic vapor phase epitaxy to synthesize a wide range of thin films such as InSb, InGaP, InP, and GaN. The recently completed EPICENTER (a joint activity of the Electronic Science and Technology, Materials Science and Technology, and Chemistry Divisions) is dedicated to the production of multilayer microstructures using in situ surface analytical techniques in either of two ultrahigh vacuum, molecular beam epitaxy growth chambers—one for III-V semiconductors and the other for magnetic materials and II-VI semiconductors.

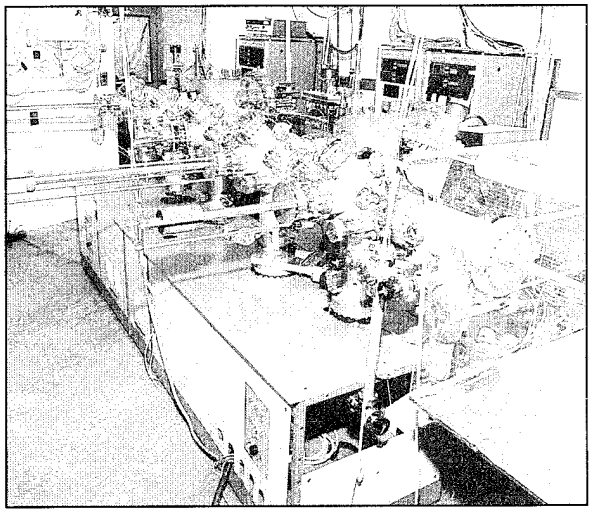

The EPICENTER (supported by the Electronics Science and Technology, Materials Science and Technology, and Chemistry Divisions) includes two MBE systems (rear of photograph) connected by a long, high vacuum tube (front of photograph). A transfer cart in this chamber facilitates the transfer of thin films from one chamber to the other.

Bio/Molecular Science and Engineering

The Center for Bio/Molecular Science and Engineering conducts research and development using biotechnological approaches to solve problems for the Navy, DoD, and the nation at large. Problems currently being addressed include advanced material development (for electronic, biomedical, and structural applications), combat casualty care, environmental quality (including pollution cleanup and control), and biological warfare defense. The approach to these problems involves long-term research focused on the study of complex materials systems, coupled with integrated exploratory and advanced development programs. The staff of the center is an interdisciplinary team who performs basic and applied research and development in areas that require expertise in bio- and surface chemistry, biophysics, genetic engineering, cell biology, advanced organic synthesis, solid-state and theoretical physics, and electronics and materials engineering. In addition, the center has many collaborations throughout the Laboratory, at universities, and in industry to ensure that a broad base of the required expertise and critical evaluations are part of the research and development programs. Highlights of the program include the development of liposome-based blood substitutes, the manipulation of biologically derived structures on the nanometer scale, the development of ferroelectric liquid crystal systems with microsecond response times, discovery of an advanced resist system for high-speed, high-density integrated circuits, and the patterning of neuronal cells to form neural networks.

Acoustics

NRL's facilities in support of acoustical investigations are located at the main Laboratory site; at Stennis Space Center in Bay St. Louis, Mississippi; and at the Underwater Sound Reference Detachment (USRD) in Orlando, Florida. At the main Laboratory site, there are

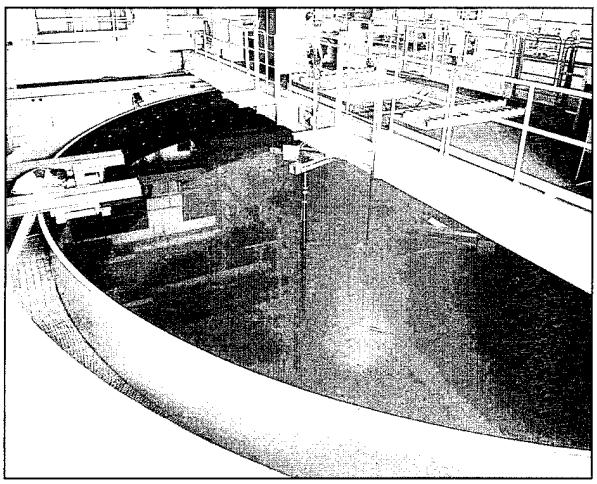

The large acoustic tank is the core research capability for structural acoustics studies undertaken by the Acoustics Division. The steel cylindrical tank is 55 ft in diameter, 50 ft in depth, and contains 800,000 gallons of deionized water. The entire tank is vibration and temperature isolated. This unique laboratory is also instrumented with precise measurement systems that include large workspace in-water robotic scanners capable of generating nearfield acoustic holography radiation and scattering databases.

three research tanks instrumented to study echo characteristics of targets and to develop devices. The most significant of the three is located in the NRL Laboratory for Structural Acoustics in Building 5, which includes a state-of-the-art acoustic pool for conducting scale-model scattering and radiation studies. Capabilities include near-field acoustic holography for studying complex 3-D sound fields near a target and the vibrations of the target itself. NRL has successfully produced the first near-field acoustical-scattered hologram in this facility. Among the benefits of the holographic capability is that near-field measurements can be projected to the far field, and target strengths can be obtained in any desired direction. In general, the pool complex permits model studies and demonstrations to be carried out at scales ranging from about 30 to 1 to several hundred to one. Projects involving modeling include—but are not limited to—target strength, radiation, signature reduction, classification, and structural acoustics. Advanced hull sensor technologies can be studied at any scale. There is also an underwater acoustic holography facility for research in acoustic fields and a water tunnel that has a large blow-down channel, with a 15-m test section used for acoustic and flow-induced vibration studies of towed line arrays and flexible cables.

The division also has several acoustic receiver array systems used to collect data for coherent signal processing. The primary system consists of a 64-element towed seismic-type receiver array with the associated tow cable, winch, and electrical components. The towed array component can be replaced with a 64-element fixed bottomed array or 64-element vertical array. There are also two radio telemetered buoyed acoustic receiver array systems with 20-element arrays capable of being vertically or horizontally deployed. All receiver arrays are interfaced into the At-sea Data Acquisition, Recording, and Real-time Processing System.

The division operates high-frequency (up to 600 kHz) acoustic measurement systems to obtain scattering, target strength, and propagation data using four large bottom-moored instrumentation towers and a high-speed, remotely operated vehicle. These data are used to simulate the performance of weapons and mine countermeasure sonars in shallow water environments. The midfrequency (30 to 1000 Hz) towed horizontal array system is used to understand the three-dimensional characteristics of the acoustic ambient noise field; these measurements are used to develop tactics and advanced systems to exploit these characteristics. An acoustic simulation capability plus a dedicated laboratory based on multiple workstations that are linked to the NRL CM-5/200, Cray Y-MP EL, and national high-performance computer facilities provides benchmark simulations of acoustic performance based on high-resolution oceanographic and atmospheric environmental information.

Remote Sensing

The Remote Sensing Division conducts a program of basic research, science, and applications to develop new concepts for sensors and imaging systems for objects and targets on the Earth and in the near-Earth environment and in deep space. The research, both theoretical and experimental, leads to discovering and

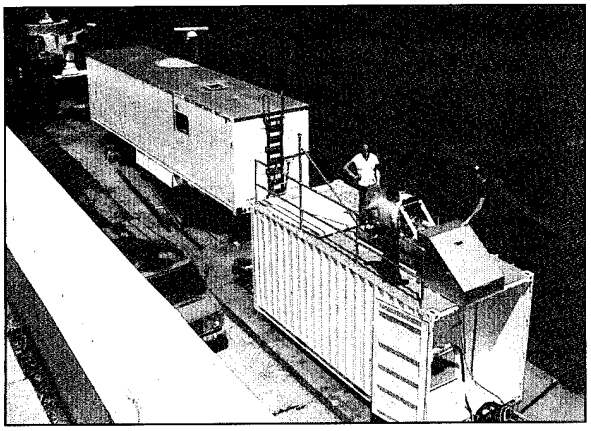

The Remote Sensing Division has several laser systems that are used in research functions associated with aerosol measurements (air/sea interface), altimetry, and nonacoustic ASW. Scientists are shown conducting laser experiments at the Chesapeake Bay Detachment site.

understanding the basic physical principles and mechanisms that give rise to the background environmental emissions and targets of interest and to absorption and emission mechanisms of the intervening medium. Accomplishing this research requires the development of sensor systems' technology. The developmental effort includes active and passive sensor systems used for the study and analysis of the physical characteristics of phenomena that evolve from naturally occurring background radiation such as that caused by the Earth's atmosphere and oceans and manmade or induced phenomena, such as ship/submarine hydrodynamic effects. The research includes theory, laboratory, and field experiments leading to ground-based, airborne, or space systems for use in remote sensing, astrometry, astrophysics, surveillance, nonacoustic ASW, improved meteorological/oceanographic support systems for the operational Navy, and the environmental/global climate change initiatives. Special emphasis is given to developing space-based platforms and exploiting existing space systems.

Oceanography

The Oceanography Division is the major center for in-house Navy research and development in oceanography. It is known nationally and internationally for its unique combination of theoretical, numerical, and experimental approaches to oceanographic problems. Theoretical research makes extensive use of the Maury Oceanographic Library (jointly operated by NRL-Stennis Space Center (NRL-SSC) and the Naval Oceanographic Office), which is recognized as one of the best and most comprehensive oceanographic libraries in the world. The division numerically models the ocean and coastal areas of the world. This modeling is conducted on the Navy's and DoD's most powerful vector and parallel processing machines. To study the results of this intense modeling effort, the division operates a number of highly sophisticated graphic systems to visualize ocean and coastal dynamic processes. The seagoing experimental programs of the division are particularly well supported. Unique measurement systems include: towed sensor and advanced microstructure profiler systems for studying micro- and fine-scale ocean structure, an integrated absorption cavity and optical profiler system for studying ocean optical characteristics, and self-contained bottom-mounted upward-looking acoustic profilers for measuring ocean variability. In the laboratory, the division operates an environmental scanning electron microscope and a laser confocal scanning microscope for detailed studies of biocorrosion in naval materials.

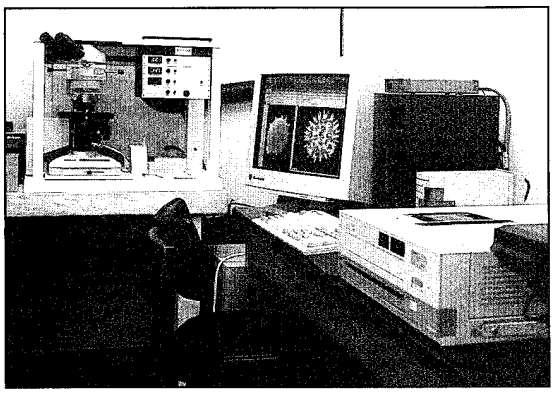

The Oceanography Division's laser confocal scanning microscope is used for microbally induced corrosion studies.

Marine Geosciences

The Marine Geosciences Division is the major center for in-house naval research and development in marine geology, geophysics, geoacoustics, and geotechnology. It is also the Navy's lead activity for mapping, charting, and geodesy research and development. The division has acquired unique instrumentation suites for its studies of the seafloor and its subbottom. These include sidescan sonar systems; deep-towed, low-frequency acoustic reflection systems; parametric acoustic swath subbottom mapping systems; remotely operated vehicles; and electromagnetic mapping sensors. These systems allow studies ranging from sediment classification to mapping of inclusions and changes in the seafloor subbottom structure. The division deploys ocean bottom and subbottom seismometer systems for use in studies ranging from tectonic noise to studies of whale migration. Specialized seafloor probes allow measurement of the water pressure in sediment pores and acoustic compression and shear wave velocity and attenuation. Laboratory equipment includes a transmission electron microscope with an environmental cell to carry out sediment-fabric and sediment-pollution adsorption studies.

The Map Data Formatting Facility, a collection of computers and work stations with associated graphics manipulation software, is used to compress map information onto compact disk read-only memory for Navy and Marine Corps aircraft digital moving maps. The division also operates the NRL Magnetic Observatory at SSC. This facility includes two specially built wooden buildings with minimal ferrous content and arrays of magnetometers that extend radially from the building. The Magnetic Observatory measures the ambient magnetic field, its changes, and other magnetic phenomena. The Observatory is part of a worldwide observing system.

In addition to in-house laboratory work, the division incorporates the Chief of Naval Operations (CNO)-sponsored Tactical Oceanographic Warfare Support Program Office, which develops high-resolution atmospheric, oceanographic and bathymetric instrumentation systems, and measurement techniques in support of CNO-endorsed requirements.

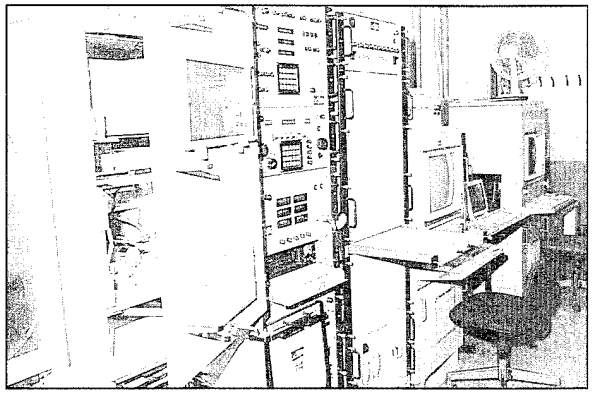

The Marine Meteorology Division's Tactical Environmental Support System Version 3 (TESS (3)) laboratory is functioning as an R&D testbed for new tactical and environmental decision aids, object-oriented databases, and graphical-user interfaces. This system will serve as a basis for a future shipboard atmospheric environmental analysis/forecasting system.

Marine Meteorology

The Marine Meteorology Division is located in Monterey, California. NRL-Monterey (NRL-MRY) performs both basic and applied research in meteorology in applications relevant to both central-site and shipboard meteorological analyses and forecasts. Located adjacent to the Fleet Numerical Meteorology and Oceanography Center (FNMOC), the Navy's operational forecast center, NRL-MRY has developed both the global and regional forecast systems that are run at FNMOC and that provide worldwide Navy forecasts. NRL-MRY is also the technical direction agent for TESS(3), a minicomputer-based environmental diagnosis/forecast system designed for shipboard use. Advanced technologies in use include satellite meteorology, advanced numerical techniques, and artificial intelligence.

Space Science

NRL is the Navy's main laboratory for conducting basic research and development in the space sciences. The Space Science Division conducts and supports a number of space experiments in the areas of upper atmospheric, solar,

and astronomical research aboard NASA, DoD, and other Government-agency space platforms. Division scientists are involved in major research thrusts that include ultraviolet remote sensing of the upper atmosphere, spectrographic studies of the solar atmosphere, and astronomical radiation ranging from the ultraviolet through cosmic rays. In support of this work, the division maintains facilities to design, construct, assemble, and calibrate space experiments. A network of computers, workstations, image-processing hardware, and special processors are used to analyze and interpret space data. Among the division's space science data acquisition and analysis efforts are the following:

- mission operations and data analyses of the NRL's Oriented Scintillation Spectrometer Experiment (OSSE) for NASA's Compton Observatory;
- observation of the Sun's interaction with the upper-Earth atmosphere through the Solar Ultraviolet Spectral Irradiance Monitor (SUSIM) experiment in support of NASA's Upper Atmosphere Research Satellite (UARS) and Atmospheric Laboratory for Application and Science (ATLAS) missions; and
- observation of selected celestial targets in the ultraviolet and X-ray bands by three Advanced Research and Geophysical Observation Satellite (ARGOS) experiments—Global Imaging of the Ionosphere (GIMI), High-Resolution Atmospheric and Auroral Spectroscopy (HIRAAS), and Unconventional Stellar Aspect (USA).

The Space Science Division also operates the BMDO's Background Data Center (BDC)—a center of expertise for backgrounds phenomenology data that provide archival, management, and analysis services, and value-added products for preserving and applying data collected by satellite experimental programs. The BDC's architecture consists of fully functional classified and unclassified processing environments that include operational data processing systems and science analysis stations. Automatic data processing equipment includes Digital Equipment Corporation (DEC) VMS and Unix platforms, Sun workstations, Silicon Graphics workstations, Macintoshes, and IBM-compatible personal computers. These platforms support a wide variety of standard scientific analyses software packages, including Ingres RDBMS, IRAF, IDL, KHOROS, and the MOSAIC/Worldwide Web. Unclassified processing environments are linked to scientists throughout the world via the Internet. Data files can be received by or sent from the BDC by using FTP or other protocol.

Space Technology

In its role as a center of excellence for space systems research, the Naval Center for Space Technology (NCST) designs, builds, analyzes, tests, and operates spacecraft, as well as identifies and conducts promising research to improve spacecraft and their support systems. NCST facilities that support this work include large and small anechoic radio frequency chambers, clean rooms, shock and vibration facilities, an acoustic reverberation chamber, large and small thermal/vacuum test chambers, control system interaction laboratory, satellite command and control ground stations, fuels test facility, and modal analysis test facilities. NCST has a facility for long-term testing of satellite clock time/frequency standards under thermal/vacuum conditions linked to the Naval Observatory; a 5-m optical bench laser laboratory; and a hologram research laboratory to conduct research in support of the development of space systems.

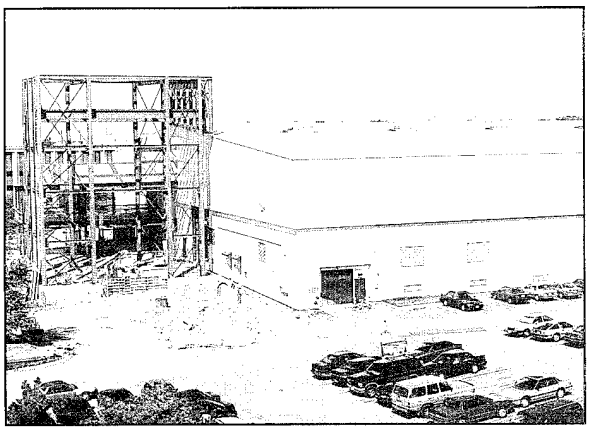

Building A59 is being readied for future NCST occupancy.

Research Support Facilities

Technical Information Services

The Ruth H. Hooker Research Library and Technical Information Center contains more than one million items, including current journals. Its collections can be searched by computer-based catalogs. The Library also provides interlibrary loans, on-line literature searches, access to CD-ROM databases, loans of microcomputer software and laptops, and a full range of reference services, including assistance in selecting and using microcomputer software. Library resources that include an online catalog, a number of CD-ROM databases, and INTERNET can be accessed from offices and laboratories through the InfoNet campus-wide information system. A networked document dissemination through TORPEDO combines full text search and on-line display and priority of selected journal and report page images.

Publication services include writing, editing, composition, phototypesetting, and publications consultation. The primary focus is on using computer-assisted publishing technology to produce scientific and technical information containing complex artwork, equations, and tabular material.

The research conducted at NRL requires a diversity of graphic support such as technical and scientific illustrations, computer graphics, design services, photographic composites, calligraphy, display panels, sign making, and framing. A high-end workstation provides and delivers a new level of electronic airbrushing and photographic retouching.

Photographic services include high-speed motion picture, video, and still-camera coverage for data documentation both at NRL and in the field. A photographic laboratory offers custom processing and printing of black and white and color films. Photographic images can also be captured with state-of-the-art digital cameras and still video. Video services include producing video reports of scientific and technical programs. A video studio and editing facility with 3/4 in. and VHS editing equipment are available to support video production.

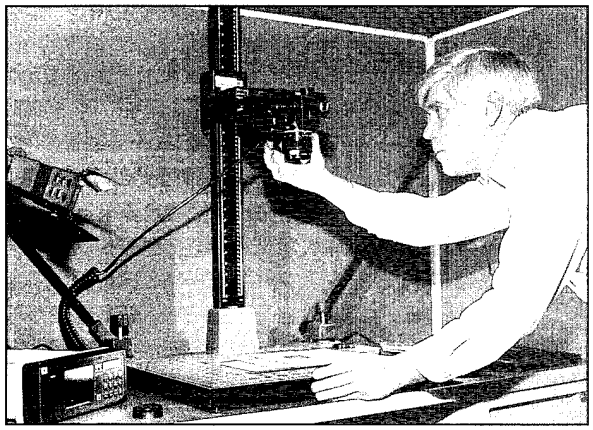

A photographer demonstrates the Technical Information Division's digital camera that can capture images as a digital data file.

The Electronic Imaging Center offers high-quality output from computer-generated files in PostScript, PICT, TIFF, and DICOMED DDC formats. The Imaginator film recorder produces high-resolution 35-mm slides, viewgraphs, and negatives. Photographic quality color prints and viewgraphs are available from the Kodak XL7700. The Canon CLC500 scans color photographs to a Macintosh or PC disk. The Linotron Imagesetter produces gray-scale prints and transparencies at 1293 dpi.

Center for Computational Science

The Center for Computational Science (CCS) conducts research and development to further the advancement of computing and communications systems to solve Navy problems. Promising technologies are transitioned to production systems. The CCS operates and maintains computer systems and networks that provide support for NRL, Navy, and DoD research. The CCS features two Connection Machines (massively parallel computer systems), a 16-K processor CM200, and a 256-processor CM-5E with 32 Gigabytes of memory and a 6 Terabyte Convex 3220 E-Mass D2 tape storage system. The CCS operates high-performance network testbeds, including an ATM/SONET experimental wide-area network. These leading-edge systems and networks are being investigated and developed by the CCS.

The CCS also manages and operates production computer systems and networks. A Cray Y-MP EL provides support for vector computing. The CCS supplies lab-wide data storage support with NRL's File Server/Archiver (FS/A) system. The FS/A provides 69 Gigabytes of online storage and 3 Terabytes of nearline storage, featuring advanced robotics from Storage Technology in an automated tape cartridge system.

The CCS Scientific Visualization Lab functions as an information center, video production unit, and training center for the latest tools in scientific visualization. By using powerful workstations, graphics workstations, and a networked digital video editor, researchers can conveniently turn the results of their computations into color prints, 35-mm slides, or animations on video tape. The Scientific Visualization Lab also provides assistance and training in workstation system administration and clustered workstation programming.

The CCS facilities are accessed through NRL's local area network, NICEnet, which includes a new local FDDI network. NICEnet provides external connections to network and computer systems worldwide. Dial-in modem access is also available.

FIELD STATIONS

NRL has acquired or made arrangements over the years to use a number of major sites and facilities for research. The largest facility is located at the Stennis Space Center (NRL-SSC) in Bay St. Louis, Mississippi. Others include a facility at the Naval Postgraduate School in Monterey, California (NRL-MRY), the Chesapeake Bay Detachment (CBD) in Maryland, and the Underwater Sound Reference Detachment (USRD) in Orlando, Florida. Additional sites are located in Maryland, Virginia, Alabama, and Florida.

Flight Support Detachment (NRL FSD)

Located aboard the Patuxent River Naval Air Station in Lexington Park, Maryland, NRL FSD operates and maintains five uniquely configured P-3 Orion turboprop aircraft as airborne research platforms. FSD provides these airborne platforms for worldwide operations in support of scientific research. In FY 94, FSD was involved in various programs such as Project Birdseye, involving hydroacoustic research; RASTER-J, a multisensor ground environmental survey suite; and Integrated Electronic Warfare System (IEWS), evaluating the performance of various shipboard electronics. Additionally, Spaceborne Imaging Radar C (Project SIR-C) operated in conjunction with NASA's Space Shuttle programs to verify Earth surface mapping. These aircraft are the sole airborne platforms for numerous projects such as bathymetry, electronic countermeasures, gravity mapping, and radar development research. The detachment has a flawless safety record, having amassed over 49,000 hours of accident-free flying over a 31-year period.

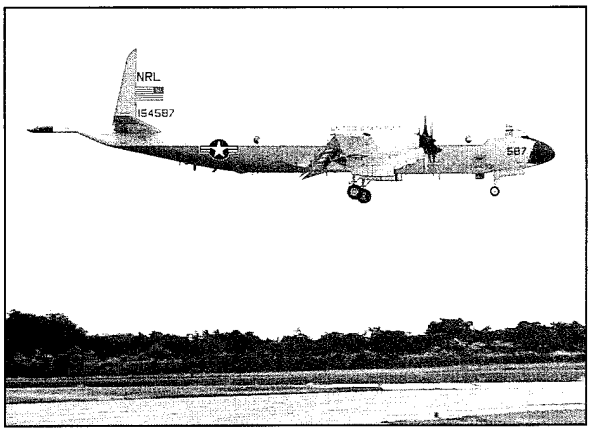

One of the two newly acquired Flight Support Detachment aircraft, 154587, returns from a mission at Patuxent River, Maryland.

Chesapeake Bay Detachment (CBD)

CBD occupies a 168-acre site near Chesapeake Beach, Maryland, and provides facilities and support services for research in radar, electronic warfare, optical devices, materials, communications, and fire research. Because of its location high above the Chesapeake Bay on the western shore, unique experiments can be performed in conjunction with the Tilghman Island site 16 km across the bay from CBD. Some of these experiments include low clutter and generally low-background radar measurements. By

using CBD's support vessels, experiments are performed that involve dispensing chaff over water and radar target characterizations of aircraft and ships. Basic research is also conducted in radar antenna properties, testing of radar remote-sensing concepts, use of radar to sensor ocean waves, and laser propagation. CBD also hosts facilities of the Navy Technology Center for Safety and Survivability, which conducts fire research on simulated carrier, surface, and submarine platforms.

Underwater Sound Reference Detachment (USRD)

Located at Orlando, Florida, USRD functions as a link in the traceability of underwater sound measurements to the National Institute of Standards and Technology and also performs R&D for sonar transducers and related acoustic materials. Its semitropical climate and clear, quiet lakes (nearly circular and 11-m deep) are distinct assets to its research and development on sonar transducers and underwater reference standards and to its improvement of techniques to calibrate, test, and evaluate underwater acoustic devices. USRD has two large, high-pressure tanks for simulating ocean depths to approximately 700 m and 2100 m. Smaller pressure tanks simulate depths to approximately 7000 m. A spring-fed lake, located in a remote area about 40 miles north of USRD (the Leesburg Facility), provides a natural tank for water depths to 52 m, with an ambient noise level 10 dB below that for sea-state zero; larger objects can be calibrated here. A conical shock tube (15-cm muzzle) simulates 60 lb of high explosive at a range of 20 ft for shock testing small sonar transducers. The detachment provides acoustic equipment and calibration services not only to hundreds of Navy activities and their contractors but also to private firms and universities not engaged in DoD contracts.

Marine Corrosion Test Facility

Located on Fleming Key at Key West, Florida, this facility offers an ocean-air environment and clear, unpolluted, flowing seawater

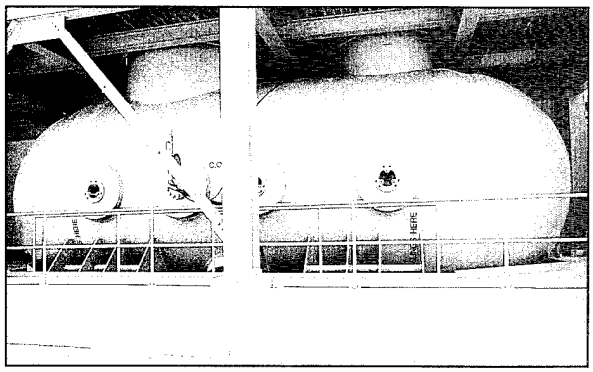

USRD's newest acoustic measurement tank is capable of testing transducers or materials to 3000 psi at temperatures from 2° to 40°C.

for studies of environmental effects on materials. Equipment is available for experiments involving weathering, general corrosion, fouling, and electrochemical phenomena, as well as coatings, cathodic protection devices, and other means to combat environmental degradation.

Naval Research Laboratory-Stennis Space Center (NRL-SSC)

NRL-SSC, a tenant activity at NASA's Stennis Space Center (SSC) is located in the southwest corner of Mississippi, about 50 miles northeast of New Orleans, Louisiana, and 20 miles from the Mississippi Gulf Coast. SSC encompasses over 200 square miles of land area, including a perimeter buffer zone to insulate surrounding civilian communities from the noise of rocket engine testing by NASA. Other Navy tenants at SSC include the Commander, Naval Meteorology and Oceanography Command and the Naval Oceanographic Office, who are major operational users of the oceanographic and atmospheric research and development performed by NRL. The Naval Oceanographic Office provides access for NRL researchers to one of the Navy's largest supercomputers. This unique concentration of operational and research oceanographers makes SSC the center of naval oceanography and the largest such grouping in the Western world.

NRL-SSC provides administrative and business operations support for NRL's Center for

A new building was dedicated at the Stennis Space Center in the fall of 1993. The new building houses research facilities and the Systems Support Requirements and Public Affairs Offices.

Environmental Acoustics, Remote Sensing Applications Branch, Oceanography Division, and Marine Geosciences Division. NRL-SSC occupies over 200,000 square feet of research, computation, laboratory, administrative, and warehouse space, and other facilities at SSC. Facilities include a number of large antennas to receive available oceanographic and meteorological satellite data, a Magnetic Observatory building constructed of nonferrous materials in an electromagnetically quiet area of SSC, a Pattern Analysis Laboratory, a Map Data Formatting Facility, a water-wave channel, and numerous laboratories for acoustic and oceanographic computation, instrumentation, analysis, and testing. Special areas are available for constructing, staging, refurbishing, and storing seagoing equipment.

Marine Meteorology Division Monterey, California (NRL-MRY)

Located in Monterey, California, as a tenant activity of the Naval Postgraduate School (NPS), this facility is collocated with the Fleet Numerical Meteorology and Oceanography Center (FNMOC) to support development and upgrades of numerical atmospheric forecast systems and related user products. NRL-MRY's mission has broadened considerably to include basic research and support to other customers. Collocation with FNMOC allows NRL-MRY access to the Navy's largest vector supercomputer mainframe and workstation resources. This access provides real time as well as archived global atmospheric and oceanographic databases for research on-site and at other NRL locations. Interfaces to the Defense Research and Engineering Network through FNMOC and Defense Simulation Internet at NPS have been established.

NRL-MRY's experience extends to prototype regional and shipboard atmospheric prediction systems. A third generation Navy system, the Tactical Environmental Support System (TESS(3)), developed for SPAWAR, is installed and has undergone various upgrades on-site to provide networking capabilities in line with the Copernicus architecture and remote workstation access. TESS(3) is functioning as an R&D testbed for new tactical/environmental decision aids (TDAs/EDAs), object-oriented databases, and Motif/X windows user interfaces. State-of-the-art graphics workstations (SGIs), network fileservers (Suns), and TAC 3 (HP) systems have been acquired for use by researchers. Environmental components of future systems are being developed within a system rooted in commercially available distributed database management software. This system, the Naval Environmental Operational Nowcasting System (NEONS), creates an environment that allows new products for weather and ocean forecasters to be developed by blending satellite and conventional data. Both orbiting and geostationary data receivers are located at NRL-MRY.

Other Sites

Some field sites have been chosen primarily because they provide favorable conditions to operate specific antennas and electronic subsystems and are close to NRL's main site. Maryland Point, south of NRL, operates two radio telescopes (25.6 and 26 m in diameter) for radio astronomy research. Pomonkey, a field site south of NRL, has a free-space antenna range to develop and test a variety of antennas. The antenna model measurement range in Brandywine, Maryland, has a 4.6-m diameter turntable in the center of a 305-m diameter ground plane

for conducting measurements on scale-model shipboard and other antenna designs. A site on the cliffs overlooking the Chesapeake Bay provides an over-the-water range of approximately 10 miles to Tilghman Island.

Midway Research Center

The Midway Research Center (MRC) is located on a 158-acre site in Stafford County, Virginia. Located adjacent to the Quantico Marine Corps' Combat Development Command, the MRC has 10,000 square feet of operations and administration area and three precision 18.5-m diameter parabolic antennas housed in 100-ft radomes. The MRC, under the auspices of the Naval Center for Space Technology, provides NRL with state-of-the-art facilities dedicated solely to space-related applications in Naval communications, navigation, and basic research.

Research Platforms

Mobile research platforms contribute greatly to NRL's research. These include five P-3 Orion turboprop aircraft and one ship, the ex-USS *Shadwell* (LSD-15) birthed in Mobile Bay, Alabama. The ex-*Shadwell* is used for research on fire suppression techniques onboard ship.

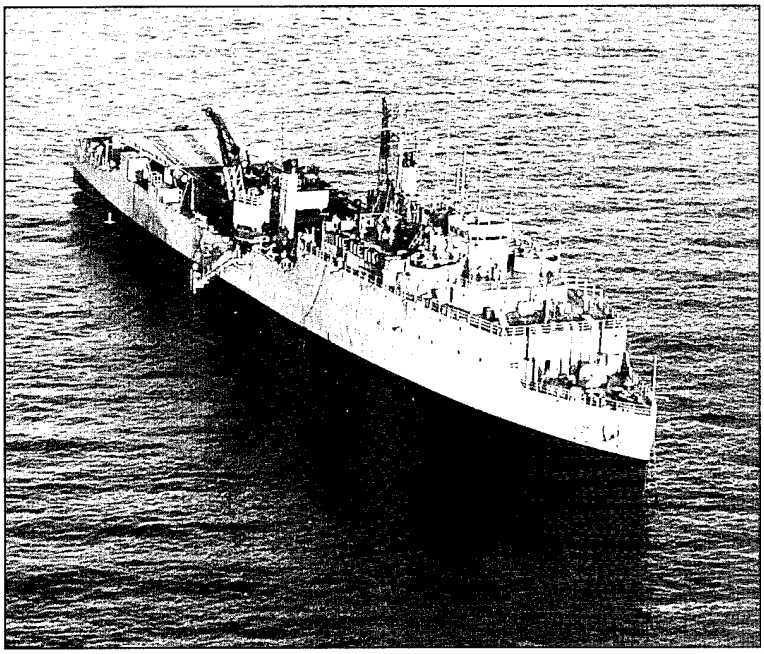

NRL's fire research ship, the ex-USS *Shadwell* (LSD-15).

NRL in the Future

To continue its growth and provide preeminent research for tomorrow's Navy, NRL must maintain and upgrade its scientific and technological facilities at the forefront. Its physical plant to house these facilities must also be adequate. NRL has embarked on a Corporate Facilities Investment Plan to renew its physical plant. This plan and future facility plans are described below.

THE CORPORATE FACILITIES INVESTMENT PLAN (CFIP)

The CFIP is a financial spending plan to provide modern research facilities at NRL by the year 2000. The plan calls for both Congressional and Laboratory investment and is updated and altered as changes occur in scientific emphasis and Congressional attitude. Over the past several years, Congressionally approved military construction (MILCON) funds were used to construct the new Electro-Optics Laboratory. In addition, construction has begun on a high bay satellite assembly building for the Spacecraft Engineering Department of the Naval Center for Space Technology. This is the first step in a proposed MILCON program that will house a large portion of the Center in a single location.

Another initiative that will require Congressional support is the proposed Nanoscience Research building. This facility will serve as the focal point for nanoscience research involving three NRL divisions.

Complementing the MILCON construction program, the Laboratory has also embarked on an ambitious renovation effort called the Laboratory Modernization Plan. Using internally generated funds, existing buildings are being renovated to bring them up to the most modern standards of contemporary laboratory design. The renovation of Building 30 for the Center for Bio/Molecular Engineering has been completed as has the renovation of Building 3 for the Materials Science and Technology Division. An in-house renovation project has provided a new facility for the Remote Sensing Division. This project colocates a division which was previously scattered among four buildings into a single location.

The complete renovation of Building 12 has begun, and planning has started for the renovation of Building 1. These two buildings will house the Information Technology Division when they are finished. Other projects that are either in progress or planned for the near future include renovations for the Plasma Physics Division, the Acoustics Division, the Center for Computational Science, and the Marine Geosciences Division.

Long-Line Hydrophone Calibrator Facility

A major facility for the acoustic evaluation of towed arrays and other line arrays of hydrophones will be operational at the Underwater Sound Reference Detachment (USRD) in 1995. This facility will contain a 57-m long, water-filled pipe that can be temperature and pressure controlled to simulate ocean environmental conditions. Piezoceramic projectors distributed in the pipe will ensonify an enclosed line array or module up to 48-m long with well-controlled sound fields that provide full through-the-beamformer calibration. The calibrator will be housed in a new building located at the USRD Leesburg Facility.

Plasma Physics

A major 2-kJ KrF-laser facility will be established in the Plasma Physics Division by the end of FY 95. This facility is being initiated to provide intense radiation for studying inertial confinement fusion target heating at short wavelengths. A large-volume (2-m diameter by 5-m long) space chamber facility is operational to conduct space plasma physics research in the laboratory. A uniform axial magnetic field up to 1 kG and adjustable plasma density

and temperature allow great flexibility to study laboratory simulation of space phenomena under controlled conditions.

Electronics Science and Technology

Important division emphasis is focused on the continual upgrading of the Nanoelectronics Processing Facility (NPF) and expanding activities in the nanoelectronics, heterostructures, and vacuum electronics science and technology programs. A new penthouse processing facility in Building 208 will open in FY 95. It is dedicated to processing III-V semiconductor devices in addition to serving the hands-on fabrication needs of individual scientists within the division. The Laboratory for Advanced Material Synthesis facility will continue to upgrade its organometallic vapor phase epitaxy equipment to meet program needs for thin-film semiconductors. Upgrades include safer and more environmentally benign processing and waste disposal techniques. The EPICENTER (a joint activity of the Electronic Science and Technology, Materials Science and Technology, and Chemistry Divisions) will continue to provide new insight into epitaxial semiconductor growth processes. Knowledge of these growth processes will be used for improved control of film properties for use in the electronic devices of tomorrow.

Center for Bio/Molecular Science and Engineering

In January 1993, renovations began of Building 30 to accommodate the growing and diverse research programs of the Center for Bio/Molecular Science and Engineering. When completed, the center will have over 28,000 square feet of modern laboratory and office space. These facilities will include laboratories for biochemistry, organic synthesis, surface chemistry, and spectroscopy. Specialized facilities will include controlled-environment rooms, an advanced computer-graphics laboratory, electron and scanning microprobe laboratories, and a submicron and nanostructure fabrication and characterization laboratory. Ample space will be provided in which the center's interdisciplinary staff can meet and discuss joint projects.

Ocean Acoustics Research Laboratory

NRL's Ocean Acoustics Research Laboratory (MILCON Project P-006), a 62,000-square foot building, will place 90% of NRL-SSC in one closely located area. This project will provide secure laboratory and computing facilities for research and development in underwater acoustics and for mapping, charting, and geodesy. Completion and occupancy should occur in FY 96.

Vacuum Ultraviolet Space Instrument Test Facility

The Space Science Division facilities include a state-of-the-art, ultraclean solar instrument test facility in Building A-13 on the main NRL campus. The new facility is designed to satisfy the rigorous contamination requirements of state-of-the-art solar spaceflight instruments. The facility has a 400-square foot Class 10 clean room and a large Solar Coronagraph Optical Test Chamber (SCOTCH). This completely dry-pumped, 550-cubic foot vacuum chamber is maintained at synchrotron levels of cleanliness. Solar instrumentation up to 1 m in diameter and 5 m in length may be physically accommodated in the chamber. The instrument optical performance is probed and calibrated with a variety of visible and XUV sources mounted on the chamber's 11-m beamline. The optical testing and characterization of the Large-Angle Spectrometric Coronagraph (LASCO) instrument for the European Space Agency's Solar Heliospheric Observatory satellite was conducted in this chamber. Coronagraph stray-light characterization was carried out by mounting a set of baffles in the main beamline, illuminating the instrument with a simulated solar beam, and measuring the residual radiation. A stray light background measurement of 10^{-12} was successfully measured in the LASCO C3 channel. Coronagraph calibration was carried out by installing back-illuminated, calibrated opals in front of the instrument entrance aperture. Instrument polarization properties were analyzed by using a variety of polarizers installed in a wheel located between the opal and the instrument. The wheel was remotely controlled from outside the chamber. Instrument Mueller matrices were

verified with a 12-in. diameter two-plate partial polarizer. Calibration and focus of XUV solar instrumentation is accomplished by exposing the instrument to an XUV windowless collimator at the end of the tank. The facility also has a small thermal bake/vacuum test chamber used for vacuum conditioning and thermal testing of spaceflight components and subassemblies. Both the SCOTCH and the small test chamber are instrumented with temperature-controlled quartz crystal monitors and residual gas analyzers for real-time, quantitative measurements of volatile contamination.

Remote Sensing

The construction of the Navy Prototype Optical Interferometer (NPOI), a major facility for the Remote Sensing Division, began in August 1992 and will be operational in FY 95. The NPOI will make high-angular-resolution optical observations of stars for wide-angle astrometry and fundamental astrophysics. High-resolution measurement of stellar positions provides essential data for Earth rotation and celestial reference frame determinations. This enables the determination of stellar masses. High-resolution imaging of stellar surfaces and near-surface structures provides basic data on stellar structure and activity. When this facility is completed, it will be the most advanced high-resolution-imaging optical interferometer in the world. It will provide astrometric data at the level necessary to meet Navy requirements as set by the U.S. Naval Observatory.

REHABILITATION OF SCIENTIFIC FACILITIES

Specialized facilities are being installed or upgraded in several of the research and support divisions.

Flight Support Detachment

NRL's Flight Support Detachment (FSD) decreased its aircraft complement from six to five platforms. Aircraft number 149670 was placed in "mothballed" status at Arizona's Davis-Monthan Air Force Base. Aircraft 154589 received its final flight certification, and it was fitted with fiber-optic data lines for wing station pods. A specially configured bomb bay pallet will enable the aircraft to mount up to 2000 pounds of equipment with 216 cubic feet of instrument space. Navigation and communication upgrades were installed on aircraft 149674, 153442, 154589, and 158227. Aircraft 227 is also capable of extended range missions due to an added sixth fuel tank. These upgrades and modifications ensure that NRL will have the finest airborne research capabilities well into the next century.

Information Technology

The Information Technology Division continues to upgrade its local area network and research into high-performance network testbeds, including ATM/SONET technology. The 256 processor CM-5E massively parallel computer will be upgraded in FY 95. The upgrade will include the addition of 100 Gigabytes of scalable disk array, 32 additional processor nodes, device/processor expansion cabinets, and an upgraded interprocessor router. An additional scalable massively parallel computer system will be acquired. The new system will allow for continuing research into heterogeneous parallel processing in connection with the existing NRL CM-5E and will provide an alternative globally shared memory programming paradigm. The need for additional facilities to supplement research in virtual environments and Global Grid demonstrations will lead to gradual development of a demonstration/VR and conference center in Building 34. An upgrade for the Human-Computer Interaction Laboratory will integrate and enhance its video and audio presentation and recording capabilities.

Materials Science and Technology

Renovation is in progress for Building 3, which is composed of two of the original five buildings at NRL, to contain modern laboratories for studies of thin-film deposition and characterization, superconducting materials, magnetic materials, and other materials science projects. The new space will feature the most modern molecular beam epitaxy and other materials synthesis and processing equipment, an up-to-date fatigue and fracture laboratory, and state-of-the-art diagnostic equipment, including electron microscopes, spectrometers, and

electron and X-ray diffraction equipment. The renovated building will also contain office and laboratory space for approximately 70 technical personnel.

Plasma Physics

A state-of-the-art short-pulse (< 1 ps) high-intensity (> 1 TW) Table-Top Terawatt (T^3) laser has been procured for a variety of physics studies. The T^3 laser will be integrated into the Pharos III Nd-laser facility to boost its power into the 10 to 100 TW range. This will provide a facility to do fundamental physics experiments in intense laser-plasma interactions and intense laser electron beam interactions.

A low-frequency (300 MHz to 10 GHz), high-power microwave facility that uses a relativistic klystron concept is being upgraded to produce multigigawatt coherent radiation pulses. A new laser facility is also planned. It will use a powerful KrF laser and a target chamber to conduct inertial confinement fusion research.

A new electric mass launcher facility has been established to investigate the evolution of the plasma armature in a high-velocity railgun. This facility is being upgraded to accelerate larger masses (~200 g) by using a 4-m long, 2.5-cm bore railgun powered by a 5 MJ capacitor bank.

Electronics Science and Technology

In a move to further meet existing safety standards, potentially hazardous III-V semiconductor processes and associated chemicals will be moved to the new penthouse facility in Building 208. This facility employs a single-pass air-ventilation system to minimize hazards to personnel.

Remote Sensing

From 1920 through 1990, Building 2 (one of five original buildings at the Laboratory) housed the Engineering Service Division (ESD). ESD is no longer an active division, and renovation of Building 2 to house the Remote Sensing Division is currently in progress and scheduled for completion in 1996. After completion, Building 2 will contain office and laboratory space for approximately 100 personnel of the Remote Sensing Division. Two major laboratories—the Free Surface Hydrodynamics Laboratory and the Optical Calibration Facility—are currently under construction. The Free Surface Hydrodynamics Laboratory will be used to study free-surface turbulence interactions, wave generation phenomena, jet-flow phenomena, vorticity dynamics, and free-surface/surfactant interactions. These studies will help validate numerical and theoretical efforts that are occurring within the Remote Sensing Division. The Optical Calibration Facility will be used for the characterization and calibration of in-water optical instrumentation and aircraft imaging spectrometers. The laboratory will include facilities for spectral radiance and irradiance calibrations relative to National Institute of Science and Technology standards sources and reference radiometers.

Highlights of NRL Research in 1994

MK-92 Radar Improvement

Radar Division

A product improvement system for the MK-92 Mod 2 radar was developed and successfully tested at a land-based test site and on the USS *Copeland*. Because the MK-92 Mode 2 radar has difficulty detecting sea-skimming missiles in clutter, a joint program with NRL, APL, and UNISYS was begun to improve clutter cancellation in multiple interval clutter and automatic tracking with low false track rates in the presence of clutter. Algorithms were developed by NRL (1) to cancel multiple interval clutter, (2) to measure target radial velocity using echoes from targets embedded in clutter obtained from a random pulse repetition frequency coherent sequence of pulses having pulse-to-pulse random phase relationships, and (3) to use the new added radial velocity for rapidly promoting target detections into tracks while maintaining a low false track rate. The model is being moved to production based on the successful sea skimmer intercepts and the number of sister ships that failed without it.

Fiber Bragg Grating Fabrication During Optical Fiber Drawing

Optical Sciences Division

Fabrication of multielement fiber Bragg grating (FBG) strain sensor arrays has been demonstrated during the drawing of an optical fiber from a preform. Since the surface of the fiber, which is exposed to the ultraviolet laser beams that write the grating is pristine, higher laser fluences are possible. Additionally the protective polymer jacket is applied in-line immediately after exposure so that the pristine fiber strength is maintained. FBGs have been fabricated at a sustained rate of approximately 2000 per hour. FBG arrays provide the smart structures community with a powerful means for real-time, absolute, short gage-length measurements of strain throughout extended structures. Applications include air frames, fuel storage tanks, ships hulls, robotics, and space structures.

Phase II MMIC (Microwave Monolithic Integrated Circuit) EW (Electronic Warfare) Receiver

Tactical Electronic Warfare Division

A MMIC/EW triple conversion superheterodyne receiver covering 0.5 to 18 GHz was demonstrated in October 1994. This receiver, while exhibiting superior or equivalent performance characteristics, is 1/22nd the size of its best current equivalent. It is 1/12th the weight, requires 1/3rd the power, and is only 1/6th the cost of the current equivalent receiver. The receiver permits the low cost introduction of EW systems on numerous small craft. It provides for increased capability of aircraft and submarines by permitting remote mounting. The NRL Phase II MMIC/EW receiver can be used on EW and surveillance systems for ship, air, submarine, land, UAV, and national systems to improve the performance of existing systems. It can also be applied to EW countermeasures and radar warning receiver (RWR) system development where size, weight, and cost are critical factors.

High Voltage SiGe Transistors for Microwave Power Applications

Electronics Science and Technology Division

NRL has demonstrated for the first time that high breakdown voltage, high performance microwave transistors can be achieved for the SiGe heterojunction bipolar transistor (HBT) technology. In addition, NRL demonstrated that the breakdown voltage of a SiGe HBT is nearly identical to that of a silicon bipolar transistor with a similar collector design. The performance achieved is a BV_{CBO} of 40 V, f_T of 10 GHz, and f_{max} of 25 GHz. In addition, breakdown of 70 voltages was obtained for an S-band transistor design and 100 V for an L-band transistor design. This is the first demonstration that high breakdown voltages can be achieved for SiGe HBT technology. Previous results reported for SiGe have been only for small signal applications. The advantages of SiGe HBT technology include low base resistance and small base transit time, which provide improved microwave performance. The SiGe technology has the advantage that it can be a lower cost solution for microwave power than III-V or SiC technologies because it builds on the large silicon microelectronics infrastructure. The primary applications for the SiGe microwave power transistor technology is for solid-state microwave power sources for active aperture radars and microwave communication systems.

Liquid Crystal Display Devices from Conducting Polymer Substrates

Center for Bio/Molecular Science and Engineering

A new type of liquid crystal display devices has been developed in which transparent films of a conducting polymer are used as the electrode substrates. This accomplishment constitutes the first operating liquid crystal device using specially developed optically transparent conducting polymer films as substrates. This is different from all existing liquid crystal display devices, which use indium-tin-oxide (ITO) coated glass or plastic substrates. It also establishes a proof-of-principle for patterning a conducting polymer surface using selective area absorption. Such a display device in which the conducting polymer replaces the ITO-coated glass or plastic has impact in the areas of displays for field applications and heads-up or helmet-mounted displays for virtual-reality applications.

Polar Ozone and Aerosol Measurements (POAM II)

Remote Sensing Division

The Polar Ozone and Aerosol Measurement (POAM II) instrument began operation during FY 94. It measures ozone, aerosols, and several molecular species critical for understanding the ozone chemistry in the polar regions by using solar occultation techniques. The POAM II instrument was launched on the French SPOT 3 satellite; it began its measurements on 16 October 1993. It measures the transmitted solar radiation through the Earth's atmospheric limb during each sunrise and sunset (as seen from the satellite) in nine wavelengths, from the ultraviolet through the near infrared. No other current instrument is capable of providing comparable measurements to POAM's on the polar ozone and its chemistry. In addition to addressing key global change issues, POAM II characterizes the propagation of radiation through the polar stratosphere and upper troposphere, which is critical for predicting the operational performance of many DoD electro-optical systems.

Long Time Period Adjustment of the Large Scale Ocean Climate

Oceanography Division

Research involving satellite data and global ocean models has revealed changes in ocean circulation and climate occurring on decadal scales due to what was once believed to be short anomalous events. The variations forcing on the ocean occur at relatively short time scales, on the order of weeks to a year. The ocean circulation and climate driven by these changes in forcing can take from years to decades to respond at the large scale. The long time period response is provided through Rossby waves. Research work conducted at NRL was the first to reveal Rossby waves produced by extreme climate events such as the 1982-83 El Niño. Model results indicate that the climate variations produced by these waves are very predictable. This research will have a direct impact on understanding oceanic influence on global climate change.

Variability of Coastal Atmospheric Refractivity (VOCAR)

Marine Meteorology Division

For two weeks in the fall of 1993, an intensive observing period of the VOCAR experiment was conducted in the southern California bight from Point Conception to San Diego. Throughout this period, a high resolution version of the Naval Operational Regional Atmospheric Prediction System was run in a data assimilation cycle. VOCAR was designed to observe the mesoscale structure of the atmospheric boundary layer in the bight to accurately characterize the temporal and spatial variability of the microwave refractivity field. Preliminary results have demonstrated a significant impact on atmospheric boundary layer (or the refractions trapping layer) structures by the combination of land/sea difference, coastal terrain, coastal low-level jets, and configuration of the coast lines. The results also showed that the high resolution model is capable of depicting the temporal changes of the refractivity structure. The positive results have led to the development of a new generation of the on-scene shipboard analysis system; its first application demonstration takes place in February 1995.

Technical Accomplishments and Prospects of the LASCO Triple Coronagraph

Space Science Division

In May 1994, NRL delivered the Large Angle Spectrometric Coronagraph (LASCO) instrument to the European Space Agency for integration with the Solar Heliospheric Observatory satellite. The mission is expected to be launched in the fall of 1995. LASCO will obtain the highest quality images to date of the solar corona. The panoramic field of view will allow observations of coronal and the solar wind plasmas from the solar disk into interplanetary space. The spectroscopic measurements obtained will allow temperature, electron density, and magnetic field measurements in various coronal structures using emission line diagnostics. It is anticipated that the first 24 hours of observations with the instrument will produce more high quality observations of the inner corona than have been obtained in a century of eclipse observations.

Deep Space Program Science Experiment, or *Clementine*

Space Systems Development Department

The Deep Space Program Science Experiment (*Clementine*) Program demonstrated newly developed spacecraft hardware and performed a highly successful lunar mapping mission. The program, sponsored by the Ballistic Missile Defense Organization (BMDO), was launched in January 1994. The lunar imaging effort was an outstanding success—a complete imaging of the lunar surface in 11 discrete wavebands with coarse altimetry over most of the lunar surface. The spacecraft also demonstrated use of Spacecraft Command Language for autonomous spacecraft control for an entire 5-hour mapping orbit. The first space application of new hardware and software technologies qualifies them for other military and commercial space applications. *Clementine* images will help resolve a variety of scientific issues, such as the character and evolution of the primitive lunar crust, thermal evolution of the moon and lunar volcanism, and the impact record and redistribution of crustal and mantle materials; this will facilitate man's return to the moon and provide a broader understanding of the nature of our nearest-orbiting neighbor.

Development of Cenosphere Technology for Low Observable Applications

General Science and Technology Directorate

The need to develop low cost, high performance radar-absorbing materials has become increasingly important, and NRL has played a major role in guiding the scientific development of these materials. Early work using cenospheres (silver-coated microballoons developed by Spectro Dynamics from a by-product of coal-fired power plants) for IR and RF applications showed that they exhibited interesting properties in the RF region. NRL has characterized the electromagnetic properties of these cenospheres and has gained insight into how they behave. NRL has also facilitated their use on Navy SEALS' craft and is exploring their use for aircraft applications. Indications are that these or similar materials may form the basis for a new, low cost, low observables treatment for numerous applications.

Automated Consistency Checking of Requirements Specifications

Information Technology Division

Because the earliest errors in software are the most costly to fix, techniques that detect errors in software requirements specifications are especially valuable. At present, checking requirements specifications for consistency errors is done manually. A prototype tool has now been developed and demonstrated that automates this checking process. The tool detects undesirable nondeterminism, omitted cases, undefined variables, and type mismatches. Although the properties that the automated consistency checking test looks for are usually quite simple, the number of times such properties need to be checked in practical requirements specifications can become very large. A software tool that does consistency checking automatically can save reviewers of requirements specifications considerable time and effort. Moreover such tools may be more effective than humans in finding instances of inconsistency. Automated consistence checking of requirements specifications can help drive down software life-cycle costs.

Discrete-Event Dynamic Systems' Modeling Techniques and Voice/Data Integration in Radio Networks

Information Technology Division

The performance evaluation and control of integrated voice/data communication networks are formidable problems because of the difficulty in obtaining exact analytical network models or, in some cases, the complexity of evaluating analytical models that are available; therefore simulation is usually necessary. However conventional simulation techniques can be time-consuming and expensive, especially when evaluating performance for a large number of control policies. The recently developed standard clock (SC) parallel simulation technique is an efficient method to simulate a system's operation, however the basic SC approach is applicable only to systems with exponential interevent times. In this study, the SC method has been extended to permit the modeling of integrated networks. New, efficient techniques have been developed for the optimization and control of integrated voice/data communications networks and other discrete-event dynamic systems. These are based on the use of parallel simulation techniques and ordinal optimization methods that provide an approximate ranking of policies from best to worst in terms of desired performance. Remarkably accurate policy rankings can be obtained, thereby potentially reducing the time needed to determine good control policies by orders of magnitude.

Acoustic Signal Processing Application of Advanced Processor Technology

Information Technology Division

Regional conflicts involving quiet diesel submarines in cluttered shallow water require new concepts in operational ASW. Among these are rapid deployment of arrays in multidimensionally distributed configurations and methods for improved detection and high resolution tracking. These require advanced computationally intensive algorithms to process and correlate high dimensionality data. The Advanced Processing Technology Testbed on the NRL Connection Machine Facility was applied to process and evaluate broadband signal characteristics from shallow water acoustic data involving diesel submarines. Successful split array and interarray correlation results demonstrate exploitability of broadband acoustic signals for detection and localization in shallow water environments. The successful demonstration of commercial high-performance parallel processors for acoustic signal processing opens the door to deploying future advanced acoustic array configurations with massive computational requirements.

Development of a Neutrally Buoyant Capacitive Displacement Sensor

Underwater Sound Reference Detachment

Currently the most common method for measuring the surface vibration of a fluid-loaded structure is through the use of accelerometers mounted on the surface. When this surface consists of a low density compliant material, it is necessary to use small, low mass accelerometers to avoid mass loading of the surface. For high frequency measurements, the low sensitivities are not a problem, and these accelerometers are acceptable. However at low frequencies, where the acceleration is small, the signal-to-noise ratio obtained with the low sensitivity accelerometers is unacceptable. Thus to make

low frequency measurements of the vibration of a submerged compliant surface, scientists have developed a class of neutrally buoyant capacitive displacement sensors. The dynamic mass of these sensors is equal to the mass of the displaced fluid, thus the sensors do not add additional loading to the surface. Since these sensors respond to the displacement of the surface, they are ideally suited for low frequency measurements. This represents a cost savings to the Navy since characterization of panels at lower frequencies previously required the construction of more costly, larger acoustic panels.

Rational Design of Neuroactive Drugs

Laboratory for the Structure of Matter

The opioid receptor endorphin system consists of saturable enantioselective, high affinity μ, δ, and κ opioid receptor types located in well-defined areas of the mammalian central nervous system. This system mediates the analgesic, euphoric, and addictive effects of narcotic drugs and regulates numerous physiological and behavioral functions. Generally the endogenous mammalian opioid peptides and the naturally occurring nonpeptide ligands are not selective at any of the opioid receptors. Hence systematic rational approaches for the design of potent and selective analogs are needed. Early approaches to this problem included imposing conformational restraints of enkephalin analogs. Two highly potent and site-specific peptide antagonists (Tyr-DThur-Gly-Phe-Leu-Thr and Tyr-DPen-Gly-Phe-DPen) were developed, and their structures were determined at NRL. Incorporation of topographical restraints into the structure has become an important tool, and we have determined the structure of the very highly site-specific antagonist Try-Tic-Phe-Phe. Structural characterization of a series of potent morphinoid agonists and antagonists has also been completed. These structural parameters, along with those from many other studies, contribute to the basis for modeling of receptor sites. Structural information for these materials may be obtained from modeling, NMR, and X-ray diffraction. The solid-state X-ray structures determined at NRL give a clear picture of at least one low-energy conformer for these important opioids, which may lead to a better understanding of their bioactive conformation.

Phthalonitrile Composites

Chemistry Division

Strong, moisture and fire resistant organic polymeric composites are needed for use in aircraft, ship, submarine, and rocket applications. Thus polymeric composites are seeing increased use in primary and secondary components for aerospace and marine applications due to their high specific strength and stiffness, compared to metals. This composite project is aimed at developing and exploiting advanced flame-resistant composite systems based on easily processable NRL-developed high temperature phthalonitrile resin matrix materials having thermal and oxidative properties similar to carbon. These resins display outstanding flame resistance and retention of superior mechanical properties relative to current state-of-the-art thermosetting materials after extended aging of the resin at 315°C in air. The curing, processing, and fabricating parameters are being derived and the mechanical properties of fiber-reinforced composites determined. The phthalonitrile technology is being readied for transition from an applied Navy program to industry.

Power Applications of Superconductivity

Materials Science and Technology Division

The development of high-temperature superconductor (HTS) wire has been a difficult process to accomplish because the material is extremely brittle and cannot easily be dawn into fine wire. Also it must be oriented in a specific crystallographic manner uniformly throughout the kilometer lengths of wire needed to wind magnets. High formation temperatures and the complex, multicomponent chemistry make processing a very exacting procedure. The objective of this joint program with the Naval Surface Warfare Center/Annapolis Detachment, universities, and industry is to demonstrate the utility of high-temperature superconductors in the form of wires and tapes for making magnets of sufficient performance for use in superconducting motors. An existing homopolar motor that uses low-temperature superconducting wire will be used as the test bed for the HTS magnets. This work will include the testing of conductors and magnets supplied by industry, development of improved manufacturing methods for the conductors, and development of improved processing procedures. There are many applications for the HTS magnets—for naval electric propulsion systems, in mine-sweeping applications, and magnetic separation systems for environmental control, down leads for large energy storage systems, and magnets for electrical power conditioning.

Simulation of Torpedo Launch Dynamics

Laboratory for Computation Physics and Fluid Dynamics

An important class of complex engineering problems can be accurately represented by the incompressible Naiver-Stokes equations. Typical problems are unsteady aerodynamic flows and turbulent separating flows over complex vehicles such as submarines. The flow field generated during a torpedo launch from a submarine is quite complex. The complexities arise due to the flow outside the submarine entering the cavity of the torpedo bay during the initial stages of the launch, the induced flow field due to the relative motion of the bodies present, and the effect of the water jet employed to propel the torpedo. Recent advances in computer speed and memory allow the simulation of these flows about complex geometries such as those of the fully appended submarine by using an unstructured grid approach. This offers the greatest flexibility with the fewest degrees of freedom. By using high performance parallel computing, a new capability for computing launch dynamics and the trajectory of underwater weapons and vehicles has been developed and is of interest to the Navy.

Negative Electron Affinity and Low Work Function Surface: Cesium on Oxygenated Diamond

Condensed Matter and Radiation Sciences Division

Electron emission from surfaces is an important process for a variety of devices—from cold cathodes to optoelectronic components. Normal semiconductors have a positive electron affinity so that even if carriers are excited into the conduction band, strong applied fields may be necessary to obtain electron emission. Recent developments in the science and technology of wide bandgap semiconductors suggest the possibility that they might be made to exhibit intrinsic negative electron affinity (NEA) behavior and promote more efficient emission or new applications. An oxygenated C(100)

surface cesiated at the half-monolayer level has been studied with self-consistent electronic structure methods. Cesiation shifts the 2.45 eV positive electron affinity oxygenated surface to a surface with the bulk diamond conduction band 0.85 eV above the vacuum level, creating an NEA. The resulting surface is metallic due to Cs-O-C surface states and thereby also provides a low work function of 1.25 eV. The combination of the NEA bulk material with a low work function surface promotes noncharging electron emission that makes this type of surface promising for diamond-based (and other wide bandgap semiconductors-based) optoelectronic devices.

Eruptive Solar Events and Their Terrestrial Influence

Plasma Physics Division

The mechanisms causing eruptive solar phenomenon have been a central problem in solar physics. A theoretical and simulation program has been developed to investigate the eruption and subsequent propagation through interplanetary space of magnetized solar coronal structures. A new mechanism responsible for a class of eruptive solar events has been identified, enabling the calculation of dynamical behavior of erupting solar structures. The initial results are consistent with observed eruptions of filaments at the Sun. The predicted plasma structures at one astronomical unit and beyond are in good agreement with in situ measurements of physical quantities such as size, speed relative to the ambient solar wind, and magnetic field profiles. By using the calculated magnetic field, the response of the Earth's magnetosphere has been studied using a magnetohydrodynamic model. These accomplishments represent the first successful model of the coupling of the Sun and the Earth via plasma structures ejected by the Sun. Understanding the physical processes responsible for the eruption and propagation of solar plasma structures is a necessary scientific component of any space weather forecasting system that can serve DoD and non-DoD activities.

Tactical Oceanography Simulation Laboratory

Acoustics Division

Distributed simulations are accepted as the most efficient, comprehensive, and cost-effective methods of assessing environmentally sensitive sensors, weapons, and systems in variable environments. The Tactical Oceanographic Simulation Laboratory (TOSL), with its progressive architecture, draws together models, databases, system simulation algorithms, and graphic analysis tools to address current and conceptual performance questions in a simulated environment. TOSL simulates complex undersea warfare scenarios in realistic and marginal sea environments. An overall system architecture and individual software tool design have been created that are extensible and adaptable to existing and conceptual issues. This design makes software reuse easy, affordable, and allows other customers to leverage existing software development into their projects. Also the modular design of TOSL allows for easy upgrades of components whether they be databases, models, or graphics.

Signal Detection Using Fluctuation-based Processing

Acoustics Division

Fluctuations are viewed as detrimental to the signal detection process in most propagation media. A primary objective of many signal processors is to suppress the fluctuations to improve the detection. Therefore a signal processor that capitalizes on the fluctuations to improve the signal-to-noise (S/N) ratio can be considered to be tapping a new source of gain. A processing scheme that takes advantage of signal fluctuations to produce enhancements in S/N ratio has been developed. Applications have

already demonstrated that the method enables the detection of submerged acoustic sources that were too weak (relative to noise) to be detected by conventional methods and increases spacial and temporal resolution. The technique is not limited to acoustics. Other potential applications include reduction of jamming in radar and improved optical resolution in astronomy.

Wave Packet Decomposition Techniques

Acoustics Division

The active classification of targets under low Doppler conditions is problematic. The echo from any target includes contributions from several principle physical components and can, in principle, be broken down into a sum of the contributions from each of these components. The techniques for decomposing signals into distinct physical contributions have been developed and successfully demonstrated with experimental data from a finite, ribbed cylindrical shell. Unique scattering features associated with these targets occur in predictable frequency bands, and the development and demonstration of techniques that can decompose received echoes into principle components or search for specific components in an echo will provide the fundamental underpinning for the development of low Doppler active classification algorithms.

Object-Oriented Digital Nautical Chart Prototype

Marine Geosciences Division

Scientists developed and demonstrated the first object-oriented digital nautical chart database. This database is 12 times faster than standard relational techniques used in current Defense Mapping Agency vector product format databases. Additionally, feature and attribute information can be easily updated by producer or user, thereby improving database currency and accuracy. The new approach can be readily extended to accommodate all vector mapping databases produced by the Defense Mapping Agency for DoD and commercial use. The digital nautical chart will replace paper charts on most Navy ships within the next few years. This research has significant DoD impact by providing rapid updating capability for vector databases, faster access time at the producer and user levels, flexibility to deliver information to users in either the object-oriented or vector product format structure, and advanced query support, allowing users to ask complex questions of vector mapping databases.

AOPP: An Analytic Orbit Propagation Program

Spacecraft Engineering Department

An analytic orbit prediction program that includes perturbations to Keplerian motion from the Earth's potential and the third bodies of the Moon and Sun has been developed. The theory includes more perturbations and incorporates analytic transformations to a higher order than the existing operational program, PPT2, which it is intended to replace at the Naval Space Command. The theory is developed in the mathematics of Lie Transformations and relies heavily on computerized algebraic manipulation to effect the mathematical development. This development is expected to improve accuracy and reduce the number of objects that require special processing caused by the inaccuracy of the current propagator.

Meet the Researchers

NRL is proud of its numerous researchers. Every year, we feature some of these people so that you may get to know them and, as a result, understand how their diverse backgrounds come together to keep the Laboratory on the horizon of discovery.

Dr. G. Charmaine Gilbreath, head of the Electro-optics Technology Section in the Naval Center for Space Technology, conducts and manages research to develop technologies pertinent to free-space optical communications for satellite-based applications. Her areas of research expertise include photorefractive research for optical wavefront manipulation and laser ranging for high-precision position estimation of satellites and other spaceborne objects.

"NRL offers enormous opportunity for the development of vision and investigation into new technologies to potentially make that vision real. I have been fortunate to be able to investigate fundamental questions as they relate to real-world problems in satellite technology. There is simply no feeling like the one you have when your work puts you at the edge of knowledge. It is especially gratifying when you know that what you are investigating could translate into an application that might really make a difference."

Dr. Warren W. Schultz is the program manager for Biotechnology and Chemical and Biological Warfare Defense within the Materials Science and Component Technology Directorate and the Environmental Quality R & D Manager for the Laboratory. He develops, markets, and executes programs with biological and chemical approaches and develops new materials and fieldable products for military and civilian uses. Besides having oversight of the Laboratory's environmental R & D efforts, he is the principal investigator on a large, military jet-fuel bioremediation project, which has collaborators from the EPA, academia, small industry, and the large-scale end-user.

"I have the greatest and most rewarding job in the Navy. This is made possible because of the very nature of NRL where the heartbeat of scientific achievement and technological accomplishment is exceptional human resources. This highly interdisciplinary body of talent, which is unsurpassed anywhere in the world, works together as a family, continually proving the critical importance of having a tech base of unparalleled strength to produce solutions and products for military problems and needs. We make the difference in maintaining Fleet and general superiority as well as helping to maintain a strong civilian economy. I am fortunate to be a part of this continuing excellence."

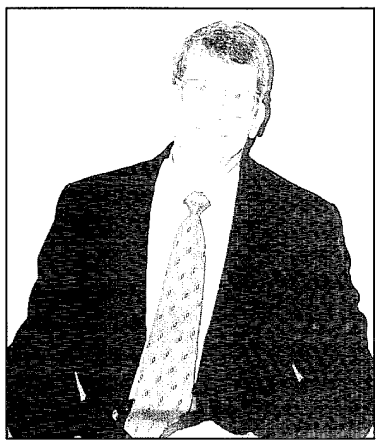

Dr. Herbert C. Eppert, Jr. is superintendent of the Marine Geosciences Division at NRL-Stennis Space Center, Mississippi, and Washington, D.C. The division conducts a multidisciplinary scientific and technological program to provide increased knowledge of the geology of the oceans through a better understanding of the processes that are forming and continually modifying the upper crust; these include the overlying sediments and the resulting geophysical, geomorphologic, and geoacoustic signatures observed today. The goals of the division are to quantify the effects of the seafloor on naval systems and operations and develop advanced seafloor mapping techniques, seafloor models, and digital database concepts to improve the navy's mapping, charting, and geodesy capability.

"I find these to be exciting times to be a part of NRL. The shift of naval interest to littoral regions and increased national concern for environmental quality are providing our division with new opportunities and challenges. To meet these, I have been working with the division to initiate new research directions focusing on hydrodynamic and sedimentary processes in the coastal regions, genesis and distribution of gaseous sediments, and the role of marine sediments in isolating and dispersing contaminants in the ocean. To support these new research directions, we are setting up a Center for Geomaterials Research, which will take advantage of the unique scientists and equipment capabilities in the division."

Ms. Cindy Hartman is NRL's Supply Officer. The Supply Division provides NRL and its field activities with small-purchasing and supply management services. In administering and directing these services, the division continually endeavors to meet the challenging demands of the research community.

"In the ever-changing world of research and development, it is a challenging and rewarding experience to provide support to NRL's scientific and technical community. An unrestricted level of interaction between the researchers and support personnel has developed into a successful partnership. We look forward to continually providing support to a research community that is in the forefront of discovery and achievement."

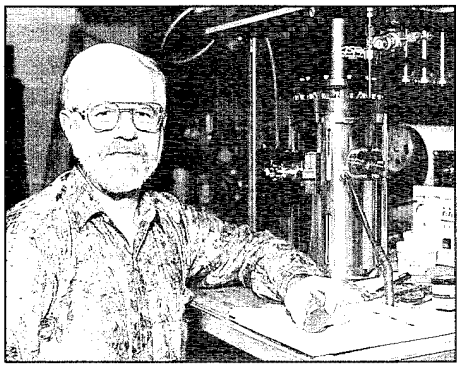

Dr. James E. Butler is a research chemist and head of the Gas/Surface Dynamics Section in the Chemistry Division. He conducts research on the chemical processes that occur at surfaces relevant to advanced materials and structures important to the Navy, DoD, and industrial partners. Through the use of lasers, optical diagnostics, and ultrahigh vacuum surface science techniques, his group studies the chemical vapor deposition or plasma etching of advance materials like diamond, SiC, BN, AlN, GaAS, and Si. Dr. Butler is a leading authority on chemical vapor deposition processes, particularly for diamond films. He has established a Chemical Vapor Processing Facility at NRL with unique capabilities that have attracted major industrial partners for the development of technologies important to the Navy and industry.

"NRL is a fertile environment where the researcher has access to a large and diverse array of colleagues in many different fields, as well as the physical resources of a well-established institution. This encourages many cross-disciplinary efforts and discoveries, as recently exemplified by NRL's contributions in the development of the science and technology of growing diamond films from gases. I enjoy the ability to work on fundamental research issues and projects where my efforts impact DoD and society in general."

Color Presentation

For visual interest, we present some of NRL's latest scientific achievements.

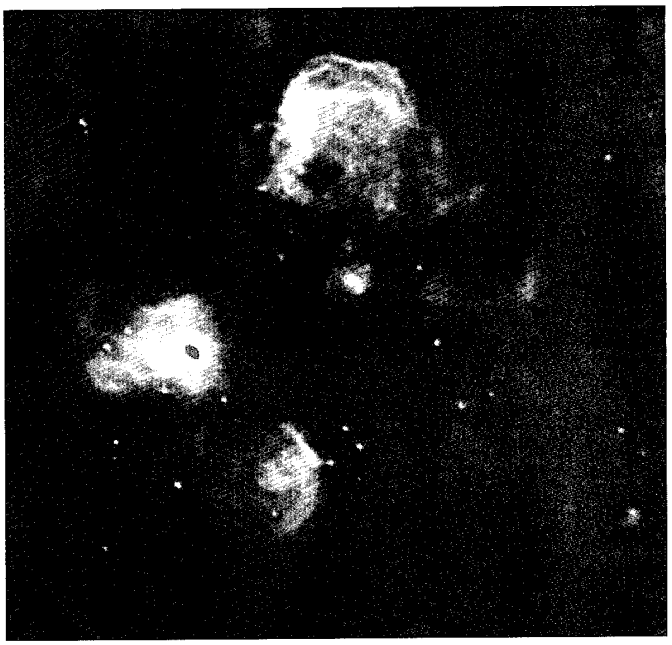

Using new technology available on the Very Large Array (VLA) telelscope at 1-m wavelength and powerful new supercomputers, NRL researchers are able to make uniquely detailed maps of large portions of the sky. This photo depicts a large, $3° \times 3°$ area containing two supernova remnants (top and bottom)–the remains of stars which exploded about 20,000 years ago–and two ionized hydrogen regions (middle) which could have been the birth places of the exploding stars. A pulsar known as PSR 1757-24 was ejected so violently (more than 1700 km/s) from the stellar explosion that it has overtaken and punctured the right side of the outracing gas shell from the bottom supernova remnants. Only long wavelength, wide field imaging being pioneered at NRL can yield such detail and sensitivity. A portion of this image has appeared on the March 1994 cover of the *Astronomical Journal*. (N. Kassim and K. Weiler, Remote Sensing Division)

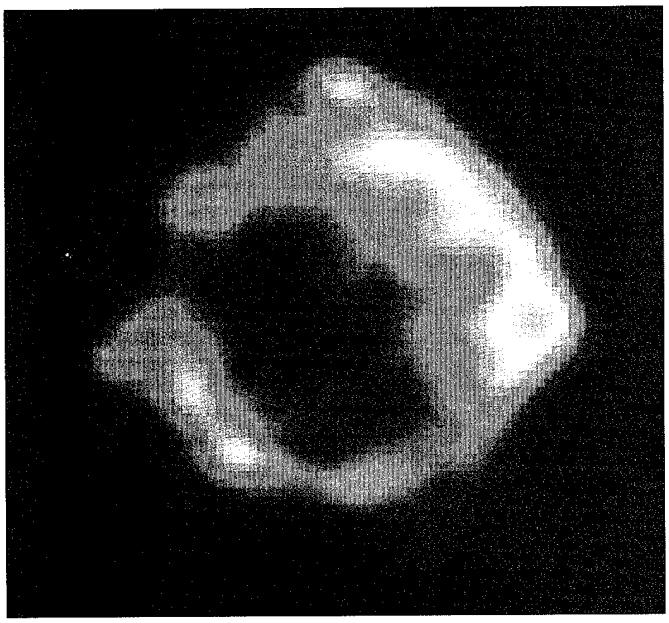

New clues to understanding the death of massive stars are captured in this supercomputer-processed image of the 300-yr old Cassiopeia A supernova remnant. In the past, high resolution imaging of astronomical radio sources at frequencies below 100 MHz has been impossible due to the effects of the ionosphere on measurements. NRL has developed a new technique, called "dual frequency ionospheric phase referencing," that when applied to a prototype system operating at 74 MHz at the Very Large Array radio telescope in New Mexico, opens a new, high resolution window on the electromagnetic spectrum. (N. Kassim, Remote Sensing Division)

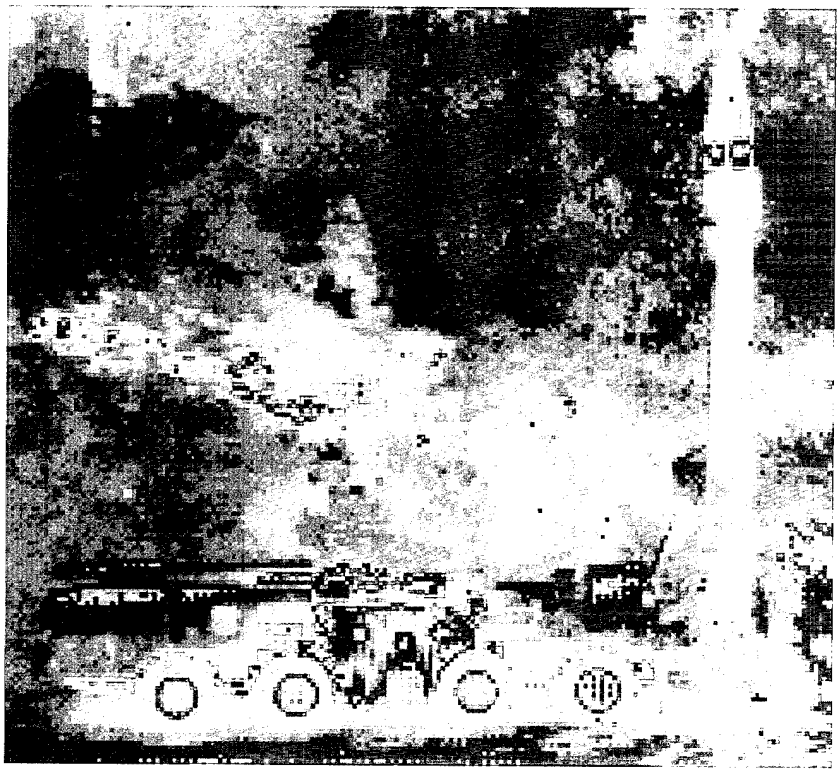

During June of 1994, NRL scientists made multispectral IR measurements of a Scud missile and Transportable Erectable Launcher (TEL) as part of the Symptom Slew collection at Wright Patterson Air Force Base. The figure presents a false-color broadband 3-5 μm image taken using an Amber IR camera with selectable IR filters. The TEL and missile were in a launch-ready mode. Measurements of this type are used to develop algorithms for Scud detection, classification, and identification. (M.R. Surette, W.A. Shaffer, J. Fisher, J.V. Michalowicz, and J.C. Kershenstein, Optical Sciences Division)

An atomic force microscope (AFM) image of *Pseudomonas chlororaphis* BC2 bacteria. Mutant strains of this bacteria produced at NRL manufacture a polyurethane degrading enzyme which NRL hopes to incorporate into an environmentally safe paint-stripping formulation. The AFM is being used to study the interaction of the bacteria and enzyme with sample paint surfaces as a means of characterizing the surface adhesion, distribution, and degradation products. The figure shows a 35 × 35 μm AFM image of an aggregated region of bacteria along with an 8 × 8 μm close-up inset. (D.Turner, L. Kondracki, and M. Montgomery, Center for Bio/Molecular Science and Engineering)

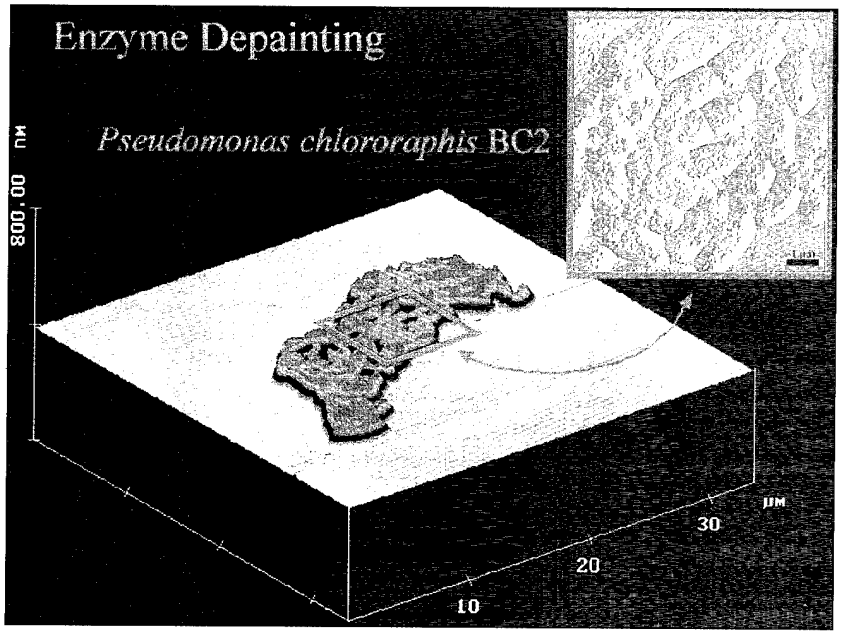

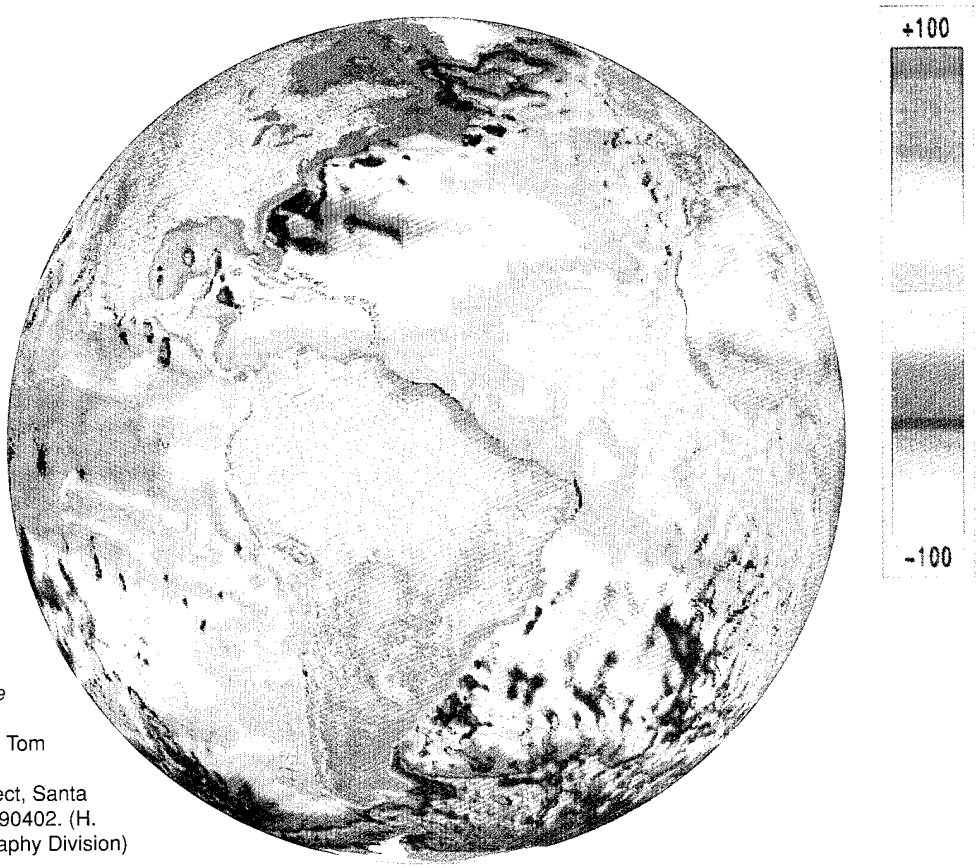

One frame (31 Jan 1983) of a 10-year video animation of sea surface height predicted by the NRL 1/4° Global Ocean Model projected on the GeoSphere™. Acknowledgment: *Satellite Composite View of the Earth*, Copyright 1990, by Tom Van Sant and the Geosphere™ Project, Santa Monica, California 90402. (H. Hulburt, Oceanography Division)

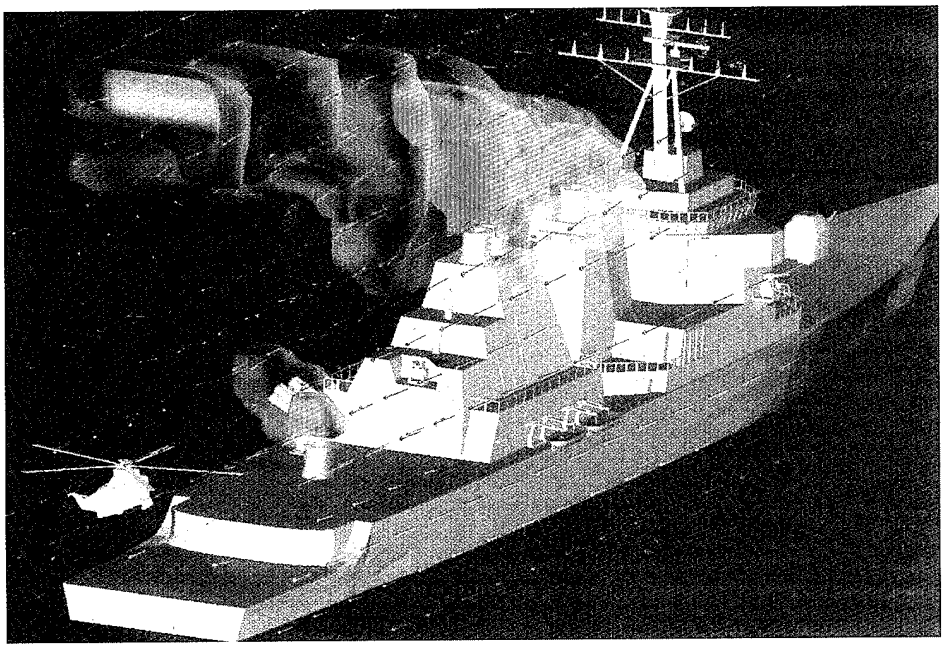

The unsteady velocity and temperature field over a Burke (DDG-51) class destroyer interacting with the downwash created by the main rotor blades of a hovering helicopter. Simulations performed on an Intel iPSC/860 and Intel Paragon. Velocity vectors show magnitude and direction of the flow field. Temperature isocontours show regions of hot exhaust gases (red) and cooler gases (yellow). (A.M. Landsberg, T.R. Young, Jr., J.P. Boris, and W.C. Sandburg, Laboratory for Computational Physics and Fluid Dynamics)

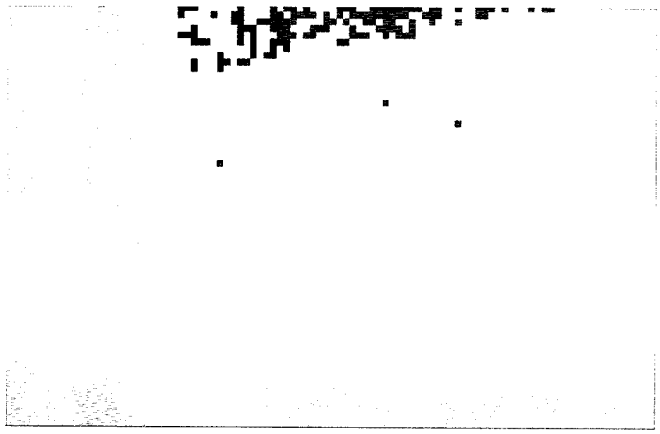

Underwater acoustic images of a foot-long cylinder resting on a sandy bottom, taken with a 3 MHz acoustic lens. The cylinder has a hexagonal pattern of bolt heads on its side. The images are (top) range image (red is close, blue is far); (bottom) acoustic "photograph." Note the reflection of the bottom in the cylinder and vice versa. (B. Kamgar-Parsi, Information Technology Division)

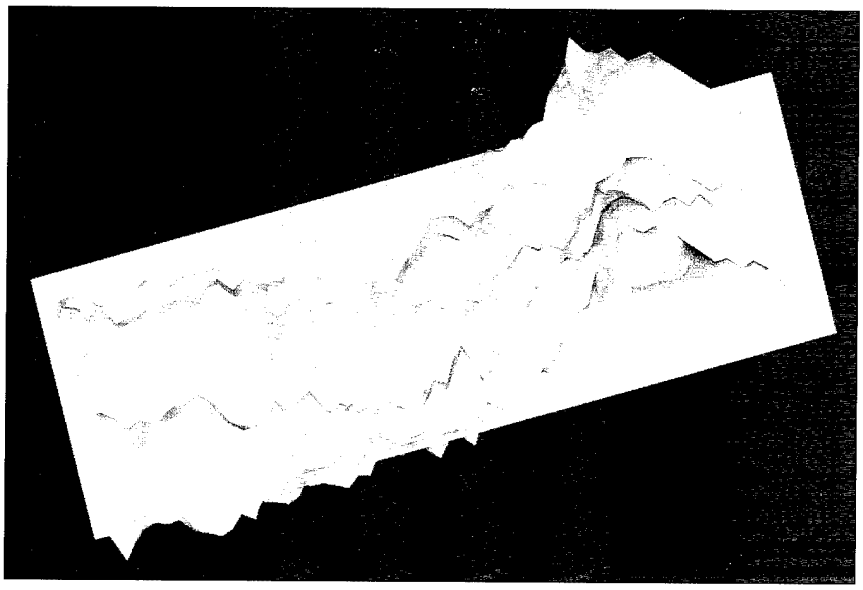

A visual display of the 32-channel detector output from a millisecond pulsar (PSR J1713+0747) found as part of the NRL/Penn State University high-latitude search program being conducted with the 305-m radio telescope at Arecibo, Puerto Rico. The data are processed on a variety of supercomputers, including NRL's CM-5. The figure shows the pulse intensity as a function of pulse period (4.57 ms) and radio frequency after correcting for interstellar dispersion (8 MHz total bandwidth). (R. Foster, Remote Sensing Division)

Clementine—A Mission to the Moon (and Beyond)

Donald M. Horan and Paul A. Regeon
Naval Center for Space Technology

BACKGROUND

Representatives of the Naval Research Laboratory's (NRL's) Naval Center for Space Technology (NCST) were first briefed on the *Clementine* mission in November 1991 while at the Strategic Defense Initiative Organization (SDIO) in the Pentagon to discuss the on-going Low-power Atmospheric Compensation Experiment (LACE) Program. The NCST representatives were casually asked if they had extra time to listen to a concept for a new space mission of interest to SDIO. The concept involved a lunar imaging and asteroid flyby mission using a Scout rocket as a launch vehicle. The key to the use of such a small launch vehicle was the successful development (under SDIO sponsorship) of a multitude of small, lightweight space components. A skeptical group of scientists headed back to NRL that afternoon to begin calculating the feasibility of the proposed mission.

Initial calculations produced discouraging results. Launch, using the small Scout rocket, was impossible but had appeared viable to SDIO because kilograms had been mislabeled as pounds. However SDIO progress in producing lightweight versions of essential hardware had been so great that launch by the next larger class of launch vehicles (Taurus, Conestoga, Titan II) might be possible. The size of the launch vehicle is important because a larger launch vehicle means greater mission cost for both the rocket and the spacecraft. In mid-December 1991, NCST began a 3-month effort to verify the feasibility of the *Clementine* mission by working through a preliminary mission plan and spacecraft design. After 2 months, it was clear to NCST and SDIO that the concept was feasible but risky. In the enthusiasm to get the mission started, SDIO sent several million dollars immediately rather than wait for the formal acceptance of the program by NRL management, which did occur in mid-March 1992.

Several months before the initial contact with NCST, SDIO had approached the National Aeronautics and Space Administration (NASA) to see if there was any interest in the data the *Clementine* mission might provide. NASA was interested and quickly appointed an ad hoc Science Advisory Committee, which initially would be responsible for defining the scientific goals of the mission. This committee worked closely with the NCST personnel during the 3-month effort to produce the mission plan and spacecraft design. Later NASA would use a competitive process to formally appoint a NASA Science Team (April 1993) to support the mission until the time the data are deposited in an archiving center. Thus when the Deep Space Program Science Experiment (DSPSE) mission was accepted by NRL, the primary objective was to provide a long-term test in space of hardware and algorithms developed by SDIO; the secondary objective was to obtain data useful for scientific investigations. Additionally in its mission to develop new technology for spacecraft, NCST was interested in the hardware developed by SDIO and also in testing hardware and software that had been developed through NCST.

THE MISSION

The NASA Science Advisory Committee defined the scientific goals as imaging of the entire lunar surface and imaging of the asteroid 1620 Geographos during a close flyby. SDIO's primary objective would be accomplished by

adding specific tests and demonstrations while achieving the scientific goals. Significant time constraints were imposed by the close flyby of Geographos. The asteroid would be closest to Earth in late August 1994 and then would move rapidly out of range. Figure 1 shows a timeline of the flown mission. The *Clementine* spacecraft was launched into a low-Earth orbit by a Titan IIG on January 25, 1994, only 22 months after formal acceptance of the program by NRL. On February 3, a solid-fueled rocket integral to the spacecraft was fired to achieve a trajectory to the Moon. In contrast to the *Apollo* missions, which had large fuel reserves to support a direct trajectory to the Moon with arrival in approximately 4 days, *Clementine* used fuel-efficient phasing loops to get to the vicinity of the Moon and fired its liquid-fueled propulsion system to enter lunar orbit on February 19. On February 21, the spacecraft was maneuvered into the 5-hour period, polar orbit that would be used to take images of the entire lunar surface. After several days of testing to ensure proper exposure settings for the cameras and to perfect operations, systematic imaging started on February 26 and continued until April 22. Several additional days in lunar orbit were used to make special observations, and the spacecraft propelled itself from lunar orbit on May 3. The plan was to again use phasing loops around Earth and then leave the Earth-Moon system on May 27, with an assist from lunar gravity. However an onboard malfunction on May 7 caused the attitude control fuel to be used completely and left the spacecraft in a spin, which ultimately prevented generation of adequate electrical energy to operate the spacecraft. The flyby of the asteroid 1620 Geographos was no longer possible, and the mission was effectively ended, although attempts to regain some control over the spacecraft continued for several weeks.

Definition of the desired lunar orbit to achieve complete imaging of the lunar surface was difficult because of several competing factors. The orbit had to be a polar one in order to provide the opportunity to image the entire surface. The NASA Science Advisory Committee desired that the angle between the plane of the orbit and the vector from the spacecraft to the Sun be no greater than approximately 30° throughout the systematic imaging phase. (This angle changes approximately 1° per day because of the motion of the Earth-Moon around the Sun.) If the cameras were too close to the lunar surface during imaging, the surface included in each image would be inadequate to ensure overlap between adjacent imaging strips. However, imaging from longer distances reduced resolution. Also the laser ranger used as an altimeter had a maximum range of only 640 km because of a design feature that could not be changed quickly enough to support the January 1994 launch. With these altitude constraints, the imaging portion of each orbit would require approximately 2 hours. During the 2 hours of imaging, between 5000 and 6000 images would be collected and stored aboard the spacecraft. The data transmission rate was constrained by hardware available in time for the launch. By using data compression acceptable to the NASA

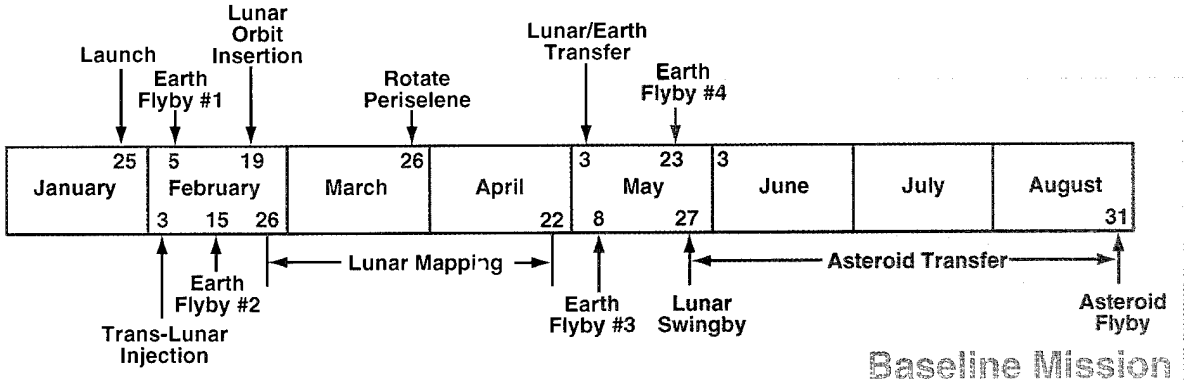

Science Team, it would take slightly over 2 hours to transmit the data collected on one imaging run. As the Moon moved around the Earth each month, communications blockages lasting a little over an hour would occur. Thus the lunar orbit used for systematic imaging had to have a period of at least 5 hours to allow 2 hours for data collection, 2 hours for data transmission, and 1 hour of communications blockage. The orbital period had to be in synchronization with the rotation of the Moon to ensure that the paths traced on the lunar surface by the fields of view of the cameras over a sequence of orbits would result in adequate overlap between adjacent images.

The lunar orbit used for systematic imaging had a 5-hour period with a periselene altitude (orbital point closest to the lunar surface) maintained between 400 and 450 km. The aposelene altitude (orbital point farthest from the lunar surface) was allowed to vary to keep the period constant as the periselene was adjusted to keep it within its acceptable limits. Typically the aposelene altitude was near 2950 km. During the first 28 days of systematic imaging, as the Moon rotated once beneath the spacecraft's orbit, the south-to-north paths traced on the lunar surface by the cameras' fields of view had gaps between them. These gaps were narrower than the cameras' fields of view and were covered by the imaging paths of the second 28 days of systematic imaging. A significant orbital adjustment had to be made at the end of the first 28 days of systematic imaging to ensure that the imaging paths of the second 28 days filled in the gaps left during the first 28 days. It was recognized that, since the imaging paths converged in the polar regions, the polar regions would be completely imaged after the first 28 days of systematic imaging. However placing the periselene in the Southern Hemisphere during the first 28-day imaging period would allow imaging of the south pole from a lower altitude, thus with better resolution than if the periselene were positioned over the lunar equator for the entire imaging cycle. When the orbital adjustment was made after the first 28 days of systematic imaging to ensure that the gaps between imaging paths would be filled during the second 28 days, the periselene could also be rotated into the Northern Hemisphere to allow higher-resolution imaging of the north pole during the second 28 days of systematic imaging. This procedure was followed, and both poles were imaged completely from an altitude of 800 km instead of the 1200-km altitude that would have resulted if the periselene were held over the equator. The lunar orbit was selected so that the angle between its plane and the vector from the spacecraft to the Sun was approximately 30° and decreasing at the start of systematic imaging on February 26. By the end of systematic imaging on April 22, the vector had passed through the orbital plane, and the angle between it and the orbital plane was again approximately 30° but increasing.

NCST trajectory experts had no experience with translunar trajectories, lunar orbits, and heliocentric trajectories. Therefore the Flight Dynamics Facility at NASA's Goddard Space Flight Center was given the primary responsibility for trajectories and orbits until departure from the Earth-Moon system, which was to occur on May 27. After May 27, the Jet Propulsion Laboratory (JPL) was to take primary responsibility for the heliocentric trajectory to 1620 Geographos. NCST trajectory experts duplicated the calculations of these external groups as a check on their results and as a learning experience for NCST.

NEW SPACECRAFT TECHNOLOGY

The primary purpose of the *Clementine* mission was to test hardware and algorithms in space that had been developed under the sponsorship of the Ballistic Missile Defense Organization (BMDO), which is the new name for SDIO. In addition to BMDO-developed space technology, new components and software developed through NRL or by commercial enterprise were also carried by *Clementine*. A brief description of the new technology flown aboard *Clementine* and its importance for space use follows.

Common Pressure Vessel NiH_2 Battery

For many years, nickel-cadmium (NiCd) batteries have been used in spacecraft. A significant disadvantage of NiCd batteries is the

inability to repeatedly carry them to significant depths of discharge (DOD). For repeated discharge cycles, accepted practice with NiCd batteries is to hold the DOD below 20% to avoid shortening the lifetime of the battery. For such uses, a battery with 15-A · h nameplate capacity has a cycling capacity of less than 3 A · h. Nickel-hydrogen (NiH_2) batteries have long been recognized as an improvement over the NiCd batteries for use in space. A NiH_2 battery can be repeatedly carried to a DOD of 40% to 50% without shortening its lifetime, thus providing more than double the cycling capacity of a similarly rated NiCd battery. Although NiH_2 batteries have only recently become the preferred battery for spacecraft, many have been flown since their first use in space in 1976. However, until *Clementine*, all NiH_2 batteries flown have been packaged so that each cell of the battery was sealed within its individual pressure vessel (IPV). This adds great mass and volume to the battery and causes its specific energy (watt-hours per kilogram) to be slightly worse than for a NiCd battery, and its energy density (watt-hours per liter) to be almost 10 times worse than for a NiCd battery. Sealing all of the cells within a common pressure vessel (CPV) provides a significant decrease in mass and volume. The 22-cell CPV NiH_2 battery flown for the first time on *Clementine* had an energy density only half that of a comparable NiCd battery but a specific energy twice as great. Thus the 15 A · h CPV NiH_2 battery used on *Clementine* provided the greater cycling DOD characteristic of NiH_2 batteries plus double the specific energy of either NiCd or IPV NiH_2 batteries, with a volume penalty only twice that of a NiCd battery and only one-fifth that of an IPV NiH_2 battery. Also the charge state of a CPV NiH_2 battery is linearly related to the battery's pressure, which can be directly measured by means of a pressure transducer. The charge state of NiCd and IPV NiH_2 batteries is known by continuously monitoring the current into and out of the battery. The CPV NiH_2 battery first flown in space aboard *Clementine* was developed by Johnson Controls, Incorporated.

GaAs/Ge Solar Cell Arrays

Typically spacecraft that operate near Earth use solar cell arrays to convert sunlight into electrical energy. As the demand for electrical energy aboard spacecraft continues to increase, the area of the solar arrays must also increase. For many years, spacecraft have used silicon solar cells. Gallium arsenide on germanium (GaAs/Ge) cells provide a 20% increase in electrical energy conversion-per-unit area over the silicon cells. Although GaAs/Ge cells have had some limited use in space before *Clementine*, the cells carried by *Clementine* are the thinnest GaAs/Ge cells that have been flown. The thinner cells thus add a mass advantage to the area-density advantage of previously flown cells. The thin GaAs/Ge cells used by *Clementine* were developed through a manufacturing technology program of the USAF Wright Aeronautical Laboratory and built by Applied Solar Energy Corporation.

Solid-State Data Recorder (SSDR)

Storage of large volumes of data aboard spacecraft is a problem which the SSDR carried by *Clementine* may contribute greatly to solving. Although there has long been a strong desire to advance beyond use of tape recorders in spacecraft, reliable solid-state devices have generally not been available. Tape recorders carried in spacecraft must be hermetically sealed to provide an atmosphere for the proper operation of the recording heads. The sealing enclosure adds a great mass penalty. The linear placement of data on the recording tape makes retransmission of missed data a time-consuming process because the recorder has to execute a linear search for the missed data. For spacecraft with precise pointing requirements, the effect of the rotating reels of the tape recorder must be canceled. Early SSDRs were excessively sensitive to the radiation environment in space, and errors were introduced into the stored data at an unacceptable rate. The SSDR carried by *Clementine* provides four times more data storage capacity than any previously flight-qualified

SSDR. *Clementine's* SSDR used commercially available dynamic random access memory (DRAM) devices packaged as multichip modules to provide 1.6 Gbits of storage capacity with 20 Mbits/s data input and output rates and very low error rates. At 2100 cm^3 and 4.1 kg, the SSDR was smaller and less massive than a tape recorder by almost an order of magnitude. The SSDR had a radiation tolerance of 30 krad(Si) plus an active error detection and correction capability. Aboard *Clementine*, many single bit errors were detected and reliably corrected. The SSDR can detect but not correct double bit errors. No double bit errors were detected during the *Clementine* mission. The *Clementine* mission goal of imaging 100% of the lunar surface could not have been attained without the random access capability of the SSDR. Errors from a variety of sources occurred during transmission of data from approximately 20% of the orbits during systematic imaging. The random-access capability of the SSDR made it an easy task to quickly retransmit the missed data before it was overwritten on a later orbit. The *Clementine* SSDR was produced by SEAKR Engineering, Incorporated.

Inertial Measurement Units

The *Clementine* spacecraft carried two inertial measurement units (IMU), partially for redundancy, but primarily to provide the first test in space of lightweight units based on two different gyroscope technologies. Inertial measurement units provide a continuous measurement of linear and angular accelerations that can be used to calculate trajectory changes, linear and angular velocities, and to control the orientation of the spacecraft. *Clementine* carried one IMU based on ring laser gyroscope (RLG) technology and one based on interferometric fiber optic gyroscope (IFOG) technology. Both units were developed using Ballistic Missile Defense Organization (BMDO) and company resources for large production helicopter and missile applications. Size and mass reduction had been accomplished through use of application-specific integrated circuitry and lightweight packaging. The *Clementine* attitude measurement subsystem comprising the IMUs and star-tracker cameras provided performance comparable to conventional space subsystems but with a 75% reduction in mass, size, and cost. The RLG-based IMU was produced by Honeywell Space Systems Group and the IFOG-based IMU by Litton Guidance and Control Systems.

Reaction Wheels

Clementine provided the first test in space of lightweight reaction wheels produced by Ball Aerospace and developed with combined BMDO and company funding. Reaction wheels provide precision pointing control and low acceleration slews for a spacecraft. Mass and volume reduction for the reaction wheels were accomplished by incorporating all drive electronics into the wheel housing.

Composite Materials

Significant mass savings on the *Clementine* spacecraft were achieved through use of composite materials. A graphite/epoxy mounting structure was developed at NRL for the CPV NiH_2 battery. This structure was unique in that it used different types of graphite fibers. One type of continuous fiber provided the heat path from the battery to the mounting panel for temperature control, and a different type of fiber provided strength and stiffness. The mass of a standard magnesium and aluminum battery mount would have been 7.3 kg. The mass of the composite mount for *Clementine* was 1.2 kg. A metal matrix graphite/aluminum material developed at the Naval Surface Weapons Center was used in several electronics boxes to reduce base plate temperatures as much as 10°C and weighed less than comparable aluminum heat sinks. Graphite/epoxy material was used for the supporting longeron structure and shell for *Clementine's* interstage adapter (ISA). The ISA carried structural loads during launch and the firing of the solid-fueled rocket to leave low-Earth orbit and later became a separate satellite in a highly elliptical Earth orbit. The use of composite materials instead of aluminum in the ISA provided a mass savings of 3.8 kg. Graphite/epoxy face sheets were used over an aluminum honeycomb core for the solar panels. The

composite material used for the solar panels was developed for BMDO through the USAF's Phillips Laboratory. Use of the composite material instead of aluminum for the face sheets of the solar panels provided a mass savings of 0.5 kg per array wing. Although this mass savings appears insignificant, it is important to realize that 8 kg of fuel are required to carry 1 kg of spacecraft to the asteroid 1620 Geographos. Therefore a saving of 1 kg in spacecraft mass resulted in a 9-kg reduction in launch mass.

Lightweight Release Device

Clementine also provided the first use in space of a lightweight release device called Frangibolt™. Release devices are used aboard spacecraft to securely hold components in place for an indeterminate period and then release the components upon command. Frangibolt™ provides a 40% mass reduction over a conventional pyrotechnic release device and also eliminates the safety concerns for ground handling and the pyrotechnic shock to delicate spacecraft components at release. The Frangibolts™ were produced by TiNi, Incorporated.

Commercial 32-bit Processor

Clementine provided the first use in space of a commercial 32-bit reduced-instruction-set-computer (RISC) processor. Images taken by *Clementine's* cameras had to be processed aboard the spacecraft within a small fraction of a second for various spacecraft control functions. Available, space-qualified, radiation-hardened processors for space use were not capable of processing the images quickly enough. Therefore the commercially available, nonhardened IDT R3081 32-bit RISC processor capable of executing 18×10^6 instructions-per-second was used aboard the *Clementine* spacecraft. The processor module, designed by Telenetics, Incorporated, provided error detection and correction capability, 2 Mbytes of RAM, and 1 Mbyte of electrically erasable, programmable, read-only memory (EEPROM).

Data Compression Chipset

Clementine provided the first use in space of an advanced, integrated chipset to provide highly controllable data compression in hardware. The storage of between 5000 and 6000 images during each lunar orbit would have provided too many bits to transmit in 2 hours unless data compression was used. However the NASA Science Team was extremely concerned about information loss through data compression and insisted that data compression be carefully controlled and minimized. Matra Marconi Space (France) offered use of their newly developed chipset, with highly controllable data-compression levels. After careful testing of data-compression results using the new chipset on lunar images from earlier missions, the Science Team agreed that the information loss could be held close to normal noise effects and would be acceptable.

Spacecraft Command Language

Also, *Clementine* provided the first use in space of NRL's Spacecraft Command Language (SCL) flight software. SCL provides an improved capability aboard the spacecraft for processing information and subsequent spacecraft control autonomy. SCL provided *Clementine* with a rule-based environment whereby the spacecraft could react to external events in an autonomous fashion. By using SCL, the spacecraft could command itself into different operating modes based on results of internal processing or changes in parametric values. For example, throughout the mission, the *Clementine* spacecraft processed startracker images to measure its own attitude, compared its measured attitude to the desired attitude, and corrected any errors. After the systematic imaging phase was completed, a significantly more stressing demonstration of autonomous control was successfully conducted in which the spacecraft duplicated all of the operations of a 5-hour lunar-imaging orbit based on onboard calculations of its location in its orbit. Progress in the development and use of SCL will lead to reduced operating costs for space missions because the spacecraft will be more capable of controlling its own operations. In addition to SCL, the flight software aboard *Clementine* provided the first use in space of a commercially available operating system. By using VxWorks from Wind River Systems as the

operating system, coding of the higher-level applications software was made easier and, given the time constraints of *Clementine*, even feasible.

Lightweight Imaging Sensors

Under BMDO sponsorship, the Lawrence Livermore National Laboratory (LLNL) developed several extremely lightweight cameras. These cameras were used by the *Clementine* spacecraft to collect scientific data and to control the spacecraft's attitude. The cameras are identified as ultraviolet visible (UV/Vis), near infrared (NIR), high resolution (HiRes), long-wavelength infrared (LWIR), and star-tracker. The UV/Vis camera uses silicon charge-coupled-device (CCD) technology with a 288 × 384 pixel array sensitive to light with wavelengths between 0.25 and 1 μm. Its field of view is 4.2° × 5.6° with an instantaneous field of view (IFOV) (the field of view of a single pixel) of 255 μrad. Pass bands are defined by a six-position filter wheel as 395 to 435 nm, 745 to 755 nm, 890 to 910 nm, 935 to 965 nm, 985 to 1015 nm, and 400 to 950 nm. All except the broad pass band were selected by the NASA Science Advisory Committee. Each of the five narrow pass bands of the UV/Vis camera was to be used to image the entire lunar surface. The UV/Vis camera used on *Clementine* weighed less than 410 g and, when compared to similar sensors in use, represents a factor of 2 to 4 decrease in mass and a factor of 3 decrease in power consumption.

The NIR camera uses an indium antimonide (InSb), 256 × 256 pixel array mechanically cooled to 70 K and sensitive between 0.9 and 3.1 μm. Its field of view is 5.6° × 5.6°, with an IFOV of 396 μrad. As developed by LLNL, the NIR camera had a single pass band. At the request of the NASA Science Advisory Committee, a six-position filter wheel was added to the instrument. The six pass bands are 1070 to 1130 nm, 1220 to 1280 nm, 1470 to 1530 nm, 1970 to 2030 nm, 2570 to 2630 nm, and 2630 to 2750 nm. All except the longest-wavelength pass band were selected by the NASA Science Advisory Committee. Each of the six pass bands of the NIR camera was to be used to image the entire lunar surface. The NIR camera used on *Clementine* weighed 1920 g, including the Stirling-cycle cryocooler; this represents a significant decrease in mass when compared to similar sensors.

The LWIR camera uses a mercury cadmium telluride (HgCdTe), 128 × 128 pixel array mechanically cooled to 65 K. Filters define a single pass band between 8 and 9.5 μm. Its field of view is 1° × 1°, with an IFOV of 143 μrad. The LWIR camera used on *Clementine* weighed 2.1 kg, including the Stirling-cycle cryocooler. The HiRes camera uses a silicon CCD, with a microchannel plate intensifier. It has a 288 × 384 pixel array sensitive between 0.35 and 0.80 μm. Its field of view is 0.3° × 0.4°, with an IFOV of 18 μrad. However photocathode and microchannel intensifier effects cause a blur circle with a diameter close to 40 μrad. Pass bands are defined by a six-position filter wheel as 395 to 435 nm, 535 to 585 nm, 625 to 675 nm, 725 to 775 nm, and 450 to 800 nm, with an opaque disc in the sixth position to protect the intensifier. All except the broad pass band were selected by the NASA Science Advisory Committee. The HiRes camera used on *Clementine* weighed only 1120 g.

The startracker is a star-imaging sensor designed primarily for attitude determination, although it was also used to collect scientific data. *Clementine* carried two startrackers mounted to ensure that one would always have the Sun excluded from its field of view. The startracker uses silicon CCD technology with a 384 × 576 pixel array sensitive between 0.4 and 1.1 μm. It has a wide field of view, 29° × 43°, to make more stars available for attitude determination. Its IFOV is 1.3 mrad. The LLNL startrackers used on *Clementine* each weighed less than 290 g and, when compared to other startrackers, represented a decrease in mass by a factor of 3 to 10, a factor of 2 decrease in power consumption, and a factor of 2 to 5 lower cost. An image from a startracker was processed aboard the spacecraft by using a computer program, Stellar Compass, provided by LLNL. Stellar Compass compared the angular relationships of stars in a startracker image to those provided by a stored star catalog of only 600 stars distributed over the celestial

sphere. Stellar Compass and the star catalog were resident in the R3081 RISC processor. Typically attitude determination could be made within 100 ms by using a single startracker image. The LLNL startracker and Stellar Compass provide attitude determination of medium accuracy, which is better than 150 μrad in pitch and yaw and 450 μrad in roll.

Laser Ranger

LLNL developed a laser-ranging system (also under BMDO sponsorship) that was successfully used for lunar altimetry. The transmitter is a diode-pumped Nd:YAG laser emitting at 1064 nm with 180 mJ per pulse and a pulse duration of 10 ns. The transmitter can run continuously at a 1 Hz pulse rate with short bursts at 8 Hz limited by thermal effects. The laser transmitter and power supply weighed 1.25 kg and were very compact. They represented a factor of 10 improvement in mass and volume when compared to earlier units. The receiver for the laser ranger was an avalanche photodiode within the HiRes camera and shared its optics. Range measurements could be made to a maximum of 640 km, with a resolution of 40 m.

DATA FOR SCIENTIFIC RESEARCH

Although the bravely stated secondary goal of the mission was to image the entire lunar surface in 11 narrow pass bands of the UV/Vis and NIR cameras, there was a tacit recognition that this goal would not be fully achieved. If we succeeded in imaging 75% of the lunar surface, it would be a major accomplishment. NASA's DSN ground stations in Madrid, Canberra, and Goldstone, California, shared the communications tasks with our NRL site in Pomonkey, Maryland. As a matter of policy, DSN would only commit to 90% of the support requested of them because of the large number of space programs using DSN. However 1 week into the 8-week systematic imaging phase of the mission, it was clear that imaging of the entire lunar surface was indeed possible. Although a few images had already been missed, operational procedures and opportunities to regain the missed images were quickly identified. Therefore the *Clementine* operations team became determined not to miss a single image, and their determination inspired DSN as well. The obvious delight of the NASA Science Team with the quality and quantity of the lunar images also fueled our determination.

The *Clementine* spacecraft delivered approximately 1.8 million digital images, most of which were obtained during the period of systematic imaging from February 26 until April 22. Every 5 hours, between 5000 and 6000 images were transmitted. As each image arrived in the *Clementine* operations center in Alexandria, Virginia, it was processed and was available for use by operations personnel and the NASA Science Team within 15 minutes. As the images became available, sensor experts from NRL and LLNL, representatives of the NASA Science Team, and other operations team personnel would use them to quickly verify the proper operation and targeting of the sensors. Thus adjustments identified from the images of one orbit could often be transmitted to the spacecraft before collection of images began for the next orbit. Selected images were frequently made available over the Internet electronic mail system; this created great interest in the *Clementine* mission.

Figure 2 shows a refined version of a mosaic of UV/Vis camera images covering the Moon's south polar region, from approximately 70° S latitude to the pole. The south pole would be completely imaged with the best resolution for this mission during the first month of systematic imaging because the periselene was in the Southern Hemisphere. At the arrival of the first polar images, members of the NASA Science Team from the U.S. Geological Survey (USGS) started assembling a mosaic of UV/Vis images of the south polar region as a check on the quality of the data. As new images were transmitted, the Science Team would fit them into the mosaic and carefully examine the overlap with adjacent images and picture quality. This effort provided early identification of a minor spacecraft timing anomaly, which caused some misalignment of image strips from adjacent orbits. The early identification resulted in a quick correction so that analysis of the data

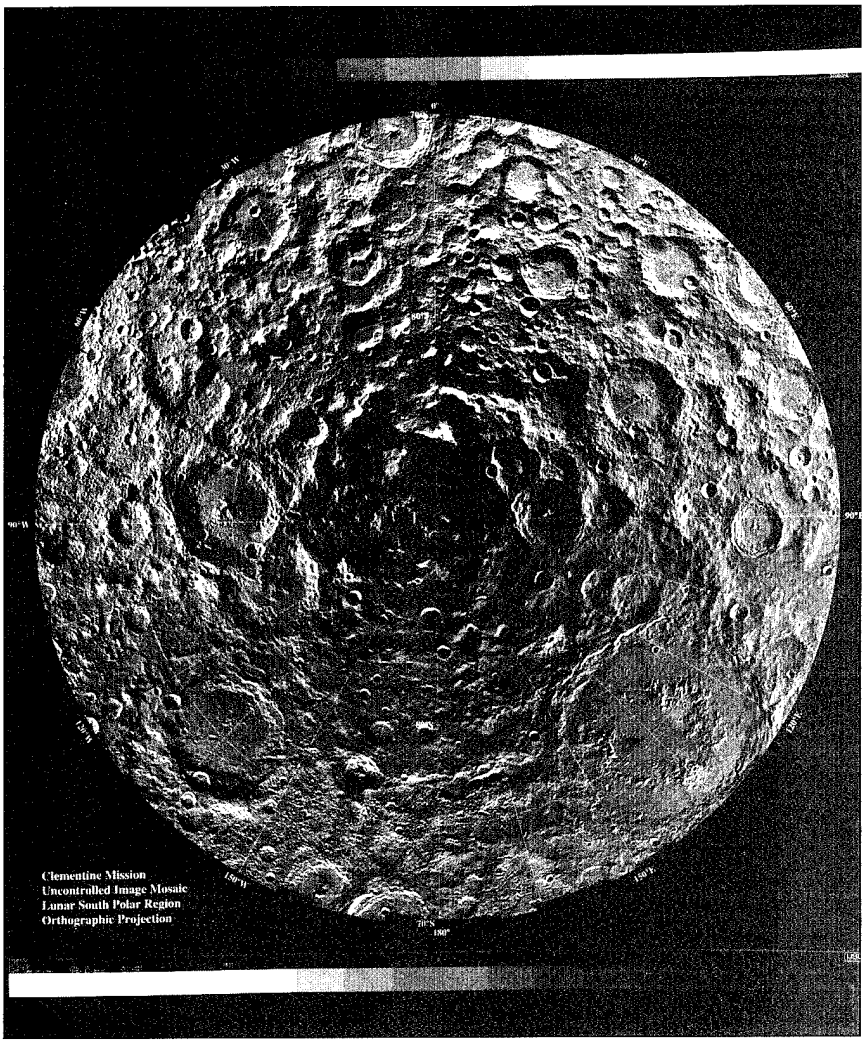

Fig. 2 — Mosaic of over 1500 *Clementine* UV/Vis camera images produced by U.S. Geological Survey and showing the Moon's south polar region, with 200-m resolution.

from subsequent orbits was made easier. As the mosaic took shape, it appeared to reveal a region surrounding the pole that received no sunlight even though the Moon completely rotated once. Although it will require extensive analysis to determine whether sunlight is always excluded from this region, the possibility of an extremely cold, perpetually shadowed region collecting and freezing water molecules for eons invited an attempt to find ice in the shadowed area. In consultation with representatives of JPL and by using a technique based on characteristic changes in the polarization signature of radio frequency (RF) radiation with reflection from ice or rock, the spacecraft's high gain antenna was aimed at various south and north polar regions, including the shadowed area so that the RF signal would bounce from the selected lunar surface area to the ground stations on Earth. Since this is an experiment that was not foreseen prior to launch, no processing software had been prepared. Thus after the data were collected, software for an extremely intricate data processing sequence had to be prepared. Final analysis of this data is not yet complete. Initial lower-order analyses reveal no ice, but there is hope that ice might still be revealed in the later stages of the analysis.

Figure 2 is also significant for what it promises from the *Clementine* images. Between

1500 and 1600 images from a single pass band of the UV/Vis camera were used to create the mosaic. With an altitude near 800 km at the poles, the resolution (based on the field of view of a single pixel) is 200 m for the UV/Vis camera and 300 m for the NIR camera. At the 400-km minimum periselene altitude, resolution was 100 m for the UV/Vis camera and 150 m for the NIR camera. Thus the *Clementine* images cover the entire lunar surface with a resolution between 100 and 200 m for the five pass bands of the UV/Vis camera and a resolution between 150 and 300 m for the six pass bands of the NIR camera. Images of equal or higher resolution were available for most of the lunar surface before *Clementine* from *Lunar Orbiter* and *Apollo*. However, these earlier images were almost entirely in the form of nondigital hard copies. The digital format of the *Clementine* images will allow not only easier storage and distribution but also digital processing to enhance selected information and more easily align adjacent images. *Clementine* does provide significantly higher resolution than previously available for the higher latitude regions, especially on the Moon's far side. Presently available charts from USGS and National Geographic show significant areas poleward from 70° S latitude between 90° and 120° W longitude labeled "unsatisfactory photography." The *Clementine* images will certainly remove this luna incognita. Mosaics, with resolution equal to or better than in Fig. 2, can be made by using *Clementine* data for every region of the lunar surface. The overlap of image paths in both polar regions is such that mosaics like Fig. 2 can also be made by using images from the HiRes camera with 30-m resolution. Since the HiRes mosaics will include over 70,000 images, they will not be available soon.

The use of the same cameras to image the entire lunar surface adds information. Many discrete areas of the Moon have been imaged with better resolution than *Clementine* provides. Surface features within these regions can be precisely located relative to each other. However precise location of features within one region relative to features in another region separated by an expanse of lower-resolution images is very difficult, especially if different sensors were used for the two regions. The *Clementine* data provide the first opportunity not only to achieve precise relative locations for all resolvable features on the lunar surface but also to accurately define an absolute reference grid for the entire lunar surface.

The 11 narrow pass band filters of the UV/Vis and NIR cameras were selected by the NASA Science Advisory Committee to provide information useful to identify the distribution of minerals over the lunar surface. Relative responses among the various filters can identify regions dominated by minerals rich in iron, magnesium, titanium, or other elements. Lunar samples provide a calibration of the mineralogy at the *Apollo* landing sites. During spacecraft integration at NRL, *Apollo* samples were used to provide calibration information for the *Clementine* sensors. Figure 3 shows how multispectral images will be used to identify mineral content and distribution. Over 100,000 UV/Vis images were used in three pass bands to cover the entire lunar surface. The average response for each image was calculated from the response of each of the 100,000-plus pixels of each image. The red images centered at 750 nm were used as the reference and combined with the relative response of the bands centered at 415 and 950 nm to form Fig. 3. The nonuniform distribution of minerals over the lunar surface can clearly be seen. Use of the individual pixels of the images will provide much higher resolution. Lunar geologists can use the results of these multispectral displays to estimate the ages of different regions, trace ejecta paths from craters, and recognize when material from below the surface has been uncovered.

Doppler-based range and velocity measurements were made on the spacecraft while in lunar orbit so the location of the spacecraft could be precisely known for later interpretation of the images and to obtain measurements to improve the model of the Moon's gravitational potential. Since the lunar potential model was quite accurate before the *Clementine* flight, improvements to the model are expected to be small. However the accurate measurements of the location of the spacecraft throughout the mission, coupled with the use of the laser ranger to provide altitude measurements, will

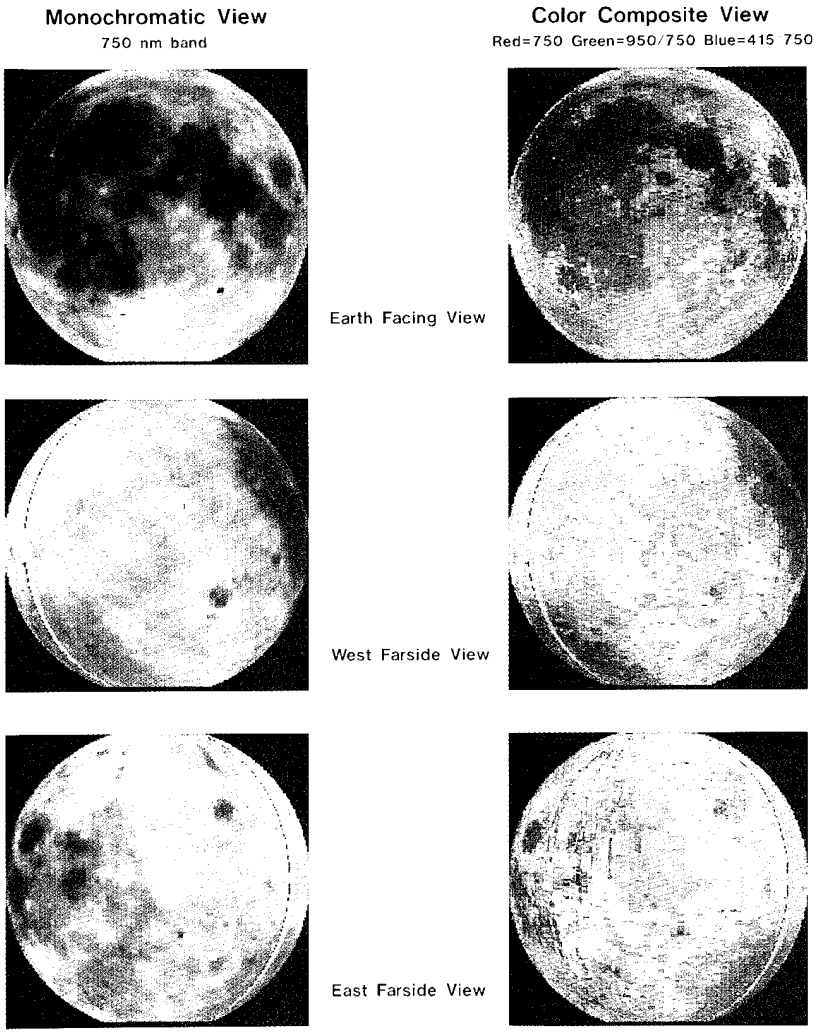

Fig. 3 — Example of the use of multispectral images from *Clementine* to identify the distribution of minerals over the lunar surface.

greatly extend the knowledge of lunar topology. Since the laser ranger had a maximum range of 640 km, good altimetry data were obtained from 70° to 10° S latitude during the first 28 days of systematic imaging and from 10° to 70° N latitude during the second 28 days. Additional data of lesser quality were obtained between 70° and 75° in both polar regions and within 10° of the equator. Although the laser ranger pulsed at 1 Hz, only about 25% of the pulses provided an interpretable return. Therefore the *Clementine* altimetry data provides strips of measured points at intervals averaging 10 km running from 70° S to 70° N latitude. The strips are approximately 75 km apart at the equator and closer at higher latitudes. The laser ranger can resolve altitudes to 40 m. The Doppler measurements and lunar potential model can locate the spacecraft to 100 m [1] relative to the center of mass of the Moon. Thus a coarse surface profile for latitudes below 75° can be generated from the *Clementine* data. Superficial, initial analysis of these data has already verified the existence of suspected old basins, revealed the presence of at least one unsuspected old basin, and shown the huge south pole Aitken Basin on the far side to

be larger and far deeper than previously recognized [2]. Altimetry measurements near the lunar equator were also made by *Apollo* flights. Attempts will ultimately be made to combine the *Clementine* and *Apollo* altimetry into a single grid. In an attempt to provide some surface-profile information for latitudes greater than 75°, dual images of both polar regions were made to provide stereoscopic coverage.

The *Clementine* operations team could not resist taking images of Earth from the spacecraft's unusual vantage point. Figure 4 is a splendid color mosaic of Earth assembled by the USGS from multispectral HiRes camera images taken from lunar orbit. New pictures of Earth arriving in the control center always created a stir. Although everyone clearly understood the physics involved, photographs showing our round Earth with no visible support were awesome.

All data from the *Clementine* mission are being processed for submission to NASA's Planetary Data System (PDS) for archiving in the standard PDS format. This task is being closely monitored by the NASA Science Team. The image data are being combined with pertinent ancillary information from the spacecraft, such as sensor temperatures and spacecraft orientation, which will be needed for proper analysis of the data. High-precision orbit information supplied by NASA's Goddard Space Flight Center is being used to locate the spacecraft for each image. Calibration information for each sensor will be included with the archived data set. Data archived in the PDS are easily available to all potential users at modest cost, especially including universities and other research institutions, government agencies, and the general public. It is expected that the *Clementine* data will keep lunar scientists occupied for at least 10 years.

SUMMARY

The *Clementine* mission is considered to be highly successful in achieving its primary and secondary objectives. Although it would have been desirable to operate the new technological components in space for a longer period, the highly stressing use while in lunar orbit, combined with the flawless performance of the devices, have made them clearly the hardware

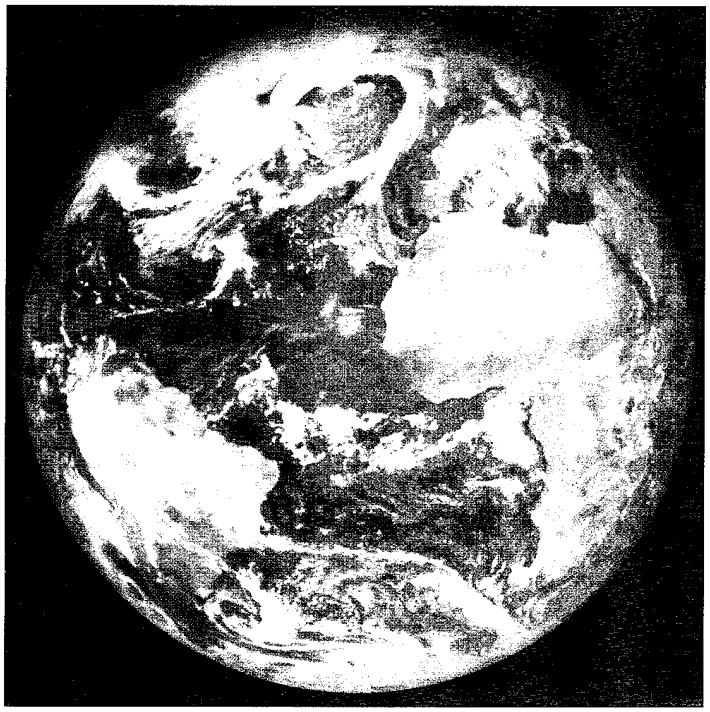

Fig. 4 — Mosaic of *Clementine* HiRes images produced by the U.S. Geological Survey, showing Earth from lunar orbit.

of choice for subsequent NCST space missions. The performance of Spacecraft Command Language on this mission provides encouragement for additional development of this spacecraft control software. Although there was universal disappointment that the flyby of Geographos could not be performed, the abundance of high quality lunar data (which greatly exceeded expectations) overwhelms any attempt to say the mission failed to achieve its secondary goal.

ACKNOWLEDGMENTS

A difficult mission such as *Clementine* cannot be successful without the participation of many dedicated people and organizations. We acknowledge the sponsor, the Ballistic Missile Defense Organization, for insight in recognizing the viability of the mission and tenacity in keeping it moving over many programmatic obstacles. We acknowledge the Lawrence Livermore National Laboratory for their advanced, lightweight cameras, NASA Goddard Space Flight Center's Flight Dynamics Facility and the Jet Propulsion Laboratory for their support with trajectories, and the Deep Space Network for their communications support. We acknowledge the enthusiastic assistance of the initial Science Advisory Committee and the NASA Science Team for mission planning and operations.

We were privileged to have the opportunity to play leadership roles for the *Clementine* mission. We greatly appreciate the determination and competence of the members of the *Clementine* team—both government and contractor—who were the real difference between success and failure on many occasions.

REFERENCES

1. M.T. Zuber, D.E. Smith, F.G. Lemoine, and G.A. Neumann, "The Shape and Internal Structure of the Moon from the *Clementine* Mission," *Sci.* **266**, 1839 (1994).

2. P.D. Spudis, R.A. Reisse, and J.J. Gillis, "Ancient Multiring Basins on the Moon Revealed by *Clementine* Laser Altimetry," *Sci.* **266**, 1848 (1994).

THE AUTHORS

Donald M. Horan began working at the Naval Research Laboratory (NRL) in 1959, immediately after earning a B.S. degree in physics from Canisius College in Buffalo, New York. His initial assignment at NRL was with the Electronics Division where he conducted research on tunnel diodes. In 1965, he joined the Metallurgy Division where he conducted research on the thermoelectric effect in metallic materials. In 1966, he earned an M.S. degree in physics from the University of Maryland and joined NRL's Space Science Division where he began a long involvement with the Solar Radiation (SOLRAD) Satellite Program. He participated in design, construction, tests, operation, and data analysis for the SOLRAD 9 satellite, which was launched in 1968, and the SOLRAD 10 satellite, which was launched in 1971. He served as experiments manager for the pair of SOLRAD 11 satellites, which each carried 25 experiments into a 50,000 nautical mile circular orbit in 1976. While with the Space Science Division, he earned a Ph.D. in physics in 1970 from The Catholic University of America and also participated in solar research experiments flown on NASA's Orbiting Solar Observatories (OSO) and Orbiting Geophysical Observatories (OGO). In 1982, Dr. Horan transferred to NRL's Aerospace Systems Division where he conducted research on satellite survivability concepts. In 1985, he participated in the initial studies which evolved into the Low-power Atmospheric Compensation Experiment (LACE) satellite for which he was the chief scientist and director of operations. He became a member of the Space Systems Development Department of NRL's Naval Center for Space Technology in 1986. In late 1991, he led the translation of the initial concepts for a lunar imaging mission into a set of spacecraft and mission requirements, which evolved into *Clementine*. Dr. Horan is presently the chief scientist and director of operations for the *Clementine* Program.

Paul A. Regeon received a B.S. degree in electrical engineering in 1980 from the George Washington University, in Washington, D.C. He came to the Naval Research Laboratory (NRL) after graduation. He is now head of the Systems Integration Section of the Spacecraft Engineering Branch of the Space Systems Development Department. Mr. Regeon has served in key roles for several NRL projects. He was the electrical systems manager for the Low-power Atmospheric Compensation Experiment (LACE) satellite, a Strategic Defense Initiative Organization spacecraft launched in 1990. He was program manager for the Sea Launch and Recovery X-3 launch vehicle and for the Special Sensor Ultraviolet Limb Imager (SSULI), an advanced ionospheric sensor for the Defense Meteorological Satellite Program. Mr. Regeon is the program manager for the *Clementine* Program; he also performed additional, technical duties in support of *Clementine*. Mr. Regeon is also responsible for the coordination among the various government agencies participating in the *Clementine* mission.

Processing-Microstructure-Property Relationships in Advanced Naval Steel Welds

George Spanos, Richard W. Fonda and Roy A. Vandermeer
Materials Science and Technology Division

INTRODUCTION

Modern high-strength, low-alloy (HSLA) steels, which have commercial applications in the construction of buildings, bridges, pipelines, and ships, can provide an excellent combination of strength (the resistance of a material to deformation) and toughness (a measure of the mechanical energy required to achieve failure by fracture). In particular, the Navy desires plate steel for ship and submarine construction with higher yield strengths, no loss of toughness, and reduced processing costs. Advanced HSLA steels have the potential to meet these criteria. However welding can still degrade the microstructure, properties, and geometric compatibility of structural components, leading to very costly problems, including cracking within weldments and welding-induced distortion. It is therefore of great interest to the Navy (and to industry) to develop adequate weld-processing procedures and weld-filler materials for these advanced steels without increasing processing costs. Our research program thus provides processing-microstructure-property relationships that enhance one's ability to understand and control the development of the microstructure and the mechanical properties of welded HSLA steels.

Weld problems may be encountered both in the fusion zone (molten during welding) and in the heat-affected zone (the region adjacent to the fusion zone, which heats up significantly but remains solid during welding). In the fusion zone, a number of new phase distributions may form due to solidification and subsequent solid-state reactions during cooling. During heating of certain regions in the heat-affected zone (HAZ), the matrix phases will transform to the high temperature, solid austenite phase, and fine strengthening precipitates within the original matrix phases will coarsen and/or dissolve. During subsequent cooling, the austenite will retransform to new matrix phases and new precipitate distributions. These microstructural alterations can degrade the mechanical properties (for example, strength, hardness, and toughness) of the welded structure.

Although there have been a number of investigations of HSLA steels within the last few years, most researchers have studied mechanical properties and relied predominantly upon optical microscopy to correlate the microstructure with these properties. The investigations that used higher resolution techniques (such as transmission electron microscopy (TEM)) have usually focused on the effects of alloying elements and/or isothermal aging treatments (rather than commercial processing procedures) on microstructural development. TEM studies of the detailed microstructural changes that occur during welding of HSLA steels and the subsequent effects of these changes on the mechanical properties have been seriously lacking.

The present investigation was undertaken to study systematically the detailed microstructural changes (particularly at the TEM level of resolution) that occur during welding of advanced HSLA steels. We first investigated the microstructural changes that occur in a commercial HSLA-100 steel thermally cycled to simulate weld HAZ behavior under tightly controlled processing conditions. Optical microscopy, dilatometric analysis, and microhardness studies were also performed to provide correlations with the TEM findings.

More recently we have extended our investigation to study both the HAZ and the fusion zone in commercial weldments of HSLA-100 made with new, low-alloy filler metals.

MICROSTRUCTURES IN HSLA STEELS

Microstructure refers to the distribution of microconstituents in a material. A microconstituent is either a single phase or a composite structure of multiple phases, with a characteristic morphology and internal structure. Single crystals of a phase (in which all atoms have the same structural arrangement and lattice orientation) are called grains. Due to the importance of microstructure in dictating the physical properties of materials, it is useful to describe in advance the most important microconstituents that are present in HSLA steels.

Matrix Phases/Microconstituents

The matrix phases in steels are composed of a lattice of iron atoms with small amounts of solute alloying elements (carbon, niobium, copper, nickel) dispersed throughout the iron lattice. The important matrix microconstituents in HSLA-100 steel are described below.

Austenite is a high temperature phase which begins to form at about 700° C or above and which is the sole equilibrium phase at temperatures of about 850° C or greater in HSLA-100 steel. Under nonequilibrium conditions, small amounts of austenite can also be retained at room temperature (retained austenite). Austenite has a face-centered-cubic (fcc) crystal structure, whereas all of the other matrix phases in low alloy steels are based on a body-centered-cubic (bcc) atomic lattice. *Equiaxed ferrite* (also referred to as polygonal ferrite) forms from the austenite during cooling and has a relatively equiaxed morphology in three dimensions. It is typically the softest of the room-temperature matrix microconstituents in these steels. *Lath ferrite* forms from austenite at lower temperatures than does equiaxed ferrite. It has a finer, more elongated morphology, roughly resembling that of a wood lath, and it is typically harder than equiaxed ferrite. *Untempered lath martensite* is the hardest phase in HSLA steels and forms from austenite at temperatures lower than those of ferrite by a diffusionless phase transformation in which no alloying elements are partitioned between the martensite and the parent austenite from which it forms. For any given material, martensite can only form at or below a characteristic "martensite start temperature," M_s. Large amounts of this relatively brittle microconstituent can be detrimental to weldments, resulting in cracks within the welds. *Tempered lath martensite* results from untempered lath martensite that has been subsequently aged (tempered) at temperatures below those which will allow austenite formation. The aging results in redistribution of the solute atoms from the iron lattice of the untempered martensite into small particles of new precipitate phases embedded in the tempered martensite. These fine precipitates are typically at least an order of magnitude smaller than the matrix martensite grains.

Precipitate Phases

Fine *copper* particles in commercial HSLA steels possess an fcc crystal structure and can form within either ferrite or tempered martensite. These particles contribute to the high strength of these steels. *Niobium carbonitrides* are particles that are usually finer than the copper precipitates and are composed of an ordered lattice that possesses the following stochiometry: Nb(C,N). They are stable up to much higher temperatures than the copper precipitates and, in addition to providing strength, help to inhibit austenite grain growth during high temperature processing. *Cementite* is a carbide that forms during the tempering of martensite or during the eutectoid decomposition of austenite to ferrite-plus-carbide microstructures. It is based on an Fe_3C stoichiometry and possesses a complex orthorhombic crystal structure. It is quite brittle and when formed in large, continuous morphologies can be a source of fracture.

HSLA-100 BASE PLATE

We initially studied a 5.7-cm thick plate of a commercial HSLA-100 steel manufactured by Lukens Steel Company and supplied to us by the Naval Surface Warfare Center (NSWC) at Annapolis, Maryland. The as-received base plate had been subjected during processing to two separate austenitization and quench cycles to refine the structure and develop optimum toughness, followed by aging at 640° C for 7 hours, to achieve the desired mechanical properties. The as-received base plate was investigated first in order to provide a baseline for subsequent investigations of the effects of weld processing cycles on this material.

Our TEM observations demonstrate that the matrix microstructure of the as-received base plate consists of a majority of heavily tempered lath martensite (due to the quench-and-age processing) and a minority of lath ferrite. A relatively wide size distribution and high density of copper and niobium-carbonitride particles are observed within the heavily tempered martensite laths. Additionally somewhat larger particles are often observed at the martensite and ferrite lath boundaries.

Very coarse particles, which can occasionally be impinged and run continuously for lengths of 1 μm or greater, are present along some of the prior austenite grain boundaries. [Prior austenite grains refer to austenite grains which transform to martensite or ferrite during cooling; prior austenite grain boundaries are identified in room temperature TEM specimens as regions where a packet of martensite or ferrite laths come to an abrupt termination because they cannot grow across austenite grain boundaries.] Electron diffraction analysis shows many of these precipitates to be cementite. Since coarse-grain-boundary cementite is known to be an embrittler, these particles could provide potential fracture paths. However this may not be a serious problem because the particles are only present on a minority of prior austenite grain boundaries in the as-received base plate.

We thus observed three types of precipitate distributions in the base plate: (1) coarse particles at prior austenite grain boundaries, (2) somewhat smaller precipitates at lath boundaries, and (3) relatively fine intralath precipitates. By analyzing many specimens with TEM, we were able to construct Table 1, which shows the size ranges, morphologies, and identification of the precipitates at each type of site.

LABORATORY SIMULATED HAZs

We simulated the behavior of HAZs during welding by using a heating/quenching dilatometer to perform eight different thermal cycles chosen to bracket the behavior associated with different positions in the HAZ and different weld processing parameters (for example, heat input and preheat) [1,2]. Specimens were heated inductively at a rate of 100° C/s to one of four different peak temperatures (see below). They were then immediately cooled to room temperature, following a Newtonian relationship (that is, $\frac{d\Delta T}{dt} = -k\Delta T$, where T is temperature, t is time, and k is a constant) such that an average cooling rate between 800° C and 500° C of either 60° C/s or 5° C/s was obtained. (For peak temperatures below 800° C, the cooling profile was extrapolated from the 800° C to 500° C range following the Newtonian relationship.) We chose peak temperatures (*Tp*) representative of those observed at various locations in typical heat affected zones [1,2] and which also correspond to (1) a temperature within the ferrite matrix phase field: 675° C; (2) a temperature within the equilibrium ferrite-plus-austenite two-phase field: 750° C; (3) a low temperature in the single phase austenite regime: 900° C, and (4) a much higher temperature (near the melting point) in the single phase austenite regime: 1400° C. Figure 1 shows an example of a thermal cycle taken from the output of the dilatometer. In addition to providing precise heating and cooling control and to obtaining detailed thermal histories during these cycles (see Fig. 1), using the dilatometer to simulate weld thermal cycles provides another major advantage. Since the dilatometer measures minute dilatations and/or contractions during phase changes in the specimens, analysis of the

Table 1 — Location, Size, Morphology, and Identification of Precipitates Found at Three Different Types of Site in the Base Plate.

Location	Size Range (μm)	Typical Size (μm)	Morphology	Type
Prior austenite grain boundaries	0.054 - 0.360	0.15	Allotriomorphs (some equiaxed)	Cementite
Ferrite and martensite grain boundaries	0.009 - 0.065	0.02 (200 Å)	(1) Elongated rods/plates with low aspect ratio ($\leq$ 3) (2) Equiaxed	Cu + Carbonitrides
Intragranular sites	0.003 - 0.066 (33 Å - 660 Å)	0.013 (130 Å)	(1) Mostly spherical (2) Rodlike at large sizes	Cu + Carbonitrides

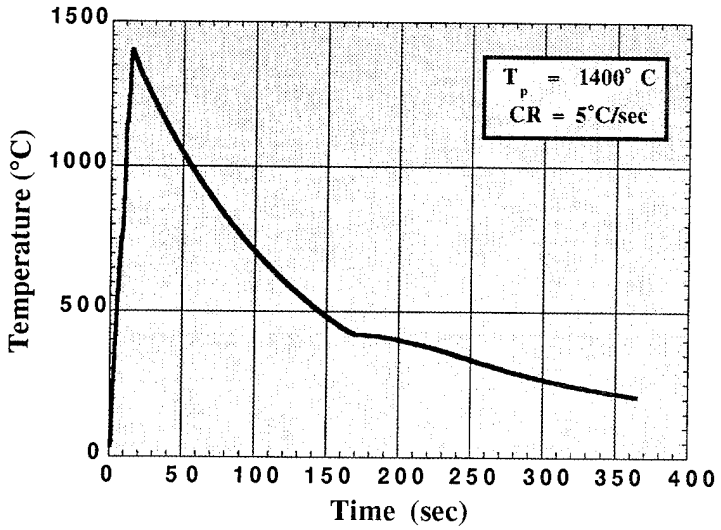

Fig. 1 — Thermal profile taken from the dilatometer during the *Tp* = 1400° C, 5° C/s cooling rate thermal cycle.

length change vs temperature data obtained during the cooling portion of each thermal cycle allows estimation of the austenite fraction transformed to other phases as a function of temperature and time. This is possible because the differences in atomic volume between austenite and ferrite (or martensite) give rise to measurable dilatations during austenite decomposition.

The microstructural changes due to the thermal cycling were systematically investigated primarily by TEM. Conventional optical microscopy studies, prior austenite grain-size measurements, microhardness measurements, and dilatometric analyses were also performed. The interrelationships among all of the observations proved to be essential to the final processing-microstructure-property relationships that we developed; the details of these relationships will now be presented.

Prior Austenite Grain Size and Microhardness Measurements

Since austenite grain size strongly affects the formation rate of ferrite and can thus affect the mechanical properties of welded materials

[1], the average prior austenite grain size of the base plate and of the thermally cycled specimens was measured (see Fig. 2). There is a small refinement of the prior austenite grain size relative to the base plate material for peak temperatures up to 900° C and a large increase in the prior austenite grain size for the 1400° C peak temperature. The cooling rate has a relatively minor effect on the prior austenite grain size. These data will be considered in more detail and correlated with the TEM and microhardness results in the next section.

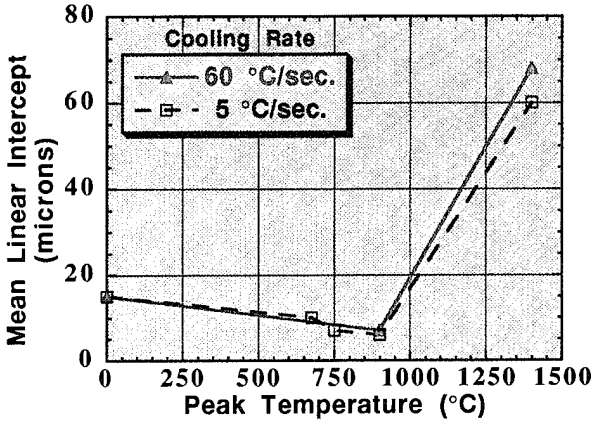

Fig. 2 — Prior austenite grain size as a function of peak temperature and cooling rate.

Figure 3 shows microhardness measurements for the base plate and the thermally cycled specimens. Unlike the prior austenite grain size, the microhardness is a function of both the peak temperature and the cooling rate. For the fast cooling rate, there is a sharp increase in microhardness with increasing peak temperature up to 900° C followed by a small drop in the microhardness between the 900° C and 1400° C peak temperatures. Alternatively, for the slow cooling rate, the microhardness drops—going from the 750° C peak temperature to the 900° C temperature—then rises again for the 1400° C peak temperature. To understand this behavior, the microhardness data must be interpreted in terms of the specific microstructural changes resulting from the thermal cycles.

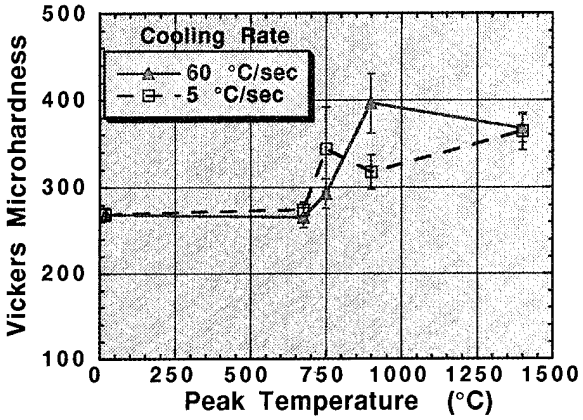

Fig. 3 — Average Vickers microhardness as a function of peak temperature and cooling rate.

Effects of Thermal Cycling on Microstructure and Correlations to Microhardness and Dilatometry Results

(1) Tp = 675° C

The microstructures corresponding to the 675° C peak temperature were essentially the same as those of the base plate, with one minor exception; the precipitates at lath boundaries coarsened slightly during the slow cooling rate cycle. This was insufficient to cause an appreciable change in microhardness. No significant volume fraction of fresh austenite was formed during the thermal treatments associated with this peak temperature, as indicated by dilatometric analysis and verified by TEM.

(2) Tp = 750° C

A major difference between the Tp = 750° C, 5° C/s cooling-rate microstructure and that of both the base plate and the Tp = 675° C specimens becomes obvious only at the TEM level of resolution; there are some regions of very low precipitate density in the former microstructure. These areas correspond to portions of the base plate that had retransformed to austenite at and near the peak temperature and then decomposed to freshly formed lath martensite (and some lath ferrite)

during the cooling portion of the thermal cycle. The copper particles also dissolved in these areas and the few precipitates that are observed are mostly undissolved niobium-carbonitrides, which have a dissolution temperature well above 750° C [3]. There are also untransformed regions in these specimens, characterized by a high volume fraction of precipitates in both the lath ferrite and the heavily tempered martensite (see Fig. 4). These precipitates are undissolved copper particles (and niobium-carbonitrides) that were present in the original base plate. Analysis of the diffraction pattern in Fig. 4 demonstrates that the structure and lattice parameter of the precipitates in this predominantly untransformed region correspond to epsilon-copper (fcc). The 60° C/s cooling rate caused much less fresh austenite formation and copper precipitate dissolution since it allowed for significantly less time at temperatures high enough to form austenite (above about 700° C).

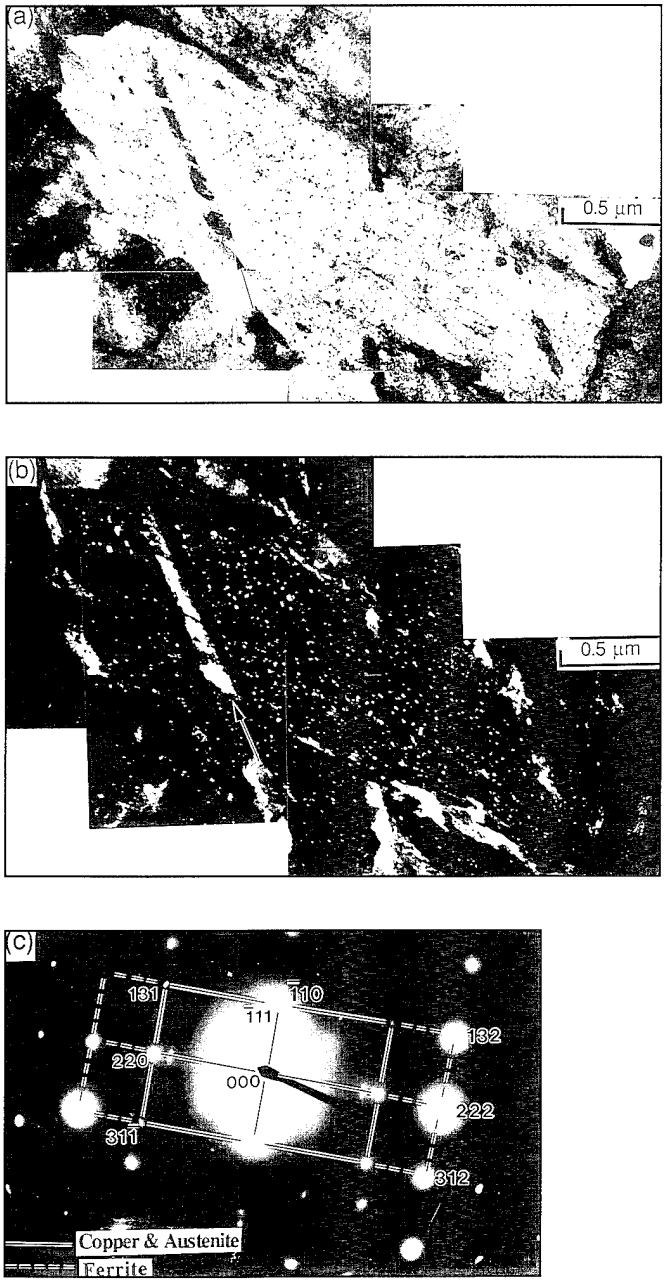

Fig. 4 — TEM micrographs of acicular ferrite containing freshly formed (and retained) austenite (arrowed) and copper precipitates in a specimen subjected to the *Tp* = 750° C, CR = 5° C/s thermal cycle: (a) bright-field micrograph, (b) dark-field micrograph taken from an austenite and an overlapping copper reflection, and (c) diffraction pattern demonstrating the Kurdjumov-Sachs orientation relationship between both the copper and the ferrite and the retained austenite and the ferrite.

Plots of the volume fraction of austenite transformed during cooling for the various thermal treatments (as determined by dilatometric analysis) are quite consistent with the TEM findings and are presented in Fig. 5. Curves corresponding to the 675° C peak temperature are not shown in this figure since the dilatometric technique could not detect fresh austenite formed in these cases. Likewise the Tp = 750° C curve for the fast cooling rate is absent from Fig. 5 because not enough fresh austenite was formed to allow for meaningful quantitative dilatometric analysis even though the length change vs temperature curve clearly showed deflections that indicated qualitatively that some fresh austenite had been formed.

For the Tp = 750° C slow-cool cycle, the TEM observations of some fresh lath ferrite and more freshly formed martensite are in complete agreement with the Tp = 750° C curve shown in Fig. 5(a). This curve indicates that about 25% of the retransformed austenite decomposed between 520° C and the M_s temperature of 420° C. This austenite could not have transformed to martensite and therefore must have decomposed to ferrite since the specimen was above the M_s temperature during this portion of the cooling cycle. The remaining 75% of austenite transformed below M_s and thus would be expected to form a majority of fresh martensite, as observed microstructurally.

The freshly formed martensite produced during both thermal cycles causes the increase in microhardness shown in Fig. 3. The hardness increase is much greater for the slower cooling rate than the faster cooling rate due to the formation of more austenite, and thus a higher volume fraction of freshly formed martensite decomposed from the austenite during the slower cooling cycle, as demonstrated by both TEM and dilatometric analyses.

(3) Tp = 900° C

The microstructure corresponding to this peak temperature is significantly different from that associated with the two lower peak temperatures. In particular, the ferrite and heavily tempered martensite matrix phases originally present in the base plate were fully retransformed to austenite during the heating portions of the thermal cycles associated with both cooling rates, as indicated by dilatometric analysis. The original copper precipitates (but not the niobium carbonitrides) dissolved during both thermal cycles, as demonstrated by TEM.

Considering first the slow cooling rate (5° C/s) treatment, the TEM results indicate that the matrix microstructure produced consists of a mixture of a majority of freshly formed equiaxed (and some lath) ferrite and a minority of lath martensite. The ferrite first begins forming at about 580° C (see Fig. 5(a)); the high transformation temperatures allow for some reprecipitation of copper within the ferrite during cooling. On the other hand, no precipitation occurs within the freshly formed martensite.

The microstructure corresponding to the fast (60° C/s) cooling cycle is significantly different from that formed during the slow cool. Austenite decomposition began at a much lower temperature, about 480° C (see Fig. 5(b)), indicating that there was less time available for ferrite formation, in agreement with the TEM observations. In particular, this microstructure consists predominantly of freshly formed lath martensite containing undissolved niobium carbonitrides and a minority of lath ferrite.

The fine austenite grain size associated with the two Tp = 900° C thermal cycles (Fig. 2) enhances ferrite nucleation since it is well known that austenite grain boundaries serve as nucleation sites for ferrite. The decrease in microhardness for the slow (5° C/s) cooling rate and 900° C peak temperature (Fig. 3) is associated with the high volume fractions of freshly formed equiaxed and lath ferrite observed by TEM and the corresponding decrease in the amount of freshly formed martensite. Alternatively, the fast (60° C/s) cooling rate results in a large increase in microhardness with increasing peak temperature (Fig. 3) since the matrix consists primarily of the harder, freshly formed lath martensite for this thermal cycle. In this case, the cooling

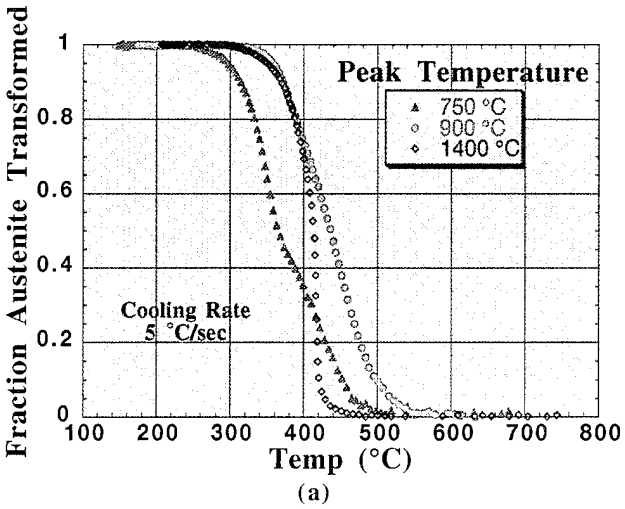

Fig. 5 — Austenite volume fraction transformed as a function of temperature during the cooling portions of the simulated HAZ thermal cycles, as determined by dilatometry. The curves correspond to various peak temperatures and cooling rates of (a) 5° C/s and (b) 60° C/s.

rate was simply too fast to allow a large amount of ferrite to form despite the fine austenite grain size.

(4) Tp = 1400° C

The thermal cycles associated with this peak temperature resulted in complete dissolution of both the matrix phases and the precipitates (including the niobium carbonitrides) to austenite, as evidenced by both TEM observations and dilatometric analysis. The prior austenite grain size was 5 to 6 times larger than that of the base plate and about 10 times larger than that of the 900° C peak temperature specimens; this is due to the dissolution of the niobium carbonitrides and the strong temperature dependence of grain growth. The large austenite grain size caused a drastic decrease in the nucleation rate of ferrite, resulting in a majority of precipitate-free, freshly formed lath martensite for both cooling rates.

A small amount of lath ferrite did form during the slow cool cycle only, beginning at a temperature of about 480° C (see Fig. 5(a)). Fine precipitates were rarely observed in either

the martensite or the lath ferrite since there was not enough time available during cooling for significant reprecipitation of niobium-carbonitrides from austenite, and copper precipitation from within the ferrite was inhibited by the low ferrite formation temperature.

The microstructure corresponding to the 60° C/s cooling rate is somewhat different from that formed during the slow cooling cycle. No ferrite was observed with TEM, and no austenite decomposition above M_s was detected by dilatometric analysis. There is a bimodal size distribution consisting of fine, precipitate-free lath martensite as the majority matrix phase and a coarser martensite as the minority constituent (see Fig. 6). As demonstrated by the multiple variants of cementite shown in Fig. 6, the coarse martensite was "autotempered" (that is, carbides precipitated) during even the relatively fast cooling portion of this thermal cycle. It has been reported that precipitation of cementite is greatly enhanced in coarser martensitic structures [4]. We also performed detailed isothermal experiments which unequivocally demonstrated that this product was indeed tempered martensite and not a diffusional microconstituent formed below M_s. Additionally two-surface optical micrographs revealed that the morphology of this coarse martensite is that of a plate and not a lath. As far as we are aware, this new microconstituent (coarse autotempered plate martensite) has never been previously reported in HSLA steels [5].

The hardnesses associated with this peak temperature are nearly the same for the two different cooling rates and are significantly greater than those of the base plate (Fig. 3) due to the abundance of freshly formed lath martensite. Although the minority constituent is different for the two cooling rates, the new autotempered coarse martensite of the fast-cooled microstructure is expected to be significantly softer than the freshly formed untempered lath martensite (and might be of comparable hardness to the lath ferrite formed in the more slowly cooled microstructure).

COMMERCIAL WELDMENTS MADE WITH NEW FILLER METALS

We extended our investigation of the HAZ of simulated welds produced under tightly controlled processing conditions to commercial weldments in which we could study both the HAZ and the fusion zones. In the case of

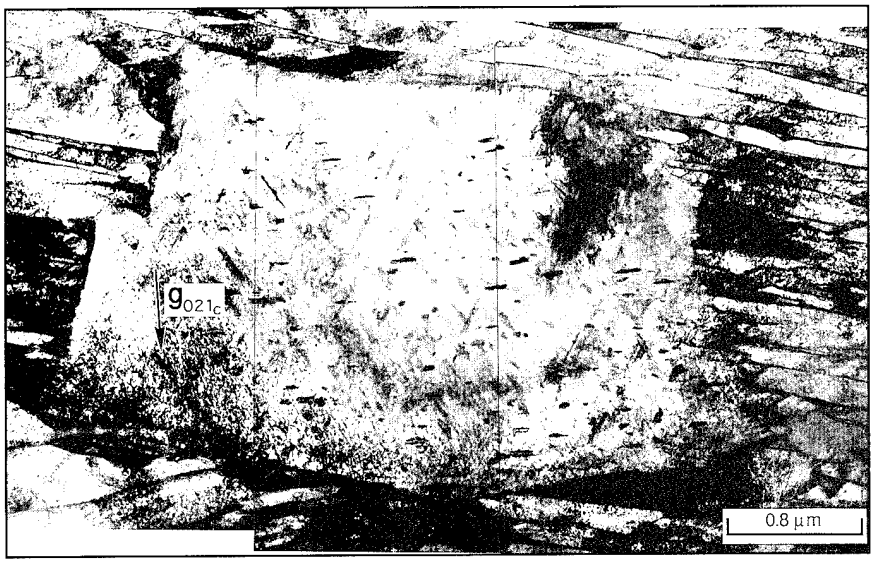

Fig. 6 — High magnification TEM micrograph showing large cementite plates within the coarse autotempered martensite formed during the *Tp* = 1400° C, 60° C/s cooling rate thermal cycle.

HSLA steels, the fusion zone is typically made with a different "filler" material, but adequate filler metals have yet to be developed specifically for these newer steels. In this study we are therefore collaborating with Concurrent Technologies Corporation (CTC), which is developing optimum filler metal compositions and weld procedures for these new HSLA steels under the Navy's MANTECH (Manufacturing Technology) Program. CTC has supplied us with HSLA-100 gas-metal arc welds (GMAWs) made with new filler metal candidates under different sets of weld conditions (heat input and preheat). They have also provided us with mechanical properties data on yield strength and impact toughness as a function of filler metal composition and weld-processing parameters. We in turn are able to develop processing-microstructure-property relationships that provide an understanding of how the filler metal composition and weld conditions affect the microconstituents and the subsequent weld properties. Another important consequence of our investigation is that the results can be used to test the applicability of some of the empirical models that CTC employs to design new filler-metal chemistries. In particular, we perform detailed microstructural and microhardness analyses and correlate these results to each other, to the weld chemistry, to the weld processing conditions, and to the strength and toughness data.

Our initial examination was on GMAWs consisting of HSLA-100 base-plate material and a new, low-alloy filler metal welded under two different sets of weld conditions: (1) no preheat, 20 to 24 kJ/cm heat input, 23 centimeters per minute (cpm) travel speed, and a maximum interpass temperature of 52° C, resulting in average cooling rates of 23° to 24° C/s, and (2) a 135° C preheat, 41 to 45 kJ/cm heat input, 13-cpm travel speed, and a maximum interpass temperature of 140° C, resulting in 6° to 6.4° C/s cooling rates. We performed detailed optical microscopy and microhardness analyses of the entire cross sections of both weldments. We developed two-dimensional color microhardness maps by taking a matrix of over 400 microhardness measurements across each weld cross section and interpolating the data on a computer. Figure 7 shows a low magnification micrograph and the corresponding microhardness map for the same weld condition. By directly overlaying transparencies of the microhardness maps over the micrographs, we are able to make a one-to-one correspondence between the weld features and variations in microhardness across the weldments. We also relate these findings to more detailed microstructural observations taken from selected regions across the weldments by higher resolution optical microscopy (500X to 1,500X magnification range) and TEM (10,000X to 250,000X magnification range).

The data indicate that the hardest regions of the GMAWs are the heat-affected zones in the base plate. The microhardness variations and preliminary microstructural observations across the HAZs agree qualitatively with the findings from our laboratory-simulated HAZ study. The softest areas lie inside the weld-fusion zone on the white arcs shown in Fig. 7(a) (and especially on intersections of multiple arcs), as demonstrated by the correspondence between the white arcs in Fig. 7(a) and the yellow regions on the microhardness map in Fig. 7(b). The white arcs correspond to regions of HAZs *within the fusion zone* that are associated with the heat transmitted to a solidified weld bead (or beads) during the subsequent deposition of another hot molten weld bead. The regions corresponding to these arcs did not become hot enough (during deposition of the subsequent weld beads) to retransform the matrix to the high temperature austenite phase. Instead any existing martensite in these regions was simply tempered, resulting in considerable softening.

The hardest areas within the fusion zone lie either just inside or directly on the bead boundaries. Since these regions experienced the fastest cooling rate after solidification, large amounts of hard, untempered martensite are expected to form from the decomposition of austenite during cooling in these areas. Additionally, because these regions lie outside subsequent HAZ arcs, the martensite in these areas should not be significantly tempered. These findings are also consistent with the results of our HAZ simulations.

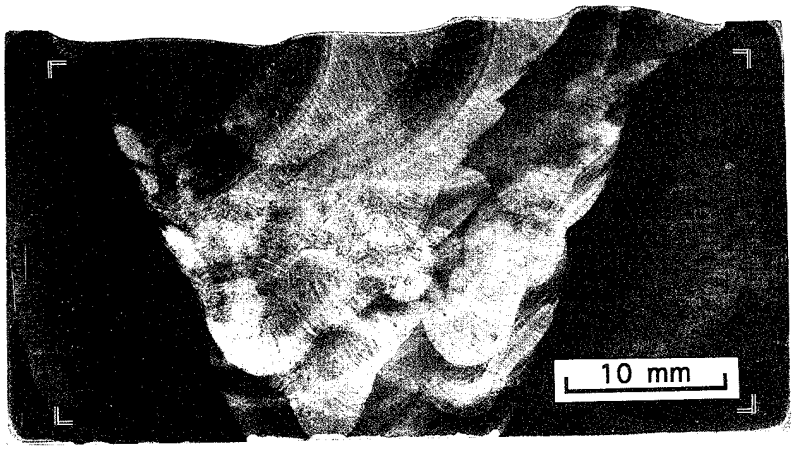

(a)

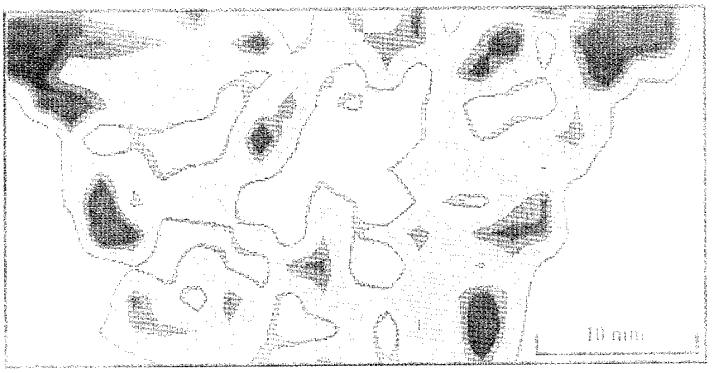

(b)

Fig. 7 — (a) Optical micrograph of transverse cross section of the low heat input gas metal arc weld; (b) corresponding microhardness map across the same transverse cross section.

Finally, the microhardness data indicate that the greatest effect of the different weld conditions (that is, the higher heat input and preheat) was the formation of a significantly softer fusion zone but that different weld conditions have very little effect on the hardness profile of the HAZ. Our microscopy studies indicate that this softer fusion zone is due to the formation of primarily soft ferrite during cooling of the high heat input weldment, as opposed to martensite, which was formed in the fusion zone of the smaller heat input weld.

SUMMARY AND CONCLUSIONS

Modern high-strength, low alloy (HSLA) steels have the potential for significantly reducing processing costs and providing excellent combinations of strength and toughness in a variety of applications, including the construction of buildings, bridges, pipelines, ships, and submarines. Since all of these applications involve the welding of structural components, it is imperative that we develop adequate weld-processing procedures and new weld-filler metals to fully realize the potential of these

advanced steels. In collaboration with the Naval Surface Warfare Center at Annapolis, Maryland, and Concurrent Technologies Corporation (a Navy MANTECH Center), we have thus transitioned our basic research programs in phase transformations and the evolution of ferrous microstructures (including an accelerated research initiative on advanced steels) to the problem of welding advanced HSLA steels for ship and submarine construction. By using transmission electron microscopy supplemented by optical microscopy, microhardness measurements, and dilatometric analysis, we have been able to establish processing-microstructure-property relationships that enhance our ability to understand and control the microstructure and mechanical properties of these steels during welding. These relationships were first established in tightly controlled laboratory simulations and are now being developed for commercial weldments. Future plans will be centered about: (1) completion of the investigation of HSLA-100 weld-fusion zones produced with new weld-filler metal candidates, (2) laboratory simulation and analysis of multipass welds, and (3) the development and dissemination of continuous-cooling-transformation diagrams for both HSLA-100 base material and new weld filler metals.

ACKNOWLEDGMENTS

Financial support from the Office of Naval Research is gratefully acknowledged. R.W. Fonda also acknowledges support from the American Society for Engineering Education. The authors are grateful to Dr. M. Vassilaros and Mr. E. Czyryka of the Naval Surface Warfare Center at Annapolis for supplying the HSLA-100 base plate and for many stimulating discussions and to Mr. Rich Green and Dr. S. Sampath of Concurrent Technologies Corporation for supplying us with the new filler metal weldments and for helpful discussions. Appreciation is expressed to Mr. Adam Matuszeski and Mr. Thad Matuszeski for assistance with the optical microscopy and microhardness measurements and to Mr. Edward Pierpoint for assistance with the photographic preparation of the figures.

The authors are also grateful to Professor G. Krauss of the Colorado School of Mines for contributions made during enlightening private discussions and to Dr. H. I. Aaronson for critically reviewing our manuscript. The authors dedicate this paper to the late Mr. W. E. King, Jr., who performed the dilatometry for this project. His quality workmanship and friendship will be greatly missed.

REFERENCES

1. K.E. Easterling, "Recent Trends in Welding Science and Technology," TWR'89, *Proceedings of the ASM International Symposium*, Gatlinburg, Tennessee, 14-18 May 1989, pp. 177-188.

2. P.W. Holsberg, J.P. Gudas and I.L. Caplan, "Recent Trends in Welding Science and Technology," TWR'89, *Proceeding of the ASM International Symposium*, Gatlinburg, Tennessee, 14-18 May 1989, pp. 593-605.

3. A.M. Sage, "Microalloyed Steels for Structural Application," *Metals Mater.*, 584-588, October 1989.

4. G. Krauss, *Steels: Heat Treatment and Processing Principles* (ASM International, Metals Park, OH, 1990).

5. R.W. Fonda, G. Spanos, and R.A. Vandermeer, "Observations of Plate Martensite in a Low Carbon Steel," *Script. Metall.* **31**, 683-688 (1994).

THE AUTHORS

George Spanos received his B.S., M.E., and Ph.D. degrees in metallurgical engineering and materials science from Carnegie Mellon University in 1982, 1985, and 1989, respectively. His dissertation topic included the study of solid state phase transformations in high carbon steels by transmission electron microscopy, optical microscopy, X-ray diffraction, and thermodynamic and kinetic modeling. He joined the staff at the Naval Research Laboratory (NRL) as a metallurgist in 1989 and is currently head of the Joining and Process Simulation Section in the Physical Metallurgy Branch. His work at NRL involves the study of phase transformations and microstructural evolution by electron microscopy, optical microscopy, X-ray diffraction, and computer modeling. His initial work was focused on phase transformations in model ferrous alloys; his current efforts additionally include developing processing-microstructure-properties relationships for the welding of advanced commercial steels and phase transformations in titanium alloys. He is author or coauthor of more than 20 publications.

Richard W. Fonda received a B.S. degree in geology and chemistry from Juniata College in 1983 and his M.S. degree in chemistry from Cornell University in 1986. He was awarded a Ph.D. degree in 1991 from the Materials Science Department at the University of Virginia. For his dissertation, he used transmission electron microscopy and interfacial computer modeling to reveal the important role of crystallography in the cellular precipitation reaction. After studying coarsening of precipitates in Al-Cu-Mg-Ag alloys in collaboration with Reynolds Metals Co., he accepted a postdoctoral position at the University of Pennsylvania to study grain boundaries and segregation using atomic resolution electron microscopy. He came to the Naval Research Laboratory as an ASEE postdoctoral fellow in 1993 and continues to work on the microstructural characterization of welded steels and shape memory alloys. Dr. Fonda has written more than 15 scientific papers.

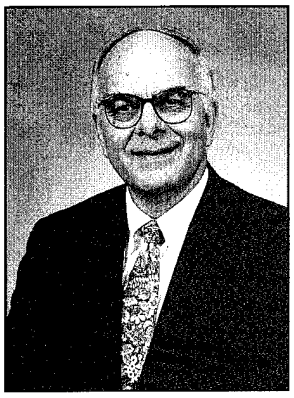

Roy A. Vandermeer earned his B.S. and Ph. D. degrees in metallurgical engineering from the Illinois Institute of Technology in Chicago, Illinois, in 1956 and 1961, respectively. His dissertation topic considered the effects of recovery and impurities on the recrystallization of zone-refined aluminum. He joined the staff of the Oak Ridge National Laboratory in 1960, where as metallurgist, group leader, and senior staff metallurgist, he continued the study of recrystallization of aluminum and began work on texture development in niobium and phase transformations in uranium alloys. In 1980, he transferred to the Oak Ridge Y-12 Plant where he was a senior development engineer. During his tenure in Oak Ridge, Dr. Vandermeer held a joint appointment at the University of Tennessee where he was a part-time lecturer and professor from 1963 until 1983. He also was appointed a visiting professor at the University of Rochester and Illinois Institute of Technology. In 1985, Dr. Vandermeer came to the Naval Research Laboratory (NRL) and for several years was head of the Physical Metallurgy Branch. He is now a branch consultant. His work at NRL involves basic research in the areas of phase transformation of steels and in quantifying microstructural evolution in a number of other physical metallurgical processes that occur by nucleation and growth. He is a member of TMS-AIME and is a Fellow of ASM International. For the past two years, he has been appointed visiting scientist at the Risø National Laboratory in Denmark. He is author or coauthor of more than 60 publications.

Pulsed-Laser Deposition of Ceramic Thin Films

Douglas B. Chrisey, James S. Horwitz, Catherine M. Cotell,
Randolph E. Treece, and Paul C. Dorsey
Condensed Matter and Radiation Sciences Division

Many important Naval systems and platforms require state-of-the-art thin films of technologically important materials. As the active elements in electronic and magnetic devices, thin films determine the electrical performance (for example, speed, input power, and signal loss) of microwave and recording systems. On the surfaces of structural materials, thin films provide resistance to mechanical, chemical, and biological degradation. The Navy has a strong interest in developing better ways to produce thin films of these materials, which range from simple to complex in composition, phase, and structure.

Advanced techniques that use high-powered excimer lasers are being developed at the Naval Research Laboratory (NRL) to deposit thin films and multilayers of complex, multicomponent materials. The processing breakthrough is called pulsed-laser deposition (PLD), and it is currently making available high-quality thin films of technologically important ceramics [1]. The properties of these materials—both structural and physical—are virtually unobtainable by more conventional physical vapor deposition techniques. Originally developed to meet the demanding challenges of processing ceramic high-temperature superconductors (HTS), such as $YBa_2Cu_3O_7$, PLD has been found to be ideally suited to the deposition of multicomponent electronic ceramics, including ferroelectrics and ferrites as well as biocompatible ceramic coatings. The production of thin films of such important materials by PLD and their emerging applications are described below.

PULSED-LASER DEPOSITION

The advantages of PLD for depositing high-quality thin films of multicomponent oxide ceramics begins with the simplicity of the experimental setup. Figure 1 shows a schematic diagram of the equipment required to deposit a thin film by PLD and a photograph of the laser-produced plume. Briefly, the focused output (laser fluence $\sim$1-2 J/cm^2) of a short-pulse (full width at half maximum $\sim$30 ns) excimer laser is used to flash-evaporate a multicomponent target. The rapid heating and evaporation of the solid by the laser results in the formation of an energetic plasma plume, which is transported through an ambient gas to the surface of a nearby heated substrate. The ability of PLD to produce films of complex materials with compositional fidelity is one of its hallmarks. The growth of the desired phase and orientation of the film is carefully controlled by the choice of substrate, its surface temperature, and the selection of background gas and pressure. Extremely high instantaneous deposition rates (up to 10^5 Å/s) and hyperthermal kinetic energy distributions of the species in the plume of evaporated material permit lower substrate temperatures for PLD when compared to other physical vapor deposition techniques. For many materials, PLD can produce single-phase, oriented thin films in situ; that is, there is no need for additional post-deposition processing. While film thicknesses of $\sim$5000 Å are most common, PLD has been used to grow films at the layer-by-layer level to 100 μm in thickness. Detailed studies of the laser-generated plasma are being conducted at NRL by using emission (vacuum ultraviolet) spectroscopy and neutral/ion mass spectrometry to identify the composition of the plasma (atom, ion, or cluster), its internal and kinetic energy distributions, and the gas phase chemistry relevant to the growth of high-quality films, some of which cannot be produced by other means.

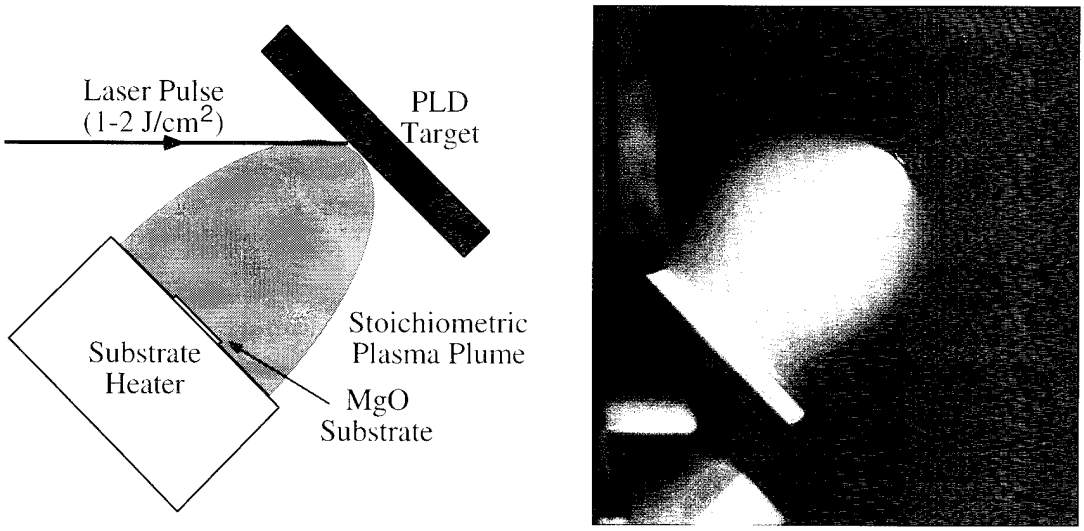

Fig. 1 — The excimer laser ablation of a $YBa_2Cu_3O_7$ target. The forward-directed plume of ejected material contains predominately neutral atoms and small molecules, ions, and electrons. The diagram shows the orientation of the laser target interaction.

HIGH T_c SUPERCONDUCTING THIN FILMS

Much of the PLD materials research at NRL has focused on the development of advanced microwave electronics based on high-quality thin films of ceramic materials. The discovery of high-temperature superconductivity renewed interest in using superconducting thin films for high-speed, low-power electronic device applications such as compact, high quality factor filters, dispersionless delay lines, and Josephson elements for high-speed, low-power switching. However realization of these benefits required a well-controlled, reliable, thin-film production technology that permits the controlled growth of superconducting thin films and multilayers. Efforts to deposit device-quality thin films and to develop electronics applications encountered a unique set of challenges because of the multicomponent, anisotropic, and reactive nature of the HTS. Similar challenges were also present for other electronic ceramics. It was the overwhelming potential of HTS electronics, however, that catalyzed the PLD breakthrough in thin-film production. PLD played a pivotal role in helping to set the unprecedented pace at which researchers at NRL and around the world produced and tested devices with HTS thin films. In particular, the success of PLD for HTS was due to the ease with which oriented and stoichiometric thin films could be reproducibly deposited in a high-pressure oxygen ambient.

Advanced microwave devices based on thin films of $YBa_2Cu_3O_7$ grown by PLD are being used in the NRL's High-Temperature Superconducting Space Experiment (HTSSE) to develop next-generation satellite communications systems. Superconducting electronics are attractive to satellite systems because they provide improved electrical performance with reduced weight, volume, and electrical input power. Satellite systems based on $YBa_2Cu_3O_7$ thin films are especially desirable because their high critical temperature ($T_c \sim 90$ K) raises the maximum operating temperature to ~ 77 K, thus reducing the cryogenic burden previously associated with the use of superconductors in space systems. The HTS devices submitted by NRL to Phases I and II of the HTSSE program are shown in Fig. 2. In Phase I, single-function devices were required, whereas in Phase II, more complicated subsystems were fabricated. For HTSSE I, PLD-deposited films on MgO substrates were used to fabricate simple passive microwave devices such as the five-pole bandpass filter shown in Fig. 2(a). The figure of merit of electrical performance in microwave devices is the microwave surface resistance R_s; this quantity is inversely proportional to the quality factor in

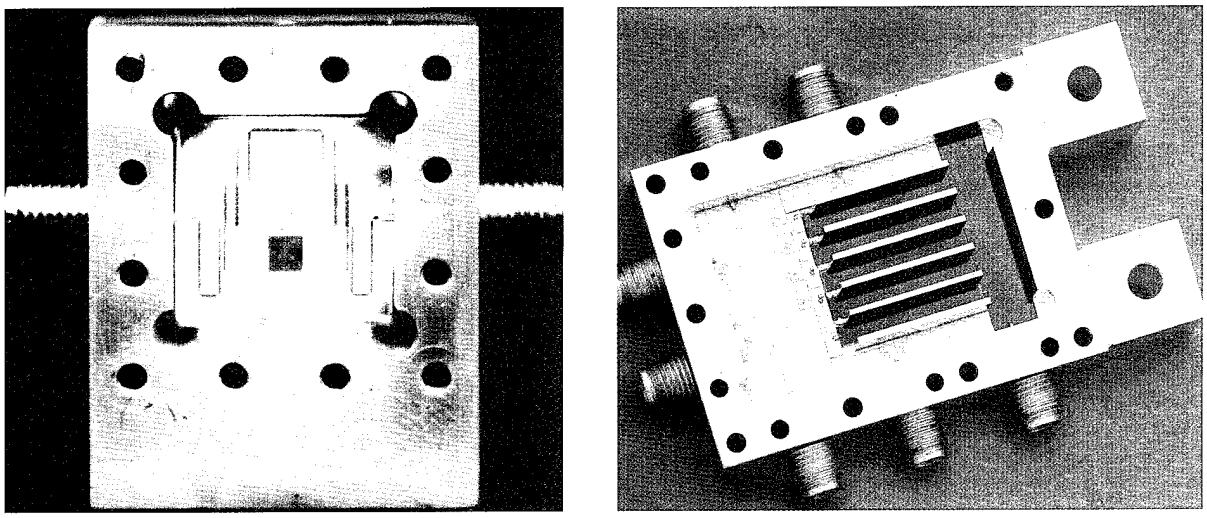

(a) (b)

Fig. 2 — The NRL HTS devices for the High-Temperature Superconducting Space Experiments (HTSSE) I and II; (a) a five-pole modified Chebychev bandpass filter designed to operate at 10 GHz on HTSSE I and (b) a channelized receiver for HTSSE II. These HTS devices are superior to conventional devices in electrical performance, size, weight, and input power.

resonant devices and directly proportional to the signal loss in transmission circuits. In addition, the electrical transport properties of $YBa_2Cu_3O_7$ are highly anisotropic, meaning that *c*-axis-oriented films are required. The bandpass filter in Fig. 2(a) is superior in electrical performance when compared to one made from conventional materials because the oriented $YBa_2Cu_3O_7$ films used in their fabrication have R_s's that are more than an order of magnitude lower at the temperature and frequency of operation. Communication satellites contain about 50 bandpass filters. A similar filter made from conventional materials is about an order of magnitude larger in size and weight. For HTSSE II, the materials requirements and the device's capability grew in complexity. The channelized receiver, shown in Fig. 2(b), represents a compact subsystem requiring high-quality HTS films to be deposited uniformly on *both* sides of a 1 in. × 1 in. × 0.010 in. MgO (100) substrate. The spatial uniformity and high quality of the superconducting properties such as the critical current ($J_c \sim 4 \times 10^6 A/cm^2$), surface resistance ($R_s$(HTS) << R_s(Cu)), and penetration depth ($\lambda \sim 1500$ Å) are important, as they directly affect the receiver's electrical design and performance. When compared to conventional channelized receivers, the HTS subsystem is advantageous because it is smaller, demonstrates higher quality factors, and can be produced at a reduced cost.

FERROELECTRIC THIN FILMS

The use of PLD to grow ferroelectric thin films was a natural extension from HTS because most of the ferroelectrics of current interest are also multicomponent oxide ceramics with a complex crystalline structure. Ferroelectrics have a wealth of interesting and useful properties because of their noncentrosymmetric crystal lattice structure, which results in spontaneous polarization. Device application areas for ferroelectric thin films include high-dielectric constant trench capacitors for high-density dynamic random access memories, nonvolatile random access memories, piezoelectric transducers, pyrolytic detectors, optical displays, and linear and nonlinear electro-optic applications. These applications for thin-film ferroelectrics have existed for many years, if not decades, but have awaited a technique capable of depositing them in an oriented and single-phase form. To meet the needs of these emerging applications, PLD has been used extensively to deposit epitaxial thin films of a number of perovskite ferroelectrics including $Pb(Zr,Ti)O_3$, $(Sr,Ba)Nb_2O_6$, $Pb_3Ge_5O_{11}$, and $(Sr,Ba)TiO_3$. In this section, we

describe a new class of active microwave devices developed at NRL based on ferroelectric thin films deposited by PLD.

Revolutionary microwave device structures are currently being developed from multilayer structures involving HTS and ferroelectric thin films. These devices make use of the active dielectric property of ferroelectrics; that is, their dielectric constant can be varied through the application of an electric field. Although the active dielectric property of bulk ferroelectrics has been known for decades, it has only been through the recent use of PLD that this property could be exploited in a thin-film device. The lack of progress in this area has primarily been a materials issue. Figure 3 shows that in a simple microstrip transmission line, the dielectric constant of a $(Sr,Ba)TiO_3$ film can be varied by 50% through the application of an electric field of 200 kV/cm (or 10 V across a 0.5-μm-thick film). All passive microwave devices based on signal transmission and resonance (including delay lines, oscillators, and filters) can now be made active by using a ferroelectric thin film as the variable dielectric because with the application of an electric field, the phase velocity in the device can be continuously varied. When compared to bulk, thin films have the added advantage that, for a given electric field, the bias voltages have been reduced from kilovolts to volts.

The ferroelectric Sr_xBa_1-$xTiO_3$ was used for this application because of its relatively low loss in the bulk state and because its Curie temperature (the temperature defining the boundary between the ferroelectric and paraelectric phases) can be continuously varied between 30 and 400 K as the Ba doping $(1-x)$ is varied between 0 and 1, respectively. With PLD, this full range of doping can be easily and reproducibly achieved through the use of targets with correspondingly different dopings. In Fig. 3, the Curie temperature occurs at the peak in the zero field curve. Controlling the Curie temperature is important since it permits the maximum tuning and device performance to be realized at or near the device operating temperature, for example, room temperature, or 77 K. In addition, $(Sr,Ba)TiO_3$ offers the potential to use $YBa_2Cu_3O_7$ as the metallization layers, as they can be grown heteroepitaxially.

An important requirement for the application of ferroelectrics in microwave devices is low dielectric loss. Dielectric loss degrades the quality factor and thus the electrical performance of a microwave device. Unusually high dielectric losses, as compared to conventional dielectrics, could preclude the use of $(Sr,Ba)TiO_3$ in active microwave devices. The dielectric loss tangent values of PLD-deposited $(Sr,Ba)TiO_3$ has been measured by cavity perturbation techniques to be as low as 10^{-3}. This

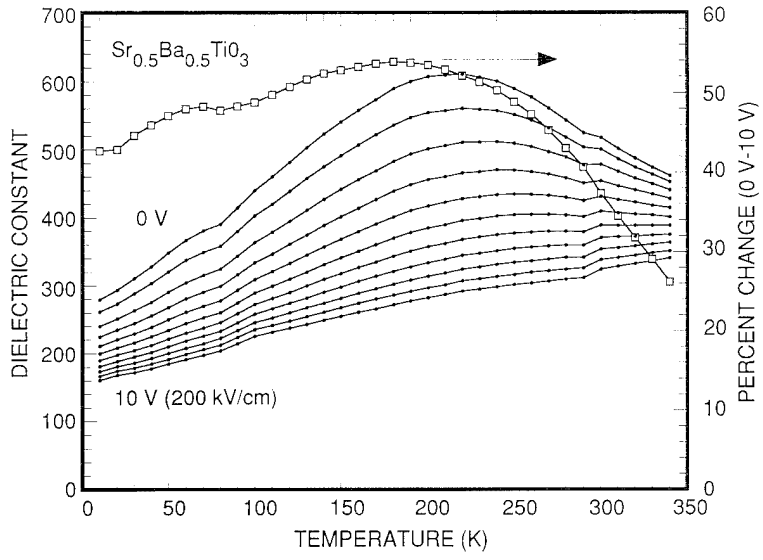

Fig. 3 — The dielectric constant for a $Sr_{0.5}Ba_{0.5}TiO_3$ ferroelectric thin film vs temperature for several applied voltages. These data illustrate the active dielectric property on which an entirely new class of microwave devices will be based. On the right is plotted the percent change in the dielectric constant between 0 and 10 V bias.

is one of the lowest values ever measured for a ferroelectric thin film. To find the origin of this low loss, one has to look no further than the X-ray diffraction pattern indicating the high crystalline quality. PLD-deposited (Sr,Ba)TiO_3 thin films exhibit true single-crystal morphology. The structural quality of a deposited film is reflected in the full width at half maximum (FWHM) of the X-ray rocking curves. Figure 4 shows that X-ray rocking curves for the (Sr,Ba)TiO_3 film (002) and the $LaAlO_3$ substrate (024) reflection measured with 8 keV monochromatic synchrotron radiation gave the FWHM to be 72 arc seconds and 36 arc seconds, respectively. Despite the large mismatch between the (Sr,Ba)TiO_3 and the $LaAlO_3$ substrate of $\sim 4\%$, the rocking-curve width is comparable or better than semiconductor films grown by molecular beam epitaxy. Low dielectric loss and high crystalline quality films like these mean that PLD may gain acceptance as an industrial electronics coating technology for microwave and other electronic devices.

FERRITE COATINGS

Ferrites are oxide materials that are good insulators with high magnetic permeability. Structurally, ferrites are composed of magnetic and nonmagnetic ions, which lie in the interstices of a close-packed oxygen lattice and can be generally classified into three categories according to their crystal structure: garnets, spinels, and hexagonals. In general, the spinels exhibit a larger magnetic anisotropy field than garnets, but the magnetic anisotropy values for both classes of ferrite are relatively small when compared to the hexagonals. For this reason, the spinels and garnets are called soft ferrites while the hexagonals are called hard ferrites (for example, a permanent magnet).

The two primary applications of ferrite thin films are magnetic recording (disk media and read/write heads) and microwave devices (circulators, isolators, filters, and resonators). Microwave devices make use of the high permeability and high resistivity of ferrites to perform control and processing functions on microwave signals. The operation of microwave ferrite devices depends on the strong coupling of an electromagnetic wave to the individual ferrite magnetic moments as the wave passes through the ferrite, but at the same time, ferrites are low-loss materials, so the electromagnetic wave undergoes minimum attenuation.

Presently most commercial ferrite microwave devices use bulk single crystal or polycrystalline ferrites, but with the relatively recent advent of monolithic-microwave-integrated circuits (MMIC), there has been renewed interest in developing ferrite thin-film deposition techniques. The use of ferrite thin films offers considerable advantages over bulk technology since bulk ferrite microwave devices constitute

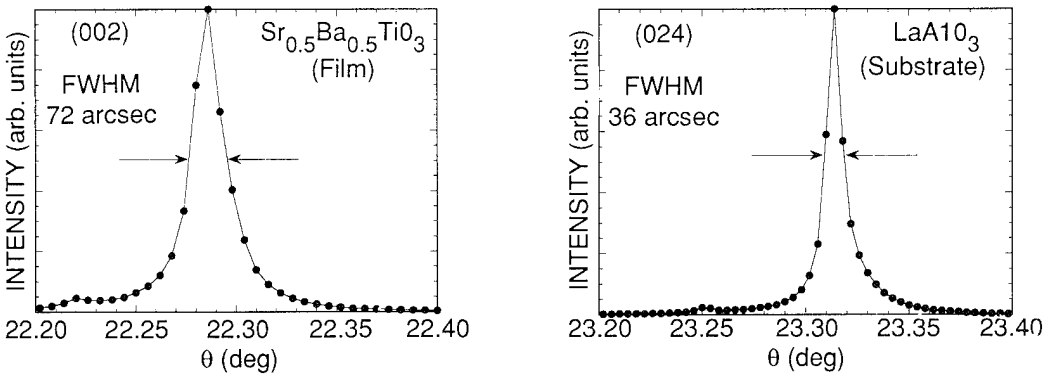

Fig. 4 — X-ray rocking curves for the (Sr,Ba)TiO_3 film (002) and the $LaAlO_3$ substrate (024) reflection measured using a high-resolution, four-circle diffractometer with synchrotron radiation (8 keV) on the NRL beam line at the National Synchrotron Light Source at Brookhaven National Laboratory. These indicate the high crystalline quality of PLD ferroelectric films.

a disproportionate amount of the total cost, weight, and size of microwave systems. In addition, thin-film technology increases the reliability and reproducibility of devices. Ideally, deposition of ferrite films would be compatible with GaAs and Si semiconductor processing techniques so that the ferrite films could be incorporated with electronics technology.

The requirement for polycrystalline, oriented-polycrystalline, or single-crystal ferrite films in microwave applications depends on the specific device. However in many applications, high-quality single crystals are required to minimize the magnetic losses and to provide a uniform crystallographic direction throughout the ferrite so that the magnetocrystalline anisotropy can be used to maximum advantage. For example, the large uniaxial magnetic anisotropy field of the hexagonal ferrites provides a self-bias for these materials so that they can be used in the millimeter-wave range with little or no external magnetic biasing.

Ferrite films have been grown using a wide range of techniques, including radio frequency and ion-beam sputtering, chemical vapor deposition, and liquid-phase epitaxy; however PLD-grown ferrite films have magnetic and structural properties superior to those of ferrite films grown by using other techniques. Unlike other techniques, PLD can be applied to a wide range of ferrite materials. For example, PLD of MnZn-ferrite and barium hexaferrite from the spinel and hexagonal categories, respectively, are typical of some ferrite materials grown using PLD. The PLD MnZn-ferrite films (1 μm) were grown epitaxially on single-crystal (100) MgO substrates in the range of 400° to 800° C and were found to have magnetic properties in good agreement with the bulk ferrite. Barium hexaferrite films (0.5 μm) grown using PLD on single-crystal *c*-plane (0001) sapphire substrates at 900° C were also found to be epitaxial, with the *c* axis oriented normal to the substrate. Figure 5 shows the magnetic hysteresis curve for a PLD barium-hexaferrite film. The film is well oriented and has high values for both bulk saturation magnetization ($4\pi M_S \sim$ 4400 G) and uniaxial magnetic anisotropy field ($H_A \sim$ 1700 G). The film saturates easily when a magnetic field is applied along the *c* axis (easy axis) but requires a large externally applied magnetic field to saturate in the plane because of the large magnetocrystalline anisotropy field along the *c* axis. In addition, the ferrimagnetic resonance (FMR) line width (ΔH) for PLD barium hexaferrite (see inset in Fig. 5) is as narrow or narrower than the line width of bulk single-crystal barium hexaferrite spheres. In general, a narrow FMR line width indicates relatively small magnetic losses. These examples demonstrate the high quality and wide range of ferrite films that can be achieved using PLD.

One of the more important issues to be addressed in the development of a technique for

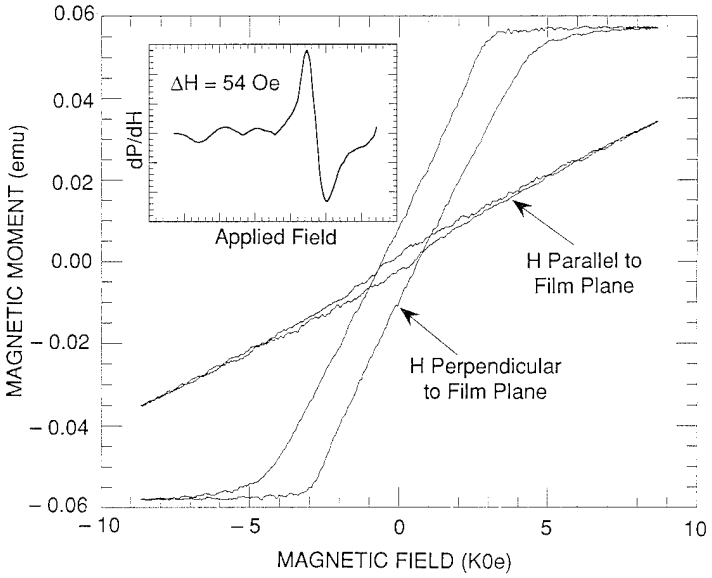

Fig. 5 — Magnetization hysteresis curves for the in-plane and out-of-plane components of an epitaxial $BaFe_{12}O_{19}$ ferrite thin film on (0001) Al_2O_3. The inset is the ferrimagnetic resonance measured at 85.7 GHz. The narrow linewidth of 54 Oe is comparable to the best bulk single-crystal values and indicates small magnetic losses.

ferrite-film microwave devices is the growth of thick ferrite films. For most microwave devices, films in the range of 25- to 100-μm thick are needed to keep device factors such as insertion loss at a minimum. At present, research is progressing on the deposition of thick ferrite films using PLD since the magnetic and structural properties of PLD ferrite thin films have proved to be in good agreement with the bulk. PLD of barium hexaferrite and MnZn-ferrite at NRL and YIG at Westinghouse has reached 20, 30, and 100 μm, respectively, while still maintaining the good structural and magnetic properties that are necessary for practical devices. The 20-μm barium hexaferrite films are especially noteworthy as the orientation was maintained throughout this thickness. Furthermore, the MnZn and YIG films can be grown at substrate temperatures low enough to make these materials truly compatible with MMIC technology. Based on these results, PLD promises to be a truly revolutionary technique for growing high-quality, thick-ferrite films.

PLD SYNTHESIS OF METASTABLE NITRIDES

In addition to depositing thin films of complete materials, PLD is also being used to synthesize new materials. Traditional synthetic approaches to solid-state chemistry, for example, use high temperatures for long reaction times to overcome diffusion limitations. These high-temperature methods usually result in the formation of thermodynamically stable phases. A considerable effort is being spent to develop synthetic methods that permit control over product phase formation to include metastable structures. Currently PLD is being developed as a new ***synthesis*** method for the formation of metastable compounds so that their intrinsic properties can be evaluated and incorporated in future device applications. With its unique nonequilibrium evaporation process, PLD may prove to be the only method to produce some metastable compounds and structures that cannot be formed by ordinary chemical methods.

We have applied PLD to the growth of thin films of various technologically important nitrides of carbon, boron, and molybdenum. Phase pure nitrides are particularly hard to synthesize due to the extremely nonreactive nature of nitrogen gas (as compared to oxygen), which is a common vacuum-deposition contaminant. Some of the applications for nitride thin films include high-speed superconducting electronics and bolometers (MoN and NbN), wide band-gap semiconductors (c-BN, GaN, and AlN), and hard, wear-resistant tribological coatings (β-C_3N_4 and c-BN). In fact, β-C_3N_4 is theoretically predicted to be as hard as diamond. The growth of the nitrides of niobium (NbN_x) by PLD proved to be particularly interesting as the synthesis of a new, previously unreported, phase of NbN was achieved. This and the PLD of NbN_x are summarized below.

Thin films of NbN_x were prepared by PLD of Nb in N_2/(10%) H_2 ambient onto (100) MgO substrates held at a deposition temperature of 600° C. By increasing the N_2/H_2 pressure in the deposition system, the phase of the deposited film could be varied from pure Nb to Nb_3N_4; intermediate phases included Nb_2N and NbN. X-ray diffraction, Rutherford backscattering, and resistivity vs temperature curves confirmed these assignments. At 60 mTorr, the deposited films were identified by X-ray diffraction as cubic NbN, which is highly textured in (100) orientation with the substrate—the well known rock-salt (B1) phase of niobium nitride. The X-ray diffraction pattern also contained odd (h00) reflections indicative of a primitive cubic distortion from the rock salt NbN unit cell. Based on their structural characteristics as revealed through the XRD patterns, the NbN films deposited at 60 mTorr and at a series of temperatures could be separated into two categories: those representative of the expected face-centered cubic (fcc) lattice and those of the primitive-cubic (PC) lattice.

The observation of the PC lattice, a new phase of NbN, was confirmed in an oscillation X-ray photograph, as shown in Fig. 6. Two sets of diffraction spots are present—one set from the single crystal MgO substrate and the other set from the deposited PC-NbN film. The presence of spots for the PC-NbN, instead of arcs or rings, indicates that it adopts heteroepitaxial

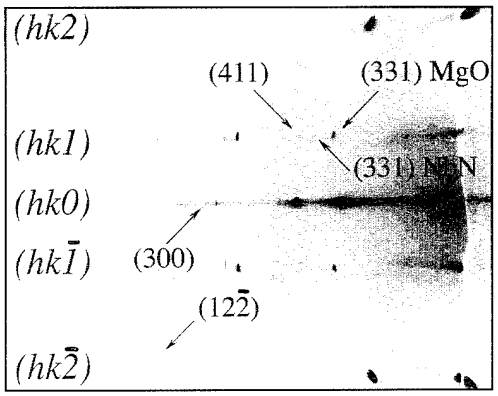

Fig. 6 — Oscillation X-ray photograph of PC-NbN film on (100) MgO substrate. The diffraction planes and selected reflections are indicated. Note the (300), (411), and (122) diffraction spots of the NbN film, which is characteristic of the primitive cubic phase.

orientation in the *a-b* plane, as well as in the *c* direction. Each substrate spot also is associated with a film diffraction spot. The difference between the fcc lattice of the substrate and the PC lattice of the film is indicated by the additional spots corresponding to the (300)-reflection in the zero layer, the (411)-reflection in the first layer, and the (12$\bar{2}$)-reflection in the second layer. The (331)-reflections for both the MgO substrate and NbN film also are indicated for reference.

The PC-NbN phase only could be synthesized at substrate temperatures between 400° and 650° C. Otherwise the films were highly (h00) oriented in the B1 phase. The PC-NbN films showed $T_c(R = 0) \approx 16.4$ K values, which exceeded the fcc-NbN films by greater than 0.5 K. This is one of the highest T_c's reported for a NbN film that is free of carbon impurities (known to raise T_c in NbN). In addition, the transition widths were sharper for the PC phase (~ 0.2 K) than for the fcc material (1 to 3 K). The PC phase also displayed a metallic dependence of resistivity above T_c while the fcc phase showed an activated temperature dependence. The room-temperature resistivity was the same for both phases (~ 50 $\mu\Omega$-cm). The J_c measured by inductive methods for a PC-NbN film was 7.1 MA/cm^2 at 4.2 K. The superior electrical transport properties of PC-NbN demonstrate that PLD can be used to discover new and metastable materials in thin-film form. Continued study of the novel physical properties of these exciting materials will permit their development into practical devices.

BIOCOMPATIBLE MATERIALS

In addition to thin films for electronic devices, PLD has been used to deposit coatings that enhance the performance and functionality of other materials. One example of such a coating is calcium hydroxyapatite (HA), the primary mineral constituent of bones and teeth. Hydroxyapatite is one of the most biocompatible materials known and has been used as a coating on orthopedic and dental implants made of titanium or cobalt-chromium alloys to promote natural bone-bonding to these devices. The coated devices take advantage of the biocompatibility of the coating and the mechanical integrity of the substrate metal. Figure 7 is a schematic diagram of the implantation orientation of a total hip prosthetic device showing those areas of the device that are in direct contact with the host bone. Hydroxyapatite coatings into which bone may grow and bond naturally may eliminate the need to use cements to fix the device to the existing bone and may minimize the incidence of corrosion products that result from direct contact of the metallic device with body fluids. Since wear debris from cements and corrosion products are the primary sources of tissue irritation and inflammation associated with implants, HA coatings may enhance the healing process, reduce convalescence times, and extend the useful life of a prosthesis.

Hydroxyapatite, a hydrated calcium phosphate with chemical formula $Ca_{10}(PO_4)_6(OH)_2$, can be difficult to deposit in thin-film form. Most thin-film deposition methods involve high-temperature and high-vacuum conditions, which typically result in coatings that consist, at least in part, of dehydrated calcium phosphates such as tricalcium phosphate or tetracalcium phosphate. Amorphous calcium phosphates are also commonly found as contaminants in coatings of hydroxyapatite. Pulsed-laser deposition offers a distinct advantage for deposition of hydroxyapatite, namely, the ability to deposit the coatings in reactive gas environments such as water vapor. By depositing HA in a water vapor-

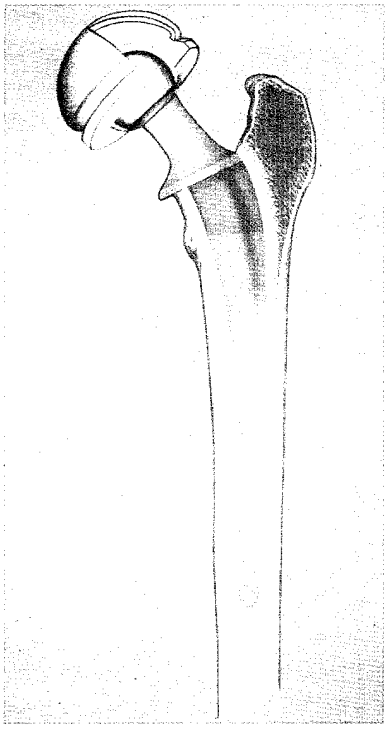

Fig. 7 — The implantation orientation of a total hip prosthesis showing areas of contact between the metal device and bone.

enriched gas environment, the OH groups are retained on the molecule. The X-ray diffraction patterns in Fig. 8 show that PLD coatings of HA are highly crystalline and free from other phases. Conditions of substrate temperature and gas environment for PLD have been identified which will produce coatings that are either amorphous or consist of other calcium phosphate phases. Since the bioresorbability of calcium phosphate coatings (rate at which a coating will dissolve in the body) is a function of their crystallinity and phase, the identification of conditions for PLD that will produce a range of phases makes the technique a powerful one for designing coatings that will match the body's natural rates of healing. For dental applications, PLD has an additional advantage. If fluorine gas is introduced during the deposition, then fluorinated apatite (fluroapatite) is formed.

In collaboration with colleagues at SUNY-Buffalo, NRL researchers have studied the kinetics of dissolution of HA coatings deposited by PLD and compared these results to those for dissolution of plasma-sprayed HA coatings. Plasma spraying is the technique that is used commercially to manufacture HA-coated prosthetic devices. Crystalline PLD HA samples remained undersaturated with respect to HA throughout the preconditioning phase of these studies when the samples were exposed to a saline solution until the surfaces reached equilibrium. The undersaturation indicated that only very small amounts of coating were released from the crystalline PLD HA surfaces. Plasma-sprayed coatings showed much higher release of calcium and phosphate during preconditioning. Furthermore, compared to plasma sprayed coatings of HA, the PLD coatings showed fewer decomposition products and dissolved at much slower rates in the dissolution phase of the studies when the samples were allowed to dissolve while the solution was maintained at a constant pH and calcium-ion concentration. These studies confirm that PLD HA coatings are more pure and free from contamination by other crystalline or noncrystalline phases than plasma-sprayed coatings and suggest that the surfaces are more uniform as well.

The availability of highly crystalline, pure, uniform HA coatings has led to fundamental research into the interaction of various cells with these surfaces. In particular, a recent study by NRL scientists in collaboration with the Biomedical Bioreactivity Characterization Laboratory at UCLA's Medical Center has concluded that macrophage cells—the giant cells generated by the body when a foreign object is introduced—will attack amorphous calcium phosphate coatings preferentially over crystalline coatings. The observation of attack of these coatings by macrophage cells implies that macrophages are capable of osteolysis (the breakdown of bone tissues) and that aseptic loosening of implant materials is not merely a physiological bone remodeling process involving only osteoclasts—the cells responsible for bone resorption—but is, at least, in part, an inflammatory reaction.

In addition to the deposition of coatings for orthopedic and dental implants, PLD has recently been used to deposit coatings on silicone rubber tubing for use in percutaneous catheters.

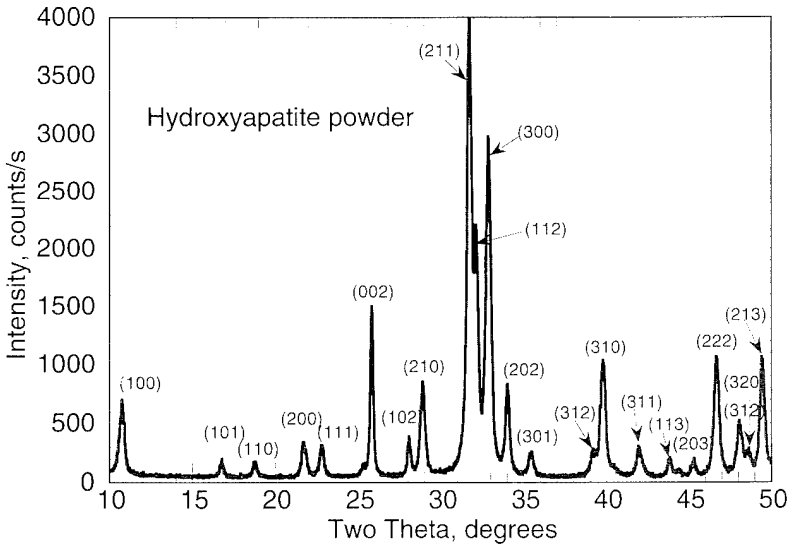

(a)

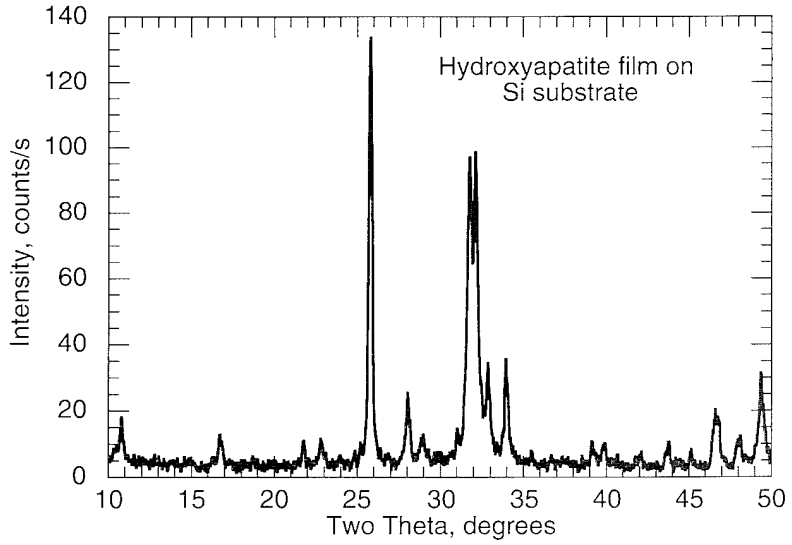

(b)

Fig. 8 — X-ray diffraction patterns for (a) a pressed powder pellet of hydroxyapatite ($Ca_{10}(PO_4)_6(OH)_2$) and (b) a thin film of hydroxyapatite deposited by PLD on a Si substrate. These data indicate the high quality of hydroxyapatite films produced by PLD.

NRL scientists hold a joint patent with a nephrologist at Lenox Hill Hospital in New York City for a catheter design incorporating HA coatings deposited by PLD. The location where catheters exit the skin is a frequent site of infection since skin will not bond to silicone rubber, and the exit site is, therefore, always effectively an open wound. Skin will, however, form a sterile bond to hydroxyapatite, and clinical studies have shown that threading a catheter through a spool of bulk ceramic hydroxyapatite results in fewer exit-site infections. Thin-film coatings of HA on catheter tubing offer a less invasive method of using HA because the flexibility of the tubing is not sacrificed. While the coatings will crack when bent, as expected for a ceramic material such as HA, they remain adherent to the tubing. In vivo testing of the efficacy of this approach for reducing the incidence of infection resulting from percutaneous catheters is under way.

The study of PLD of HA coatings has progressed from an investigation of the materials-processing structural/property relationships for this system to adapting it for particular applications. In addition, the flexibility of the technique with regard to deposition of various different calcium phosphate phases has allowed its use in basic studies of the kinetics of dissolution of these materials and cell interactions with these surfaces.

FUTURE PROSPECTS FOR PLD

Future studies of PLD of thin films can be grouped into two categories—research applications and industrial acceptance. For research applications, the future for PLD is very bright. University, industrial, and government laboratories are increasingly using PLD to meet their research needs for high-quality thin films of complex ceramics [1]. As new ceramic materials are discovered, such as the Hg-based HTS materials with T_c's approaching 160 K or the new colossal magnetoresistant materials with magnetoresistances of 10^5%, PLD can be used to rapidly ascertain the inherent single-phase properties. New application areas for PLD as a coating technique include: coating optical fibers and other nonplanar objects, characterization and explanation of the unique properties of the laser-produced plasma, and particle-assisted PLD in which ion beams are employed in concert with PLD. Industrial acceptance of PLD will be slower but seems quite certain. For a new technology to be accepted by industry, it must either do something at a reduced cost or perform a function that cannot be accomplished otherwise. Regarding the former, the capital investment of PLD is comparable to other industrial physical-vapor-deposition techniques, material use is greater, and film-to-film deposition time is much faster than competing methods. Unfortunately, there has been no overwhelming cost advantage to using PLD for industrial coatings. For the latter, there has not yet been the "market pull" vs a "technology push" required to take full advantage of PLD's unique capabilities. However the ability of PLD to produce materials otherwise unobtainable should result in the successful commercialization of this technique.

ACKNOWLEDGMENTS

The PLD program at NRL and the information presented in this article have had many important contributors: K.S. Grabowski, R.C.Y Auyeung, C.A. Carosella, G.K. Hubler, F. Smidt (posthumous), and R.E. Leuchtner, from the Surface Modification Branch; E.L. Skelton and S.B. Qadri, from the Dynamics of Solids Branch; J.M. Pond, H.S. Newman, and C. Rauscher, from the Electronics Science and Technology Division; and M.S. Osofsky, P. Lubitz, F. Ratchford, and V.C. Cestone, from the Materials Science and Technology Division.

REFERENCE

1. *Pulsed Laser Deposition of Thin Films*, edited by D.B. Chrisey and G.K. Hubler (Wiley, New York, 1994). ■

THE AUTHORS

Douglas B. Chrisey received a B.S degree in physics from the State University of New York at Binghamton in 1983 and a Ph.D. degree in engineering physics from the University of Virginia in 1987. He joined the Naval Research Laboratory as an Office of Naval Technology postdoctoral fellow in 1987, investigating radiation effects in thin films of high-temperature superconductors. Dr. Chrisey became a staff member in 1988 and is currently the head of the Plasma Processing Section of the Surface Modification Branch. As a staff member, his research at NRL has focused on the deposition of thin films of ceramics by pulsed-laser deposition and their application in electronics. He has authored more than 70 scientific papers, has given 10 invited presentations, edited a handbook on the pulsed-laser deposition of thin films, and has won three Alan Berman Research Publication awards.

Catherine M. Cotell received a B.A. degree in chemistry from Wellesley College and M.S. and Ph.D. degrees in metallurgy and materials science, respectively, from the Department of Materials Science and Engineering at the Massachusetts Institute of Technology. After 2 years as a member of the technical staff at AT&T Bell Laboratories, Dr. Cotell joined the Surface Modification Branch in the Condensed Matter and Radiation Sciences Division at the Naval Research Laboratory in 1990 as a research metallurgist. Her present research interests lie in the development of processing techniques, including pulsed-laser deposition (PLD), for the fabrication of biocompatible materials. She holds two patents relating to the use of PLD for biological and medical applications. She has published over 30 scientific papers and 2 book chapters on PLD and other surface modification techniques, has delivered 9 invited lectures on these topics, and has recently completed coediting the *ASM Handbook on Surface Engineering*. She is a member of the Materials Research Society, the Society for Biomaterials, and Sigma Xi.

James S. Horwitz is a research chemist in the Surface Modification Branch in the Condensed Matter and Radiation Sciences Division. He received a B.S. degree in chemistry from the University of New Mexico and a Ph.D. degree in Chemistry from the University of California at Santa Cruz, investigating the primary photochemical processes in visual transduction. Prior to becoming a staff member at the Naval Research Laboratory in 1989, Dr. Horwitz was a National Research Council Fellow at NRL, investigating plasma etching of semiconductors using resonance-enhanced multiphoton ionization/mass spectrometry. Dr. Horwitz's current research interests involve mechanistic investigations of the laser-solid interaction relevant to the pulsed-laser deposition of thin films and pulsed-laser deposition of single and multicomponent thin films for electronic applications. He has coauthored more than 60 papers for refereed scientific journals.

Randolph E. Treece received a B.S. degree in chemistry with departmental honors from the California State University at Los Angeles (1987) and a Ph.D. degree in inorganic chemistry from the University of California at Los Angeles (1992). His research interests have focused on the interface between chemistry and materials science and physics. As a graduate student at UCLA, Dr. Treece developed and patented a rapid, low-temperature synthetic approach to "III-V type" semiconducting and magnetic materials. After graduation, he lectured freshman chemistry at UCLA and began a postdoctoral research collaboration. There Dr. Treece prepared thin films of amorphous Sn_xSi_{1-x} alloys by laser ablation and characterized their potential for infrared detectors. Dr. Treece is currently an NRC postdoctoral research associate at NRL, where he has several projects, including growing thin films and characterizing super-hard carbon nitride, light-emitting nanocrystalline silicon, and a new phase of superconducting niobium nitride. While an undergraduate, Dr. Treece participated in Track and Field and earned All-America status in the hammer throw at the NCAA National Championships in 1987. Dr. Treece has more than 60 publications, patents, and presentations.

Paul C. Dorsey received a B.S. degree in applied physics from Xavier University, Cincinnati, Ohio, in 1986, an M.S. degree in physics from Michigan State University in 1988, and M.S. and Ph.D. degrees in electrical and computer engineering from Northeastern University in 1992. While preparing for his M.S. degree at Northeastern University, he worked on composite dielectric materials at the Army Research Laboratory in Watertown, Massachusetts. His Ph.D. research was conducted in the Microwave Materials Laboratory and focused on the deposition and characterization of ferrite thin films and high-temperature superconducting thin films using pulsed-laser deposition. He joined the Naval Research Laboratory as an ASEE postdoctoral fellow in 1993. He has published over 20 papers in the area of materials for microwave devices and is currently working on the incorporation of ferrite films with microwave integrated circuits and characterizing colossal magnetoresistance films.

Naval and Commercial Applications of Acoustic Scattering from Fish

C.H. Thompson, R.W. Nero, and R.H. Love
Acoustics Division

Many marine fishes contain air-filled sacs, called swim bladders. The primary function of a swim bladder is to enable fish to achieve near neutral buoyancy. It can also be an aid in hearing. When swim bladders are struck by acoustic energy of the proper frequency, they resonate, scattering sound in all directions. If the resonance frequencies of a sufficient number of fish are close to the operating frequency of a naval active sonar system (that is, a sonar that transmits a signal and then listens for a return), the scattered sound, called reverberation, can mask an echo from a submerged target. Although acoustic scattering by fish can be detrimental to naval operations, it is beneficial to commercial and recreational fishermen who use small, high-frequency sonars to locate fish.

Measurements and Modeling: NRL has been advancing the understanding of acoustic scattering from fish to enable the Navy to predict expected levels of biological reverberation for system development and operational purposes. Since 1988, we have conducted 10 experiments using broadband low-frequency sources and receivers to measure biological reverberation in different parts of the world. In each experiment, we measure volume scattering strength S_v (defined as the ratio of sound scattered from a unit volume of water to that incident upon it) as a function of depth, frequency, location, and time of day. The measurement technique uses small explosive charges detonated just below the surface as sources of sound and a downward-looking receiver lowered just below the ship's hull. Sound scattered back from fish is recorded and processed to produce color plots of S_v versus depth and frequency, as shown in Figs. 1(a) and (b). What appears to be intense scattering near the surface is actually the explosion; reverberation data begin at about 50 m. Figures 1(a) and (b) show two distinct scattering layers; integrating over the depth of these layers produces layer scattering strengths S_L, which we compare to model results.

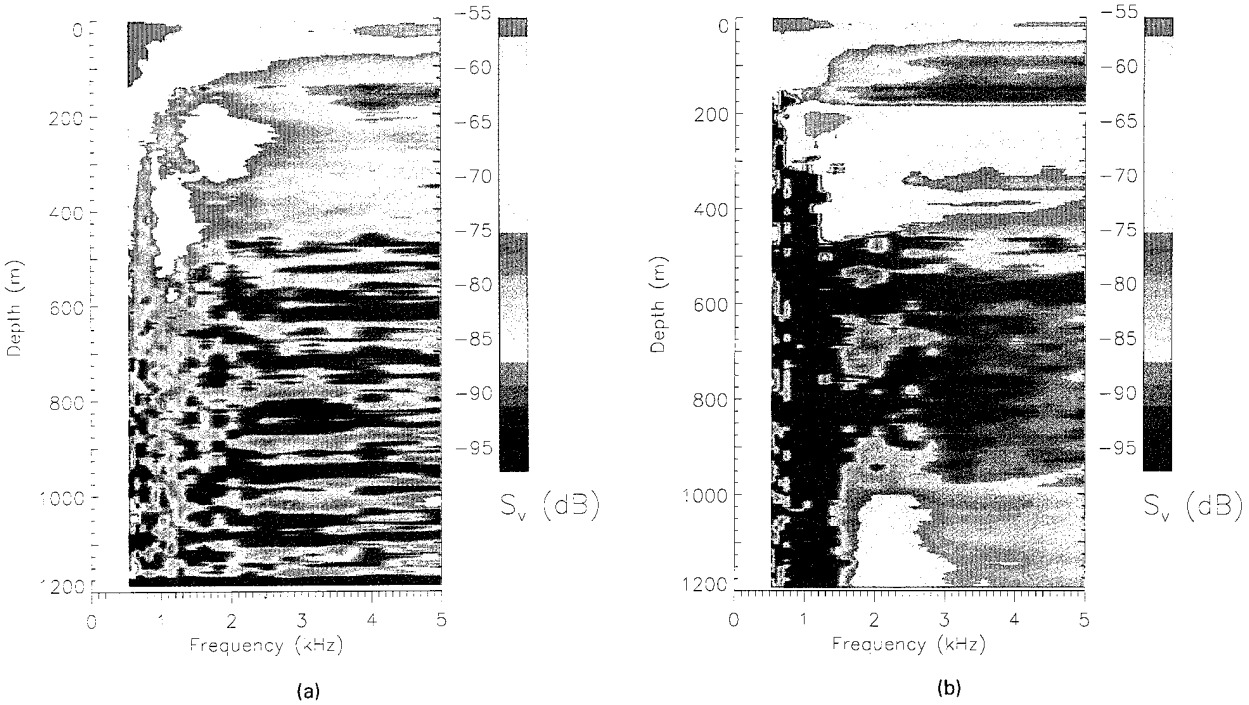

Fig. 1 — Volume scattering strengths S_V as a function of frequency and depth measured (a) in the Norwegian Sea and (b) off the coast of Oregon.

NRL has developed a theoretical model of swim-bladder scattering that calculates the scattering from individual fish and determines S_L by summing scattering from all fish in the layer [1]. The shape of an S_L versus frequency curve depends on size and depth distributions of fish in the layer, and the level of the curve depends on the density of fish in the layer. We use the model to predict and then to verify experimental results. Measurement and model results have been found to agree well for several well-known commercial fish populations. Conversely we can use the model in combination with our reverberation measurements to determine sizes and numbers of fish; this technique has been able to provide important information on fish stocks for which limited fisheries information is available.

Norwegian Sea: Figure 1(a) shows results from a location in the central Norwegian Sea. The shallower layer (between about 150 and 350 m) has a resonance peak between 1.5 and 2 kHz. The deeper layer (between about 300 and 600 m) peaks near 1 kHz.

We conducted an extensive study of fisheries' information for the region prior to the measurements. This study, which included discussions with researchers in several countries, concluded that blue whiting would be the only significant low-frequency scatterer in the experimental area [2]. Using fisheries data on blue whiting sizes and measured layer depths in the swim-bladder scattering model showed that blue whiting, at a density of 0.008 individuals/m^2, would produce the shallower layer (Fig. 2(a)). However blue whiting are not large enough to produce a 1 kHz resonance at 300 to 600 m, so a search was conducted for another possible scatterer. A re-examination of the fisheries' information indicated that redfish, which are normally considered to be near the bottom on the continental slope, have been found to occur pelagically in very deep waters. Modeling showed that redfish, at a density of 0.004 individuals/m^2, could produce the deeper layer (Fig. 2(a)). The fisheries researchers had not mentioned redfish for two reasons: (a) because the redfish fishery is confined to bottom trawling on the slope, the distribution and abundance of redfish in the deep waters of the Norwegian Sea have never been investigated, although their pelagic existence was known, and (b) high frequency echo sounders used to assess the shallower blue whiting did not have sufficient power to see the deeper redfish.

U.S. West Coast: Figure 1(b) shows results from a location on the continental slope, off the Oregon coast. The shallower layer (between about 200 and 450 m) peaks between 1 and 1.5 kHz. The deeper layer (which extends from about 1000 m to the bottom (at 1260 m)) peaks near 2 kHz.

A study of fisheries information conducted prior to these measurements indicated that Pacific hake would be a major contributor to volume reverberation in this region [3]. When size distributions obtained from National Marine Fisheries Service trawls collected nearby were used in the swim-bladder model, we determined that Pacific hake at a density of 0.08 individuals/m^2 would produce the shallower layer (Fig. 2(b)).

No fish of present commercial importance exist at the great depths of the deeper layer. Therefore no fisheries data were available. However deep-water scientific trawls conducted by Oregon State University (OSU) caught grenadiers at these depths. Using grenadier sizes and densities (0.008 individuals/m^2) from the OSU trawls in the model gave excellent agreement with the acoustic data (Fig. 2(b)), indicating that grenadiers are the cause of the deeper layer. Our measurements at seven other sites along the California, Oregon, and Washington coasts suggest that these fish are widespread and abundant. They may represent a potential alternative fishery in today's world of declining fish resources.

Summary: NRL has used a combination of measurements and models to determine the effects of biological scattering on naval sonars in a number of areas. We have found that scattering strengths can be predicted accurately if the characteristics of the fish are known. Because our low-frequency measurements penetrate to deeper depths than the usual commercial fisheries measurements and cover a broad frequency range, we have been able to locate and

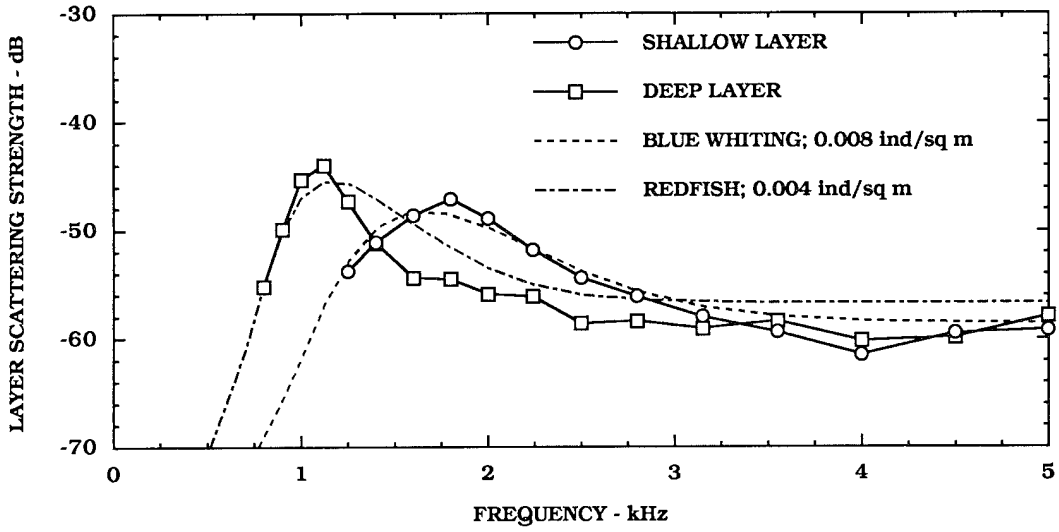

(a)

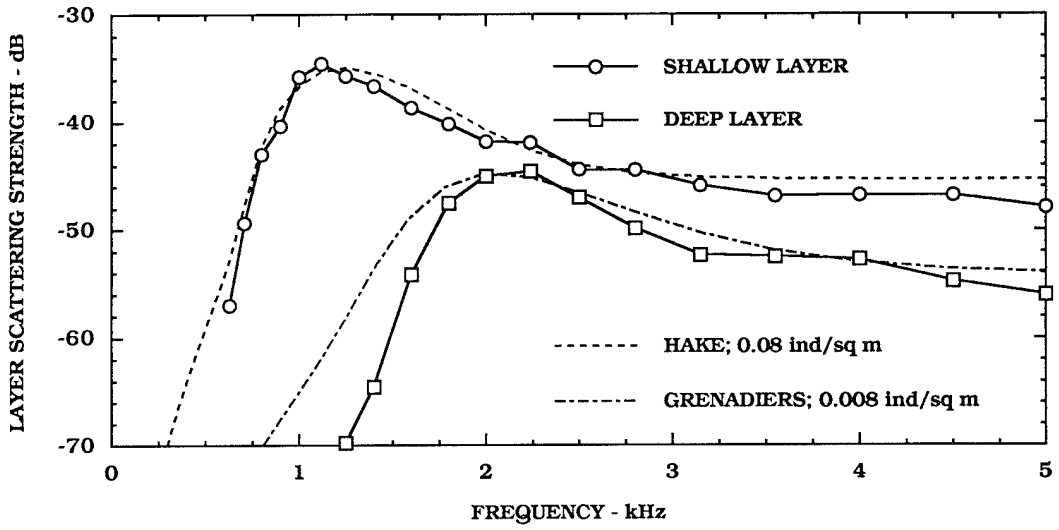

(b)

Fig. 2 — Comparison of measured and modeled layer scattering strengths S_L as a function of frequency (a) from the Norwegian Sea and (b) off the coast of Oregon.

study large fish stocks that had been dismissed as unimportant by fisheries' researchers. These stocks have the potential to be developed into viable future fishery resources.

[Sponsored by ONR and SPAWAR]

References

1. R.H. Love, "Resonant Acoustic Scattering by Swim-bladder-bearing Fish," *J. Acoust. Soc. Am.* **64**, 571-580 (1978).

2. R.H. Love, "Low-Frequency Volume Scatterers in the Norwegian Sea," FR/7174--92-9418, Naval Research Laboratory, Washington, D.C. (1992).

3. R.W. Nero, "Estimates of Low-Frequency Volume Scattering off the Oregon-Washington Coast," Tech Note 206, Naval Oceanographic and Atmospheric Research Laboratory, Bay St. Louis, Mississippi (1992). ■

Imaging the Mid-Atlantic Ridge with Reverberation

N.C. Makris, L.Z. Avelino, and R. Menis
Acoustics Division

The deterministic relationship between low-frequency ocean-basin reverberation and detailed geomorphology is documented for wide-area insonification of the western Mid-Atlantic Ridge. The establishment of this relationship is significant because it elucidates the role of reverberation as clutter in the Navy's active underwater surveillance systems, and it provides a means of exploiting the only medium currently available for real-time remote sensing of wide areas of the ocean basin: low-frequency sound waves. The bistatic reverberation data analyzed were acquired in July 1993 during the Main Acoustics Experiment of the multidisciplinary, multi-institutional, Office of Naval Research Special Research Program (SRP). The experiments and tow-ship tracks of the U.S. Research Vessel (RV) *Cory Chouest* and NATO's RV *Alliance* were designed by NRL's Acoustics Systems Branch. Beamforming and range-dependent propagation modeling are used to chart the returns in a Universal Transverse Mercator coordinate system. The newly developed techniques, Environmental Symmetry Breaking (ESB) [1] and the Global Inversion (GI) [2], are used to eliminate ambiguity in the towed-array measurements. Charted reverberation shows excellent registration with back-facing scarps on extended ridges and a high correlation with modeled transmission loss (TL). The correlation with TL is significant because it indicates that spatial variations in wide-area reverberation can be accurately modeled simply with knowledge of sound-speed structure and bathymetry.

Experimental Design: Figure 3 shows tow-ship tracks for the B′-C′ corridor experiments. These are overlain on high-resolution bathymetry (200-m grid) collected during a previous SRP experiment led by the Woods Hole Oceanographic Institution (WHOI). White lines are for RV *Cory Chouest* ship tracks, and the black lines are for RV *Alliance*. The tracks exploit a naturally occurring corridor (of length equal to twice a convergence zone (CZ)) to obtain two experiments for the price of one. That is, waterborne reverberation at 1/2 CZ (33 km) and 1 1/2 CZ ranges from the targeted bathymetric features B′ and C′ at either end of the corridor is obtained reciprocally. This is possible because

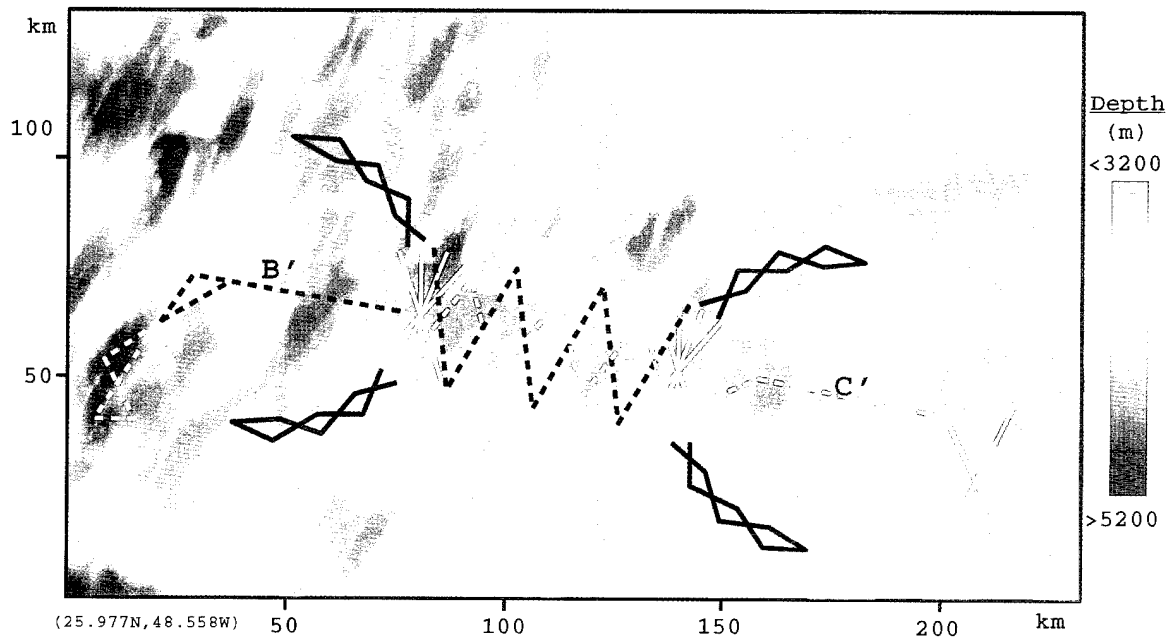

Fig. 3 — Tow-ship tracks for the B′-C′ Corridor Experiments of the SRP Main Acoustics Experiment overlain on bathymetry.

refraction in the water column causes the horizontally steered source beam to turn upwards at $n + 1/2$ CZ and downward at n CZ ranges from the source. By Snell's Law, the $n + 1/2$ CZ vertex occurs at the conjugate depth of 3800 m where the sound speed is equal to the sound speed at the source. This conjugate depth is significantly shallower than the corridor but deeper than the B′ and C′ ridges. Therefore these ridges will be strongly insonified by the main beam.

Measured vs Modeled Reverberation: Figure 4 compares (a) measured reverberation from a single 0.5-s narrowband transmission at 268 Hz (375-m range resolution) made by the RV *Cory* at the center of its eastern four-track crossing (shown in Fig. 3) and Fig. 4(b) modeled convolved TL for the same monostatic measurement. Symmetry about the receiving-array axis is due to ambiguity inherent in line-array measurement. Cross-range resolution is poorest at endfire. Elevated noise levels are apparent in the sector directed towards the tow ship. The modeled convolved TL is derived by convolving the antilog of the two-way TL with the spatially varying resolution window determined by the receiving array beampattern and transmission bandwidth. The TL is obtained by parabolic equation (PE) modeling that accounts for the full source array beampattern. Statistics of both the measured reverberation level and

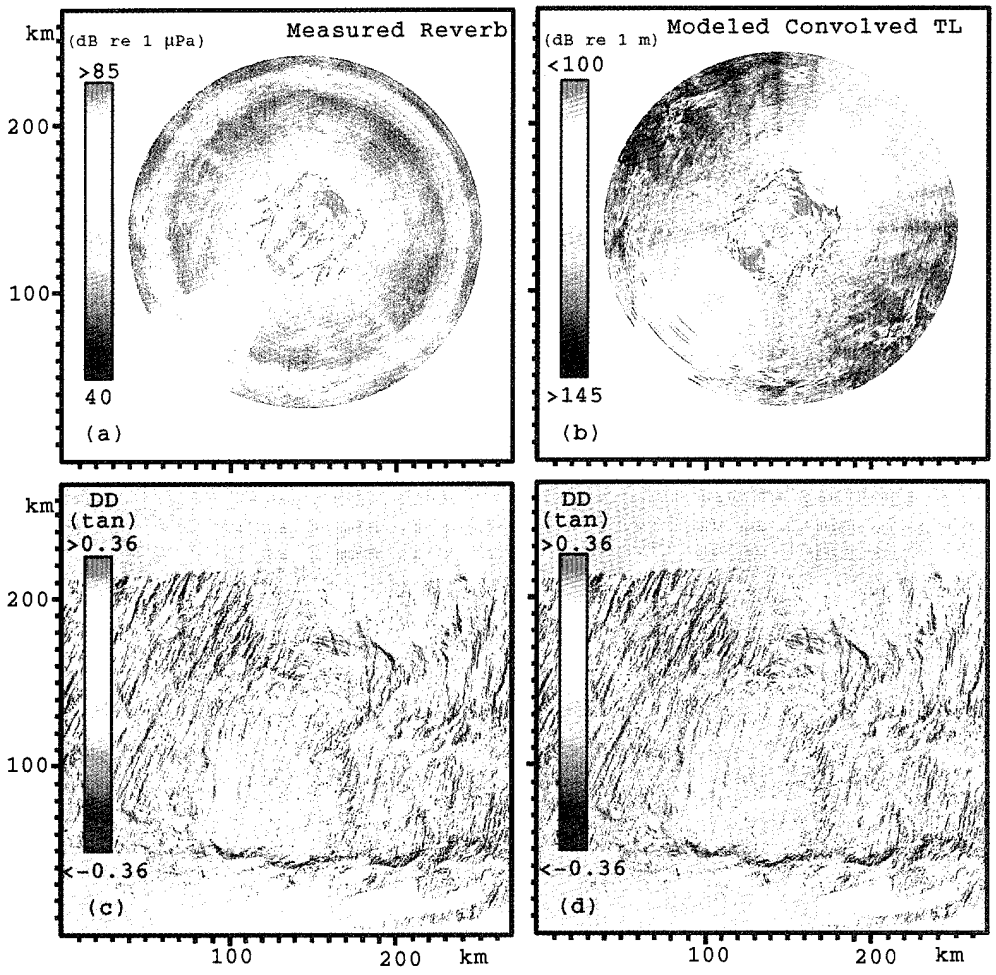

Fig. 4 — (a) Measured reverberation and (b) modeled convolved two-way transmission loss from a narrowband pulse. Ambiguity is resolved by the ESB method in (c) for this transmission and the GI method in (d) using this and three other transmissions. Prominent reverberation is overlain on the directional derivative of bathymetry in (c) and (d).

modeled convolved TL are Gaussian, making the interpretation of the 0.54 correlation coefficient between the two images unambiguous. Correlation coefficients from similar measurements are typically between 0.50 and 0.70. This indicates that reverberation may be modeled to this level of accuracy with a PE given sufficient knowledge of sound-speed structure and bathymetry.

Correlation with Bathymetry: Figures 4(c) and (d) show a color chart of the directional derivative (DD) of the bathymetry along an azimuthal vector pointing from the receiving array. Red shows slopes facing the measurement, and blue shows slopes facing away. Contours of prominent reverberation with ambiguity resolved by the ESB and GI methods are overlain. The ESB method uses PE modeling for a single measurement, and the GI method inverts independent measurements at differing array orientation to break ambiguity. High correlation between prominent reverberation and backfacing scarps is apparent as is agreement between the ESB and GI methods.

The high correlation between measured reverberation and back-facing scarps is highlighted in a detailed image of the B′ feature in Fig. 5. The DD is shown in black and white this time. Reverberation from a broadband linear frequency modulated pulse 200-255 Hz (50-m range resolution with averaging) is overlain in yellow in Figs. 5 (a) and (b). The overlay is a monostatic measurement from the RV *Cory* in Fig. 5 (a) and is the same pulse measured bistatically by the RV *Alliance* in Fig.

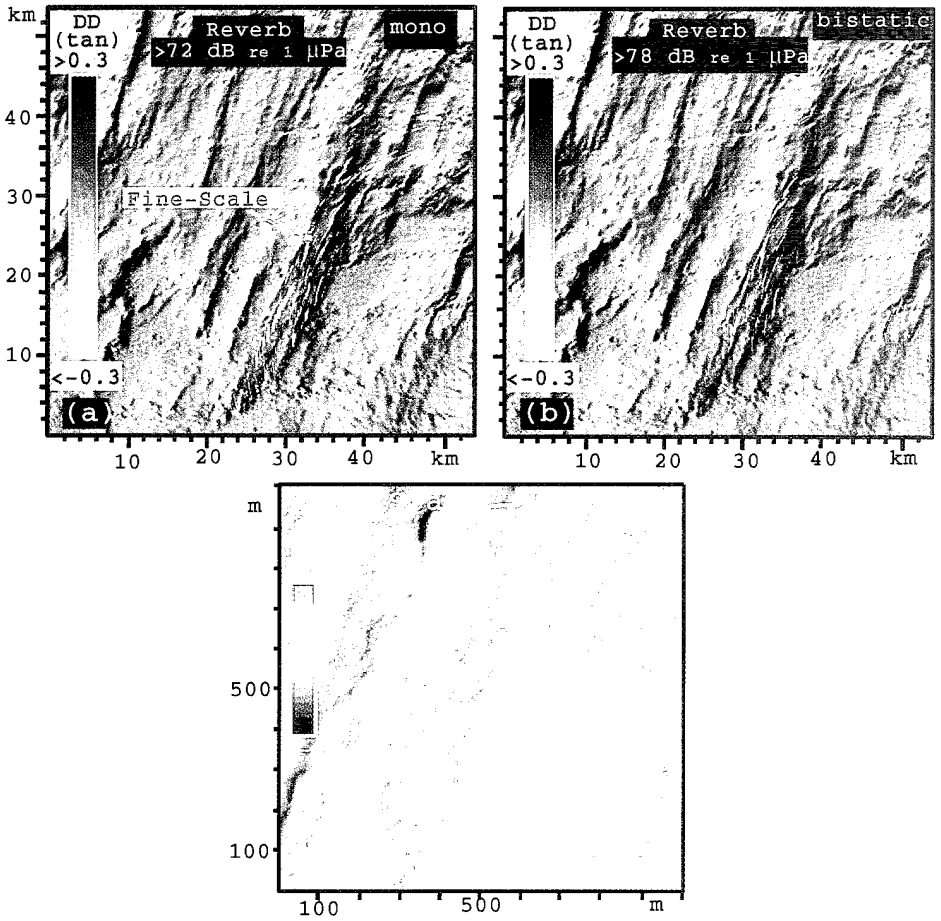

Fig. 5 — Prominent reverberation overlain on the directional derivative of bathymetry at the B′ feature for (a) monostatic and (b) bistatic reception of the same transmission. (c) A close-up view of the bathymetry over a 1 km × 1 km area at the site of the fine-scale site indicated in (a). The return is from an aggregate of steep cliff faces.

5(b). Both ships are within 1/2 CZ of B′. These results show that a single towed-array transmission from tens of kilometers or more can qualitatively image a ridge in real-time with horizontal resolution approaching that of roughly a week-long side-scan sonar survey. Finally, Fig. 5(c) shows a detailed view of the steep slopes (arctan (2.2) = 66°) that are responsible for the reverberation. The color DD is from SRP fine-scale bathymetry gridded at 5 m and collected by a previous SRP experiment led by WHOI. The white overlain contours are the same as in Fig. 5(a). Reverberation above the indicated level falls within these contours on cliff faces (red) of roughly a 50-m extent across the ridge axis. This shows that an aggregate of relatively fine-scale cliff faces is generally responsible for a prominent return.

[Sponsored by ONR]

References

1. N.C. Makris and J.M. Berkson, "Long-range Backscatter from the Mid-Atlantic Ridge," *J. Acoust. Soc. Am.* **95**, 1865-1881 (1994).

2. N.C. Makris, "Imaging Ocean-basin Reverberation via Inversion," *J. Acoust. Soc. Am.* **94**, 983-993 (1993). ■

Structural Acoustics and Interior Noise of Aerospace Vehicles

B.H. Houston
Acoustics Division

Understanding the physics of the acoustic fields on the interior of aerospace vehicles is becoming increasingly important. High levels of acoustical and vibrational energy can lead to crew performance degradation as well as acute passenger discomfort. Problems can become particularly severe in the case of helicopter interior noise where stress-related injuries are possible, and crew performance can suffer appreciably. During the early phases of a satellite launch, the development of high acoustic field strengths in the payload section from unsteady aerodynamic flow can lead to payload damage.

The physics of the interior noise problem of an aircraft in flight can be separated into a low frequency part—dominated by energy from power plants, etc., coupling into interior spatial modes—and a broadband part—where interior noise levels are primarily attributable to flow-induced excitation of the shell, with subsequent coupling into the interior spaces. Generally speaking, the low frequency region (below ~500 Hz) has higher acoustic levels associated with it and is therefore the primary spectral region of interest. The Physical Acoustics Branch is undertaking efforts to apply advanced experimental, theoretical, and control methodologies to this problem that were originally developed for the submarine community. This includes the adaptation of nearfield acoustic holography (NAH) [1] and powerful *K*-space processing and analysis tools [2].

Structural Wavenumber Response: Many aerospace structures are fabricated out of thin, reinforced aluminum shells where the reinforcing stringers and ribs contribute substantially to the bending stiffness and add much complexity to the structural response that includes Bloch-wave pass and stop bands [3]. To uncover the detailed structural acoustics, it is useful to characterize the response of a structure to a point excitation because this excites broad wavenumbers both axially and circumferentially. Experimentally, the structural response is measured with an accelerometer array or spatially scanned Doppler vibrometer. For some structures, this is also studied numerically with finite-element/boundary-element calculations that model the structural detail with interior and exterior fluid loading. Typically the shell response data are measured/calculated with sufficient spatial resolution to capture the first 16 circumferential harmonics and are further decomposed by the equivalent axial Fourier mode (or wavenumber k_z). Figure 6 shows the k_z out-of-plane wavenumber response $n = 1$ circumferential harmonic for a cylindrical aircraft section under radial force excitation at a point on the shell. The "sonic cone," which delineates the regions of subsonic and supersonic phase speed, is also

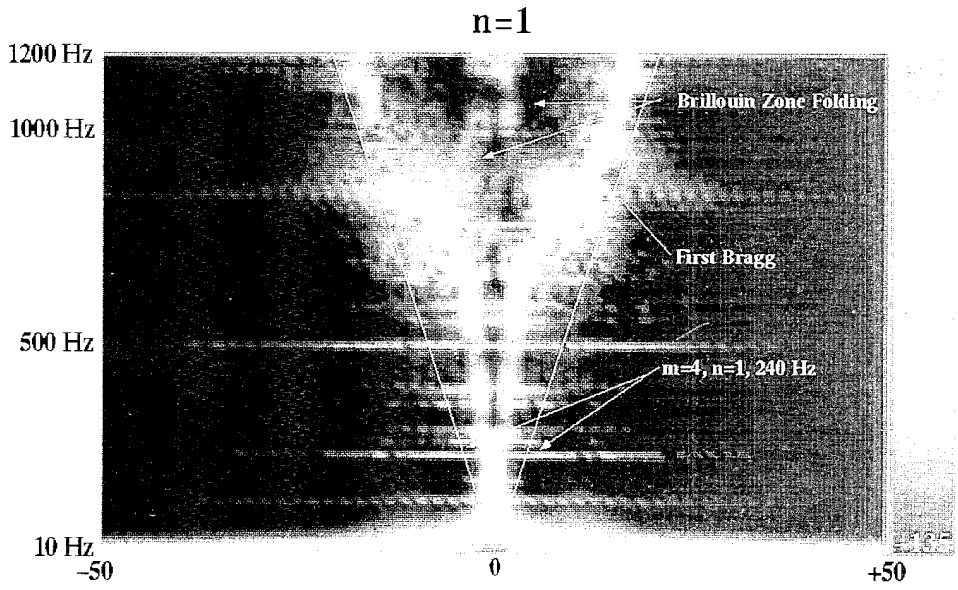

Fig. 6 — Flexural dispersion curves derived from the Fourier transformation of radial displacements in the axial direction. The color scale is a magnitude scale that represents 50 dB of dynamic range, with red indicating the highest radial normalized displacement magnitude (−85 dB re m/N) and deep blue, the lowest (−135 dB re m/N). The horizontal axis is m, the equivalent Fourier mode number equal to the number of half-wavelengths along the length of the straight section.

shown. Generally speaking, the majority of the waves in these $k-\omega$ plots occur in the supersonic region (inside the cone) and are thus well coupled to the fluid. The overall "wine glass" shape is predicted from dispersion curves generated from a normal mode series calculation for a thin-walled invacuo infinite cylinder (not shown) and are understood to be the freewaves for the *infinite* cylinder. The propagation of essentially supersonic free waves is obviously a dominant mechanism on the shell, and these results indicate that there is little or no evanescent decay of these structural waves into the fluid. However there are also strong, nearly sonic pointlike features at 240 Hz that do not lie on the freewave dispersion curve and are due to an internal volume mode at 240 Hz; to understand this, we must look at the interior acoustic response.

Interior Field: The interior acoustic response is measured by means of a robot that moves an array of matched microphones precisely throughout the interior of the structure. In this fashion, data are recorded on cylindrical surfaces, and NAH projections are performed to develop a detailed mapping of the field. As is the case for the shell response discussed above, some interior acoustic responses can be studied with high-fidelity numerical models. Figure 7 is a plot of the associated spatially rms-averaged acoustic-pressure response for the point drive case discussed in the previous section. There are a number of resonance peaks in this spectrum, with the peak at 240 Hz being the most dominant. A closer look at this indicates that the Q is very high ($\sim$500), indicating extremely low loss. The display in Fig. 8 shows the single frequency, spatial field mapping at 240 Hz, with the phase information preserved in the color scale. The standard nomenclature is used here for circular waveguides: n indicates the number of circumferential pressure nodes, p the number of concentric radial nodes, and m the number of axial maxima along the straight section. This is therefore an $n = 1$, $p = 0$, $m = 4$ mode. It should be noted that evidence of this mode in the structural response is indicated at the end of previous section. The clear and distinct pointlike features in Fig. 6 indicate $n = 1$, $m = 4$ shell motion. Thus for this resonance, there is a

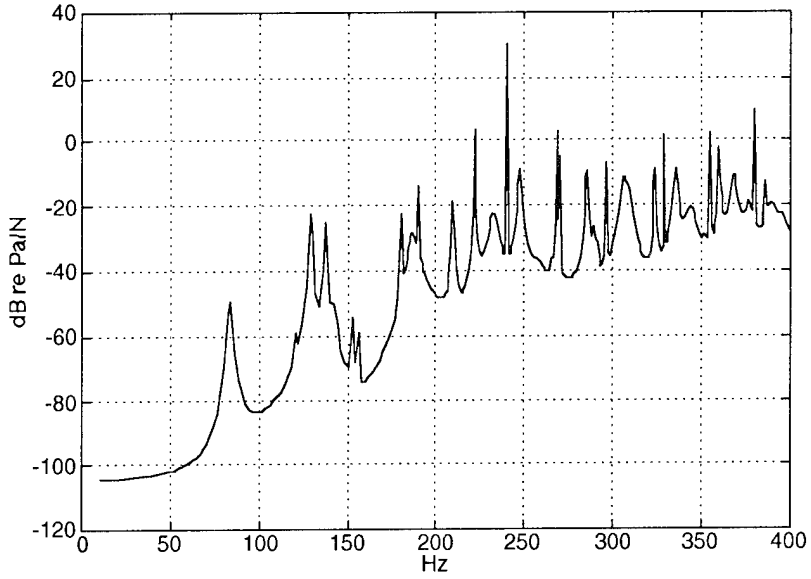

Fig. 7 — The broadband spatially rms-averaged interior acoustic response. The vertical axis is in dB referenced to 1 Pa per N drive force. The horizontal axis is frequency in Hz.

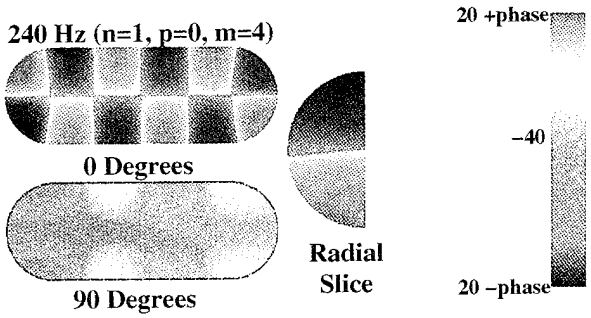

Fig. 8 — The single frequency spatial field mapping at 240 Hz with the phase information preserved in the color scale. This scale in units of dB relative to 1 Pa per N drive has an overall 50 dB of dynamic range, with red and deep blue representing the most positive and negative going values, respectively. The top cylindrical slice represents the vertical pressure distribution through the fuselage section, while the bottom slice represents the distribution in the horizontal plane. Also plotted is the radial distribution for the axial location near the right end of the cylinder.

coupling between the structural and acoustic modes. Additional analysis shows that this mode shape is a normal mode of the *cavity* and is forcing the shell into $n = 1$, $m = 4$ motion. Further the extremely low loss in this resonance is an indication that the coupling to the external fluid is weak; for example, radiation damping to the external fluid is the only source of loss for this system. The structural and interior losses are near zero.

Remarks: At different frequencies and under different forcing conditions, the mechanisms can be varied and mixed. For example, at some frequencies, two or more spatial and/or structural modes can coexist, leading to degeneracy. Generally speaking, detailed knowledge of both the structural and interior acoustic responses is essential to understand the mechanisms that lead to the high interior acoustic levels and their ultimate reduction or elimination through active control or structural design changes.

[Sponsored by NASA]

References

1. E.G. Williams, B.H. Houston, and J.A. Bucaro "Broadband Nearfield Acoustic Holography for Vibrating Cylinders," *J. Acous. Soc. Am.* **86**, 674-679 (1989).

2. E.G. Williams, B.H. Houston, and J.A. Bucaro, "Experimental Investigation of the Wave Propagation on a Point-driven, Submerged Capped Cylinder Using K-space

Analysis," *J. Acoust. Soc. Am.* **87**, 513-522 (1990).

3. D.M. Photiadis, "Anderson Localization of One-dimensional Wave Propagation on a Fluid-loaded Plate," *J. Acoust. Soc. Am.* **91**, 771-780 (1992). ■

Plate Tectonic Studies Using SOSUS Data

C. Nishimura and C. Bryan
Marine Geosciences Division

Introduction: Development of the theory of plate tectonics in the 1960s was a major breakthrough in the Earth sciences. According to the theory of seafloor spreading (one component of plate tectonics), the surface of the Earth is comprised of large, rigid, lithospheric plates formed at ocean ridges, which slide past one another along faults and are destroyed at subduction zones. Understanding plate tectonic processes is crucial in understanding the dynamics of our planet. As boundaries between plates are defined by narrow belts of high seismicity, these processes have traditionally been studied by seismologists using land-based seismometers. These seismometers are capable of detecting only earthquakes greater than magnitude 4.5 in oceanic areas; hence relatively little is known about the nature of the processes resulting in low-magnitude seismicity beneath 71% of the surface of our planet.

In this experiment, NRL analyzed U.S. Navy Sound Surveillance System (SOSUS) hydrophone data collected at the Naval Ocean Processing Facility (NOPF), Dam Neck, Virginia, to detect, locate, and interpret seismicity in the North Atlantic Ocean. Goals of this program include improved monitoring of ongoing processes occurring along the mid-Atlantic Ridge system as well as improved understanding of the tectonics of the highly complex Caribbean region.

Background: SOSUS hydrophones routinely record waterborne tertiary (T-) phases from earthquakes, submarine volcanic eruptions, and underwater explosions. T-phases propagate as compressional waves primarily through the Sound Fixing and Ranging (SOFAR) channel. The cylindrical waveguide effect of this channel, combined with the low attenuation of sound in seawater, permits T-phases to propagate to much greater distances than spherically propagating solid-Earth primary (P-) and secondary (S-) phases. It is this fundamental property of T-phases that makes them ideal for the study of low-magnitude seismicity within the oceans.

Data: On December 28, 1992, routine monitoring by the U.S. Navy of its SOSUS hydrophone arrays in the Atlantic Ocean revealed the onset of intense seismic activity north of the Virgin Islands. T-phases from this sequence were recorded throughout January 1993, with the array closest to the T-phase source region recording more than 100 events per day for several weeks. The SOSUS arrays recorded two orders of magnitude more events from this sequence than the land-based seismographs of either the Worldwide Standardized Seismograph Network or the local Puerto Rico seismic network, showing the enhanced ability of hydrophone arrays to monitor oceanic processes relative to land-based seismographs.

Method and Results: Beamforming of signals from the hydrophone arrays at preset azimuths yields not only directional information but also an increased signal-to-noise ratio relative to that from a single omnidirectional hydrophone, thus enabling the detection of lower magnitude events. Beamformed data also often reveal not only waterborne T-phases, but also solid-Earth P- and S-phases, greatly improving our ability to locate events over that possible when these additional phases cannot be identified.

The series of earthquakes included more than two dozen events of magnitude greater than 4.0. While the largest events were recorded on all arrays monitored at NOPF, many of the smaller events were also recorded by a sufficient number of arrays to yield good radiation sources. Epicenters were determined using a weighted eigenvalue method that simultaneously

minimizes the sum of the squared residuals of both the beam and time data.

Figure 9 shows epicentral locations for all events occurring during the first four days of the sequence. Epicenters lie in the frequently active region near the intersection of the Main Ridge with the inner wall of the Puerto Rico trench. Further study is necessary to determine the plate tectonic implications of these events.

Figure 10 compares our epicentral locations for events that occurred during the first 77 hours of activity with those given in the National Earthquake Information Center's (NEIC) *Preliminary Determination of Epicenters (PDE)* publication [1]. While we obtained well-constrained locations for 188 earthquakes during this time period, the NEIC's PDE lists locations for only 12 events, while the University of Puerto Rico's *Seismic Bulletin* lists preliminary locations for only 18 events. The T-phase solutions represent the radiation sources at which solid-Earth seismic energy is converted to hydroacoustic energy and may not be coincident with the associated earthquake epicenters; in general, our solutions lie to the northeast of those given by the NEIC.

Discussion: These results clearly demonstrate the importance of examining hydrophone data when studying fundamental processes affecting the dynamics of our planet. However acoustic monitoring of the world's oceans also has other important applications in such diverse fields as global climate change, marine mammal protection, fisheries enforcement, and nuclear nonproliferation. Knowledge and skills gained in analyzing signals pertaining to each of these areas can easily be transferred back to the Navy for use in its traditional tasks. In particular, the identification of earthquake and cetacean signatures has enabled Naval analysts to better identify other transient signals of greater tactical value.

[Sponsored by SPAWAR and CUSL]

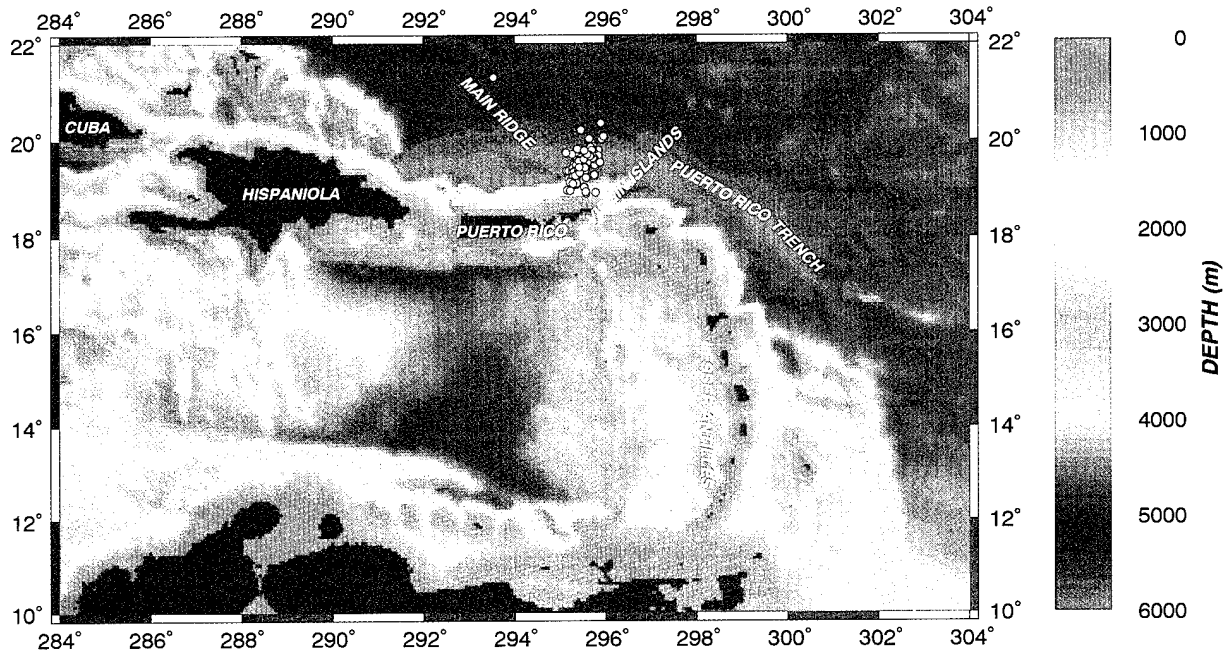

Fig. 9 — The Caribbean region, showing the well-constrained SOSUS locations for all earthquakes occurring between 1920 GMT 28 December 1992 and 0000 GMT 1 January 1993.

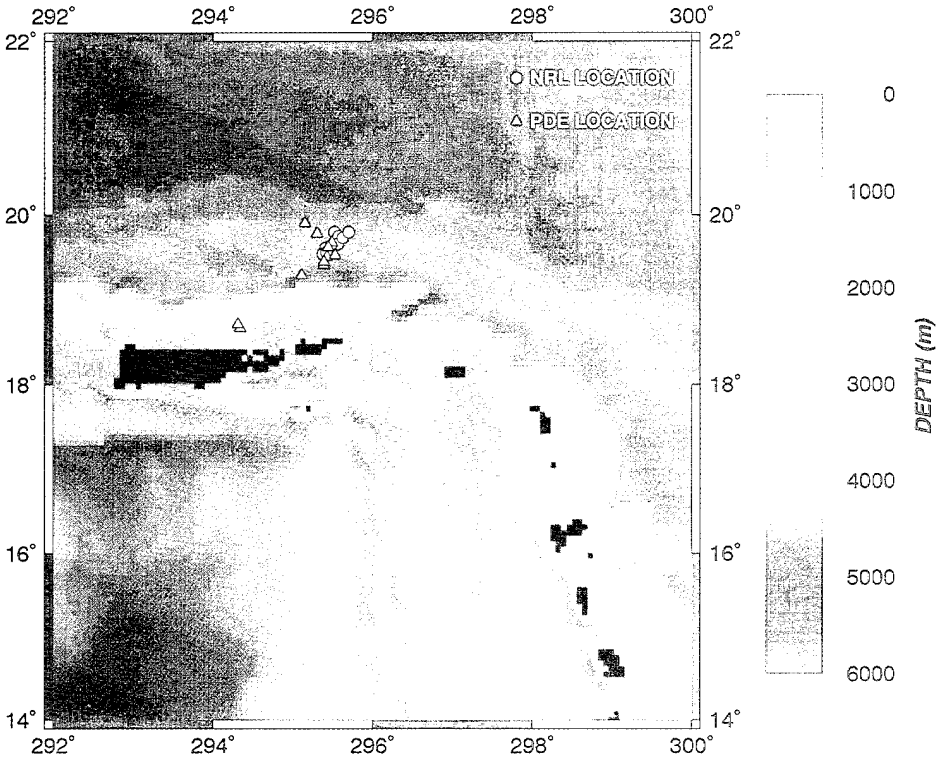

Fig. 10 — Comparison of SOSUS-derived epicentral locations for events occurring during the first 77 hours of activity with those listed in the PDE.

References

1. National Earthquake Information Center, *Preliminary Determination of Epicenters, Monthly Listing, December 1992*, U.S. Government Printing Office, 838-990 (1993).

2. *Seismic Bulletin, Preliminary Locations of Earthquakes Recorded near Puerto Rico, October-December, 1992*, University of Puerto Rico, Mayaguez Campus, Department of Geology, Seismic Network (1994). ■

Metal-Ion Biosensors for Environmental Studies

J.R. Deschamps and K.B. Ward
Laboratory for the Structure of Matter

Metal ions such as lead, mercury, zinc, and copper can be quite toxic even at low levels, and their concentrations in natural waters and in discharges into these waters are closely monitored. Conventional methods used to measure such trace metals possess sufficient sensitivity for the analysis of their ambient concentrations but suffer from problems in sample pretreatment and slow turn-around time for the analysis. An examination of the accepted "ambient" concentrations of various trace metals in the marine environment shows a trend of decreasing ambient levels as sources of sample contamination are eliminated. The analytic method chosen for a particular metal dictates what, if any, pretreatment of the sample is needed. For example, atomic absorption spectroscopy requires extensive sample pretreatment both to concentrate and to remove salts from marine samples. Ideally, it would be desirable to measure trace metals in situ, thus eliminating problems caused by sampling and storage. However such measurements are impractical using present techniques.

Enzyme-based Detection: Naturally occurring biological systems have evolved to interact with metal ions in a highly specific and sensitive fashion (Fig. 1), and we have used this fact to adapt these systems for use in a novel class of metal-ion detectors.

The metalloenzyme carbonic anhydrase requires zinc ion for activity, and we have developed methods to use this protein to detect zinc ions at nanomolar concentrations (that is, in the low parts-per-billion range). The metalloenzyme is first stripped of its metal-ion cofactor, forming an inactive apoenzyme. The apoenzyme is then exposed to an unknown concentration of the activating metal ion, which reactivates a portion of the enzyme. The concentration of this reactivated enzyme is directly proportional to the concentration of the metal ions in the sample being analyzed. We have demonstrated the feasibility of this enzymatic approach to the detection of trace metals and have submitted a patent application for this new kind of detector [1]. A prototype flow-through system that allows continuous monitoring of metal-ion concentration using this approach has also been constructed (Fig. 2).

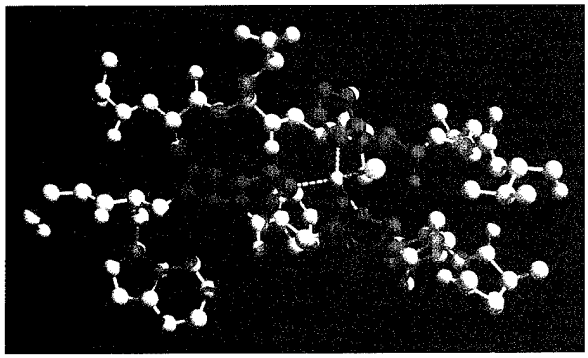

Fig. 1 — Zinc-binding site in carbonic anhydrase. The zinc ion is shown in green, the enzyme backbone is in white, the residues involved in coordination of the zinc ion are in magenta, and a bound water molecule is in cyan. Note the tetrahedral geometry of the zinc/ligand interactions shown by the broken yellow lines. The selectivity of the binding site is controlled by the binding geometry, the nature of the ligands, the size of the binding pocket, and the distance between the metal ion and the ligands.

We have identified several enzymes that could be used to detect metal ions other than zinc. Recently we extended the enzyme-based detection method to copper using the metalloenzyme tyrosinase. The large signal due to the highly colored product formed when this enzyme acts upon L-DOPA and the low noise level afforded by the slow, spontaneous degradation of the L-DOPA should result in a limit of detection for copper in the low nanomolar range. We are thus encouraged that this enzymatic approach to metal-ion detection can be generally applicable to other trace metals.

Other Biodetectors for Metal Ions: Another example of a natural biochemical system that can be used for metal-ion analysis involves the photoprotein aequorin. Aequorin, a naturally occurring protein in the bioluminescent jellyfish *Aequorea*, responds to low levels of calcium by emitting light (Fig. 3). In collaboration with scientists at the Woods Hole Oceanographic Institute, we now routinely produce recombinant aequorin in a bacterial expression system.

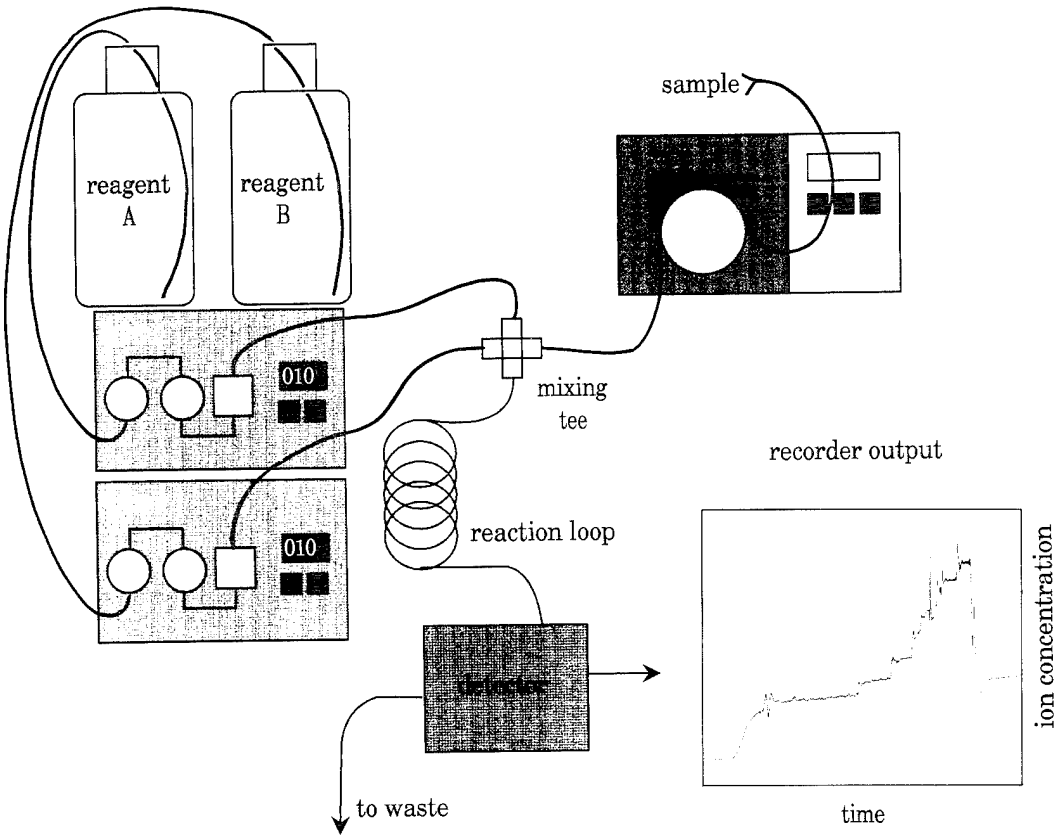

Fig. 2 — Flow-through system for continuous monitoring of zinc. The required reagents—apocarbonic anhydrase and a chromogenic substrate—are mixed with the sample, and after an appropriate reaction time, the mixture passes through an absorbance monitor. The insert shows detector response as a function of time with increasing zinc concentrations and a return to background in the absence of zinc.

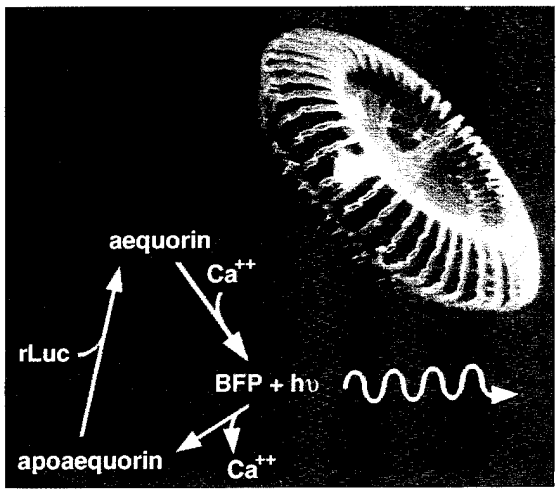

Fig. 3 — The bioluminescent jellyfish *Aequorea victoria* and the reactions involved in luminescence. When photoproteins such as aequorin bind calcium ions, light is emitted, and aequorin is transformed into the blue fluorescent protein (BFP). BFP can be recycled in the presence of oxygen to form new, calcium-sensitive aequorin.

Scientists are already using aequorin to study calcium-ion concentrations in isolated cells. By using protein engineering, we hope to tailor this recombinant protein to detect other metal ions and to report their presence by emitting light. By coupling aequorin with the related green fluorescent protein and suitably modifying that protein, we believe a detector can be constructed that emits a different color of light for each kind of metal-ion present in the sample being tested.

The importance of the analysis of trace concentrations of metal ions will continue to increase within the environmental sciences. Certain Environmental Protection Agency guidelines mandate monitoring a wide variety of trace metals to protect the environment. In response to these concerns, the Navy has developed a renewed interest in environmental monitoring. The novel metal-ion biodetectors being

developed at NRL will serve as important tools for both domestic environmental studies as well as the Navy's Marine Environmental Quality Program.

[Sponsored by ONR]

References

1. J.R. Deschamps, K.B. Ward, and W.R. Light, An Enzyme-based Detector for Trace Metals, Application for Letters Patent, Navy Case No. 75,296. ■

Molecular Hydrodynamics of Detonations

C.T. White and D.W. Brenner
Chemistry Division

D.H. Robertson
NRL-NRC Resident Research Postdoctoral Associate

Undisturbed, solid explosives rest quietly in their metastable states but, when struck, can undergo rapid exothermic chemical reactions, often with catastrophic results. Once begun, a detonation travels through a solid explosive as a shock wave accompanied by rapid rises in temperature and pressure that initiate the exothermic chemical reactions that sustain it. This shock front—only several lattice spacings deep—separates the unreacted material from the shocked material, which experiences temperatures of several thousand degrees Kelvin and pressures of several hundred thousand atmospheres while flowing at rates of several kilometers per second. Propagating as a shock wave, a detonation consumes the explosive at velocities several times the speed of sound in the material, resulting in the release of chemical energy at rates that can exceed 10^{11} W for a 10 cm^2 detonation front—a figure comparable to the total electrical generating capacity of the United States.

In spite of advances in the understanding of detonations over the last several decades, their nanometer-scale behavior in solids remains poorly understood. Continuum theories can only indirectly address this domain while the extremely short time and length scales of the processes involved, together with their destructive nature, make experiment difficult and costly, if not presently impossible. This state of affairs is unfortunate because a better understanding of nanometer-scale behavior of detonations in energetic materials could prove crucial to the Navy in designing safer, more powerful explosives.

Atomistic Detonation Simulations: Processes at condensed-phase shock fronts can occur on such short time (subpicosecond) and length (subnanometer) scales that they are ideal for classical molecular dynamics (MD) simulations that follow individual atomic trajectories. Although starting from an atomic-scale description, MD simulations have also proven able to treat enough atoms for long enough times to describe continuum properties of planar shock waves in nonenergetic materials—including such complex hydrodynamic behavior as shock-wave splitting caused by a polymorphic phase transition [1]. Therefore MD simulations hold great promise both for studying discrete shock-induced chemistry in energetic materials and for directly relating this atomic-scale chemistry to the continuum properties of planar detonations successfully described by the hydrodynamic theory of compressive reactive flows.

However MD simulations of chemically sustained shock waves in energetic materials require interatomic potentials that allow for the simulation of thousands of atoms while including the possibility of chemical reactions with well-defined reactants and products. These potentials should not only incorporate the strong intramolecular forces that bind atoms into molecules but also the weak intermolecular forces that bind molecules into molecular solids. These potentials must also yield realistic barriers to the exothermic reactions that drive the detonation and well-defined molecular products after reaction. We have recently developed many-body reactive empirical bond-order (REBO) model potentials that have these essential ingredients [2,3].

We have found that two-dimensional MD simulations of a generic AB model explosive

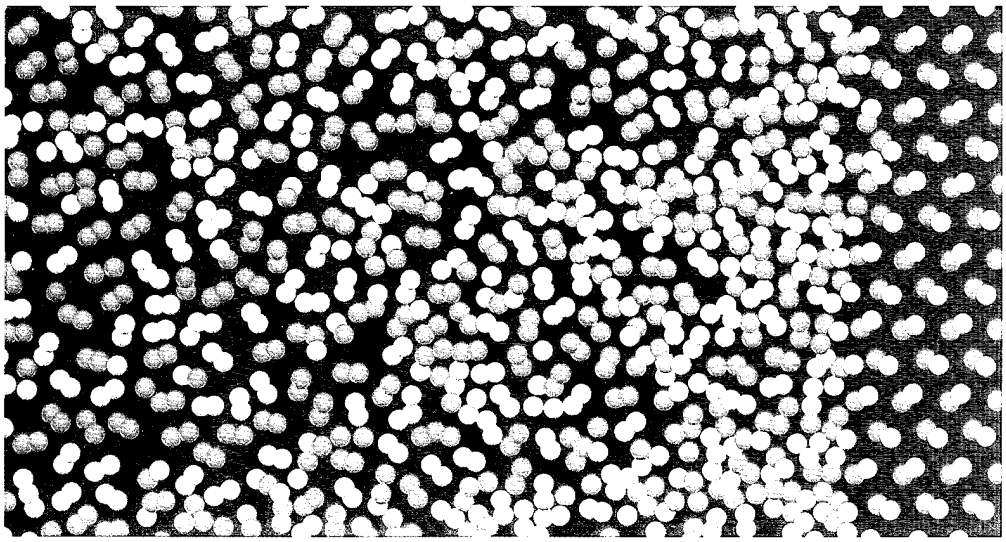

Fig. 4 — Snapshot of a shock front propagating into a generic model of an energetic material—a crystalline molecular solid composed an diatomic A-B (blue-gray) molecules with 0.12-nm bond length, which when shocked can undergo rapid exothermic chemical reactions to form the more stable A_2 (gray-gray) and B_2 (blue-blue) products. The physical parameters characterizing this model such as bond distances, vibrational frequencies, binding energies, speed-of-sound, and barriers to chemical reaction are all well within physical norms. To the right of the shock front is the unreacted two-dimensional crystal at ambient condition. Already visible 1 nm behind the shock front are the product molecules—prior to expansion—which are flowing from left to right at an average velocity in excess of 4 km/s while experiencing an effective pressure of over 400,000 atm. Part of the chemical energy released in the formation of products is used by the system to sustain the shock wave at a constant velocity several times the speed of sound in the crystal.

described by chemically realistic REBO potentials can yield chemically sustained shock waves with calculated temperature and pressure, particle flow and shock velocities, and power generation all consistent with a macroscopic detonation [3]. Remarkably we also have found that when a chemically sustained shock wave is achieved in the model, the results of these simulations reach near steady flow conditions near the shock front in under 100 ps, yielding results in excellent agreement with continuum hydrodynamic theory [2-4]. Figure 4 shows and describes a snapshot of a simulated detonation that can result in this model molecular solid.

Conclusions: Our promising results demonstrate that MD simulations using reactive many-body potentials provide a powerful new probe of the interplay between the continuum properties of shock waves and the atomic-scale chemistry they induce in condensed-phase detonations. The REBO potential form can also be extended to model more complex energetic solids. In addition, this potential form can be used to study the role of radical defects thought important in some accidental detonations. Moreover new numerical algorithms able to follow the dynamics of 10^6 atoms on parallel computers should soon make possible three-dimensional MD simulations of shocks in these more complex systems. The results of such simulations could prove crucial to the Navy in the design of safer, more powerful explosives.

[Sponsored by ONR]

References

1. D.H. Robertson, D.W. Brenner, and C.T. White, "Split Shock Waves from Molecular Dynamics," *Phys. Rev. Lett.* **67**, 3132 (1991).

2. C.T. White, D.H. Robertson, M.L. Elert, and D.W. Brenner, "Molecular Dynamics

Simulations of Shock-Induced Chemistry: Application to Chemically Sustained Shock Waves," in *Microscopic Simulations of Complex Hydrodynamic Phenomena*, M. Mareschal and B.L. Holian, eds. (Plenum Press, New York, 1992), pp. 111-123.

3. D.W. Brenner, D.H. Robertson, M.L. Elert, and C.T. White, "Detonations at Nanometer Resolution Using Molecular Dynamics," *Phys. Rev. Lett.* **70**, 2174 (1993).

4. "Shock-wave Chemistry of Explosives Simulated," *C & EN News*, December 7, 1992, p. 23; T. Studt, "Energetics Research Booming," *R & D Magazine*, April 1993, p. 67; C. Holden, "Explosive Anatomy," *Sci.* **260**, 618 (1993). ■

Single Molecule Detection

R.J. Colton and D.A. Kidwell
Chemistry Division

L.A. Chrisey
Center for Bio/molecular Science and Engineering

G.U Lee
NRL/ASEE Postdoctoral Research Associate

The three-dimensional structures of complex biological molecules are not determined exclusively by the strong covalent bonds between atoms but by relatively weak intermolecular forces such as electrostatic, van der Waals, hydrogen bonding, and hydrophobic forces. Because these forces may exist concurrently during intermolecular interactions, they are termed collectively molecular recognition forces. Understanding and controlling the nature of these forces will foster a deeper understanding of biological processes and create new diagnostic tools with important medical and environmental applications.

Until recently, our knowledge of molecular recognition was based on indirect physical and thermodynamic measurements such as X-ray crystallography, light scattering, nuclear magnetic resonance spectroscopy, and calorimetry. To measure forces directly requires highly sensitive techniques that can record force and position with high resolution and accuracy. The Atomic Force Microscope (AFM) has both high force sensitivity (10^{-15} N/$\sqrt{\text{Hz}}$ or four orders of magnitude more sensitive than the force of a hydrogen bond) and position control (0.01 nm), and can probe areas as small as 10 nm^2 under physiological conditions. By attaching one type of molecule to the end of a force-measuring cantilever beam and its complement to a flat substrate, we can measure directly the intermolecular forces between a single receptor-ligand complex, for example, when the cantilever first contacts the substrate and then pulls apart.

Receptor-Ligand Complexation: Streptavidin and biotin molecules comprise a common receptor-ligand system that mimics an antibody-antigen interaction but with high binding affinity. Specifically, the streptavidin molecule contains four binding sites for biotin. By placing streptavidin on one surface of the AFM and tethering biotin to the other surface using a short linker chain, we can measure the force necessary to rupture the intermolecular interaction once the surfaces are placed in contact and then pulled apart. The rupture force is 0.34 $\pm$ 0.12 nN, which is larger than the force of 0.06 $\pm$ 0.04 nN when the streptavidin sites are blocked with free biotin. The histogram in Fig. 5 shows the force measurements taken many times. Detailed analyses of the magnitude and distribution of the force indicate that we have measured the intermolecular force between two streptavidin-biotin molecules.

DNA Hybridization: Similarly, the two opposing surfaces can be functionalized with complementary strands of DNA and their binding interaction measured. Using oligonucleotides consisting of five repeating units of four base-pairs (that is, $(ACTG)_5$), we measure strong adhesive forces ($\sim$1.6 nN) between the surfaces only when the base sequences of the oligonucleotides are complementary that is, $((CAGT)_5)$. Furthermore the magnitude and distribution of the rupture forces change and can be interpreted

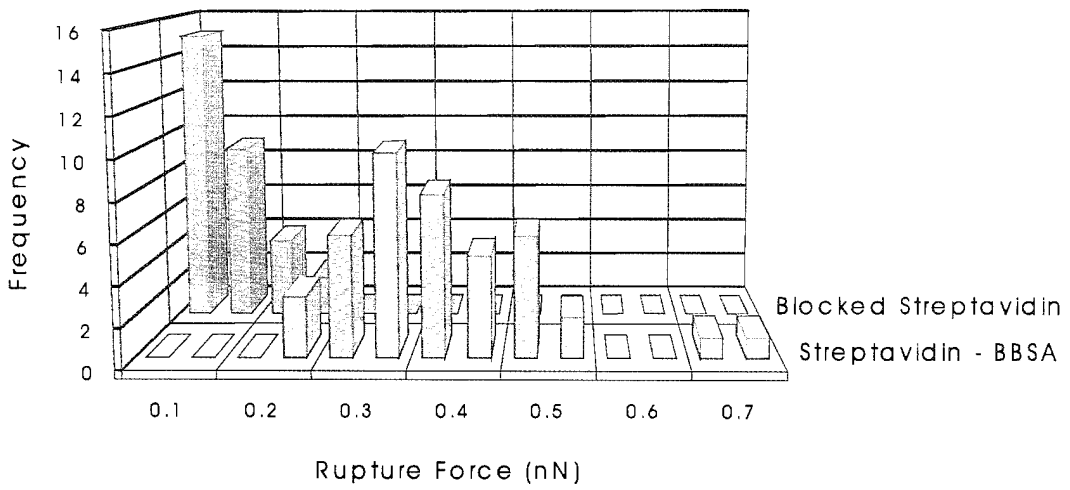

Fig. 5 — Histograms of the magnitude of the adhesive forces between biotin and streptavidin with the streptavidin sites open or blocked.

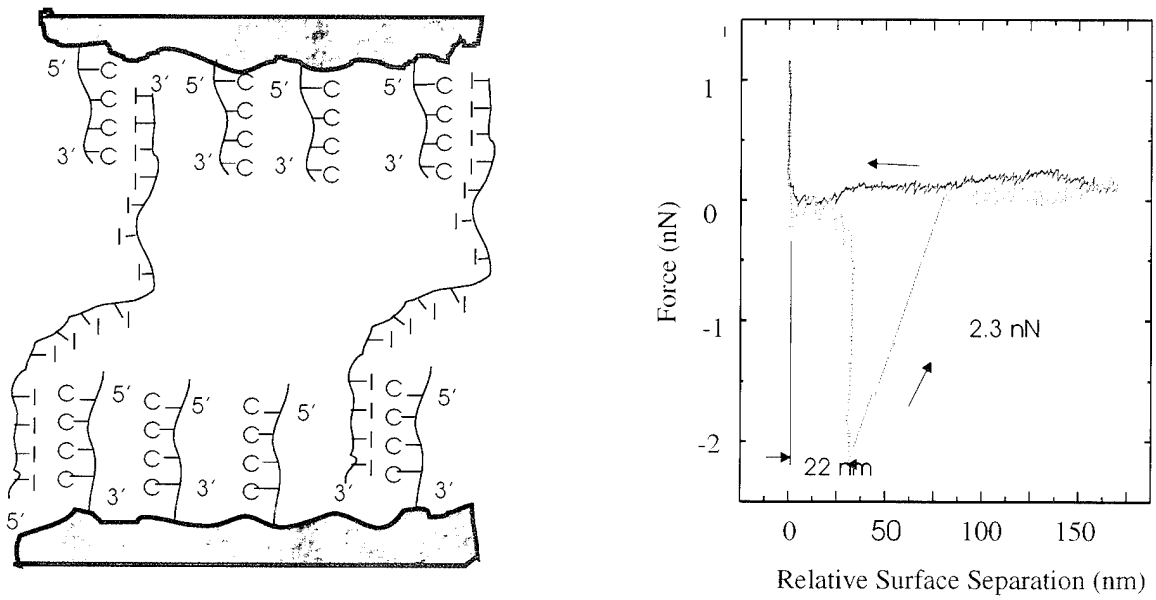

Fig. 6 — Diagram (left) showing two strands of polyinosine (I) interacting between two surfaces terminated with its complement—cytosine (C_{20}); force vs relative surface displacement plot (right) measured between a C_{20}-poly(I) surface and a C_{20}-functionalized probe.

as a direct measure of the interchain forces associated with Watson-Crick base pairing between 20, 16, and 12 base-pairs of individual molecules.

In Fig. 6, we illustrate a different type of assay in which noncomplementary oligonucleotides are immobilized on opposing surfaces, and a complementary homopolynucleotide is placed between them. The addition of the homopolymer does not change the magnitude of the adhesive force but increases the distance (up to 400 nm in some cases) between the surfaces at which the bond rupture occurs. As the surfaces are separated, an exponentially increasing force is required to elongate the molecule, resulting in a measure of the molecule's elasticity. Careful examination of the force curve reveals fine structure that may be interpreted as the force

necessary to uncoil and elongate single-stranded DNA. These results demonstrate that the AFM can measure *intra*molecular as well as *inter*molecular forces in complex macromolecular systems.

Sensors with Single Molecule Detection Sensitivity: We have used the force sensitivity and position control of the AFM to develop a molecular recognition tool capable of detecting single molecule-molecule interactions. The concept could produce a viable sensor after means are developed to introduce only a few molecules into the system and deliver them to the appropriate areas of the sensor where they can be detected. Such a sensor could potentially detect single molecular entities. This work is now in progress.

[Sponsored by ONR]

References

1. G.U Lee, D.A. Kidwell, and R.J. Colton, "Sensing Discrete Streptavidin-Biotin Interactions with Atomic Force Microscopy," *Langmuir* **10**, 354 (1994).

2. G.U Lee, L.A. Chrisey, and R.J. Colton, "Direct Measurement of the Forces Between Complementary Strands of DNA," *Sci.* **266**, 771 (1994). ■

Inorganic/Organic Hybrid Polymers For High-Temperature Applications

T.M. Keller
Chemistry Division

An emerging technology that holds promise for extending the temperature stability of polymers is inorganic-organic hybrid polymers. The polymeric hybrid combines the desirable features of inorganics and organics within the same polymeric system, such as thermal and oxidative stability and processability.

High-Temperature Inorganic/Organic Hybrid Polymers: The search for polymeric materials with new and improved high-temperature properties has led to the investigation of inorganic/organic hybrid polymers containing carborane-siloxane, siloxane, and acetylene segments in the backbone of linear polymers [1,2]. These polymers behave as precursors to thermosets and ceramics, which have exceptional thermal and oxidative stabilities (see Figs. 7 and 8). The major advantage of our approach is that the desirable features of inorganics and organics, such as high thermal and oxidative stability and processability, are incorporated into the same polymeric chain. The siloxane units provide thermal and chain flexibility to polymeric materials. Siloxane-acetylenic polymers have also been made but lack the thermal and oxidative stability that the carborane units possess. The chemistry involved in synthesizing poly(siloxane) and poly(carborane-siloxane) has been modified to accommodate the inclusion of an acetylenic unit in the backbone. The novel linear polymers have the advantage of being extremely easy to process and convert into thermosets or ceramics since they are either liquids at room temperature or low-melting solids and are soluble in most organic solvents. They are designed as thermoset polymeric precursors. The cross-linked density of the thermosets is easily controlled as a function of the quantity of reactants used in the synthesis. The acetylenic functionality provides many attractive advantages relative to other cross-linking centers. The acetylene group remains inactive during processing at lower temperatures and reacts either thermally or photochemically to form conjugated polymeric cross-links without the evolution of volatiles.

Surface Analysis: Scanning electron microscopic and scanning auger microprobe studies show that a protective bilayer or film composed mostly of silicon oxide and boron oxide forms on the outer surface of a thermoset or pyrolysate formed from a poly(carborane-siloxane-acetylene) upon exposure to air at high temperatures. The bulk of the thermoset and pyrolysate remained unchanged upon oxidative heat treatment at elevated temperatures. The film protects the bulk of these materials against oxidation. Prolonged oxidative aging results in the

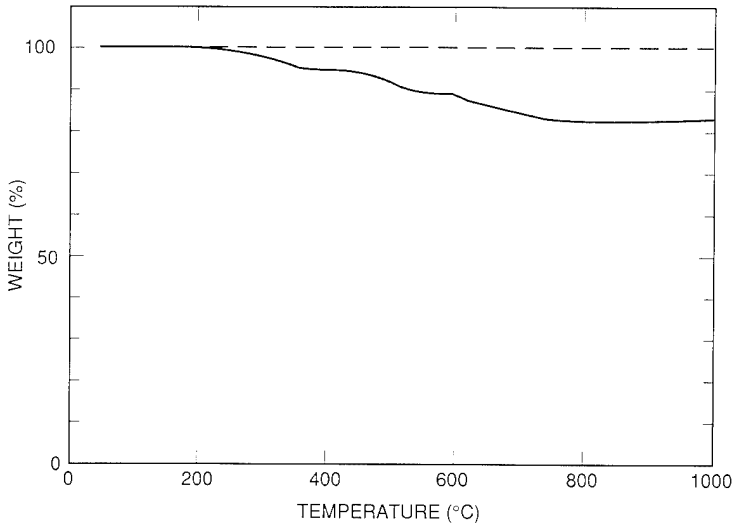

Fig. 7 — TGA thermograms of: poly(carborane-siloxane-acetylene) cured and pyrolyzed under nitrogen atmosphere (solid line) and cooled and rerun pyrolysate in air (dash line).

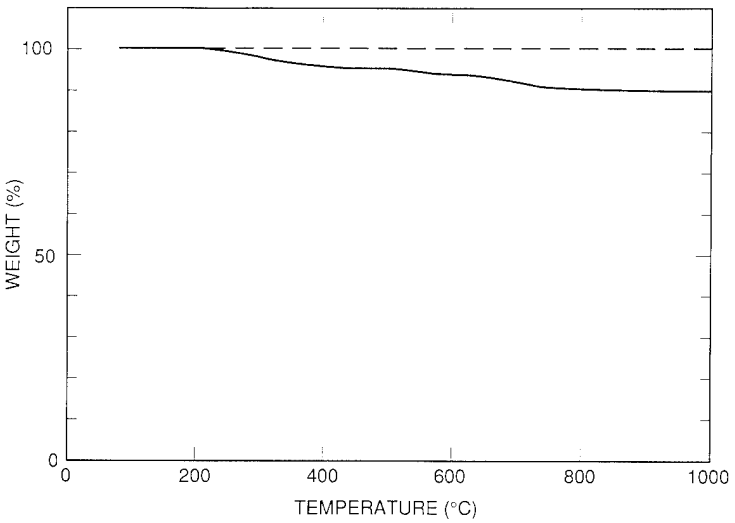

Fig. 8 — TGA thermograms of: poly(carborane-siloxane-acetylene) cured and pyrolyzed under air (solid line) and cooled and rerun pyrolysate in air (dash line).

volatilization of boron oxide, leaving an almost pure layer of silicon oxide, which blends into the silicon and boron concentrations at the interface between the surface layer and the bulk. As observed from the these studies, the extent of the oxidation and thus thickness of the film is dependent on the oxidative temperature and duration of the heat treatment.

Potential Applications: The linear siloxane-acetylenic and carborane-siloxane-acetylenic polymers provide advanced structural materials (thermosets and ceramics) for applications above 400° C and in excess of 1000° C in an oxidizing environment. These advanced materials could be used in the fabrication of advanced ceramic fibers and as high-temperature, high-performance structural materials for nuclear and fusion power generation, high-performance heat engine, gas turbine engines, the high-speed civil transport, the national aerospace plane, reusable launch vehicles/boosters,

heat exchangers, medical devices, cutting tools, as coatings to protect carbon/carbon composites against oxidation, and numerous other aerospace applications.

Conclusion: Linear poly(carborane-siloxane-acetylene)s and poly(siloxane-acetylene)s are precursors for high-temperature thermosetting polymers and ceramic-based materials that exhibit outstanding thermal and oxidative properties. Our studies have shown that relatively modest amounts of carborane in diacetylene-siloxane polymers can greatly enhance the thermal and thermo-oxidative stabilities of the resulting thermosets and ceramics formed during heat treatments at elevated temperatures. Further studies are under way to evaluate and exploit the linear polymers as matrix materials for high-temperature and carbon/ceramic composites.

Acknowledgment: The author is grateful to Dr. David Y. Son (NRC postdoctoral associate) and Dr. Leslie J. Henderson (ONT postdoctoral associate) for the synthetic efforts and Dr. Pehr Pehrsson of the Surface Branch of the Chemistry Division for the surface analysis studies.

[Sponsored by ONR]

References

1. L.J. Henderson and T.M. Keller, *Macromolecules* **27**, 1660 (1994).

2. D.Y. Son and T.M. Keller, *Polym. Mat. Sci. & Eng.* **71**, 305 (1994). ■

Fabrication of Patterned DNA Surfaces

L.A. Chrisey, C.E. O'Ferrall, and C.S. Dulcey
Center for Bio/molecular Science and Engineering

G.U. Lee
Chemistry Division

Spatially controlled, selective attachment of DNA molecules to surfaces is a key step in the development of sensing arrays for multiple genetic targets (for example, biological warfare agents and infectious and genetic diseases), the fabrication of combinatorial DNA libraries for screening of potential pharmaceuticals, and the evolution of new optical materials based on DNA. Through a unique combination of expertise in molecular biology, materials science, and chemistry at the Naval Research Laboratory, we have developed methodologies for the formation of patterned DNA surfaces to help advance these emerging applications. Self-assembled monolayers of aminosilanes on silicon substrates have been used as surfaces for the covalent (as well as electrostatic) attachment of synthetic DNA molecules in geometric patterns [1,2], by using two photolithographic methods. These achievements represent significant progress toward our goal of immobilizing multiple DNA species (with a theoretical maximum of 10^8 discrete DNA elements/cm^2) in well-defined arrays. The most immediate application of such arrays would be as rugged, field-compatible biosensors for the multiplexed detection and identification of various genetic targets (for example, specific DNA or RNA sequences), including biological warfare agents. A multiplexed detection system of the type described represents a significant increase in efficiency over DNA-based sensors that are presently available.

DNA Attachment Methods: One of the primary challenges in creating DNA patterns was to devise methods for attaching the DNA to surfaces. We have exposed two approaches: (1) electrostatic binding of negatively charged synthetic DNA oligomers to a positively charged aminosilane monolayer (one-step, direct deposition of DNA from solution) and (2) covalent attachment of an activated, thiol-modified synthetic DNA oligomer to an aminosilane film using a heterobifunctional crosslinker (two steps). The crosslinker has two reactive groups, one capable of reaction with the accessible amine portion of the aminosilane film and a second moiety, which reacts specifically with the thiol portion of the modified DNA molecule [2]. Each method resulted in detectable DNA films, however, the covalent attachment

approach is preferred due to the greater stability of the resultant DNA film.

Formation of Patterned DNA Surfaces: Key to our ability to define DNA pattern was the identification of surfaces to which DNA can be selectively bound, as well as surfaces which have low affinity for the DNA. We developed two methods for the creation of geometric patterns of DNA using either electrostatically bound or covalently bound DNA oligomers, as shown in Fig. 9. The first method involves photochemical modification of an aminosilane monolayer by irradiation through a mask using ArF laser (193 nm) pulses; this treatment results in removal of the silane molecule in regions exposed to laser light, exposing the underlying oxidized Si surface [3], which does not bind DNA. Treatment of this surface with a labeled DNA oligomer using either of the two attachment methods described above yields a DNA pattern detectable using an enzyme-linked colorimetric assay. Using this approach, DNA features on the 2 to 10 μm scale have been achieved.

Patterns were also formed using an aminosilane film on Si, which was then spin-coated with a negative photoresist. Exposure and development of the resist through a lithographic mask using appropriae conditions reveals the underlying aminosilane in unexposed regions (negative tone image); treatment with DNA as described above results in a detectable DNA pattern (Fig. 10), also with features on the μm scale; the figure shows 10-μm width bars. This resolution is significantly greater than that achieved by others working in this area and suggests that a very high density of unique DNA elements in an array can be achieved by sequential exposure of the aminosilane surface and treatment with individual DNA oligomers.

Significance: By using the DNA attachment and pattern-formation methods described above, we have achieved controlled immobilization of synthetic DNA on the micron scale. We have also demonstrated that DNA immobilized in this way retains its ability to recognize and bind to a complementary DNA strand in a highly specific and selective process called hybridization, a property that is key to the development of this technology into a practical biosensor. Fabrication of arrays of large numbers of immobilized, discrete DNA molecules—each of which is capable of recognizing its own unique complementary partner strand—forms the basis for a sophisticated and highly efficient biosensor for the detection of targets including bacteria, viruses, and genetic disorders.

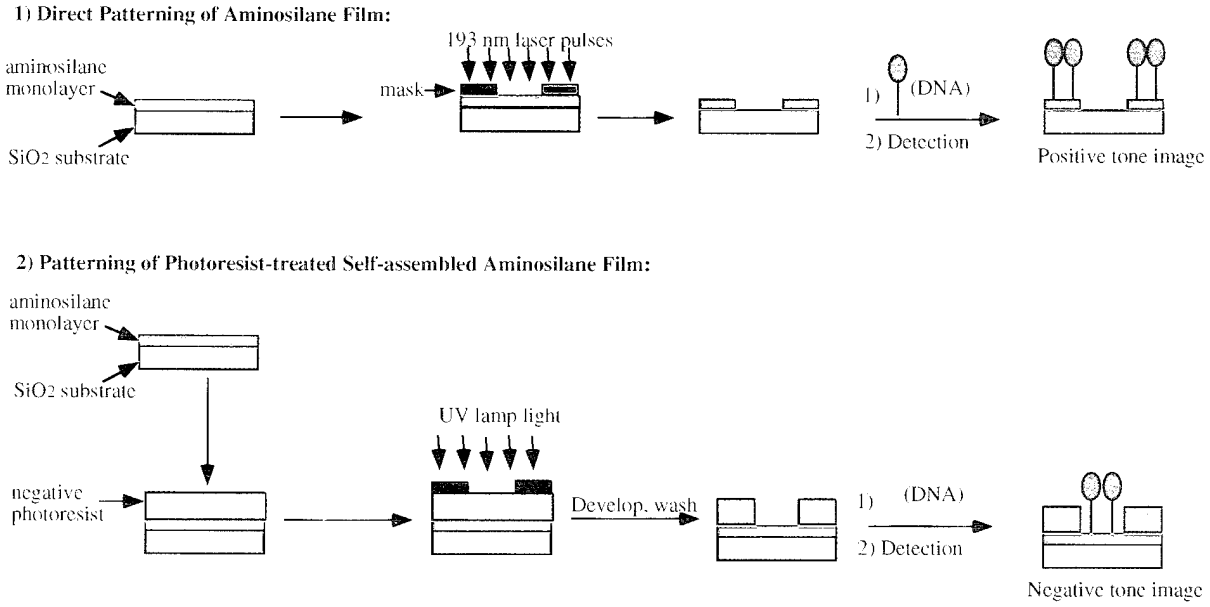

Fig. 9 — Methods of forming DNA patterns using self-assembled aminosilane films.

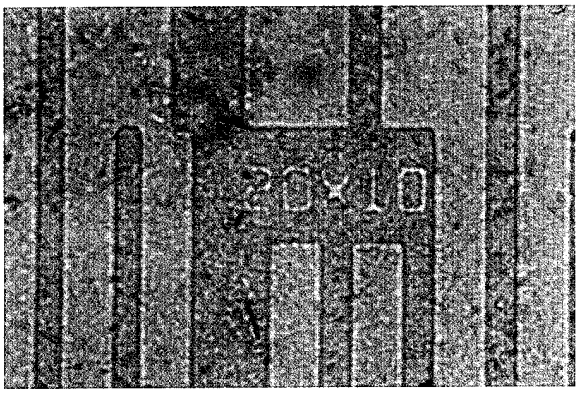

Fig. 10 — 40X brightfield image of a DNA pattern achieved using a photoresist-coated aminosilane surface. A biotin labeled DNA oligomer (20 bases long) was attached to the resultant patterned aminosilane film using a crosslinker, then visualized with an enzyme-linked colorimetric assay specific for the biotin group. The dark blue regions represent the immobilized DNA, which only binds regions bearing the aminosilane; minimal binding to areas bearing the resist is detected.

Acknowledgments: J.M. Calvert of the Center for Bio/Molecular Science and Engineering contributed to the microlithography aspects of this research.

[Sponsored by ONR]

References

1. L.A. Chrisey, P.M. Roberts, V.I. Benezra, W.J. Dressick, C.S. Dulcey and J.M. Calvert, "Selective Attachment of Synthetic DNA to Self-Assembled-Monolayer Functionalized Surfaces," *Materials Research Soc. Symposium Proc.* **330**, 179-183 (1994).

2. G.U Lee, L.A Chrisey, and R.J. Colton, "Direct Measurement of the Forces Between Complementary Strands of DNA," *Sci.* **226**, 771-773 (1994).

3. J.M. Calvert, in *Organic Thin Films*, A. Ulman, ed. (Academic Press, Boston, in press, 1994). ■

Portable Electronic Warfare Environment Simulator

M.S. Olson
Tactical Electronic Warfare Division

To support checkout of shipboard Electronic Support Measures (ESM) systems, simple RF signal sources are used in the Fleet. However these signal sources lack the versatility and realism for effective operator training purposes. Typically operator training can only occur when large threat simulator "vans" are installed. In response to this need, the ESM Branch of the Tactical Electronic Warfare Division has developed a portable EW environment simulator that meets both equipment checkout and operator training requirements in a single unit. It is designed to provide up to 1023 simultaneous signals in the frequency range from 0.5 GHz to 18 GHz and small enough to be housed in a 17-in. × 18-in. × 12-in., 50-lb case. The simulator operates under "Windows" control software on a laptop computer. The simulator supports complex pulse repetition interval (PRI), frequency, and amplitude modulations and provides the capability to simulate the most sophisticated radar signals. This article describes the design and technology incorporated into the portable simulator (Fig. 1) and its application as valuable training equipment for Navy and other service platforms.

Simulator Design/Technology: Figure 2 illustrates the functional design of the simulator. The laptop computer functions as the system controller and user interface. It has menu-driven software for creating scenarios composed of emitters with specific on and off times. When a scenario is started, the emitters are downloaded over an Ethernet link to the embedded PC in the simulator. The embedded PC and the digital subsystem communicate via the Versa module eurocard (VME) bus, which provides a bi-directional high-speed data-transfer capability. The digital subsystem translates the emitter parameters into pulse data words that describe the RF pulse to be generated. The RF subsystem houses the RF components, which are driven by the pulse data word to generate the actual RF pulses. The RF subsystem uses a voltage-controlled oscillator with a frequency feedback control system to increase frequency accuracy and decrease noise susceptibility of the generated RF.

System Capabilities: The portable simulator system is the most capable simulator developed for generating high fidelity signals of its size. It models antenna and scan pattern effects on a pulse-to-pulse basis and simulates complex PRI and RF modulation types. Specific RF modulation types include staggers, switching, agile, periodic functions, and continuous wave. Specific PRI modulations generated are staggers, jitters, synchronization, and phase-coded

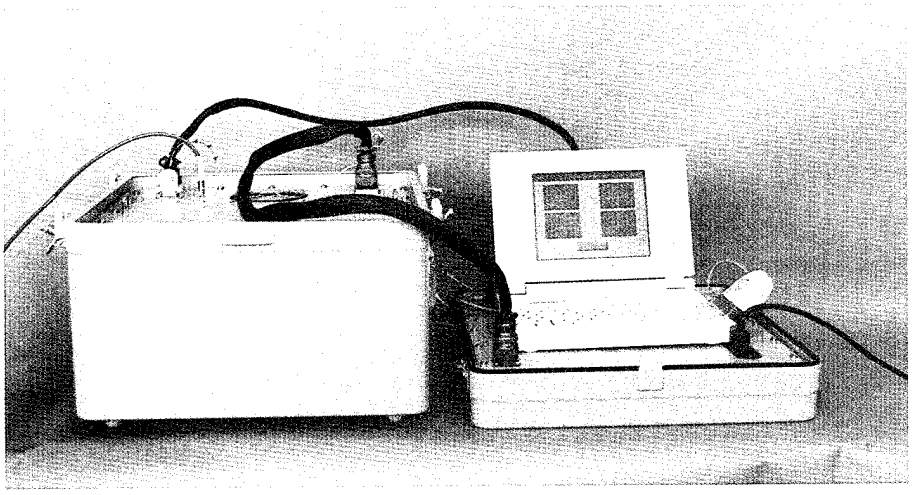

Fig. 1 — The portable electronic warfare environment simulator.

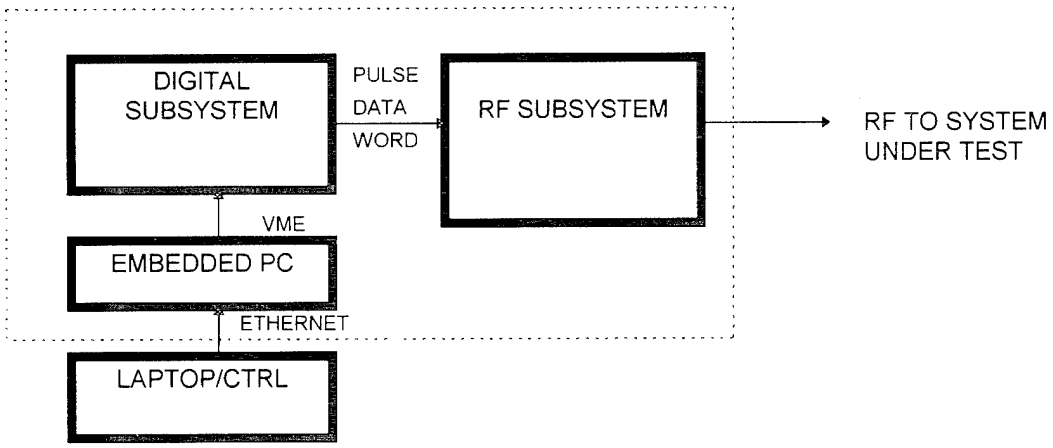

Fig. 2 — Portable simulator.

modulation. The VME bus architecture provides a very high pulse throughput capability. The simulator can generate up to one-million pulses-per-second and over 100 simultaneous signals. The system is also capable of generating signals directly from the Electronic Warfare Integrated Reprogrammable (EWIR) library and can store more than 100 EWIR signal modes at a time in its internal database (on the laptop computer).

Conclusion/Transition Plans: The first portable simulator demonstration unit has been completed, tested, and is currently being used as a testing device for ESM receivers under development at the Naval Research Laboratory. Plans for FY 95 include transitioning the unit for specific Fleet use in both airborne (EP-3) and sea platforms. Software development is also under way to enable the creation of realistic mission training scenarios involving multiple platforms and real-time platform motion simulation. This will enable the system to extract signals directly from the EWIR library and create a realistic RF signal environment for a given geographic/mission conflict area. By FY 96, miniaturization of the simulator to one-half the size of the demonstration unit is planned to enhance its versatility as carry-on training equipment for all Navy (or other service) EW platforms.

[Sponsored by ONR] ■

Target Recognition with Surveillance Radar

G.J. Linde and C.V. Platis
Radar Division

Long-range target identification is vital for a timely and correct response to unidentified targets in hostile situations. Friendly and civilian aircraft are presently identified with active transponders on the aircraft; however these systems are not always reliable, and they are not useful to identify hostile aircraft. Air surveillance radars can detect targets at long ranges and provide target position measurements; usually that is not sufficient information about the target for identification or classification. A project at the Naval Research Laboratory has demonstrated target recognition with a long-range, two-dimensional air-surveillance radar. The normal radar surveillance continued but was modified by replacing a few of the surveillance pulses with wideband pulses. Classification was into one of the perceptual classes of: large commercial jet, small jet interceptor, large propeller driven, small propeller driven, helicopter, and missile.

Information Obtained from Wideband Pulses: Normal radar air-surveillance uses pulses with a bandwidth of about 1 MHz, which is sufficient to resolve targets separated by more

than 150 m. To obtain information about a single target, several 200 MHz pulses are inserted in the radar dwell. These pulses will resolve individual scattering points separated by 1 m. This radar uses 100-μs pulse widths with linear frequency modulation (LFM). The pulses are compressed to obtain high range resolution target profiles. Figure 3 shows an example of the real-time computer display from a set of seven wideband pulses. In the middle left part of the screen is a drawing of an aircraft showing its relative position to the radar. This provides the operator with a visual indication of the aspect angle and target location. The upper left screen shows the amplitude of the return as a function of time. Since the pulse is LFM, this screen is also the frequency response of the target. Radial velocity is needed for time alignment of range profiles. Because of the large signal bandwidth, radial velocity can be obtained by measuring target movement from the first to last pulse. Measured target movement and the calculated radial velocity are displayed in the lower left screen. Range profiles from seven pulses are shown in the upper right screen. Time alignment was used to superimpose the profiles so that the pulses could be averaged. Note that for this aircraft, a 757, the individual scatterers are constant for all of the pulses. This is typical for jet-powered aircraft. From the average range profile (lower right), a target extent can be measured, and when combined with the aspect angle, a length or wingspan can be estimated. This aircraft is correctly classified as a "large jet."

Figure 4 is an example of a propeller-driven aircraft, a P-3. A photograph of the aircraft is included to show the location of the individual scatterers. The signal returns from the nose and tail areas are constant in all of the pulses while returns from propellers show large fluctuations. The modulation power in all of the individual scatterers is measured and used in the classification process to differentiate between jet-powered and propeller-driven aircraft. This aircraft is also correctly classified as a "large prop."

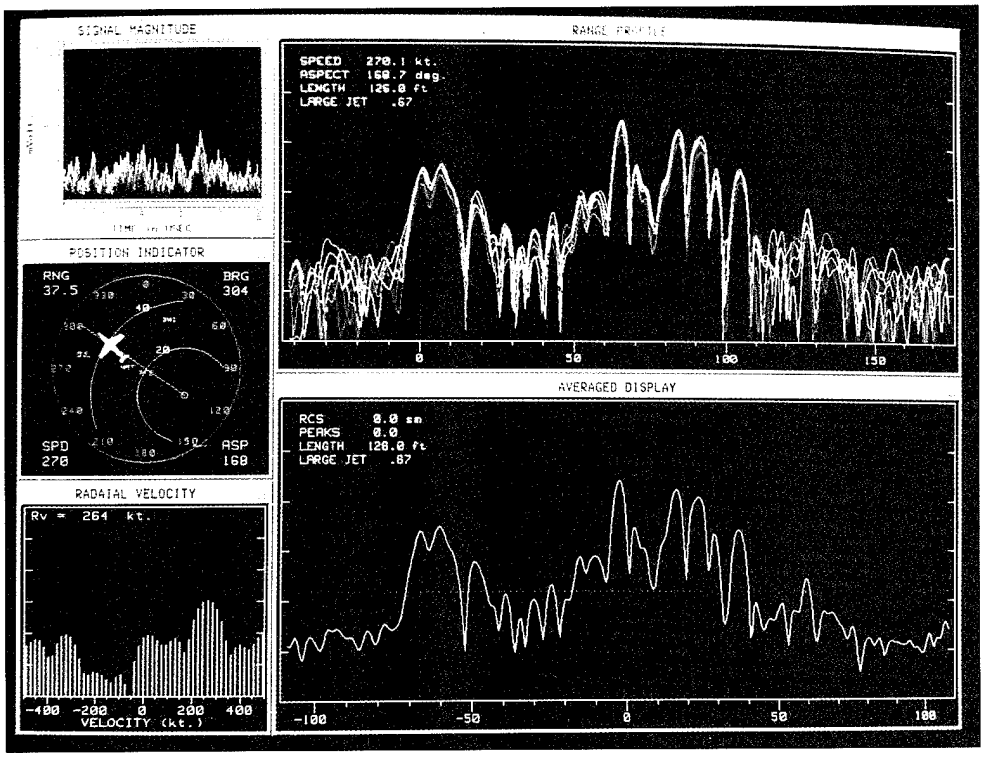

Fig. 3 — Radar display of high range resolution data.

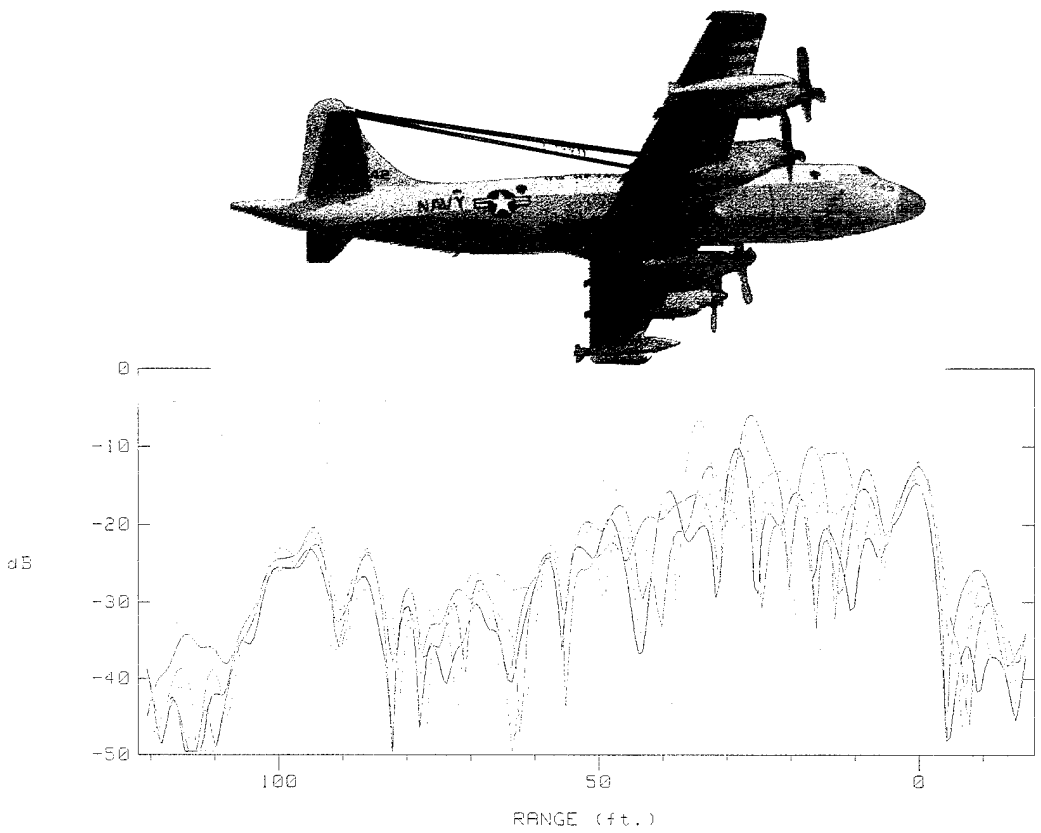

Fig. 4 — Range profile of P-3 aircraft showing location of propellers.

Classification process: From high resolution profiles, several target features are measured, including extent, cross section, and modulated scatterer location. The features are combined with target speed and aspect angle obtained from normal surveillance tracking data. Measured target features are converted to logic variables that are used in a rule-based classification system. The experimental system has demonstrated a 90% classification accuracy of aircraft flying in the Washington, D.C. vicinity, showing that it is possible to perform air surveillance and classify uncooperative targets into useful, perceptual classes.

[Sponsored by ONR] ■

The Development of Over-the-Horizon Radar at NRL

J.M. Headrick and J.F. Thomason
Radar Division

The Naval Research Laboratory's (NRL) initial development of high-frequency (HF) over-the-horizon (OTH) radar has been followed by fielding Navy operational radars, the AN/TPS-71 relocatable over-the-horizon radar (ROTHR). NRL's successful development of HF OTH radar is one of the most significant radar accomplishments since WWII. This is especially true when one considers that NRL succeeded where others had given up. Microwave radar, as developed and employed during WWII, has its range limited by the curvature of the Earth, just as visual ranges are limited. At the end of the War, a number of investigations in several countries were initiated to try to dramatically increase radar range by an order of magnitude; the concept was to operate in the HF band and use the ionosphere to refract rays back to the Earth at distances far beyond the optical horizon. Also there were programs aimed at using HF propagation by the surface-attached wave to extend ranges a modest distance beyond the horizon. A major difficulty with OTH radars is the sea-clutter echo that occurs at the same ranges as that of targets; the amplitude of this clutter is many orders of magnitude greater than

that of desired targets, and 1950s signal processors were inadequate for separating targets from the clutter. By the mid-1950s, most of the programs were terminated because of marginal or no success.

NRL Program: In the 1950 timeframe, NRL recognized that technology in several areas was progressing such that HF OTH radar might be realizable in the near future, and a program was started. The concept was to exploit matched-filter processing (or, as referred to then, "cross-correlation processing") so that targets were separated from the clutter and each other in the Doppler velocity dimension. By 1955, NRL had in operation a low power HF radar called MUSIC (multiple storage integration correlation). OTH sea backscatter and line-of-sight aircraft target properties were examined, and with this knowledge, success was predicted for OTH radar, including system requirements. Although the NRL effort was aimed at air targets, with the MUSIC radar, it was discovered that the ionospheric disturbance that accompanied nuclear tests was easily detected; this was followed shortly by another first, the detection of a rocket launch because of its distinctive disturbance of the ionosphere. Along with the MUSIC radar experiments, the MADRE (magnetic drum radar equipment) development was started, which culminated in a high-power, high antenna gain system located on the Chesapeake Bay. Figure 5 shows the antenna. With this radar, aircraft detection and tracking across the Atlantic was achieved in 1961—the primary goal of the program. Recognition of the potential of narrowband, high dynamic range processing was a major component of NRL's success. With the MADRE, nearly all of the fundamental capabilities of HF OTH radar were first discovered and demonstrated: ship detection, sea state determination and storm tracking, vectoring aircraft to intercept, and Battle Group early warning. Computer model development was started that enabled realistic design of future systems. The

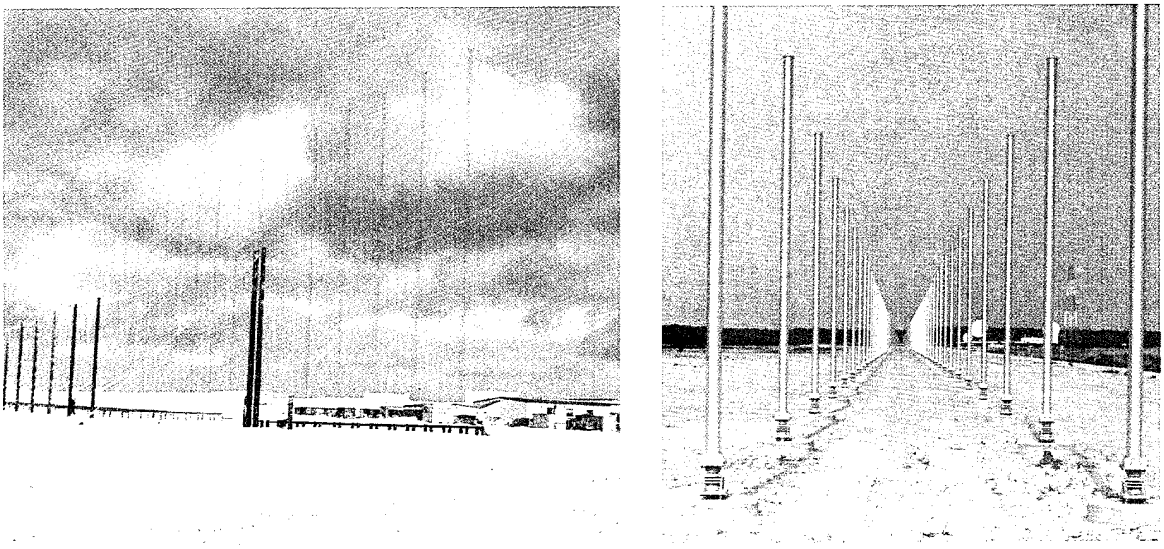

Fig. 5 — On the left is a picture of the ROTHR transmit antennas. Two arrays cover 5 to 28 MHz; each array is composed of 16 log periodic elements. A single pair of log periodic elements used for the oblique backscatter sounder covers 5 to 28 MHz for ionosphere diagnostics. The width across all of these arrays is about 850 m. On the right is a picture of the receive array. The elements are endfire monopoles 372 in number and disposed over 2700 m. The transmit and receive antennas are separated by sufficient distance to permit simultaneous operation and thereby greater flexibility in waveform selection.

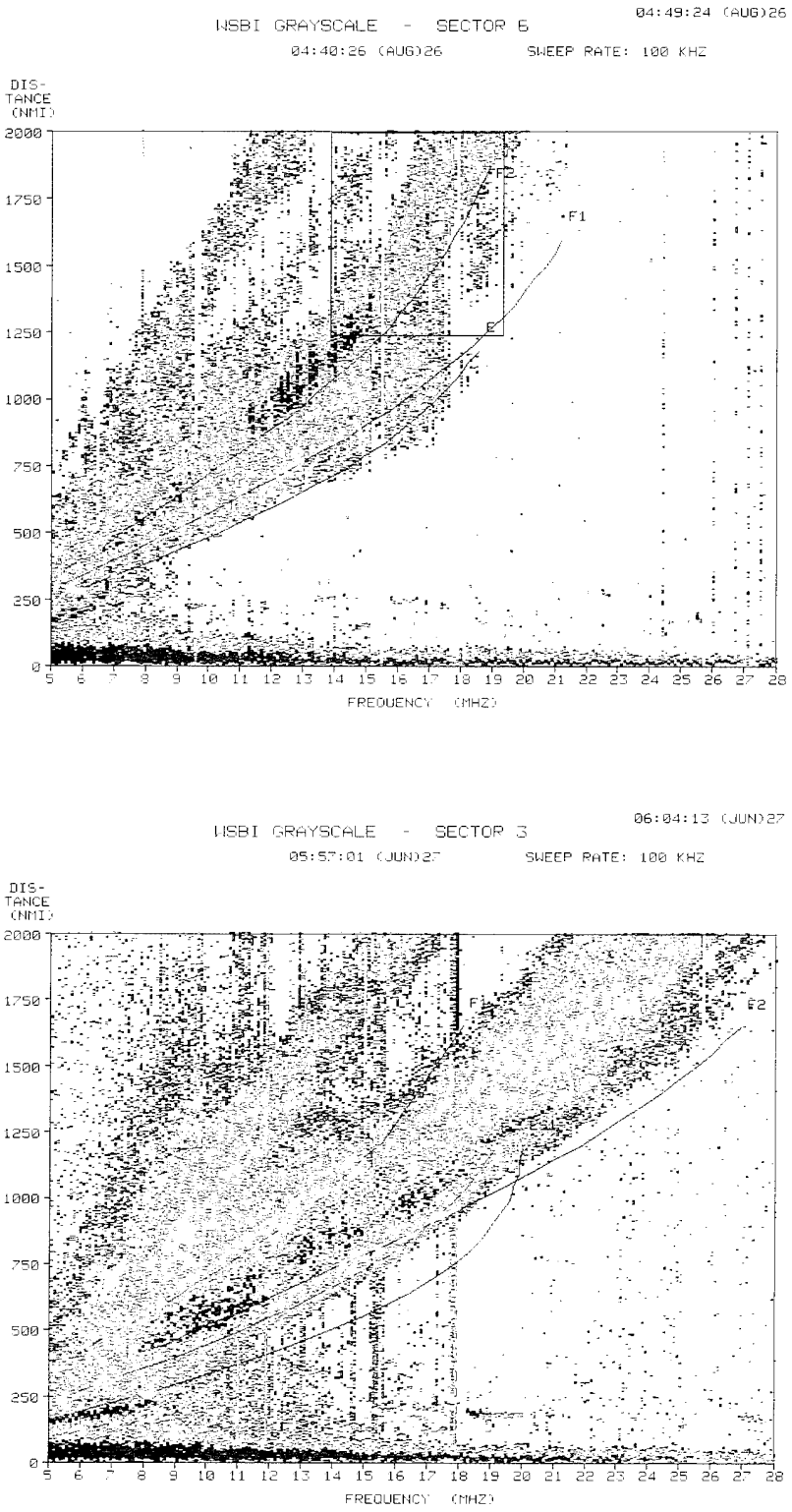

Fig. 6 — Two examples of the oblique Earth backscatter soundings are shown. The vertical axis indicates range and the horizontal frequency. Amplitude of backscatter is shown by color where yellow indicates the greatest amplitude. The examples were made at about the same time but on different days and indicate how radar frequency selection must be adaptive to existing conditions.

NRL developments in OTH radar have provided the base that led to operational systems such as the Air Force AN/FPS-118 radar for continental air defense and the Navy ROTHR, as well as influencing HF radar development in Australia and other parts of the world. Over the years, other organizations have made contributions to the OTH technology, however NRL made the basic discoveries and demonstrations. The major factors in making OTH radar practically realizable are the advances in digital signal processing hardware.

Operational System Realization: The AN/TPS-71 ROTHR is the current operational payoff of the earlier NRL research and development. During acquisition and at present, NRL is the principal technical advisor to the ROTHR Program Office. The primary mission of this radar is to provide long-range air surveillance for the Battle Group at sea. The ROTHR can illuminate an area nominally 8° wide and up to 500 nmi deep and receive with 16 half-degree-wide beams. This footprint can be stepped over an area bounded by 80° in azimuth and between 500 and 2000 nmi in range and thereby scan over an area of more than a million square miles. Figure 5 has pictures of the antenna systems. A major difference from the OTH radar over conventional radar is that its operating frequency and waveform must be matched to the variable and not entirely predictable ionosphere and environment. Figure 6 displays diagnostics that address this requirement. Figure 7 gives coverage and scan examples. In 1989, a procurement for three production radars was initiated with Raytheon at a cost of $270M. A prior-constructed prototype was installed and tested in Virginia and then relocated to Amchitka, Alaska. Operational testing deemed

Fig. 7 — A nominal potential surveillance area, 500 to 1600 nmi by 64°, is shown. Selected search areas are superimposed and the radar moves sequentially through these areas.

the radar worthy, and the first production unit has been deployed to Chesapeake, Virginia; it is being used by the Navy to provide surveillance of the Caribbean. The second unit is being installed in southern Texas where it will also provide coverage of the Caribbean and adjacent land areas. The third production unit is in storage awaiting a deployment decision. Such wide-area coverage is economically feasible only by HF radar.

Continuing Work: HF radar achieves its long ranges in effect by using the ionosphere as a gigantic mirror. This "mirror" has defects and considerable variability. This variability is only predictable on a median basis, and these predictions are derived from empirical measurements with no complete theory as yet. Data that are routinely available from the ROTHR during its operational tasking are providing excellent opportunities for increasing knowledge on ionospheric radiowave transmission, improving radar performance prediction capability, and learning how to improve performance.

[Sponsored by SPAWAR] ■

Microelectronics and Photonics Test Bed

J.C. Ritter and W.J. Stapor
Condensed Matter and Radiation Sciences Division

K.A. Clark and M.D. Frank
Space Systems Development Department

Satellite systems have to be able to operate in the Earth's radiation belts to carry out their mission. The performance of modern microelectronic and photonic devices can be degraded or destroyed by the natural space radiation environment, which consists of high-energy protons and electrons in the Van Allen belts and cosmic rays. Space radiation can affect these devices and subsystems in several ways. A single-event upset (SEU) can occur in digital electronics when an incident proton or cosmic ray passing through the spacecraft device induces a transient which causes a bit flip. A single-event latchup (SEL) is similar except that the induced current driven by the power supply does not go away until power is strobed. Radiation can also do permanent damage to devices or burn them out. There are two primary ways these effects are circumvented—by purchasing radiation-hardened devices and by qualifying radiation-tolerant devices by ground testing (shielding is not effective against high-energy radiation). Purchasing radiation-hardened devices will solve the radiation effects problem. However these devices are much more expensive than nonhardened devices (not every device is available in a hardened version), and hardened devices are typically two to three generations behind nonhardened devices in performance (about a factor of 10). Furthermore since radiation hardened devices were built primarily to withstand nuclear effects, they are becoming much less available since the end of the Cold War. The more desirable approach of qualifying radiation-tolerant devices involves performing ground-based radiation testing on nonhardened devices to determine if they will survive in the radiation environment of the orbit in question. The results of the ground-based radiation testing are used to extrapolate the device's survivability in the particular orbit. Many times this extrapolation underestimates survivability, and devices that could survive are not used. A more dangerous possibility occurs when survivability is overestimated, and a device fails in orbit.

System Program Offices (SPOs) are reluctant to fly devices unless they have been used successfully in another space system. The Microelectronics and Photonics Test Bed (MPTB) Programs seek to enhance our ability to extrapolate ground-based radiation measurements to a device's survivability on orbit. The MPTB is a satellite payload that will be used to measure the effects of space radiation on microelectronic and photonic devices and subsystems. The program can be divided into two parts—science and engineering. The scientific portion is handled by the Radiation Effects Branch of the Condensed Matter and Radiation Sciences Division. It includes the ground testing, survivability modeling, and space data analysis. The engineering portion is handled by the Space Systems Development

Department. It provides the flight hardware necessary to perform the on-orbit radiation testing.

Scientific Portion: The MPTB will be used to space-qualify and evaluate the space-radiation tolerance of microelectronic devices and subsystems, fiber optics, and photonic devices in the space-radiation environment. Functional electronic changes caused by ionizing particles and total-dose radiation will be measured in a controlled experiment, with device data telemetered to the ground. These effects will be measured: (1) SEU and SEL in memories and microprocessors; (2) bit-error-rate effects in fiber-optic data buses; (3) development of hot pixels or degradation of charge transfer efficiency in charge-coupled devices (CCDs); (4) timing degradation, threshold voltage shifts, or leakage current increases in integrated circuits; and (5) component and subsystem degradation of critical photonic technologies.

The MPTB Program includes ground test, modeling, and analysis. The purpose of this program is to perform radiation tests at various radiation facilities on the ground on each device type or subsystem to be flown. The devices will also be modeled, and predictions of their SEU rate and radiation degradation in space will be made in advance of launch. Predictions are based on our current models of the space-particle fluences. The predictions will be compared to the actual space measurements after corrections are made for the observed space-radiation environment during the mission. Only by measuring the space upset rates and the space environment simultaneously can we remove the uncertainty in the space environments and focus on the basic problems inherent in making space predictions based on ground tests. Better predictive models will be developed based on these results.

In the case of microelectronic devices, current models already exist, and these work well for some devices. For more modern, small feature-sized devices, they may be off in their predictions of SEU, for example, by an order of magnitude. For CCDs and focal plane arrays, models for radiation effects have been developed, but careful space experiments are needed to validate the models. For most photonic devices, the models are in various stages of development and are largely unproven by space tests. The MPTB flight data for these technologies in connection with ground tests will play a crucial role in model development and in qualifying these technologies for space applications.

The MPTB also contains devices to monitor the environment. These include metal-oxide semiconductor (MOS) dosimeters for total dose, silicon pulse-height analyzers for particle flux and an instrument to measure the fluxes, energy spectra, and chemical composition of energetic ions. Thermistors for temperature measurement are also included.

Engineering Portion: This portion provides the flight hardware necessary to perform the on-orbit testing. It must provide all the necessary measurement functions without requiring an excessive amount of power, size, and weight that prevent it from flying on the host vehicle. Figure 8 is a block diagram of the hardware. It can be divided into two parts—the core controller and the experiment panels. The core controller is the master controller of the MPTB. It provides the interface to the satellite, receives commands from the ground, and formats experiment data for downlink. Additionally it is the master scheduler, commanding the experiment panels to run their experiments at the appropriate time.

Each experiment panel contains an experiment-panel controller and several device-under-test (DUT) blocks. The experiment-panel controller contains a microcontroller, analog measurement tools, and power converters. The microcontroller interfaces with the DUT blocks and runs particular experiments when commanded to do so by the core controller. The analog measurement tools measure voltage and current used by the DUTs and provide analog stimulus to the DUTs, when necessary. The power converters convert the satellite voltage levels to the levels required by the DUTs. There is also the capability to remove power from individual DUT blocks.

Demonstration Model: To demonstrate the experiment panel proof-of-concept, we built a demonstration module. Figure 9 shows the

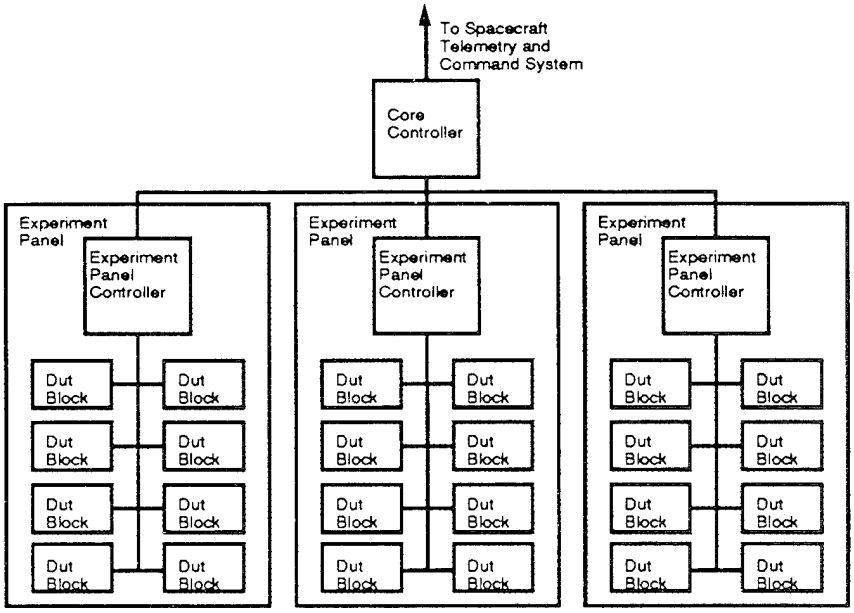

Fig. 8 — The core controller and the experimental panels.

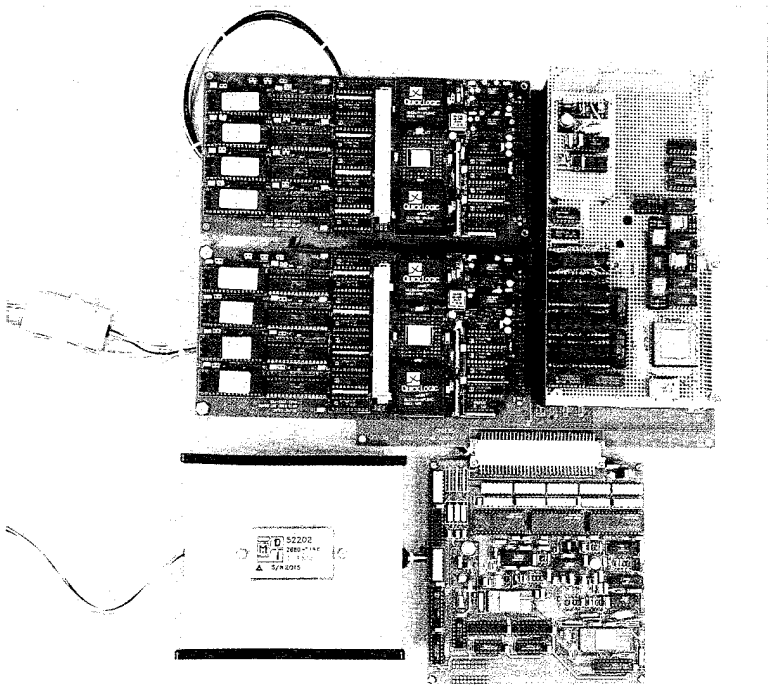

Fig. 9 — The MPTB demonstration module.

model. The computer is used to emulate the microcontroller. An analog daughterboard provides the analog measurement tools, and a dc-dc power converter converts 30 V from a bench power supply (simulating a satellite's power system) to ± 15 V and $+5$ V required by the DUTs. The module contains the following DUTs: four IBM 16-Mbit dynamic RAMs and two IDT 3081 RISC microprocessor subsystems.

Acknowledgments: The authors acknowledge Lt. Col. Glenn Kweder at the Defence Nuclear Agency and CAPT George Mitschang at the Naval Space and Warfare Systems Organization for sponsoring the program and the MPTB Working Group for participating in all phases of the design.

[Sponsored by DNA and SPAWAR] ■

High Sensitivity Measurement of Mechanical Loss

R.A. Kant and C.A. Carosella
Condensed Matter and Radiation Sciences Division

Naval Research Laboratory (NRL) scientists have developed an instrument that has extreme sensitivity to energy dissipation and frequency changes in mechanical resonators. It has many potential applications, including detecting and identifying low levels of both chemical impurities and structural defects. While previous instruments measured loss in a resonator to 1 part in 10, the new instrument measures mechanical loss to 1 part in 10^4 or better. Thus the new spectrometer can separate low-level signals from background signals that are several orders of magnitude larger.

Background: Chemical and structural defects in solids have a profound influence on the behavior and properties of solids, including electrical and thermal conductivity, corrosion resistance, hardness, and fatigue life. For many years researchers have used mechanical loss (or internal friction) spectroscopy to study a wide range of defects, including substitutional impurities, vacancies, interstitials, dislocations, and grain boundaries. Loss spectroscopy has also proven valuable for investigations of radiation damage, diffusion, and thermal processes. Today there is a renewed interest in loss-measurement techniques because of the discovery that the sensitivity and selectivity of chemical sensors are greatly enhanced by information from loss measurements. In addition, researchers have recently begun to use loss measurements in tribology to study atomic-level interactions at interfaces between sliding surfaces. However the sensitivity of conventional techniques limits the resolution in these new applications, and the small signals of interest have been difficult or impossible to detect. A new detection circuitry developed at NRL provides a thousand-fold increase in resolution and therefore makes it possible to isolate and measure effects that were previously undetectable.

Loss spectroscopy is based on the fact that defects absorb energy produced by external stresses and dissipate it as heat. A loss spectrum is made by measuring energy loss as a function of temperature while mechanically stressing a sample at a fixed frequency. Peaks appear in a spectrum when the relaxation time of a defect is comparable to the period of the applied stress. In order to make a loss measurement, a resonator is made to vibrate near a resonant frequency. In the case of quartz-crystal resonators, this is accomplished by delivering the driving signal to metal electrodes deposited directly on the quartz. When the drive signal is switched off, the amplitude of the oscillations decreases due to energy dissipated by defects in the resonator. The loss per cycle is then determined from the decay rate of the vibration amplitude. A detector circuit measures the decay of peak amplitude as a function of the number of cycles executed, and the loss is calculated from the slope of a fit to the logarithm of the decay signal. We achieve extremely high sensitivity by means of a new detector circuit and the associated software.

The NRL Loss Spectrometer: Figure 1 is a block diagram of the NRL high-resolution loss spectrometer. A computer controls all operations of the instrument and performs data acquisition and analysis. Specimens are mounted in a vacuum cryostat and maintained at any temperature from 4 K to 600 K, to within ± 1 mK. Signals from the resonator are amplified and fed to a digital detector circuit invented at NRL which, in turn, gates two counters. One counter determines the number of vibrations executed between each of a number of threshold amplitudes, and the other records the elapsed time for determining the resonant frequency. If a single relaxation process dominates the behavior of the decay, then the experimental data are indistinguishable from a least-squares fit of the data (see Fig. 2). The insert to the figure shows that the individual data points differ from the theoretical curve by less than one part in a thousand. Changes in the deviation from the best fit or unusually large deviations indicate the presence of multiple relaxation phenomena, and

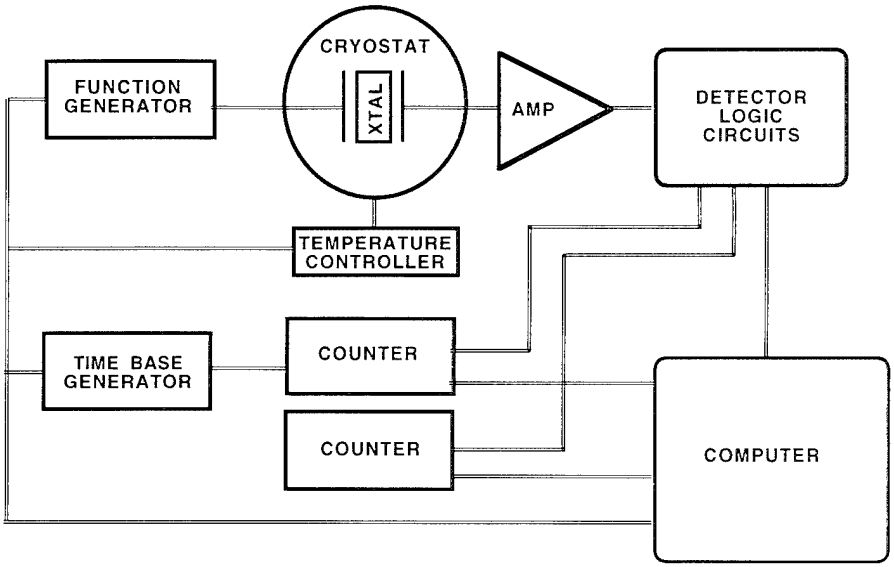

Fig. 1 — The mechanical loss spectrometer; the crystal (xtal) under test is in a temperature-controlled environment.

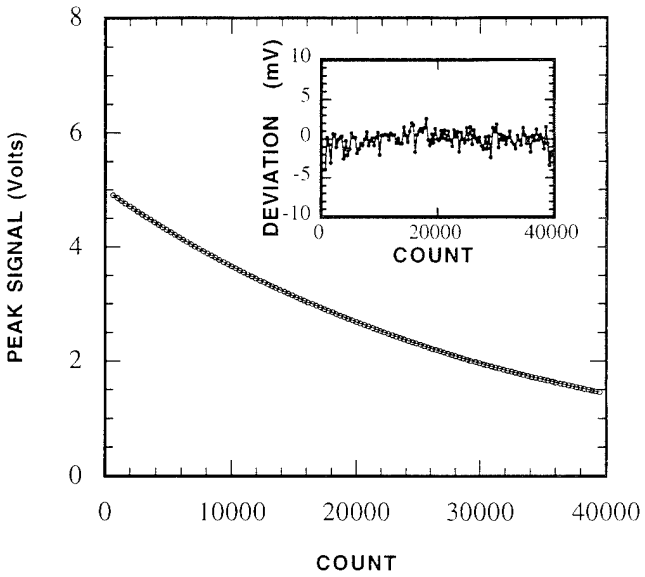

Fig. 2 — Peak amplitude of free decay signal as a function of the number of vibrations (counts). The insert shows the deviation of the experimental data from a fit to the behavior expected for a single loss mechanism.

additional analysis is needed. Fits of selected portions of each decay curve can give multiple loss rates.

Performance: Figure 3 shows the high resolution achieved with the NRL loss spectrometer. These spectra are from a high-purity, low-defect-density quartz. Figure 3(a) is displayed at a resolution consistent with a conventional spectrometer, and it reveals no small features or structure in the spectrum. In comparison, Fig. 3(b) is a high-resolution version of a portion of the same spectrum with the background subtracted. Note that the amplitude of the loss peak near 230 K in Fig. 3(b) is only 2×10^{-8}, and yet this peak is easily resolved

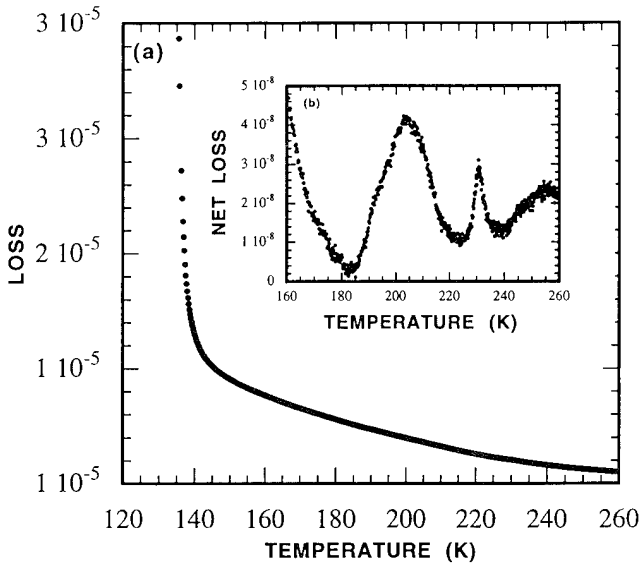

Fig. 3 — Featureless loss spectra obtained at ordinary resolution (a) is shown to have significant structure at high resolution (b) using the NRL mechanical loss spectrometer. The smoothly varying background was subtracted to obtain the high-resolution plot.

from the overall background loss of 10^{-5} in that portion of the spectrum. This illustrates the resolution achieved with the NRL mechanical spectrometer.

Relaxation phenomena with very large activation energies have high temperature loss peaks, but raising the temperature too high can significantly alter or damage the host material. The time dependence of loss at a number of temperature points well below the loss peak will yield, for example, the high temperature activation energy. The high sensitivity of the NRL spectrometer makes it well suited to take such measurements. In fact we have measured loss changes as small as 10^{-9} per hour by using the new instrument. The study of such high activation energy-relaxation processes provides a way to increase our understanding of long-term instabilities in quartz and other technologically important materials. In summary, the new, high-sensitivity NRL loss spectrometer opens the way to the study of a new range of defect densities and dynamical effects, and it may serve as the basis for a new generation of ultrasensitive chemical sensors.

[Sponsored by ONR] ■

Nike KrF Laser Facility

S.P. Obenschain
Plasma Physics Division

The Nike laser is the world's largest krypton-fluoride (KrF) laser. The laser has 56 beams, producing 5 kJ in a 4 ns pulse length. The laser was funded by the Department of Energy to address target physics and laser technology issues for direct-drive pellet fusion. Direct-drive fusion requires short laser wavelength to obtain good laser-target coupling and highly uniform laser illumination of the imploding pellet. The KrF laser has the shortest wavelength (248 nm) of existing high-energy lasers. The primary advantage of the KrF laser however is its unique capability for producing highly uniform target illumination based on a beam-smoothing technology invented at NRL. With Nike, we have obtained focal profiles that have smaller fluence nonuniformities (< 2% RMS) than that of any other laser fusion facility. The uniform Nike beams will be focused and overlapped onto planar foil targets under conditions that mimic the initial stages of a pellet

implosion. Over the next few years Nike will be used to study the laser acceleration of these targets with the goal of demonstrating sufficient uniformity for pellet fusion.

The KrF Laser: Figure 4 is a diagram of the Nike facility. Nike uses discharge-pumped amplifiers to reach energies of a few joules and two E-beam pumped amplifiers to achieve 5 kJ of laser energy. The final two amplifiers are pumped by E-beams for 120 and 240 ns, respectively. The power from the E-beam-pumped amplifiers is multiplied by means of angular multiplexing whereby numerous 4-ns duration beams sequentially extract energy from each amplifier. The beams are delayed after amplification so that all of the beams arrive at target at the same time. Nike uses a 45-m long by 6-m high laser enclosure to transport the numerous laser beams in angular mutiplexing system. Low air turbulence is achieved in this "propagation bay" by keeping all the wall temperatures the same to within 0.5° F. This good temperature control also helps maintain beam alignment. A computer-controlled system was developed for Nike that allows all 56 beams to be remotely aligned in a few minutes.

The broad bandwidth and low nonlinear index of the gaseous KrF amplifying media gives KrF lasers a unique capability for achieving uniform and controlled focal profiles [1]. An aperture at the beginning of the amplifier chain is uniformly illuminated by a multimode KrF oscillator. This aperture is then imaged through the amplifiers onto target. Because gas lasers have low nonlinear index of refraction, the uniformly illuminated aperture can be imaged onto target with good fidelity. Figure 5 shows a sample flat-top focal profile obtained after the penultimate 20-cm aperture E-beam pumped amplifier. The residual nonuniformity is less than 2%. We expect to maintain this good focal uniformity after amplification by the recently completed 60-cm aperture final amplifier.

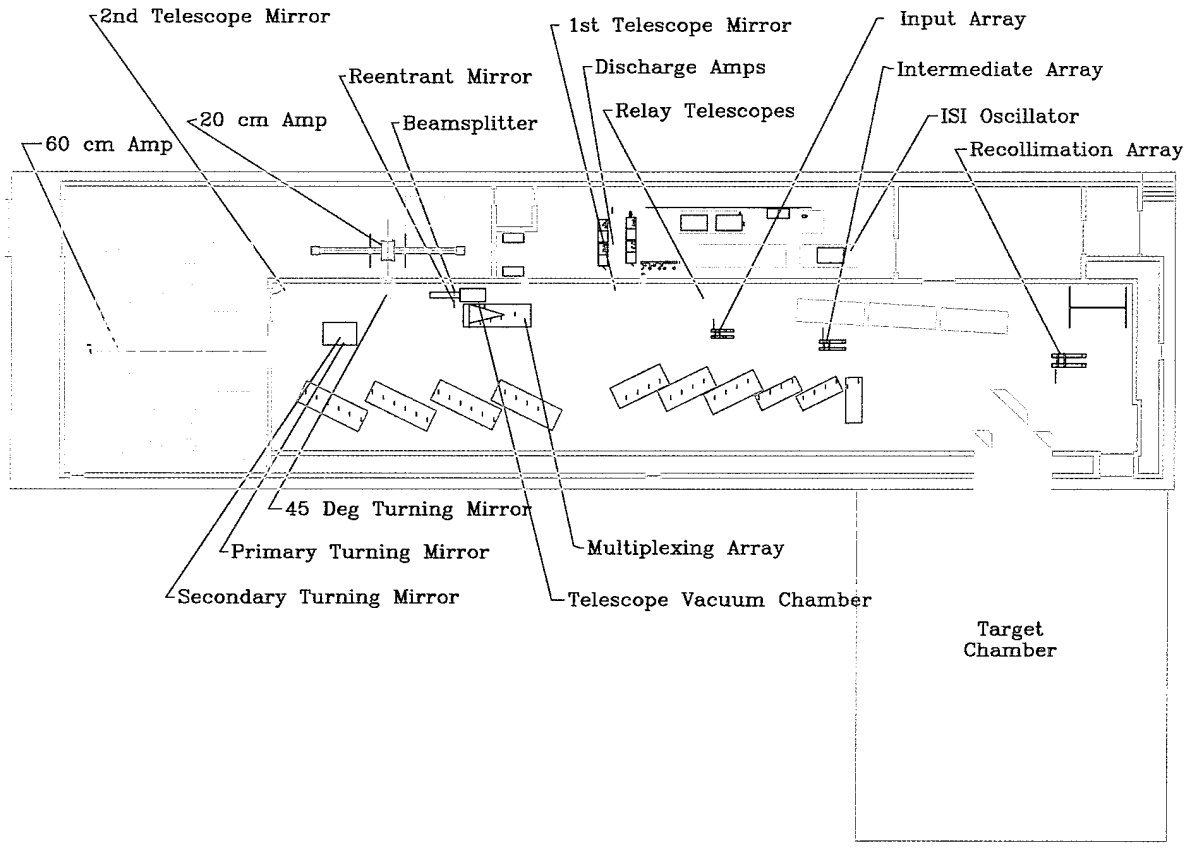

Fig. 4 — Floor plan for the Nike KrF laser.

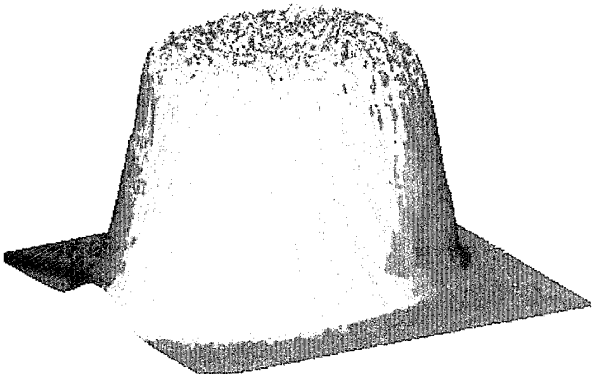

Fig. 5 — Focal profile of a Nike beam obtained after amplification by the 20-cm aperture amplifier. The profile has less than 2% RMS fluctuations—about five times better than achieved by other high-energy laser facilities.

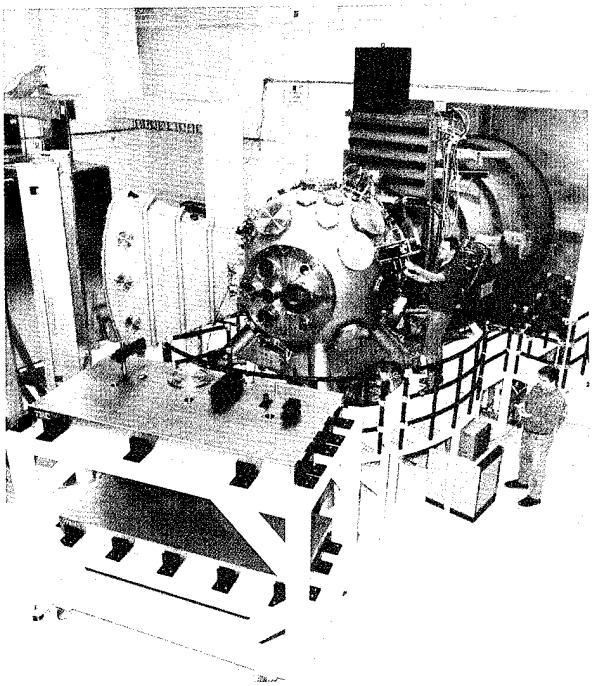

Fig. 6 — The Nike laser beams are concentrated onto thin planar targets in this vacuum chamber. The goal is to accelerate targets to high velocity with the uniformity required for pellet implosions.

Laser Accelerated Targets: The laser facility has achieved its design goal of 5 kJ energy output, and we expect to begin laser-target experiments before 1995. Figure 6 shows a photograph of the completed Nike target chamber. Forty-four of the beams will be focused and overlapped onto 1 to 10 mg/cm^2 plastic and solid deuterium targets in the target chamber. The laser is designed to achieve 2 × 10^{14} W/cm^2 illumination intensities with typical focal diameters of 600 μm. The beam overlap adds additional smoothing, and we expect to obtain effective focal intensity nonuniformities smaller than 0.4% for the target experiments. This is about a factor of 20 to 30 better than achieved at other high-energy facilities that use glass lasers. The targets will be accelerated to velocities of 100 to 200 km/s in reaction to the high pressures produced by intense laser heating of the target surface. Twelve laser beams will illuminate auxiliary X-ray-producing targets to radiograph the accelerating targets. The target experiments will explore means for inhibiting hydrodynamic instabilities that can be seeded by target imperfections as well as nonuniformity in the laser. Inhibition of these instabilities is regarded as the primary remaining obstacle to achieving direct-drive laser fusion. If the improved laser illumination available with Nike allows target acceleration with sufficiently high uniformity, then direct-drive laser fusion may be possible.

Acknowledgments: Development of the Nike laser involved the work of numerous scientists, engineers, and technicians working for NRL and its contractors. Participants include S.E. Bodner, J. Bone, D. Hardesty, K.A. Gerber, D. Gibson, R.H. Lehmberg, E.A. McLean, C.J Pawley, M.S. Pronko, J.A. Stamper, V. Serlin, J.D. Sethian, and C.A. Sullivan from the Plasma Physics Division; T. Lehecka, A.V. Deniz, and J. Hardgrove from Science Applications International; J. Sawyer from Commonwealth Technology; F. Mora and W. Webster from East Coast Engineering. Los Alamos National Laboratory provided a portion of the optics and participated in the optics design.

[Sponsored by DOE]

References

1. R. H. Lehmberg, J. Goldhar, *Fusion Technology* **11**, 532 (1987). ■

Diamond Photodetectors

M. Marchywka and D. Moses
Space Science Division

P.E. Pehrsson and J.E. Butler
Chemistry Division

S.C. Binari
Electronics Science and Technology Division

Ultraviolet light is generated by a variety of important natural and synthetic systems, including the Sun, chemical reactions such as combustion, lasers, fluorescent lights, and laboratory plasmas. In many of these systems, such as the Sun, the UV emission provides unique scientific data about the physical processes involved. In others, such as combustion systems, it can provide technologically important information for process optimization. However many applications of the UV are hindered by the lack of suitable detectors. We have investigated diamond-based detectors and found that many of the problems with existing detectors can be eliminated or reduced sufficiently to make many new applications of the UV viable. We discuss the problems inherent in prior UV detectors and how diamond detectors overcome them.

Existing Problem: The Sun provides an excellent example of a natural phenomenon that can be studied by its UV emission characteristics. It also exhibits the most common problems encountered in attempting to exploit the UV in other applications. Figure 7 shows a typical imaging UV detector. This detector is designed for the Extreme UV Imaging Telescope on the joint National Aeronautics and Space Administration/European Space Agency's Solar Heliospheric Observatory (SOHO) satellite and is representive of existing silicon detectors. The actual detector is the tan rectangle in the center of the photograph. The bulk of the apparatus is composed of support systems that are required because of limitations in the detector. The gold supporting rod is required to cool the detector to remove dark current and radiation-induced degradation. A complex optical system is required in front of the detector to remove all of the visible light from the UV signal of interest. This last problem is quite severe because the Sun's UV output is a small percentage of its visible light output, and the detector will respond to the undesired visible component as well as the UV signal of interest. Essentially all of these detector problems would be solved if the detector were fabricated from diamond rather than silicon. Such a detector could be incorporated into a future solar-observing instrument that is cheaper, more reliable, and more useful than instruments based on current technology because all of the above support systems could be eliminated.

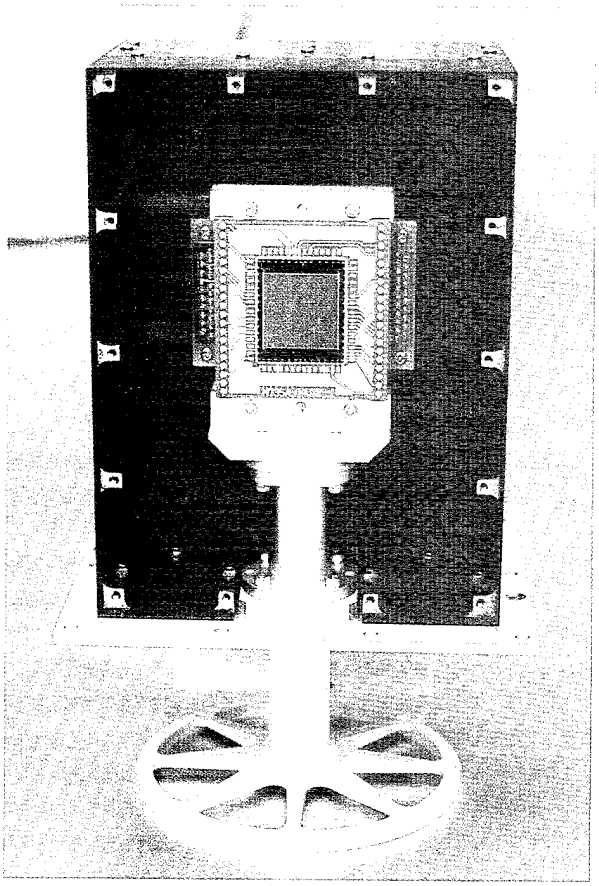

Fig. 7 — A representative UV imager mounted in a housing for a long-duration space-flight mission.

Diamond Solution; Progress and Promise: Recent work among the Space Science, Electronics Science and Technology, and Chemistry Divisions has allowed us to develop prototype detectors that prove many of the expected performance gains can be realized. This has been

accomplished by using natural diamond instead of silicon and patented processing techniques developed by careful analysis of the properties of diamond and the requirements of the detector. Both photoconductive, diamond metal-semiconductor-metal (MSM) detectors, and metal-insulator-semiconductor (MIS) devices have been successfully tested. We have observed that the diamond MSM's respond to UV light 1000 times more efficiently than to visible light. Such selectivity is sufficient to reduce the complexity of many solar-observing instruments and increase their scientific returns. We have obtained MIS devices (one picture element of an imager) with no measurable dark current (several order of magnitude better than is obtainable with today's best silicon detectors). This combination of attributes can already be used to advantage in several UV sensing applications.

The scientific return from the development program itself illustrates the synergy that can result from a focused, interdisciplinary, and interactive program. In particular, the development of a key processing step that made it possible for the MIS detectors to function was the result of considering simultaneously the behavior of the diamond surface, the detector structure, and the detector performance requirements. This integrated approach led to a novel electrochemical cleaning step (U.S. Patent 5,269,890) that can be used to exploit the benefits of diamond in other electronic device applications [1].

[Sponsored by ONR and NASA]

Reference

1. L. Pan and D. Kania, eds., *Diamond: Electronic Properties and Applications* (Kluwer Academic Publishing, Boston, 1994).

Integrated Services in Tactical Communication Systems

E.L. Althouse, J.P. Macker,
J.P. Hauser, and D.J. Baker
Information Technology Division

The Naval Research Laboratory (NRL) has developed technology to support integrated multimedia services in military tactical communication systems. Because of the limited data rate available in tactical radio-frequency (RF) transmission systems (typically less than 10,000 bps), support of multiple services within a single communication system is presently almost nonexistent. Methods are needed to replace dedicated, single-function, tactical communication networks and point-to-point circuits with systems that will support multiple uses such as tactical data broadcast, file transfer, image transfer, e-mail, command and control, interactive white boards for tactical strategizing, and interactive near-real-time voice. By transitioning unique RF multichannel architecture (MCA) networking technology previously developed under NRL's Exploratory Development Program [1], it is now possible to support integrated digital services on tactical networks. Voice is supported using recent technological advancements in vocoder technology at fixed rates of 600, 800, 1200, and 2400 bps. Somewhat lower digital rates can be obtained by adding a silence detection feature. The technology is scalable and will work well as higher data-rate tactical links become available. It will also interface with and support other integration schemes that currently exist for high-rate networks.

System Concept: For purposes of demonstration, the technology has been implemented (as Fig. 1 shows) for a ship-to-ship network using the HF surface-wave mode of radio communication for local distribution and UHF SATCOM for long-distance transfers. The same technology will also support UHF line-of-sight (LOS) networks. The system is designed to support mixed-media routing and relaying between two or more media. For example, integrated voice and data can be transferred from a distant ship or land-based site over UHF SATCOM to a ship within the battle group and then locally distributed to other appropriate platforms by using HF surface-wave or UHF LOS transmissions. The multiplexing protocol integrates multiple, simultaneous, independently routed virtual circuit and datagram services.

Virtual circuits are established and disestablished upon user request to support voice conversations and can also be used for point-to-point data transmissions such as file transfers. Establishment of a virtual circuit reserves sufficient capacity along all included links to support a guaranteed data rate (for example, 800 bps) for digital voice communication. The virtual circuit guarantees ordered delivery of packets and ensures an absolute minimum delay at each relay node in the network.

With the exception of the Joint Tactical Information Distribution System (JTIDS), which is rarely used in the Navy, the ability to relay voice over tactical networks has been essentially nonexistent. Data relay is also uncommon and is usually distributed by broadcast to platforms located within a single-hop communication range. The NRL MCA system adds an effective multihop relay capability for both voice and data.

New Tactical Networking Protocol: Tactical networks, such as UHF LOS and HF surface wave, employ monopole antennas with nearly omnidirectional coverage. Because of the omnidirectional coverage and the fact that a ship is usually in communication range of many other ships, there is potential for self-interference. Currently most systems require all nodes to transmit at the same frequency and use a time-division, multiple-access (TDMA) scheme to eliminate self-interference. The TDMA schemes in current use will not provide adequate throughput and time response to support integrated voice and data. Consequently we have developed and implemented, as part of the MCA technology, an alternative frequency-division, multiple-access (FDMA) protocol that allows each node to transmit continuously, using a frequency different from all its neighbors, and receive on a limited set of radio receivers. Each

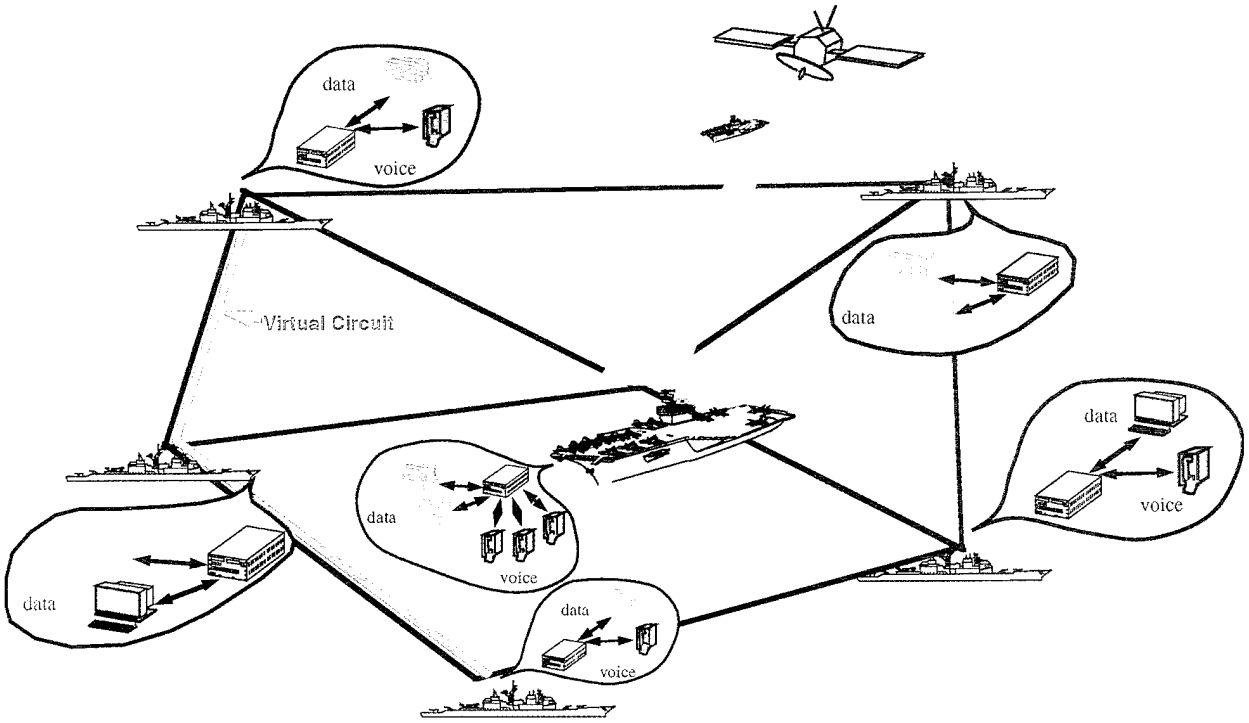

- **Independent routing for each application**
- **Virtual circuits to reserve capacity for voice**
- **Relaying for both data and voice**
- **Routing over mixed media: Long-haul (SATCOM) and local distribution (HF/UHF)**

Fig. 1 — Integrated services in tactical communication systems.

receiver can be tuned either permanently to a specific neighbor or alternately among multiple neighbors.

The ability to schedule receivers permits the automatic network control system to organize and configure connectivity based on an MCA learning algorithm that uses the results of periodic probing transmissions by all nodes. Approximately once each second and on a rotating basis, a node in the network transmits information regarding other nodes whose probe signals have been heard and the link quality on all incoming links. At appropriate intervals, a full connectivity report is transmitted. Whenever a node receives a connectivity report, it can construct routing tables to any destination in the network. The probe transmissions are interlaced with normal data communications.

The ability to retune receivers in accord with an algorithm-computed schedule requires that modem and cryptographic synchronization be reacquired each time the receiver is retuned to a different transmitter. Wireless modems that are capable of synchronizing on burst transmissions must be used. Synchronization with respect to the cryptographic sequence is achieved using time-of-day information derived from GPS and requires no additional overhead.

Flexible Multiplexing Method: The remaining key technology required to support integrated services is a flexible scheme to multi-

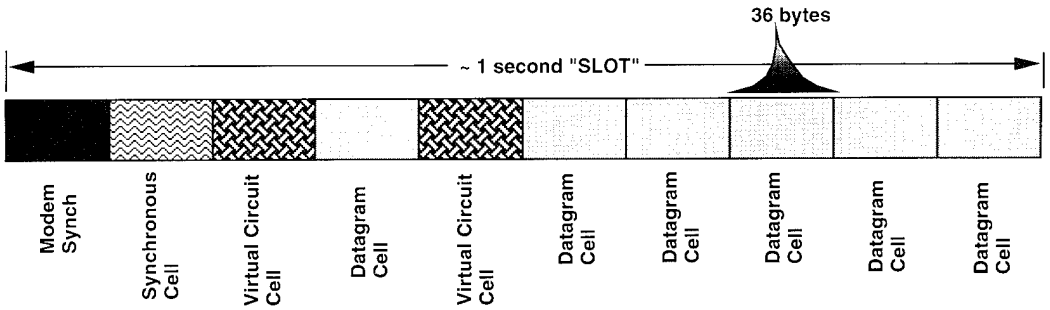

Fig. 2 — Flexible multiplexing scheme.

plex the data packets from multiple users and multiple applications. Figure 2 shows our technique. At the interface between the Network and Data Link protocols for the wireless network, data messages or packets from each user are segmented into cells of 36-byte length. Cells of this length were chosen as a reasonable compromise for limiting delay for relay of very-low data-rate voice over 2.4 kbps links. In the present design, 10 cells are bundled contiguously to form a single transmission unit, which is called a slot. The first cell position in the slot is reserved for the preamble that is used to achieve modem synchronization. The second synchronous cell position is reserved for transmitting probe signals for network control. The remaining cell positions, as well as unused portions of the synchronous cell, are used for sending data that support virtual circuits and datagrams. Cells supporting datagrams are distinguishable from cells supporting virtual circuits by virtue of cell header content. At a relay node, virtual circuit cells are retransmitted as soon as they are received; however datagram cells are buffered until the entire datagram is reassembled, integrity is checked, and a routing decision is made. Additional buffering delay may occur for datagrams if the outgoing link is congested because of commitment to virtual circuit service or higher precedence datagrams that are also in the buffer.

Project Status: An initial demonstration of integrated data and low-data-rate voice on a single 2400-bps link was conducted in December 1994. A similar demonstration in a single HF radio network will be conducted at fixed sites in the Chesapeake Bay in January 1995. The capability will be extended to include a second media, UHF SATCOM, in December 1995.

[Sponsored by ONR, OPNAV, and SPAWAR]

Reference

1. W. Thoet, D. J. Baker, and D. N. McGregor, "A Multichannel Architecture for Naval Task Force Communication," NRL/FR/5520--94-9703, Naval Research Laboratory, Washington, D.C., January 30, 1994. ■

Automatic Target Extraction in Infrared Images

B. Kamgar-Parsi
Information Technology Division

A fundamental problem in computer vision and image processing is image segmentation, or object extraction in intensity or infrared images. Current techniques require either user-supplied parameters or model-based templates. Examples of techniques requiring user-supplied parameters include thresholding and edge detection. They are convenient, but they both require threshold values which, in general, cannot be calculated automatically. Model-based techniques may not require the supervision of a human operator, but they have other deficiencies: they are slow since the image orientation or scale may be different from that of the template, and they are crude and not very dependable since the object pose in the image and the model pose in the template

may not agree. Thus model-based techniques have a low degree of resolution; for example, they may not distinguish between two types of aircraft. Target extraction is essential for many problems of interest both to the Navy and the commercial sector—object recognition, automatic target recognition, and scene analysis are a few examples. Hence it is of great importance to have a dependable automated technique for target extraction.

Infrared Images: It is well known that the detection of an object (or target) in an infrared image depends on its thermal contrast with the background. Accordingly, measures of target detectability (target metric), such as the difference between the mean target and background temperatures, or its modified versions also incorporating the standard deviation of the target's thermal variations, have been defined. These measures have been used to estimate the probability of the target detection by a human observer. They have thus been helpful in the design of infrared imaging systems. Autonomous tracking of a target begins after the detection and the identification of the target by a human operator [1]. By knowing the type and the size (in the image) of the target, an appropriate template is supplied to the tracking system. The autonomous tracking then continues by modeling the target with the template and finding its best match in a sequence of images.

The above techniques are not (fully) automated. For automatic object extraction, image thresholding has received considerable attention. The problem however is how to calculate the threshold value. For this, a variety of techniques based on the image gray-level histogram have been proposed [2]. The threshold is taken to be the gray level at the valley of a (hopefully) bimodal histogram—one mode representing the object and the other the background. A frequent problem is that the background itself may be multimodal. Furthermore, the valley is often gradual, and its bottom is not well defined.

Approach: We have developed a new technique for the automatic calculation of the threshold used for object extraction in infrared images. The technique is based on the assumption that the object of interest has a thermal contrast with the background. For clarity, in the following description we assume that the object has a higher (not lower) temperature than the background and that there is only one object which is significantly warmer than the background (note that the technique can be extended to cases where there is more than one object with thermal contrast in the image).

If, in the image, one starts from a point which is on the object and moves out along a straight line examining the gray level values at each pixel, then at the border of the object, one is likely to observe a significant drop—a gap—in the gray level value. This is because the brightness in an infrared image is proportional to the emitted heat. The gap in the gray-level profile contains the threshold. However for two reasons one needs to look at the gray level profile along many directions: (1) because of noise and the digitization of the image, it is possible that no significant gap is observed along a certain direction, and (2) the thermal gap only gives an interval containing the threshold; thus we need to narrow down the interval by seeking consistency among thermal gaps in different directions. Main elements of the algorithm are as follows. (1) Obtain the "heat center" by determining the maximum gray level value *gmax* in the image and locating pixels having gray level values within 80% to 90% of *gmax*. The center of mass of these pixels is taken to be the heat center (HC). (2) Draw a cross of N pixels long at the HC. From every pixel on the cross, move out twice: up and down from the horizontal bar of the cross and left and right from the vertical bar (Fig. 3). Along each of the $4N$ directions, look at the gray level profile and mark places where the gray level value drops significantly. The technique is not sensitive to the value of N. Further, in many applications, by analyzing successive frames one can adaptively determine a particularly appropriate value for N. (3) Determine the threshold by finding the consensus among thermal gaps. Finding consensus means finding the gray level value that is most representative of the gaps containing the threshold. (4) Extract the object by identifying pixels

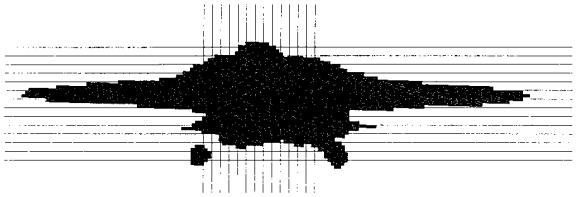

Fig. 3 — Search directions for finding gaps in gray level values.

whose gray level values exceed the threshold and are eight-connected to each other and ultimately to the heat center.

Remarks: The advantage of the above technique over gray level histogram techniques appears to be the use of many independent (directional) observations, whereas in histogram-based techniques, the entire image is added up in a one-dimensional array. Thus if the accumulation in that array is inaccurate (due to noise) or ambiguous, the outcome will be erroneous. Furthermore, unlike histogram techniques, our approach is insensitive to noisy pixels away from the object. By using our technique, we have developed software that clearly extracts aircraft approaching a carrier in infrared images (Fig. 4). The software allows the development of an automated system for the recognition of the type of landing aircraft. This is desirable in situations when a carrier does not wish to communicate with the aircraft, and consequently the approaching aircraft must be recognized from its shape. (We note that we did not find gray-level histogram techniques to be dependable for this problem.)

As was the case in the problem of aircraft extraction, our technique works well even in the presence of large temperature variations across the object. In some situations however, the application of an image-smoothing technique prior to threshold calculation may be indicated. In the absence of thermal contrast—that is, the lack of a difference between the average temperatures of the object and the local background—one may still be able to extract the object through its thermal structure (for example, hot spots such as small engines and cold regions such as large cooler fuselages). This may be done by regarding the object of interest as an

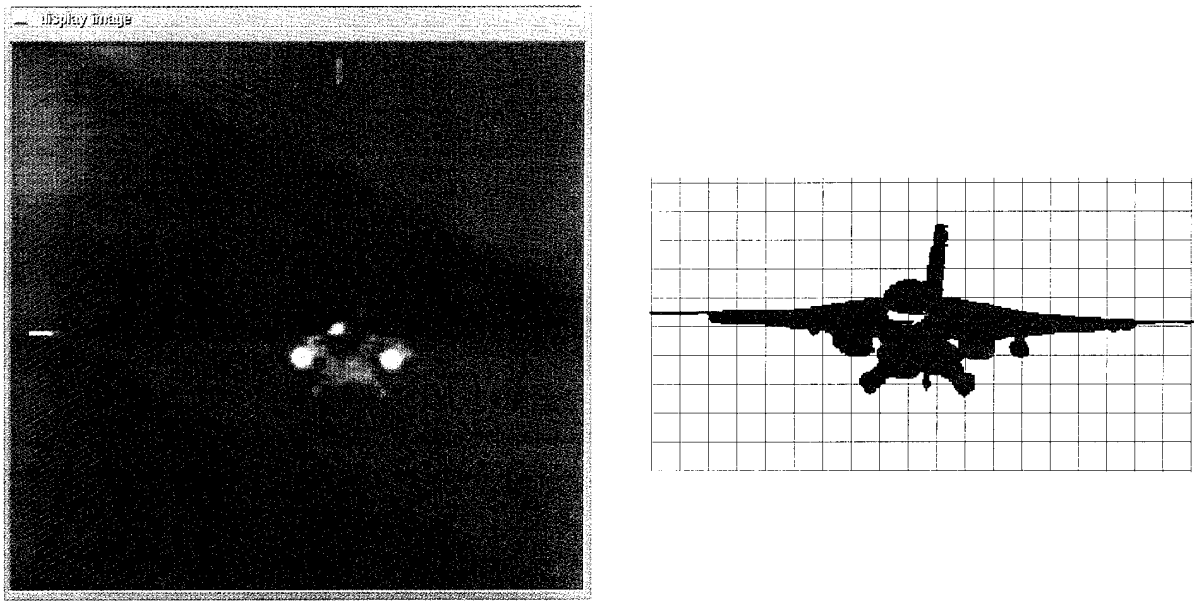

Fig. 4 — An IR image and the extracted aircraft using the newly developed automated technique.

assembly of several objects, hence calculating different thresholds or bandpass filters for each component. Although no single technique can be expected to work well on every image or object size in the image or the type of clutter, the proposed technique appears to be a significant improvement over the previously existing ones. Work is under way to better understand the scope of the applicability of the suggested technique.

Acknowledgments: Ralph Smith of the Naval Air Warfare Center, Lakehurst, NJ, provided us with data for approaching aircraft. I have benefited from discussions with Ralph Hartley of the Naval Research Laboratory and his expertise in image processing.

References

1. B.A. Brackney and J.A. Dawson, "An Integrated Approach to the Modeling of System-Level Performance for Autonomous Imaging IR Systems," *Proceedings of the SPIE* **1967**, Characterization, Propagation, and Simulation of Sources and Backgrounds, 1993.

2. J.S. Lee and M.C.K. Yang, "Threshold Selection Using Estimates from Truncated Normal Distribution," *IEEE Trans. on Systems, Man, and Cybern.* **19**, 422-429 (1989). ■

Communication Systems Network Interoperability

R.B. Adamson
Information Technology Division

Data communication systems have taken an important role in today's theater of warfare where rapid dissemination of information in the form of command and control, intelligence, or targeting data can be a deciding factor in warfighting scenarios. Recently, multinational cooperation in crisis situations has become more common. As a result, interoperable communication systems to facilitate this cooperation have become essential. The Naval Research Laboratory (NRL) is participating in the NATO Communication System Network Interoperability (CSNI) Project, which will demonstrate a multinational, interoperable radio communication network. The CSNI Project is a collaborative activity based on a NATO Conference of National Armaments Directors' Memorandum of Understanding among Canada, France, Germany, the Netherlands, the United Kingdom, and the United States, with participation by the SHAPE Technical Center (STC). Figure 5 provides an overview of the participation and radio frequency (RF) connectivity in the CSNI project.

The premise of CSNI is to demonstrate typical military communication applications with typical tactical radio links. The key to interoperability is the application of an internetworked communication architecture to provide for transfer of data among the different RF media. This discussion will focus on the communication architecture to be demonstrated, NRL's role in the project, and the issues encountered in developing a demonstration system with several different participating countries.

CSNI Communication Architecture: An objective of CSNI is to demonstrate the technical feasibility of NATO Open Systems Interconnection (OSI) concepts for military communications [1]. The basis of internetwork interoperability in the CSNI communication network is the International Standards Organization's Connectionless Network Protocol (CLNP). CLNP serves the same purpose in the OSI data communication protocol stack as the Internet Protocol (IP) does for many current computer networks. The OSI protocol suite, including CLNP, was mandated for use in the CSNI Project as a result of current NATO agreements for interoperable data communication. Although there are differences in the packet formats and some functionality between CLNP and the more widely used IP, the radio communication architecture concepts developed for CSNI are applicable to any system using connectionless data networking. As shown in Fig. 6, the primary components of the CSNI architecture are End Systems (computer workstations) and

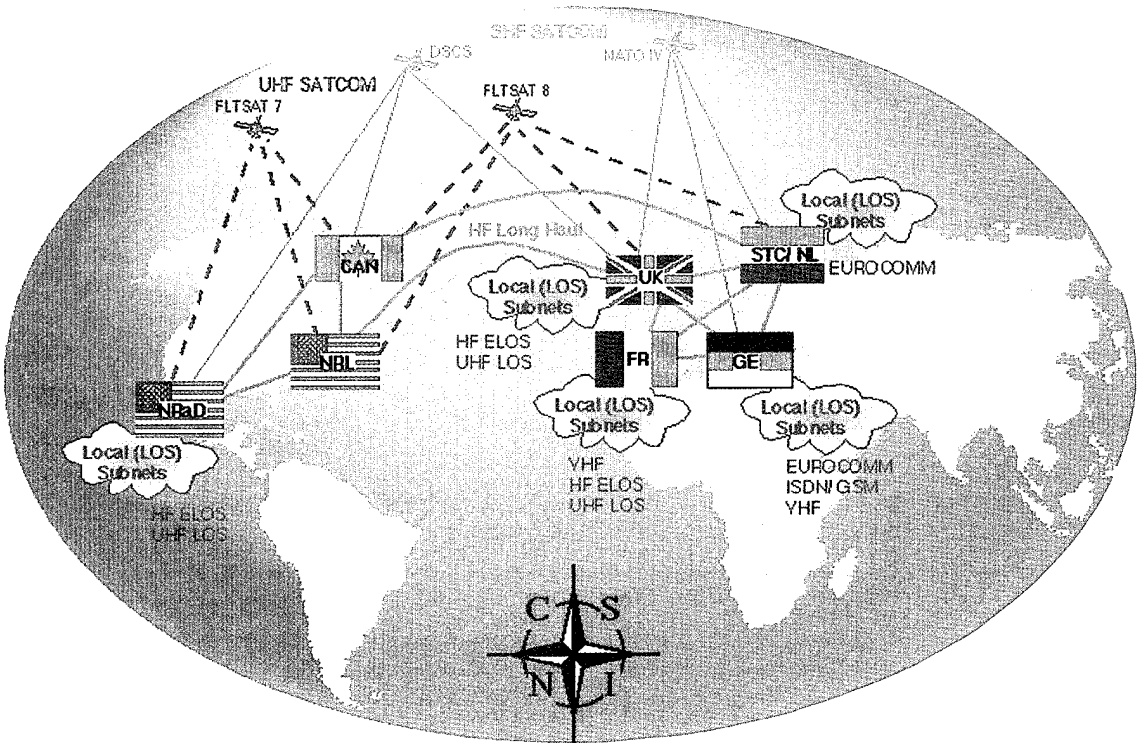

Fig. 5 — CSNI connectivity.

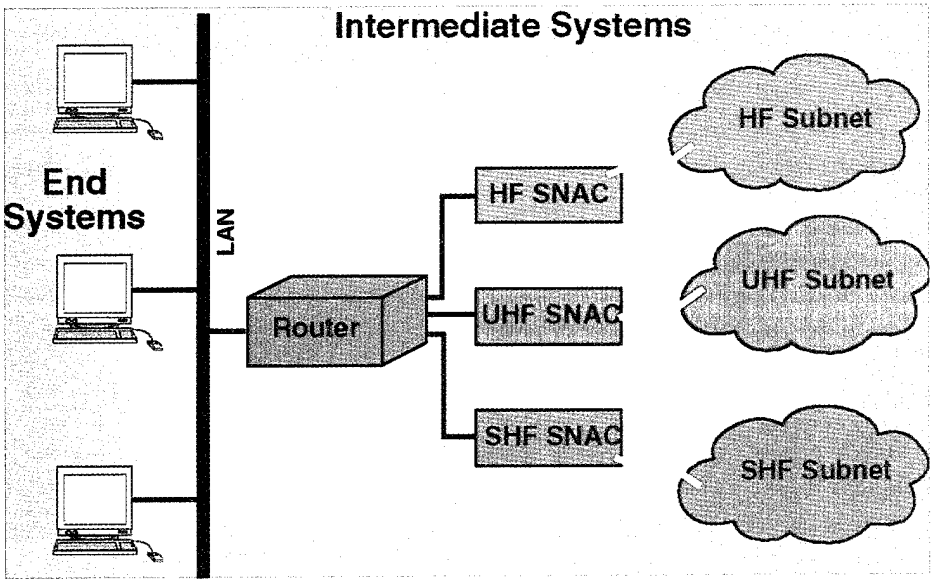

Fig. 6 — CSNI node high-level architecture.

Intermediate Systems (routers and associated network interfaces).

End System Applications: The End Systems provide the interface to the user and perform processing for user applications. In the CSNI demonstration, user applications include: (1) messaging (that is, X.400 e-mail), (2) tactical data, (3) digital secure voice; and (4) management. The X.400 messaging provides for text e-mail traffic as well as data transfer, including digital imagery, computer applications, and other computer files. A tactical data generator (TDG) is used in CSNI to simulate the network loading of tactical data communication, which generally consists of short datagram messages with information such as target type, heading, velocity, etc., on potential tactical targets. CSNI will provide real-time interactive digital voice services across its networks using voice compression at data rates of 2400 and 1200 bits per second and an interactive packet voice protocol. The management application will provide a means for controlling the CSNI communication system.

Intermediate Systems: The Intermediate Systems consist of the CLNP routing functions and the various data communication subnetworks. The primary subnetwork media are Ethernet (tying local area components together), HF long-haul ionospheric links, a UHF SATCOM network, and an SHF SATCOM network. The Subnetwork Access Controllers (SNACs) shown in Fig. 6 provide protocol processing for each of the media. For the RF media, this includes channel-access mechanisms, reliable subnetwork/link layer protocols, and connectivity monitoring tailored to each specific type of radio media. Ethernet interface cards provide the SNAC functionality for the local-area networks. The separate subnetwork and internetwork layers in CSNI allow communication and network processing unique to specific radio media to be performed independently of the more general-purpose internetwork layer. For example, the link layer protocols used in the HF long-haul subnetwork provide reliable data communication in the relatively high bit-error-rate conditions encountered in this media.

CSNI takes advantage of CLNP's ability to provide quality-of-service (QoS)-based routing. This allows the router to intelligently select the radio media route most appropriate given the data's type, destination, and current network loading. Routing metrics include link *capacity*, *delay*, and *cost*. CLNP also offers a priority field in its datagram format so that different users' or applications' data may be delivered more rapidly than others. For example, the voice application will take advantage of the QoS and priority features to attain adequate performance in the face of competing data services with less time-critical data-delivery requirements such as messaging and tactical data.

NRL's Role: NRL is participating as a node in the CSNI network. Figure 7 provides an overview of the communication equipment being installed at NRL to serve this function. NRL has represented the U.S. in the CSNI working group responsible for voice communication and has been the primary developer of the low-data-rate packet-voice application. NRL has also participated in other aspects of overall CSNI system design.

Multinational Project Coordination: Participating in a multinational project has presented many challenges including international software development efforts, electronic document exchange, and on-the-air testing across disparate time zones. The solution to many of these challenges used the very technology being applied in CSNI: a connectionless-data-communications internetwork. Internet e-mail and file exchange services have been invaluable in pursuing the goals of CSNI, and Internet connectivity has proven useful for testing CSNI applications and routing protocols.

Another key to successful coordination of the CSNI project has been its highly structured project management approach. The CSNI project has been broken down into four task areas: (1) system concept and testing, (2) applications and services, (3) multinet management and protocols, and (4) communication subnetworks. In turn, each of these task areas is broken down into separate components. For example, the

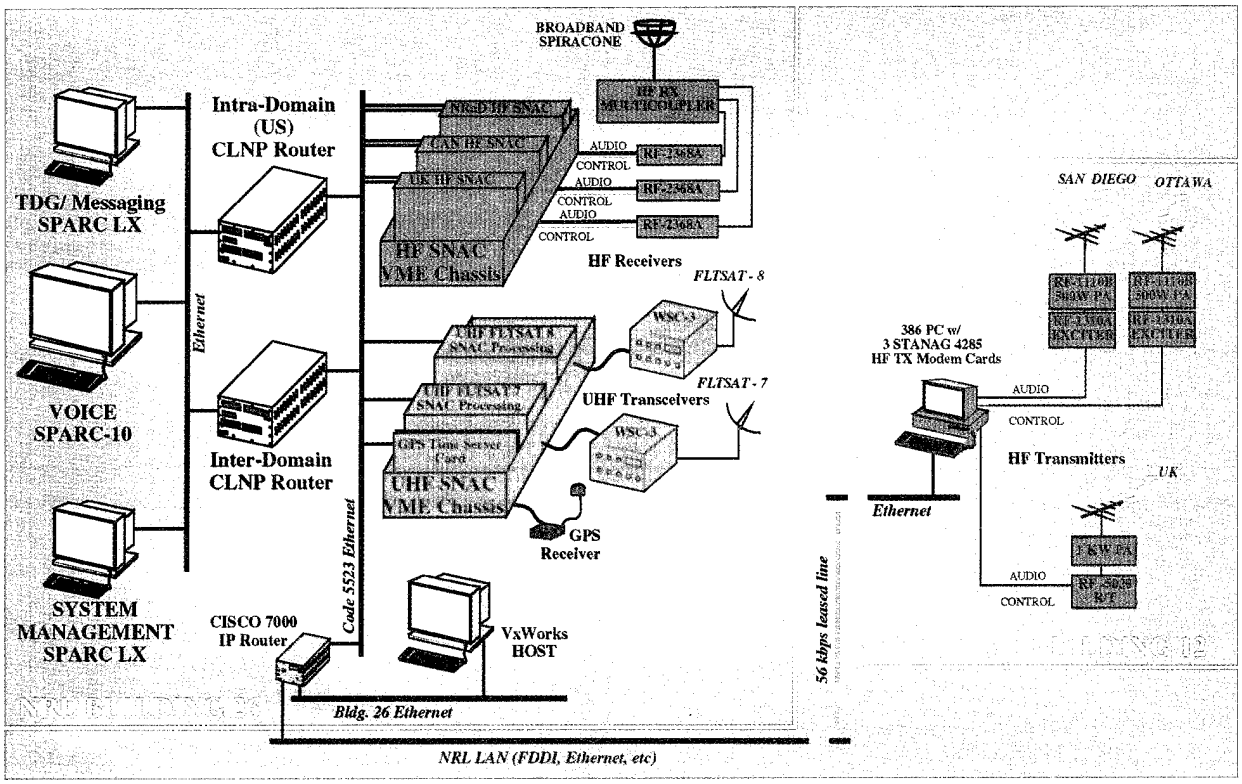

Fig. 7 — NRL CSNI node configuration.

application task area is further divided into messaging, tactical data, voice, and management while the communication subnet area is composed of HF, UHF SATCOM, and SHF SATCOM working groups. Each participating organization provides representatives to these working groups, and a separate leader is chosen for each task working group. The result is effectively sized teams of up to seven members, with one person of designated responsibility for the task area. Intertask communication is encouraged, and in most cases, members are participating in multiple working groups. A system-engineering task group facilitates more formal interworking group coordination, as needed.

Summary: The CSNI Project has offered a high degree of international technology transfer and resulted in a multinational radio communications test bed, with many of its components easily adaptable to alternative communication protocols at all layers of the communication stack. This will potentially allow further use of CSNI resources in future efforts. The CSNI Project is currently scheduled for on-the-air demonstrations in 1995.

[Sponsored by ONR and NRaD]

References

1. J.L. Robinson, "Military Communications Interoperability Through Open Systems," STC Technical Memorandum 932, SHAPE Technical Center, The Hague, Netherlands, March 1994. ■

Anomalous Temperature Dependence of the Upper Critical Magnetic Field in Bi-Sr-Cu-O

M.S. Osofsky, R.J. Soulen, Jr., and S.A. Wolf
Materials Science and Technology Division

The discovery of the high-temperature superconductors (HTS) has motivated much theoretical and experimental research directed at defining the mechanism responsible for superconductivity; it has also fostered great expectations for harnessing superconductivity for use in technology. Thus far, no definitive model for the mechanism responsible for HTS has appeared. Some of the measured properties are consistent with the well-accepted Bardeen/Cooper/Schrieffer (BCS) theory, which accounts for conventional, low-temperature superconductivity and others are not. Experiments are complicated by the complex structures and difficult syntheses of HTS materials and the fact that the superconducting coherence length ξ is on the order of the materials' unit cell dimensions, thus making the superconducting properties very sensitive to material defects. These problems have also hampered the development of technology based on superconductivity.

Upper Critical Field: The HTS are type II superconductors, which means that they have two characteristic magnetic fields—$H_{c1}(T)$ and $H_{c2}(T)$. At fields and temperatures below $H_{c1}(T)$, magnetic fields are expelled from the material. Between $H_{c1}(T)$ and $H_{c2}(T)$, the material is in the mixed state, and magnetic flux penetrates into the material in the form of quantized fluxoids. Above $H_{c2}(T)$, magnetism destroys superconductivity, making the material normal. The coherence length is calculated from the expression $H_{c2}(0) = \Phi_0/(2\pi\xi^2)$, where $H_{c2}(0)$ is the upper critical field measured near $T = 0$, and $\Phi_0 = h/2e$. For many applications such as wires and magnets, the superconductor is in the mixed state, often near $H_{c2}(T)$. Thus understanding the nature of the superconducting-normal boundary is crucial to understanding the properties of these materials and for use in technology.

Measurement of $H_{c2}(T)$: For low temperature superconductors, the measurement of the $H_{c2}(T)$ curve is not particularly difficult because its full extent lies within reach of the magnetic fields (say, 15 T), which may be generated at several laboratories. By contrast, measurements of $H_{c2}(T)$ for the HTS have been limited to temperatures near their superconducting transition temperatures T_c because H_{c2} in these materials rapidly exceeds accessible laboratory magnetic fields when the temperature is reduced to only nine-tenths of T_c. Thus the general practice [1] has been to assume conventional $H_{c2}(T)$ behavior calculating $H_{c2}(0)$ from the slope $[dH_{c2}/dT]_{Tc}$ using the Werthamer-Helfand-Hohenberg (WHH) expression: $H_{c2}(0) = 0.7\ T_c\ [dH_{c2}/dT]_{Tc}$. If for some reason H_{c2} should depart from the expected theoretical behavior, then this procedure could be subject to unanticipated error. To further compound the uncertainty in these measurements, the superconductive transitions are generally broadened in an applied magnetic field, which introduces ambiguity in choosing H_{c2}.

The $Bi_2Sr_2CuO_y$ system is an excellent choice for studying $H_{c2}(T)$ of a copper-oxide superconductor. It has a comparatively simple structure (no chains, one CuO layer), T_c is relatively low for HTS materials (20 K), and the superconducting transitions are not significantly broadened in a magnetic field. Furthermore $H_{c2}(T)$ is within laboratory reach for almost all temperatures. Superconducting films were successfully made by collaborators at Varian Corporation by using atomic, layer-by-layer, molecular-beam evaporation (ALL-MBE) [1] where the chemical composition is carefully controlled. Films approximately 100-nm thick of $Bi_2Sr_2CuO_y$ were grown on $SrTiO_3$ substrates and subsequently patterned into a geometry suitable for resistance measurements.

The resistive transition of the film in zero magnetic field indicated that the superconductive transition began at a temperature of 19 K and extended down to 12 K where the transition was complete. The magnetotransport measurements were performed with collaborators at the Service National Des Champs Magnetique Pulses, in Toulouse, France. When the magnetoresistance was measured, the film was oriented with

its *c* axis parallel to the applied field. The resistance R was measured using a standard, four-probe ac technique, as the magnetic field was pulsed from 0 to 35 T. Measurements were made at temperatures as low as 65 mK.

Figure 1 shows a series of R(H,T) curves for temperatures varying from 13 K down to 65 mK. These curves indicate that the transition widths are relatively insensitive to the applied field strength and that the quenched, normal state resistance increases below $T_c(H = 0)$. We define H_{c2} for each curve as the magnetic field where the extrapolated normal state resistance and the tangent of the transition meet (Fig. 2 inset). Because the transition is not significantly broadened by the magnetic field, we have shown that any choice of position on the R(H,T) curve defines $H_{c2}(T)$ curves with essentially the same shape.

Figure 2 displays the $H_{c2}(T)$ data extracted from the R(H,T) data shown in Fig. 1. The conventional WHH curve, matched at $dH_{c2}(T_c)/dT$, is shown for comparison. That slope is estimated to be 0.29 T/K so that $H_{c2}(0)$ is calculated to be 3.8 T. Similar results have been observed in overdoped $Tl_2Ba_2CuO_6$ [2].

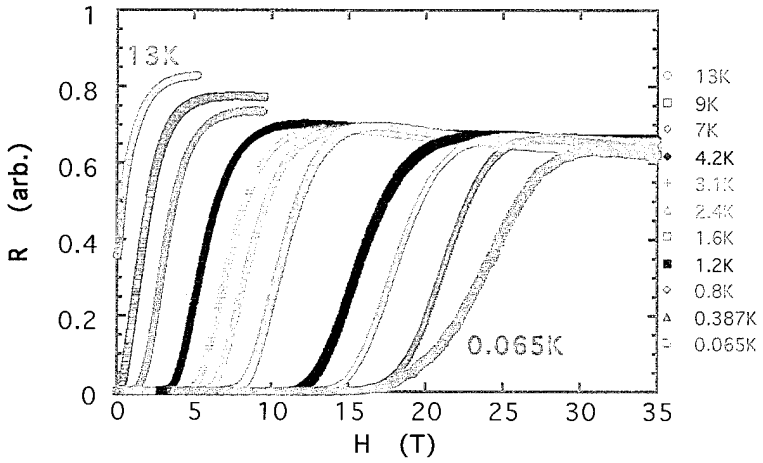

Fig 1 — Resistance R as a function of magnetic field H at several temperatures T. The temperatures decrease monotonically from 13 K (far left-hand curve) to 65 mK (far right-hand curve).

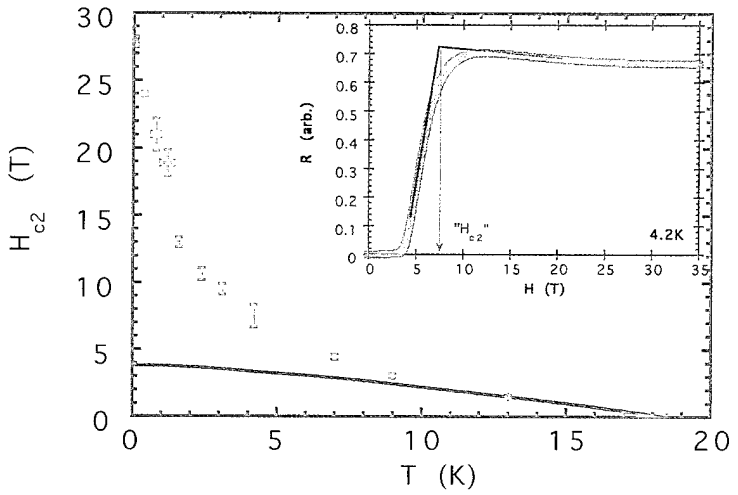

Fig. 2 — Upper critical magnetic field $H_{c2}(T)$ data derived from Fig. 1. Solid curve: WHHM theory; inset: demonstration of construction used to define H_{c2} from a measured R(H) curve.

Absence of Theory: The WHH theory predicts the shape for conventional superconductors but fails to account for the anomalous shape of $H_{c2}(T)$ observed here. Many of the peculiar physical properties of this system such as reduced dimensionality, low carrier concentration, or spin fluctuations suggest directions to pursue in finding an explanation for this behavior. Other theoretical approaches based on novel mechanisms for superconductivity have been attempted. Thus far, none of these models has proved successful in accounting for these results. Experimental studies will continue on other systems to provide more information needed to resolve the puzzle.

[Sponsored by ONR]

References

1. M.S. Osofsky, R.J. Soulen, Jr., S.A. Wolf, J.M. Broto, H. Rakoto, J.C Ousset, G. Coffe, S. Askenazy, P. Pari, I. Bozovic, J.N. Eckstein, and G.F. Virshup, *Phys. Rev. Lett.* **71**, 2315 (1993) and references therein.

2. A.P. Mackenzie, S.R. Julian, G.C. Lonzarich, A. Carrington, S.D. Hughes, R.S. Liu, and D.C. Sinclair, *Phys. Rev. Lett.* **71**, 1238 (1993). ■

Development of a New, Low-Frequency Displacement Sensor

A.D. McCleary, A.M. Young, and P.J. Klippel
Underwater Sound Reference Detachment

D.H. Trivett
D.H. Trivett, Inc.

The development of new coating materials for the "Seawolf" and the new attack submarine requires that the materials be evaluated over the hydrostatic pressure range (depths) and temperature range at which the coatings are designed to operate. This requirement leads to the use of relatively small temperature-controlled pressure vessels such as the Anechoic Tank Facility (ATF) at the Naval Research Laboratory Orlando Detachment. The finite dimensions of these pressure vessels limit the maximum size of the test samples that may be tested and the lowest frequency at which valid measurements can be made. These panels are presently evaluated by measuring both the incident and transmitted pressure when the panel is ensonified by a planewave sound field. The low frequency limit results from the edge-diffracted signal reaching the hydrophone behind the panel at the same time or earlier than the directly transmitted pressure signal. An alternative method uses neutrally buoyant accelerometers to directly measure the surface motion of the panel and eliminate the low-frequency limit caused by the edge diffraction. While this method works quite well and the accelerometers are available and inexpensive, it is characterized by a poor signal-to-noise ratio as the frequency is decreased.

A Better Sensor: If the *displacement* of the panel surface can be measured instead of the *acceleration*, a significant increase in signal-to-noise ratio at low frequencies is possible. Small, low-mass displacement sensors however are not commercially available. NRL-Orlando has developed and tested a prototype of a small, neutrally buoyant sensor suitable for directly measuring the surface displacement of compliant panels or other fluid-loaded structures. The sensor is designed as a single degree-of-freedom mass-spring system. Above the resonance frequency, the mass is inertial and functions as one-half of a parallel plate capacitor, with the sensor housing being the other half. With the application of a bias voltage between the two plates, a charge proportional to the displacement of the sensor is obtained above the resonance frequency. To maximize the bandwidth of the device as a displacement sensor, the resonance frequency is designed to be as low as possible. The prototype sensor was designed to operate in the 1 kHz to 5 kHz frequency range, and the resonance frequency of the mass-spring system was designed to be 175 Hz. The design of the mass as a thin disk and the use of a thin diaphragm as the suspension results in a highly compliant system in the direction perpendicular to the diaphragm and a

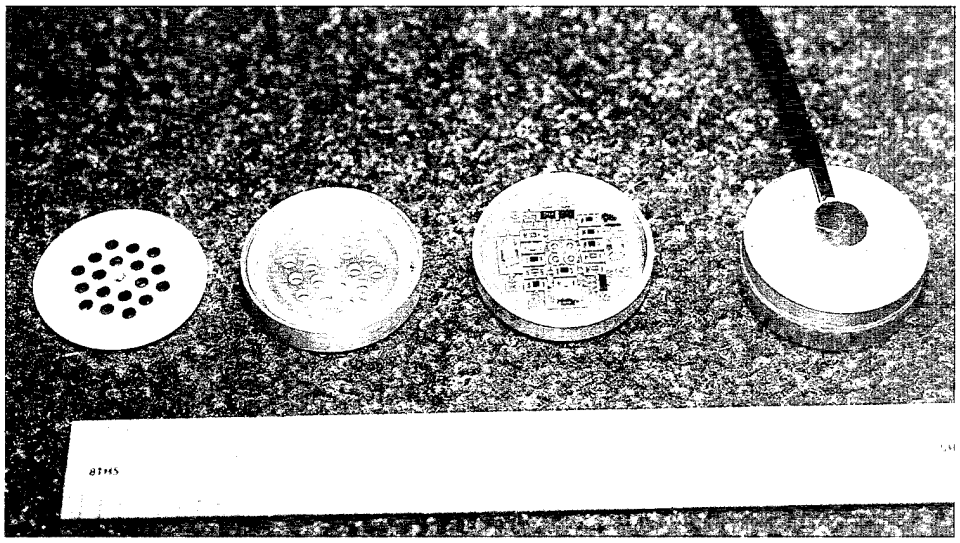

Fig. 3 — Capacitive displacement sensor—from left: suspension and inertial mass, housing bottom and capacitor plate, housing top with integral amplifier, and assembled sensor.

stiff system in the transverse directions. This design aids in reducing the sensitivity of the sensor to transverse displacements. Due to the low capacitance of the sensor, an amplifier was designed to be installed inside the housing of the sensor. The entire package was designed to be neutrally buoyant in water such that the sensor loaded the compliant material in the same manner as the fluid it displaces. Thus the sensor can be used to directly measure the normal component of the displacement of the surface without mass loading the compliant material. The prototype illustrated in Fig. (3) is approximately 1 cm in height and 3 cm in diameter and has been used to measure the displacement of compliant coatings at low hydrostatic pressures in the ATF at NRL-Orlando.

Future Research: The initial prototype was intended for use at relatively low hydrostatic pressures and over a limited bandwidth. Current research is aimed at optimizing the neutrally buoyant displacement sensor for operation at hydrostatic pressures up to the 760 kPa limit of the small anechoic pressure vessel at NRL-Orlando. A finite-element model is being developed to aid in the optimization of the sensor housing and the mass-spring system.

[Sponsored by ONR] ■

A New Method for Characterizing the Dynamic Properties of Materials

M.D. McCollum
Underwater Sound Reference Detachment

The advent of new, lightweight composite materials—both elastic and piezoelectric—has led to great improvements in the design of structures for active and passive sonar systems. The design process is often limited however by the inability to accurately determine the dynamic properties of these materials. Existing characterization techniques typically rely on the use of simple analytic equations and, therefore, ideal geometries to "back out" the important properties. A new method has been developed that avoids many of the limitations of standard methods by using finite-element (rather than analytic) models and measurements of harmonic transfer functions instead of resonance frequencies. The technique is designated by the acronym MIME (Materials Identification using Modeling and Experiment).

Description of the Method: The first step in using the MIME technique is to perform a sensitivity analysis using a finite-element model of the sample geometry. The purpose of the

sensitivity study is to determine an appropriate geometry based on the parameters that have a significant effect on the behavior of a given geometry. Once an appropriate sample geometry is selected, a set of measurements is performed at various positions on the sample and over a selected frequency range. The finite-element model generated for the sensitivity analysis is again used for the actual MIME procedure. Beginning with an assumed set of properties, the model is used to compute displacements at the measurement positions. These computed values are compared to the measured values to obtain the χ^2 error. This error, together with a derivative matrix, is used to compute the next set of properties. The specific procedure used to compute the new values is know as the Levenberg-Marquardt method. The iterative procedure is complete when the computed error no longer improves. The values of the parameters at the minimum error are taken to be the best approximation to the actual parameters over the chosen frequency range.

Application to Homogeneous Materials: For a homogeneous isotropic material, the typical parameters of interest are Young's modulus, Poisson's ratio, and the mechanical loss factor. Generally all three parameters can be obtained using a single geometry, but this geometry must be chosen carefully, keeping in mind the requirement that all three parameters be significant in the frequency range of interest.

If the material properties are frequency dependent within the frequency range of interest, an additional level of complexity is added to the computations while not affecting the required measurements. In order to determine the frequency dependence, one must perform the procedure over several different narrow frequency bands such that the parameters are approximately constant within each of the bands.

This procedure is also applicable to anisotropic materials, either elastic or piezoelectric. In this case, it is necessary to use the appropriate matrix of material properties (depending on the symmetries of the material) in the finite element model. It is important to perform a sensitivity analysis since it is very unlikely that all of the parameters will be significant for a single geometry. Because of the increased number of material parameters, the required number of measurements (frequencies and/or positions) is also higher. For the piezoelectric case, it is necessary to measure the electrical impedance of the sample.

Application to Multiphase Materials: It is often necessary to describe multiphase materials using "effective" properties. For example, the performance of piezocomposite materials consisting of piezoelectric rods in a polymer matrix is best described by effective properties because it is quite tedious to generate a finite-element model of a sample having hundreds of ceramic rods. The MIME method may be applied to such a material in the same way it is used for homogeneous materials. The set of material parameters derived using MIME is the set that gives computed displacements that most closely match the measured values.

[Sponsored by ONR] ■

Dynamics of a Vibrating Reed in a Magnetic Field

A.C. Ehrlich and R.L. Jacobsen
Materials Science and Technology Division

The vibrating-reed technique probes the elastic properties of a material by exploring the behavior of resonant flexural modes of the specimen. For example, there is a direct connection between the resonant frequencies and Young's modulus. Increasingly the technique is being used in conjunction with applied magnetic field to investigate magnetic and magnetoelastic behavior. In some experiments, a test specimen is mounted at the end of a reed [1], whereas in others, the reed itself is of interest. However in none of these experiments nor in any theory has consideration been given to the effect of magnetization per se on the reed's motion. If such an effect were present, it could obscure or confuse the other magnetic-field-induced phenomena, such as flux lattice melting in superconductors [2] that are the intended subjects of these studies. In order to address this problem, we have

investigated and resolved both theoretically and experimentally the effect of magnetic-field-induced magnetization on the resonant frequencies of reeds.

Theory: We have derived and solved the equation of motion for a reed with anisotropic magnetic susceptibility vibrating in flexure in a uniform magnetic field. The derivation is analogous to that of the usual equation for a vibrating reed or bar but with the addition of a torque of magnetic origin acting on each element of the reed as it turns in the magnetic field. This torque arises because the vibrating reed is not usually straight, and thus the applied field induces a magnetization in each element of the reed, which is a function of position (see Fig. 4). Since the susceptibility is, in general, not isotropic, the magnetization does not lie along the applied field, and therefore the magnetic-free energy is not minimal. This implies that each element of the reed will feel a torque given by the angular gradient of the magnetic-free energy. This torque is small, and the changes it causes in the resonant frequencies of the reed, which are the quantities of interest, can be calculated with perturbation theory. We have done this, and the results turn out to depend on the boundary conditions on the reed and the mode n under consideration. The square of the fractional change in each resonant frequency, called the eigenvalue, is predicted to vary, among other things, as the applied magnetic field squared.

Experiment: In our vibrating-reed experiments, a number of materials were studied, including a single crystal whisker of $NbSe_3$. In the experiment, the sample is driven into vibration and the amplitude of response measured at various applied magnetic fields. The drive frequency is swept, and a precise resonant frequency is determined by identifying the frequency at which the sample response is maximum. Figure 5 shows the results of such an experiment for several resonance modes. The curves through the data points are a fit of our theory. The agreement is excellent. The inset shows the eigenvalue at a magnetic field of 6.4 T versus the zero magnetic field resonance frequency $\omega_{0,n}$. The slope of the line fit to the data indicates the amplitude varies as $1/\omega_{0,n}$, which is also predicted by our theory. Figure 6 shows the eigenvalue dependence on the orientation of the magnetic field relative to the sample. Again the lines drawn through the data are a fit from our theory and are in excellent agreement with the data.

Conclusion: The discovery of the effect described above and its understanding has two potentially important consequences. First, it supplies the necessary context within which to interpret past and future vibrating-reed studies of more exotic magnetic-field-dependent phenomena, such as thermodynamic phase changes. Second, the phenomena may provide the basis for more sensitive measurement of magnetic anisotropy than has previously been possible.

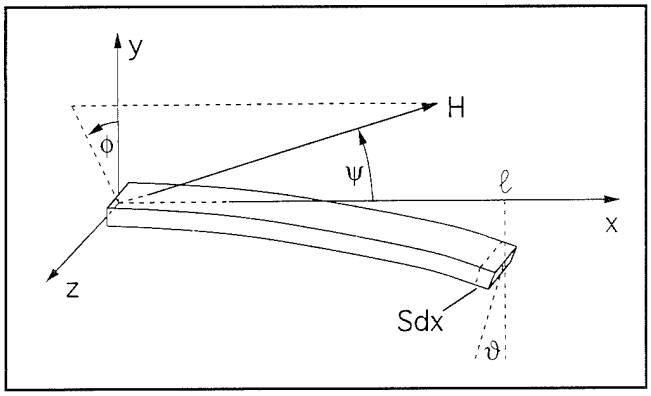

Fig. 4 — The physical arrangement of the vibrating reed and magnetic field, defining geometric parameters. The element Sdx is shown at the end of the reed but is intended to be general.

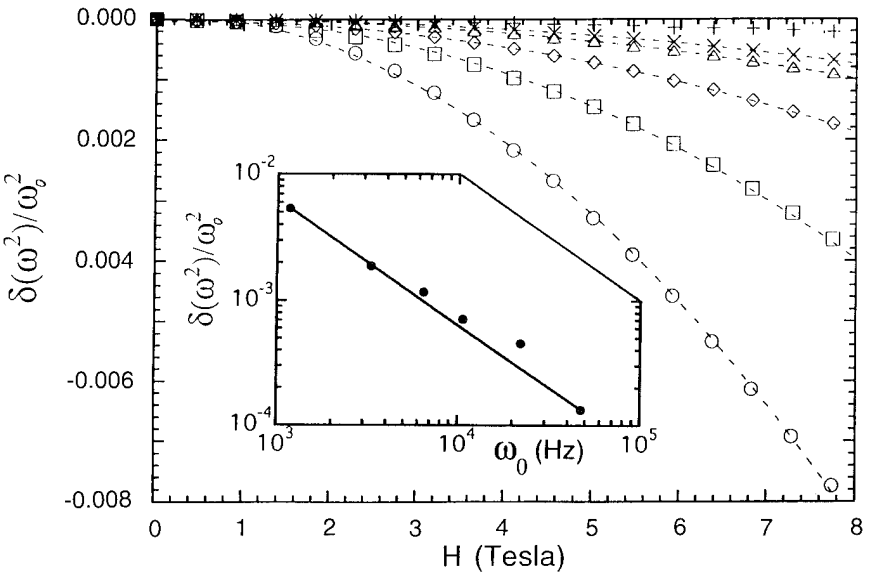

Fig. 5 — The fractional change in eigenvalue of a $NbSe_3$ reed as a function of applied magnetic field for several modes n. The dashed lines are parabolic fits to the data. Inset shows magnitude of change at 6.2 T as a function of $\omega_{0,n}$ on log scales.

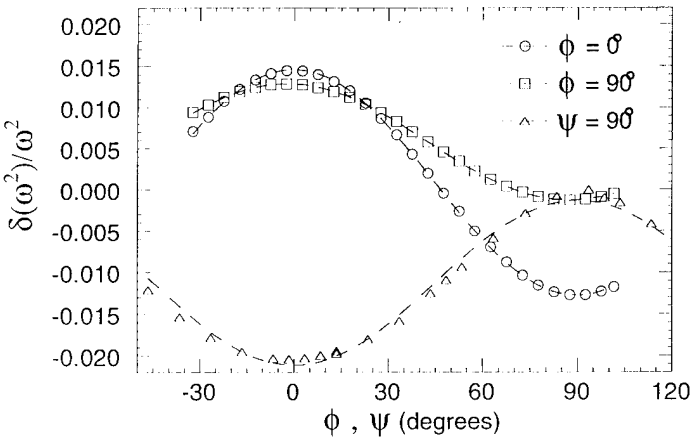

Fig. 6 — Fractional change in eigenvalue as a function of field direction at 6 T in a GY-70 carbon fiber. The dashed curves are fits to the predicted behaviors, as discussed in the text.

The frequency shift we detect with magnetic field is an extremely sensitive measure of magnetic anisotropy and in some materials is more sensitive than commercially available induction-sensing magnetometers, such as SQUID systems. This is particularly true in very small specimens since the magnetic forces involved are being sensed relative to the elastic forces of the specimen and so scale up or down together with size, whereas the detected signal is proportional to specimen size in induction-sensing magnetometers.

[Sponsored by ONR]

References

1. P.L. Gammel, F. Schneemeyer, J.V. Waszczak, and D.J. Bishop, "Evidence from Mechanical Measurements for Flux-Lattice Melting in Single-Crystal $YBa_2Cu_3O_7$ and $Bi_{2.2}Sr_2Ca_{0.8}Cu_2O_8$," *Phys. Rev. Lett.* **61**, 1666 (1988).

2. H. Drulis, Z.G. Xu, J.W. Brill, L.E. De Long, and J.-C. Hou, "Observation of an Extended Region of Magnetic Reversibility in Nb and $NbSe_2$," *Phys. Rev. B* **44**, 4713 (1991). ■

Nanofabrication with an Atomic Force Microscope

E.S. Snow and P.M. Campbell
Electronics Science and Technology Division

P.J. McMarr
Sachs/Freeman Associates

The demand for higher speeds and greater density in electronic circuits is fueling a drive for ever smaller devices. However current methods of fabrication (optical-projection lithography) are expected to reach their limits of resolution at around 0.1 μm, and attempts to replace this technology with higher resolution techniques such as X-ray and electron-beam lithography have met with much difficulty.

More recently, scientists have begun to investigate proximal probe technology as an alternative for nanometer-scale lithography. Proximal probes such as the scanning tunneling microscope and the atomic force microscope (AFM), originally developed to image surfaces with atomic resolution, have recently been used to modify surfaces at the nanometer scale and have even achieved manipulation and positioning of single atoms on a surface. This suggests that proximal probes may exceed the limits of electron-beam lithography and perhaps achieve the ultimate resolution of atom-by-atom control of the surface. This potential has motivated researchers to attempt to implement this level of control into actual device fabrication. However this task has not been easy due to the irreproducibility of the modifications, the slow "write" speed, and the difficulty of transferring such fine manipulations into a usable semiconductor or metallic structure. The challenge has been to overcome these limitations and achieve a reliable process for fabricating real devices.

Anodic Oxidation and Selective Etching: Researchers at the Naval Research Laboratory (NRL) have developed one such process in that proximal probes can be used for device fabrication. The key to this process has been the development of a fast, reliable exposure process that produces a local surface chemical modification that can be used for pattern transfer by selective etching. For the exposure, a metallized AFM tip (which is operated in air) is used to anodically oxidize selected regions of an H-passivated Si surface [1]. These oxide patterns, although only a few monolayers thick, form a robust mask for certain very selective etches that attack Si but not Si oxide. In addition, GaAs and other materials can be patterned by this technique by capping with a thin Si layer, which is patterned with the AFM and used as a mask for etching the underlying material [2].

Due to the local nature of the tip-surface interaction and the fact that the generated oxide is only a few monolayers thick, fine lateral resolution is obtainable by this technique. In practice, we can achieve 10-nm lateral-sized etched features when the exposure is performed in an air ambient (see Fig. 7). True nanometer resolution of the exposure process has been achieved in controlled environments.

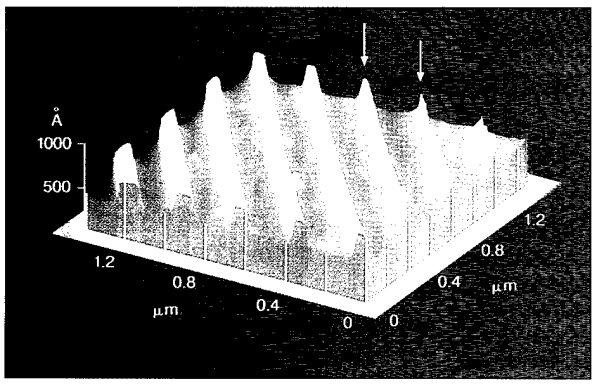

Fig. 7 — AFM image of Si wires, which were etched to a depth of 30 nm. The wires were formed by anodic oxidation with the AFM and etching with an electron cyclotron resonance source. The two lines indicated by arrows have linewidths of 20 nm and 10 nm.

Device Fabrication: A unique feature of AFM-based lithography is that the exposure and imaging mechanisms of the AFM operate independently. Thus high-resolution images of the sample can be obtained and used for precise pattern alignment. In addition, latent imaging of the oxide features allows the success of an exposure to be assessed and corrected before further processing. Combining these imaging capabilities with the high-resolution exposure process make the AFM a unique lithographic

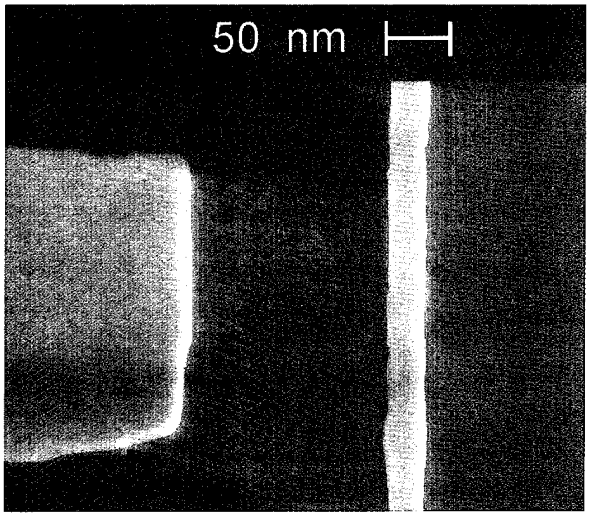

Fig 8 — SEM image of a side-gated Si field-effect transistor. The wire and gate structure shown in the figure are resting on an oxide layer, which isolates them from the underlying substrate. The wire has a width of ~30 nm.

tool ideally suited for fabricating critical features in nanometer-scale devices.

As a demonstration of this capability, we have used AFM-defined oxide patterns and selective etching to fabricate side-gated Si field-effect transistors with critical dimensions as small as 30 nm (see Fig. 8). In addition researchers at Stanford University have used this process to fabricate a 0.1 μm gate-width metal-oxide semiconductor field-effect transistor. These examples clearly demonstrate that proximal probes are viable tools for nanometer-scale device fabrication.

[Sponsored by ONR]

References

1. E.S. Snow and P.M. Campbell, "Fabrication of Si Nanostructures with an Atomic Force Microscope," *Appl. Phys. Lett.* **64**, 1932 (1994).

2. E.S. Snow, P.M. Campbell, and B.V. Shanabrook, "Fabrication of GaAs Nanostructures with a Scanning Tunneling Microscope," *Appl. Phys. Lett.* **63**, 3488 (1993). ■

GaN/AlN Growth and Electronic Device Efforts at NRL

S.C. Binari, K. Doverspike, D.K. Gaskill, and R. Kaplan
Electronics Science and Technology Division

In the pursuit of electronic devices that can operate at high-temperature and high-power levels without active cooling, the Electronics Science and Technology Division (ESTD) has initiated a major effort in the GaN/ AlN materials system. High-temperature, high-power electronic devices are expected to have applications in areas such as instrumentation and controls for jet engines, electric vehicles, nuclear reactors, and microwave radar transmitters. The ESTD program emphasizes materials growth, materials characterization, and electronic-device development. Significant progress has been made, and the Naval Research Laboratory (NRL) is now an acknowledged leader in all aspects of this field.

GaN is of interest for these applications primarily because of its large bandgap of 3.4 eV. Wide-bandgap semiconductors have low charge-carrier thermal generation rates and large breakdown fields—necessary properties for high-temperature, high-power electronic devices. GaN also has a high electron mobility and saturation velocity, which is useful for high-frequency operation. GaN-based devices can also be designed with AlN/GaN heterojunctions. This permits increased design flexibility for high-performance devices.

Materials Growth and Characterization: The organometallic vapor phase epitaxial (OMVPE) growth effort in the ESTD has concentrated on methods appropriate to the growth of high quality GaN layers on sapphire substrates [1]. Material suitable for the fabrication of GaN/AlN field-effect transistor (FET) structures that have set the state of the art for this materials system has been grown. For this effort, an inductively heated, vertical OMVPE reactor using triethylaluminum, trimethylgallium, and ammonia as sources and hydrogen as

a carrier gas was used. A thin AlN buffer layer grown on the sapphire substrate is required to obtain high quality GaN active layers. The film properties are a strong function of reactor growth conditions such as substrate temperature, reactor pressure, and gas flow rates.

The materials are characterized using the wide range of diagnostic techniques available at NRL. These techniques include temperature-dependent Hall-effect measurements, X-ray diffractometry, photoluminescence, optically detected magnetic resonance, electron-spin resonance, and ultrahigh vacuum surface spectroscopies. These characterization tools provide information on carrier mobility, dopant concentration, crystal quality, defect structure, and interface quality. This information is used to correlate the materials' properties with growth conditions. In addition, these techniques are used to determine fundamental GaN/AlN material properties.

Device Fabrication and Characterization: The device effort has concentrated on FET structures suitable for microwave, high-temperature, and high-power operation. NRL has made heterojunction FETs (HFETs) and metal-insulator semiconductor FETs (MISFETs) that show excellent microwave and high-temperature performance [2].

Figure 9 shows the device cross-section of the HFET. Both the HFET and the MISFET were fabricated with a source-drain spacing of 5 μm and gate lengths of 0.7 to 2 μm. The total gate width is 150 μm. Alloyed Ti/Al was used to form the source and drain ohmic contacts. The gate metallization was Pt/Au (500/2000 Å). For the MISFETs, an 800 Å Si_3N_4 gate insulator was deposited prior to gate deposition. The devices were isolated using He-implantation-induced damage. Helium implantation is capable of increasing the resistivity of n-type GaN material to 10^{10} Ω-cm. For He concentrations exceeding 1×10^{19} cm^{-3}, the resistivity of the damaged GaN is thermally stable to over 850° C.

Figure 10 shows the dc drain characteristics for HFETs with a gate length of 1 μm. The drain current I_{DS} is plotted vs the drain voltage V_{DS} with the gate voltage V_{GS} as an additional parameter that controls the drain current. The HFETs have a pinch-off voltage of −6 V and a maximum transconductance ($\equiv \Delta I_{DS}/DV_{GS}$) g_m of 45 mS/mm. This is the highest g_m reported for a GaN FET. The HFETs have a g_m of 22 mS/mm at a baseplate temperature of 350° C. The reduction in g_m at elevated temperatures is attributed to a reduction in electron mobility.

The S-parameters of these devices were measured as a function of frequency and bias using on-wafer probing. For a 1-μm gate-length device, the measured cut-off frequency f_T and maximum frequency of oscillation f_{max} values were 8 and 22 GHz, respectively. In terms of frequency performance, these initial results with GaN are competitive with those obtained with SiC MESFETs. Since f_T of a short-gate length FET is inversely proportional to gate length l_g, a useful figure of merit is the $f_T \times l_g$ product. The NRL GaN FETs have the highest $f_T \times l_g$ product reported for a GaN FET.

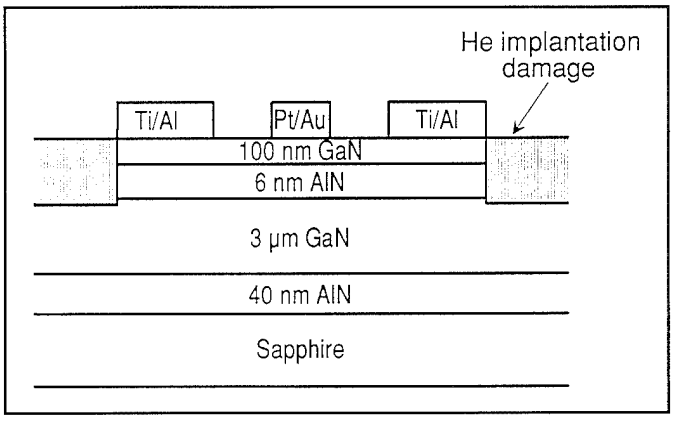

Fig. 9 — HFET cross section.

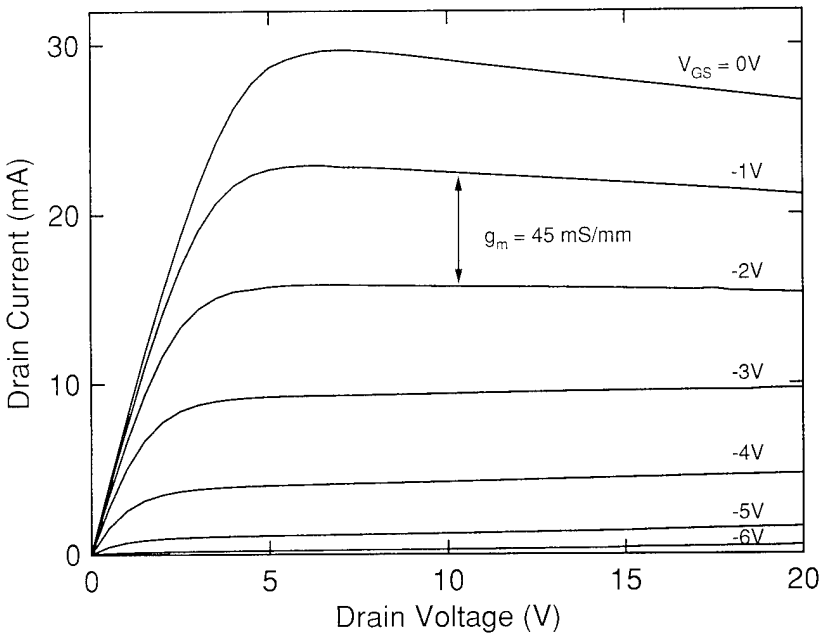

Fig. 10 — HFET drain characteristics at 30° C.

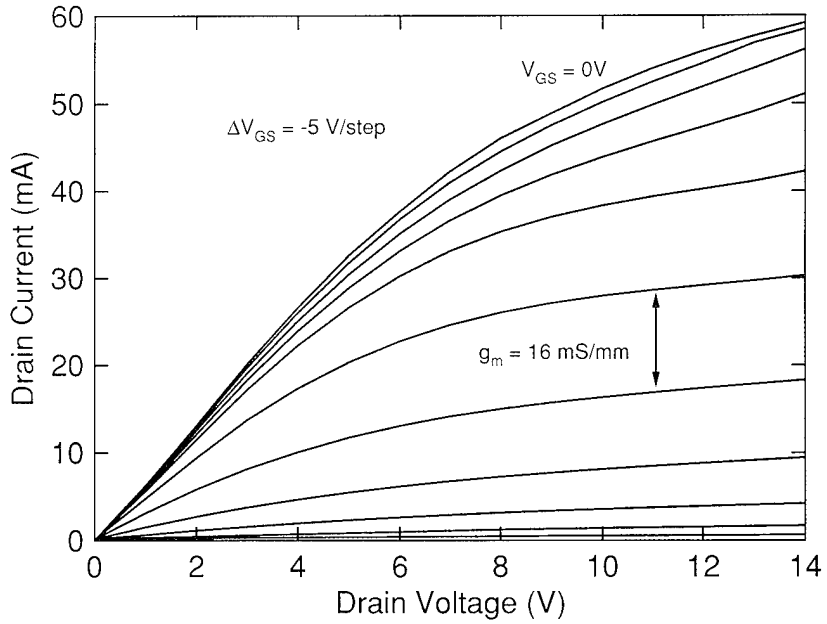

Fig. 11 — MISFET drain characteristics at 30° C.

Figure 11 shows the drain characteristics of the Si_3N_4/GaN MISFETs. This is the first demonstration of a Si_3N_4/GaN MISFET. The MISFETs have a maximum g_m of 16 mS/mm and a pinch-off voltage of −50 V. The gate leakage current was less than 0.2 μA over the entire range of gate and drain biases. The low levels of gate-leakage current show promise for high-temperature operation. The measured f_T and f_{max} values were 5 and 9 GHz, respectively. This value of f_{max} is substantially better than the value of 2 GHz obtained with SiC MOSFETs.

In summary, significant progress in GaN-based electronic devices has been achieved in the ESTD. These devices have excellent microwave and high-temperature properties and show promise for high-temperature and high-power applications.

[Sponsored by ONR]

References

1. K. Doverspike, L.B. Rowland, D.K. Gaskill, S.C. Binari, J.A. Freitas, Jr., W. Qian, and M. Skowronski, "Properties of GaN Films Grown on A-plane and C-plane Sapphire," *Proceedings of the 1994 Inter. Symposium Compound Semiconductors*, Sept. 18-22, 1994 (IEEE, Piscataway, N.J., 1994).

2. S.C. Binari, L.B. Rowland, G. Kelner, W. Kruppa, H.B. Dietrich, K. Doverspike, and D.K. Gaskill, "DC, Microwave, and High-Temperature Characteristics of GaN FET Structures," *Proceedings of the 1994 Inter. Symposium Compound Semiconductors*, Sept. 18-22, 1994 (IEEE, Piscataway, N.J., 1994). ■

Antenna Isolation Improvement

G.T. Roan and R.A. Muha

Tactical Electronic Warfare Division

The goal of this project is to develop a technology base for improving antenna isolation on decoys. Any system (or systems) that simultaneously transmits and receives at the same frequency requires some degree of antenna isolation. The electronic decoy repeater is a typical example of such a system. The decoy repeater is an electronic countermeasure (ECM) device that produces large radar returns (echoes) to jam or confuse an unfriendly radar. In its simplest form, the decoy repeater consists of a receive antenna, an electronic amplifier, and a transmit antenna that are often located on a small, offboard platform. With sufficient electronic amplification (gain), the repeater produces a larger radar return, or more precisely, a larger effective radar cross section (RCS) than that produced by a targeted ship or aircraft. The maximum electronic gain must be less than the isolation between the antennas however or the repeater spontaneously oscillates. Repeater oscillation generally produces unwanted noise and reduces the decoy's ECM effectiveness. By increasing the isolation between the receive and transmit antennas, higher electronic gain can be used to provide a larger RCS, which generally leads to an increase in the ECM effectiveness.

Basic Scattering Code (BSC): Central to the isolation improvement task is the development and application of advanced computer-aided engineering tools to predict and analyze antenna coupling on candidate platforms. The geometrical theory of diffraction (GTD) is one tool that is useful when the dimensions of the platform are much larger than a wavelength [1]. GTD is a high-frequency technique that extends the principles of geometric optics to include diffraction phenomenon. In the GTD, diffraction is treated as a highly localized phenomenon whereby the diffracted fields can be described in terms of rays. By including diffracted rays for a number of canonical shapes and surfaces, the GTD can handle electromagnetic radiation problems for large, complex structures such as ships, aircraft, and decoy vehicles. Currently we are working with a GTD-based model developed at the Ohio State University, which is called the Basic Scattering Code (BSC) [2].

In the BSC, complex structures are represented by collections of perfectly conducting flat plates and curved surfaces and thin, flat dielectric plates. Antennas are modeled singly or as arrays of simple dipoles, aperture antennas, or antennas defined by measured antenna patterns. The BSC output is provided in terms of coupling between antennas, antenna patterns, or fields at selected points. In all cases, the vector sum of the direct, reflected, and diffracted rays are calculated at the receive antenna or field point. Diffracted rays include edge diffraction from flat plates and creeping waves for curved surfaces. Reflected rays from plates and curved surfaces and reflected-diffracted and diffracted-reflected rays from plates are included, but second-order terms between cylinders and plates and other higher terms are not included at the present time.

As a check on the accuracy of the BSC, a series of measurements was carried out in an anechoic chamber for comparison to the calculations. For this purpose, a simple isolation reference model representing an airborne decoy platform was constructed that allows us to vary the placement of the antennas and measure the resultant coupling. This model is also used to measure coupling in the presence of composite dielectric surfaces and to study isolation improvement through treatment of edges and corners. The reference platform was constructed with a rectangular aluminum box for the fuselage and a thin, flat aluminum plate for the wing, with a movable slot in the fuselage for the antennas. Figure 1 shows the measured and the calculated antenna coupling at 8 GHz as a function of the receive antenna placement for the baseline reference model. The correlation is reasonably good, although some discrepancy is attributable to higher-order diffraction terms missing from the calculations and to reflections from the test setup and the imperfect anechoic walls within the chamber.

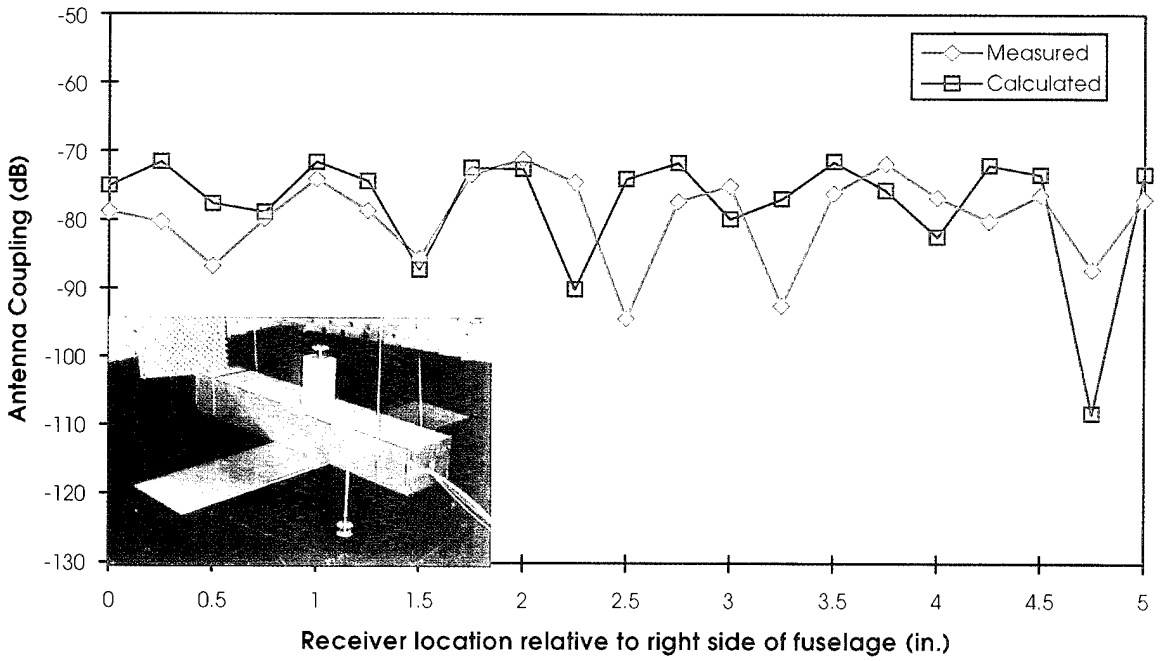

Fig. 1 — Calculated and measured antenna coupling of isolation reference model (insert).

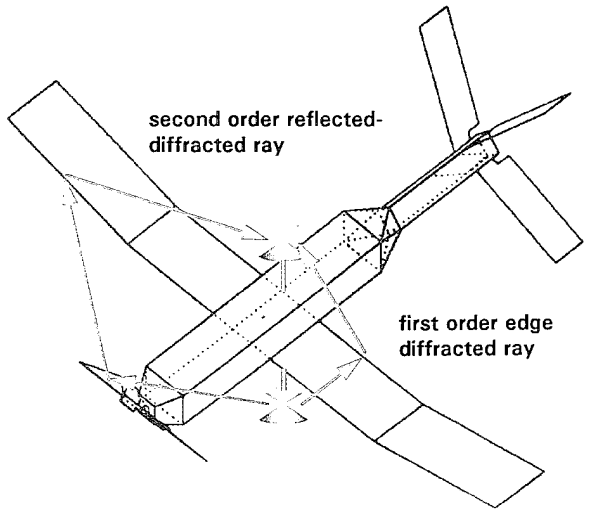

Fig. 2 — BSC model of decoy platform with examples of first- and second-order plate interactions.

BSC Model of a Decoy Platform: Figure 2 shows a computer model of a decoy platform with 33 perfectly conducting flat plates for the wings, fuselage, propeller and control surfaces, and a pair of biconical antennas. In Fig. 3, the calculated antenna coupling of this model at 8 Ghz is shown in a three-dimensional plot as a function of the receive antenna location. Calculations were made every 1.27 cm for a 1.8-m × 2.33-m area. The magnitude of the coupling between the antennas is indicated by displacement along the vertical axis and also in decibels by the color scale shown on the left side of Fig. 3. The three-dimensional visual representation is useful for quickly locating large regions of comparatively high antenna isolation. The region of lowest coupling (greatest isolation) occurs approximately midway between the wing and the tail fins. When compared to the measured antenna coupling for a decoy vehicle of similar construction, the calculated values were within 15 dB of measurements over the entire octave-plus bandwidth. The discrepancy is not unexpected since the actual decoy vehicle was constructed with composite wings, tail fins, and propeller.

Summary: Although our use of computer models for isolation improvement is preliminary, the ability to visualize antenna coupling has helped us to identify quiet zones for antenna placement and areas where edge or surface treatments would yield the most benefit. In cases where first-order diffraction terms dominate, we have found good agreement between the computer model and measurements in

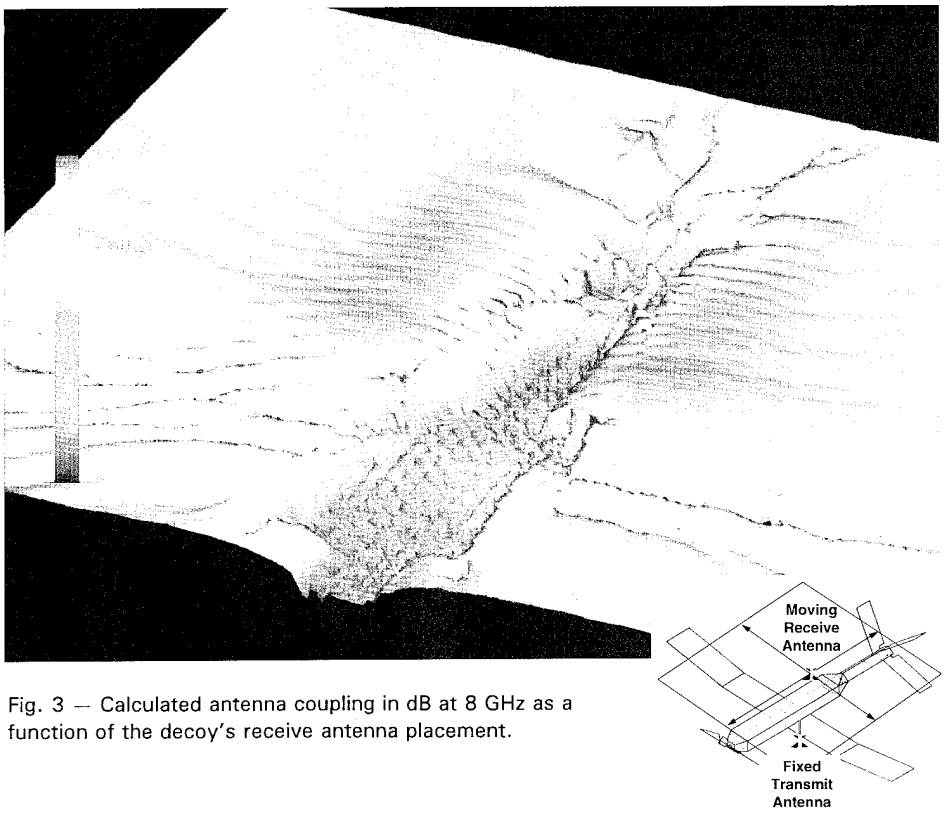

Fig. 3 — Calculated antenna coupling in dB at 8 GHz as a function of the decoy's receive antenna placement.

anechoic chambers. We will continue to work with the developers at Ohio State University to include higher-order scattering terms and more general dielectric properties in the BSC code. Other computer-aided engineering tools will be investigated for application to this problem. Once fully developed, these tools should lead to significant savings in materials and manpower over trial-and-error methods to improve antenna isolation.

[Sponsored by ONR]

References

1. P.H. Pathak, "High-Frequency Techniques for Antenna Analysis," *Proc. IEEE* **80**, 44-65 (1992).
2. R.J. Marhefka and J.W. Silvestro, "Near Zone-Basic Scattering Code User's Manual with Space Station Applications," Technical Report 716199-13, The Ohio State University Electro-Science Laboratory, Department of Electrical Engineering, March 1989. ■

Numerical Studies of Supersonic Jet Mixing and Noise

R.L. Kolbe, K. Kailasanath, T.R. Young, and J.P. Boris
Laboratory for Computational Physics and Fluid Dynamics

Noise from supersonic jet engine exhausts has been identified to be a critical technical issue in the successful development of a new, high speed, civil transport (HSCT) plane. With the current concern for a safe and sound environment, the noise for civilians from military jets during take-off and landing has also become a serious issue. Since the noise is primarily generated during the mixing of the jet with surroundings, we can alter noise by modifying the mixing of the jet. Of particular interest to us is the role of mixing enhancers, such as paddles, placed in the external flow field of a jet engine exhaust. Figure 4 shows a supersonic rectangular jet with paddles immersed from

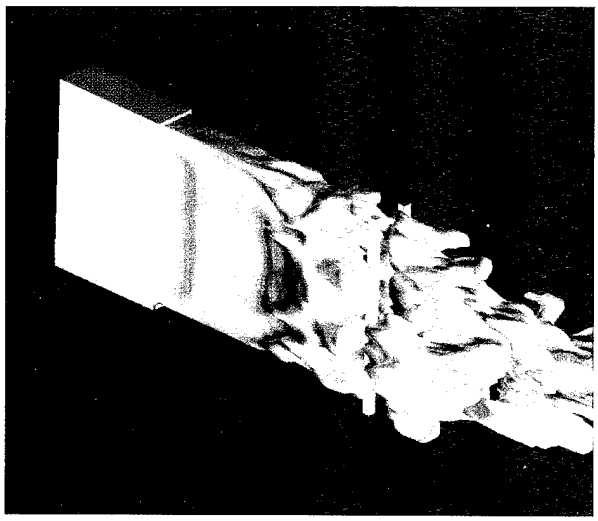

Fig. 4 — Three-dimensional view of a supersonic rectangular jet with paddles showing an x-momentum isosurface colored by density.

the sides. The jet is visualized using an x-momentum isosurface, with the color determined by the fluid's density.

Modeling and Visualizing the Jet: For this problem, we are simulating a complex, three-dimensional flow with small details, such as the paddles, in the flow field. To predict the noise, we must capture the time history of the pressure fluctuations. This time history and the motion of the jet require the solution to be time accurate. We are therefore using a large grid with approximately 10^6 points in it and marching through time with a time-step of 0.5×10^{-6} s. The solution of this problem takes several days on a supercomputer. To model the flow field of the jet with the paddles, we used a versatile simulation program, FAST3D, which solves the time-dependent, three-dimensional, gas-dynamic equations using the Flux-Corrected Transport (FCT) algorithm and the Virtual-Cell Embedding (VCE) [1] technique to represent complex objects. The three-dimensional flow visualizations were made in NRL's Visualization Laboratory, and the computations were performed on two Intel parallel processors—NRL's iPSC/860 and Wright Laboratory's Paragon.

Effect of Paddles: In Fig. 5, the flow fields of the jets without and with paddles are compared using their Pitot pressure fields. The upper frame is the free jet, and lower frame is the jet with paddles. In both frames, the jet flows from the left to the right, and the nozzle can be seen on the left. In the bottom frame, the paddles can be seen as square blocks located in the center of the figure. The effect of the paddles is to cause the jet to flap back and forth from one paddle to the other. This flapping motion quickly mixes the jet with its surroundings and generates a screech tone that further reinforces the flapping motion. This screech tone is not thought to be a problem since it can be absorbed by the use of acoustic liners in the engine's exhaust.

Jet Noise: Noise or sound is the fluctuation of air pressure that vibrates the human ear. For our numerical ear, we collect a time history of pressure at many locations within the flow field and then frequency analyze these data to reveal the noise spectrum. Figure 6 shows a sample of the amplitude-frequency response within the flow field for a jet with paddles. The amplitude-frequency plot shows multiple peaks but a very dominant peak at approximately 4700 Hz. There is a second strong peak, which is the first harmonic, at approximately 9400 Hz. If one were to stand next to this jet with paddles, one would hear a sharp tone, which is the screech tone at the dominant frequency. We have shown that this tone is present throughout the flow field and have shown that the flapping motion is at this frequency [2]. For the jet without paddles, the frequency spectrum shows multiple peaks, and no coherent structure is present. Our numerical simulations are in general agreement with experimental observations made at NASA's Lewis Research Center.

Additional Capabilities: Now that we have shown that our numerical simulations can predict the complex flow with the near-field noise, we can use our simulations to study different shape paddles and to predict the drag and mixing that these paddles produce. We have also studied the relationship between the paddle's position from the nozzle and the amount of immersion to the frequency response and thrust loss. Our analysis has also revealed a feedback

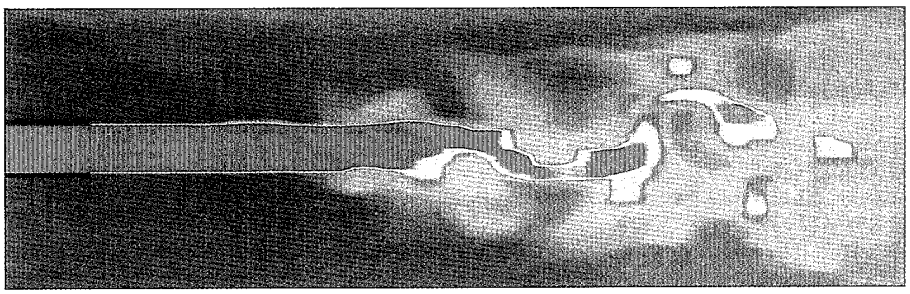

Jet without Paddles

Jet with Paddles

Fig. 5 — Effect of paddles on flow field shown by Pitot pressure distribution.

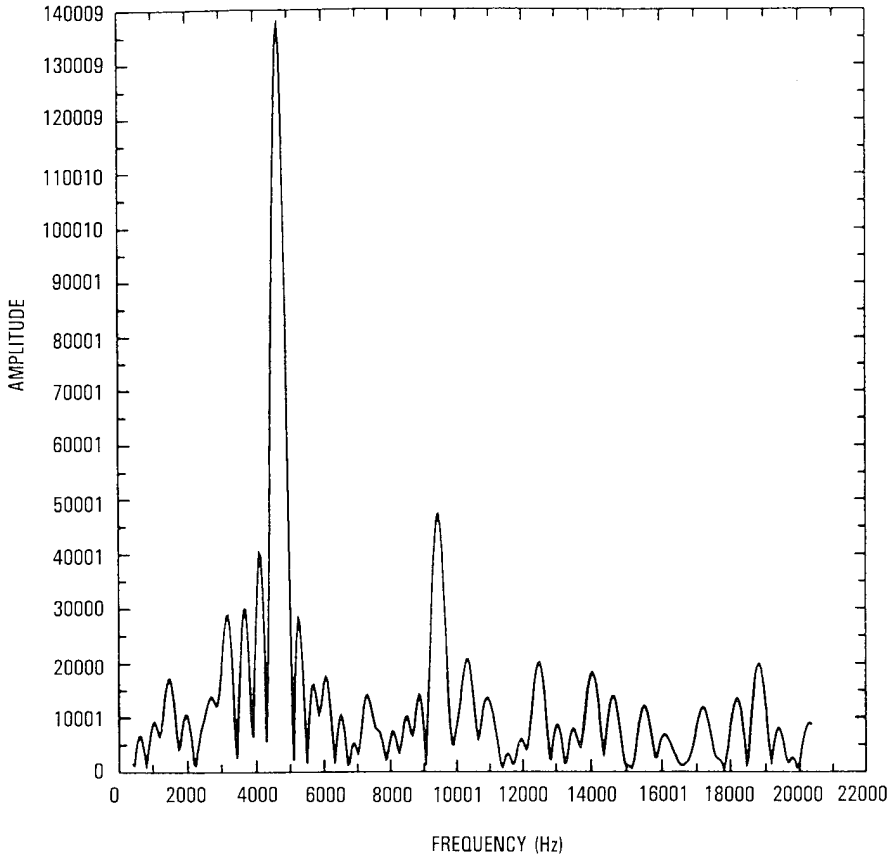

Fig. 6 — Predicted frequency spectrum of local pressure for jet with paddles at a location near the paddles.

mechanism that has the flapping motion generating the screech tone that propagates upstream and reinforces the flapping motion.

[Sponsored by NASA's Lewis Research Center]

References

1. A.M. Landsberg, T.R. Young, and J.P. Boris, "An Efficient, Parallel Method for Solving Flows in Complex Three-Dimensional Geometries," 32nd Aerospace Sciences Meeting and Exhibit, Reno, Nevada, Jan. 10-13, 1994 (AIAA paper 94-0431, AIAA Washington, D.C., 1994).

2. R. Kolbe, K. Kailasanath, T. Young, J. Boris, A. Landsberg, and E. Brown, "Numerical Simulations of Flow Modification of Supersonic Rectangular Jets," 33rd Aerospace Sciences Meeting and Exhibit, Reno, Nevada, Jan. 9-12, 1995 (AIAA paper 95-0725, AIAA Washington, D.C., 1995). ■

Compact, Portable, Hyperspectral Imaging Systems: The PHILLS Project

J.A. Antoniades and P.J. Palmadesso
Plasma Physics Division

L.J. Rickard
Remote Sensing Division

Benefits and Challenges of Hyperspectral Imaging: In recent years, several new technologies have appeared that have revolutionized the field of remote sensing. One of the most important is high-resolution imaging spectroscopy, commonly referred to as hyperspectral imaging. Hyperspectral imaging spectrographs are capable of making spatial and time-resolved measurements in the UV to LWIR. They record emission, reflection, or transmission radiation spectra from ground, air, or space-based platforms. Hyperspectral imagers produce wide-area images in the same manner as line-scan cameras but retain the full spectral profile of every pixel in the scene.

Thanks to enormous technological advances, modern imagers are very compact, modular and lightweight systems. These imagers can provide spatial resolution limited by the system optics and the pixel size of the sensor. Spectral resolution can be < 1 nm over the entire UV-to-MWIR spectrum. The high spectral resolution over hundreds of bands separates this technology from the multispectral imagers in use today (for example, Landsat), which are limited to a few noncontiguous, wide spectral bands. Equally important in this rapidly developing technology is the ability to record, manipulate, and analyze enormous quantities of data produced by hyperspectral imagers. Gigabytes of data must be handled quickly to fully use the imager's capabilities. The large number of bands allows one to simultaneously match hundreds of known absorption or reflection spectra with considerably fewer signal-to-noise ratios than other techniques. These imagers are used for a wide range of applications including environmental conservation, cleanup, pollution monitoring, fire or battle damage assessment, terrain characterization, and many others.

PHILLS Instrument Description: A modular, broadband hyperspectral imager, originally developed for BMDO and the Strategic Environmental R&D Program (SERDP) Global Climate Initiative, is now being fielded. This device, called the Portable Hyperspectral Imager for Low-Light Spectroscopy (PHILLS), is of a modular design, constructed primarily from commercial off-the-shelf components; it achieves extremely high sensitivity in a package slightly larger than a video camera. Presently PHILLS has two intensified spectroscopic modules and a high-resolution color video camera. The instrument produces in excess of 1100 spectral bands in the range of 0.3-0.95 mm, with spectral resolution of 0.55-1.5 nm. The intensified modules allow low-light operation, range gating, and blur-free imaging from rapidly moving platforms. A high-resolution color video camera is aligned with the spectroscopic modules to provide a viewfinder for easy alignment and subsequent image registration.

PHILLS was designed for both ground and airborne use. Scanning is accomplished in a

push-broom mode when the instruments are deployed from an aircraft. For ground-based operation, a stepper motor-based computer-controlled rotating platform scans the instrument across the scene. Thus far PHILLS has been deployed on the ground for gas plume monitoring as well as on the (NRL) P-3 aircraft for detection of ground-water flow for base remediation and ice measurements in the Arctic and along the eastern U.S. coast for coastal environmental measurements.

Figure 7 shows the ability of the imager to distinguish the several characteristics of the terrain such as variable amounts of moisture. The instrument was deployed on an NRL P-3 aircraft and flown over the "O-Field" area at Aberdeen Proving Grounds in Maryland.

The PHILLS system is controlled by a PC-based computer. The PC controls all analog and digital recorders that are coupled to the camera modules; further, it displays and records Global Positioning System (GPS) data and controls the scanning mount for the ground-based operation. This computer is also used for postprocessing of the acquired data.

In conjunction with the PHILLS system development, a new spectral-demixing algorithm called the filter vector algorithm (FVA) has also been developed. This method can be shown to be formally equivalent to linear least-squares demixing. This algorithm performs 100 times faster than the standard demixing algorithms. It is a fully parallelized algorithm that can be implemented on digital signal processors (Intel i860, TI MVP, ...) or neural net processors (CNAPS) to achieve real-time demixing of every pixel, even in a fast-frame multisensor system. Present tests indicate that it can locate

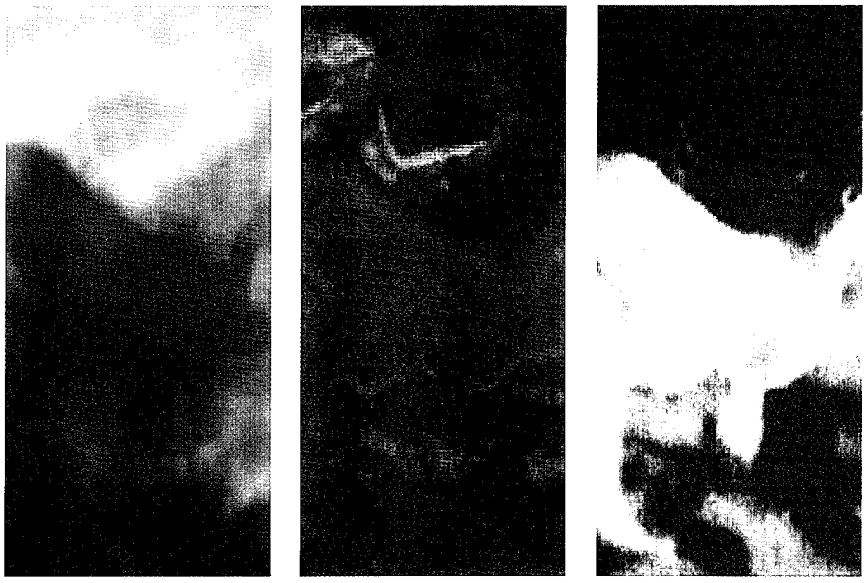

(a) (b) (c)

Fig. 7 — (a) RGB composite image taken from the hyperspectral imager of the "O-field" hazardous materials disposal section at Aberdeen Proving Grounds. The image depicts the disposal site and Watson's Creek, a tributary of the Gunpowder river. (b) Colorized plot of the reflected component of the incident illumination extracted from the spectral data. Here red is highly reflective and blue is highly absorbing parts of the scene. (c) Terrain feature separation of the area imaged in (a) using spectral signature matching techniques combined with suppression of the illuminating radiation spectrum. The separation was performed matching the spectral signature of a particular area in the field of view, in this case that of water in the creek, with the rest of the image. Brightness is determined by the degree of spectral match.

a known spectral signature within a mixture of several hundred unknowns, even at signal-to-noise levels as low as 0.2.

Current plans are to extend PHILLS to the midwave IR in its wavelength coverage to provide improved capabilities for identifying and quantifying terrestrial and atmospheric signatures. A long-wave IR (8 to 12 mm) thermal imager will also be added to the PHILLS package to provide thermal-profile mapping and complement the visible camera for nighttime operation. Coupled with the new analysis techniques, the PHILLS hyperspectral imagers are well ahead of the rapidly developing technology.

Acknowledgments: We acknowledge the efforts of Dr. Mark Baumback, Dr. Jeffrey Bowles, Mr. Daniel Haas, Mr. John Stracka, and Mr. William Dolinger, whose dedicated efforts have made the PHILLS system a working reality and continue to push the limits of technology.

[Sponsored by SERDP and BMDO] ■

Antenna Modeling on Spacecraft

W.L. Lippincott
Space Systems Development Department

Antenna modeling programs can be used as a design tool for developing antennas and antenna/satellite systems. They provide flexibility in evaluating proposed designs and in augmenting designs. There is also the future potential of very accurate modeling to replace experimental anechoic chamber testing.

Modeling Complex Structures: This research has focused on developing methods for modeling various antennas on spacecraft structures. Figure 8(a) shows the structure used to model the HTSSE (High Temperature Superconducting Space Experiment) antenna on the nadir panel of the Argos spacecraft. The HTSSE antenna (located in the center of the panel) consists of a slotted cylindrical array, with a conical monopole mounted on top. This spacecraft is scheduled to be launched in the second quarter of FY 96. The complex nature of the nadir panel causes severe degradation of the antenna patterns at certain angles. The modeling is being used to determine a flight schedule for data collection where the pattern degradation is minimized. Figure 8(b) compares experimental anechoic chamber data and modeling data for an azimuth pattern cut 60° from boresight of the antenna on the nadir panel. The NECBSC (Ohio State's Basic Scattering Code), a ray tracing and diffraction code, was used for the modeling. The modeling has the advantage over the experimental testing in that it can take into account the large solar panels (not shown), which are too large to fit in the anechoic chamber.

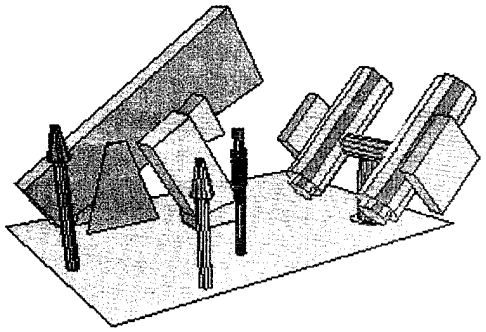

Fig. 8(a) — Model of nadir panel of the Argos Spacecraft.

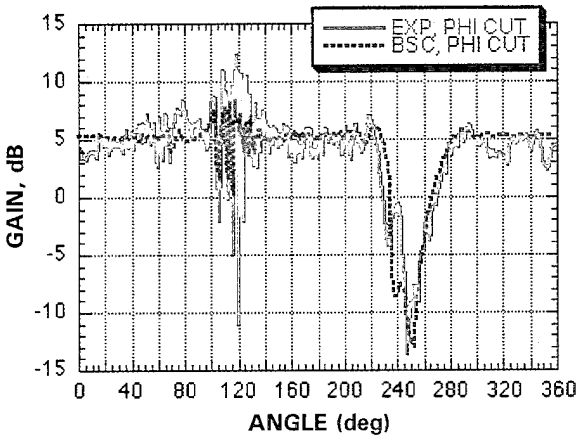

Fig. 8(b) — Experimental vs modeling results for an azimuth pattern for the slotted cylinder array antenna on the Argos spacecraft nadir panel.

Figure 9 shows the plate structure used to model a recoverable launch vehicle, previously under development by NRL's Naval Center for Space Technology. The antennas modeled on

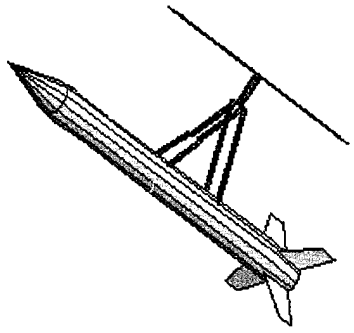

Fig. 9 — A recoverable launch vehicle.

this structure consist of opposing circularly polarized GPS-patch antennas and bent-arm monopoles. The modeling is needed to predict the effect of the deployable helicopter structure on the antenna performance. The NECBSC was used to model this system.

Multiarm Spiral Antenna: Another antenna of interest to the spacecraft community is the multiarm spiral antenna. This circularly polarized antenna is broadband and conformal to a surface, which allows several antennas to be placed near each other with minimal interaction. Two methods are currently being researched to effectively model this antenna. The first method uses the method of moments (MOM). For the MOM method, the structure being analyzed is divided into a number of straight wire subsections or surface patches, which are each small when compared to the wavelength. Each of these elements is then considered to be a point source radiating to and interacting with all of the other elements making up the system geometry.

Figure 10(a) shows the MOM model for an eight-arm, six-wind cavity spiral. Figure 10(b) shows results of MOM modeling using the Ohio State electromagnetic surface patch (ESP) code compared to experimental data for vertical polarization for the spiral set on the corner of a small ground plane with an azimuth cut 60° from boresight. The modeling predicts the general shape and gain level of the pattern reasonably well. Some discrepancies are to be expected because the model predicts a perfect feed structure, whereas for the real antenna feed, gain and phase for the eight feeds will not be perfectly matched.

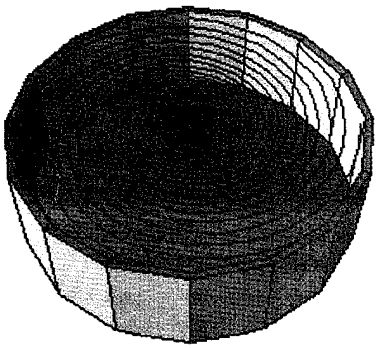

Fig. 10(a) — MOM model for the eight-arm cavity spiral.

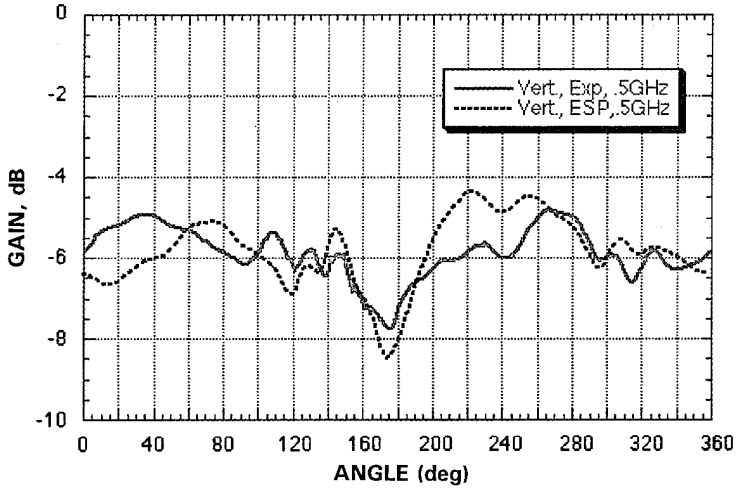

Fig. 10(b) — Experimental vs modeling results for an azimuth pattern cut for the eight-arm cavity spiral on the corner of a small ground plane.

The second method developed for modeling the spiral is a source transformation technique. This technique, developed along with Michael Kluskens and Mark Kragalott of NRL's Radar Division, models the antenna as a set of 32 sources with complex amplitudes that generate the same far-field pattern as the antenna itself. The technique is two-fold. First, the appropriate locations for a set of sources are found using an imaging technique. Second, the far-field electric field equations for general electric and magnetic sources on a surface are solved for the source magnitudes and phases. Both electric and magnetic sources are used. The sources can be used in the NECBSC to solve for the antenna's radiation pattern performance in a complex structural environment.

Acknowledgements: The author acknowledges Fred Domer for collecting the experimental data and Jeff Horner for developing a CAD interface for the modeling codes.

[Sponsored by the Air Force)

NRL's POAM-II Instrument Monitors the Ozone Hole

R.M. Bevilacqua, J.S. Hornstein,
and E.P. Shettle
Remote Sensing Division

The Ozone Hole: A tenuous layer of ozone in the stratosphere shields the Earth's surface from lethal ultraviolet components of sunlight. The absorption of ultraviolet sunlight warms the ozone layer, creating a giant temperature inversion. This temperature inversion creates the stratosphere as a distinct atmospheric region by acting as a cap on vertical motions in the lower atmosphere. In particular, the stratospheric temperature inversion limits the intensity of thunderstorms, hurricanes, and other low-pressure systems.

Each September and October, a hole develops in the ozone layer over Antarctica. The details are not clear, but the overall cause of the ozone hole is now understood. Winter occurs when either the North or South Pole is tilted away from the Sun. Because it receives no sunlight, air at the winter pole is colder than at lower latitudes. The temperature difference causes a large vortex to form in the stratosphere over the winter pole. This vortex keeps out warmer air from lower latitudes, making it even colder. The wintertime polar stratospheric vortex over the South Polar regions is particularly stable, and the air becomes so cold that polar stratospheric clouds (PSCs) form in abundance. Chemical reactions on the surfaces of PSC particles extract chlorine from harmless compounds in which it was bound with nitrogen and convert it into a form that, under the action of sunlight, can destroy ozone. The nitrogen products fall by sedimentation to lower altitudes where they are no longer available to recombine with chlorine and thereby impede the destruction of ozone. When the first spring-time rays of the Sun strike the PSC-processed air, chlorine catalytically destroys most of the ozone over a significant range of altitudes.

Most of the chlorine reaches the stratosphere only because of the human release into the atmosphere of chlorofluorocarbons (CFCs). Because they are so unreactive, CFCs are able to reach the stratosphere where the chlorine within them is released by the intense, ultraviolet-rich sunlight. The ozone hole is, therefore a recent phenomenon.

Many features of the ozone hole remain puzzling. The Antarctic ozone hole occurs at unexpectedly low altitudes (at 20 km rather than 40 km). Ozone is decreasing globally, not only in the Antarctic, and more rapidly than present models can explain. The puzzles need to be resolved to understand ozone trends all over the globe and, more generally, to predict the likely effects of other chemical changes in the atmosphere resulting from human activities and natural biological and geological processes at the surface.

Polar Ozone and Aerosol Measurement (POAM) II: An NRL instrument, POAM II, is presently obtaining data to help resolve these puzzles. POAM measures the attenuation of sunlight by the atmosphere as the satellite sees the Sun rise and set during each orbit. This solar occultation technique is self-calibrating and provides excellent vertical resolution. POAM has nine spectral channels designed to measure ozone, NO_2, water vapor, temperature, and aerosols as a function of altitude in the stratosphere and lower mesosphere. POAM II is carried by the French *SPOT 3* remote-sensing satellite, which was launched on September 25, 1993. *SPOT-3* is in a Sun-synchronous polar orbit at an altitude where it sees 14 sunrises and 14 sunsets per day.

Results: POAM-II was launched in time to observe the healing of the 1993 Antarctic ozone hole—the deepest ozone hole in history. POAM's data provided unprecedented detail about the healing. Figure 1 shows the ozone number density, averaged around a latitude circle, as a function of time. The data show clearly that the ozone hole heals from the top downward. POAM data also showed the effect of descending air in the vortex on the vertical distributions of ozone and aerosols as a function of time. Thanks to *SPOT*'s orbit, POAM was often able to sample both air inside the vortex and air outside the vortex on the same day. Figure 2 shows an example. The dark areas

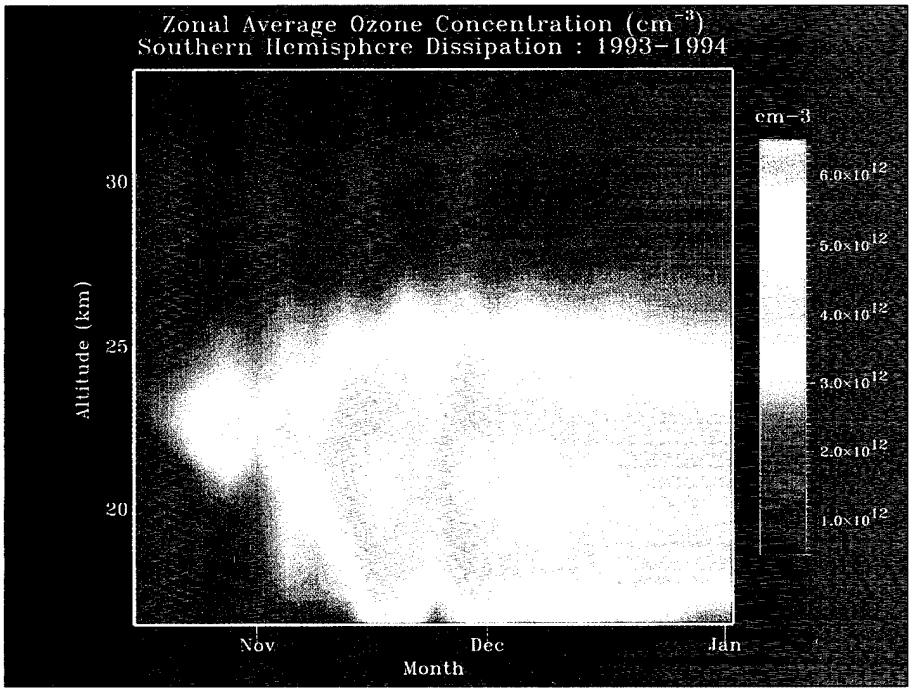

Fig. 1 — POAM II data on the vertical distribution of ozone as a function of time, during the healing of the 1993 Antarctic ozone hole.

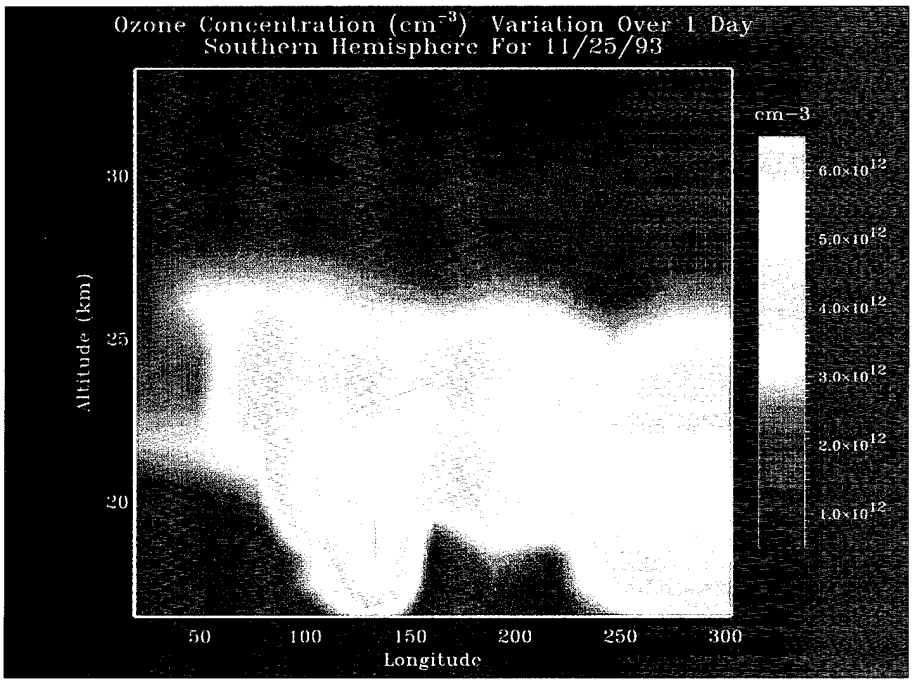

Fig. 2 — The vertical distribution of ozone around a circle of latitude on single day. On this day, POAM II sampled air inside and air outside the vortex. Inside the vortex, the ozone is missing at low altitudes; outside the vortex the abundance of ozone is much higher.

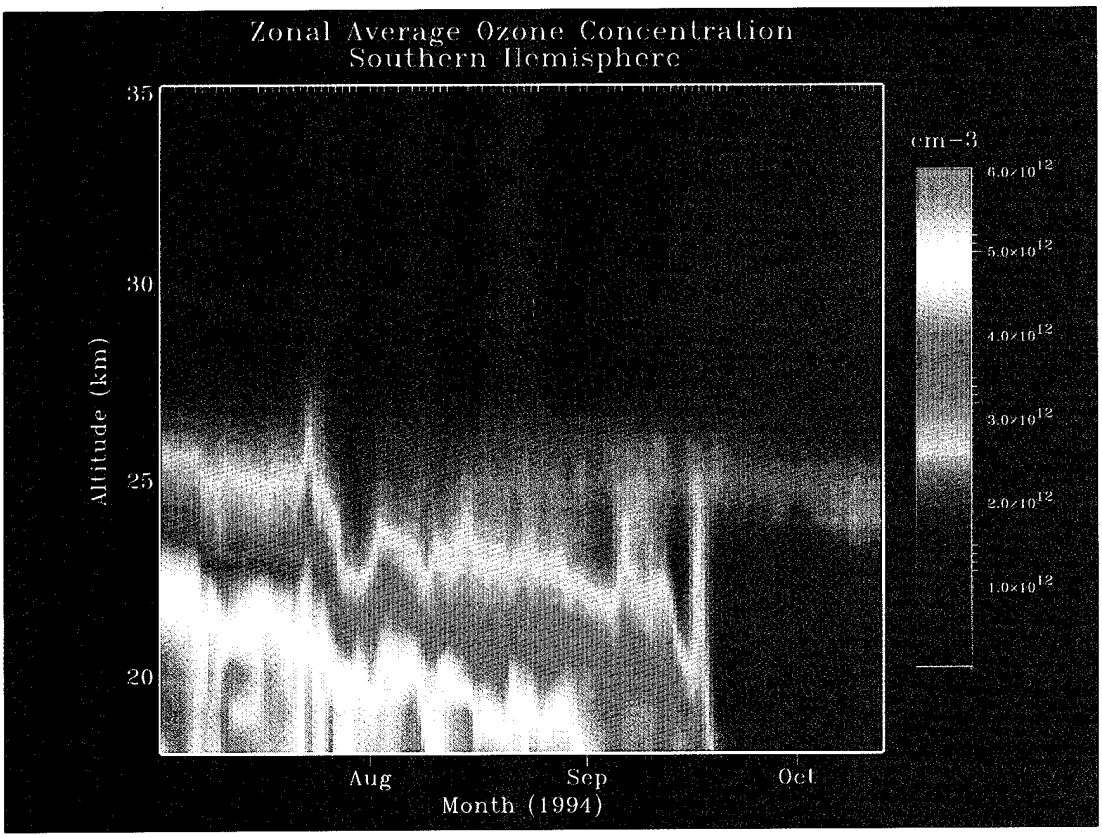

Fig. 3 — POAM II data on the vertical distribution of ozone as a function of time during the formation of the 1994 Antarctic ozone hole.

are regions of less ozone and correspond as expected to the region inside the vortex. Data such as these made it possible to show that the vortex acts more like a containment vessel than as a flow-through reaction vessel and to delineate how the containment properties of the vortex vary with altitude and time.

POAM-II observed the formation and the dissipation of the 1994 ozone hole. Figure 3 is analogous to Fig. 1 but for 1994. The figure shows that the hole developed with surprising abruptness. Other POAM data indicate that air processed by PSCs has not yet had time to fully mix with the other air in the vortex when the ozone hole begins to form. POAM-II also obtained a wealth of data on PSCs.

In addition to its contribution to studies of ozone depletion, POAM-II provides unique data on the spatial and temporal variability of the stratosphere. Figure 2 is an example. Data on stratospheric variability will be useful in designing hardware, detection and measurement algorithms, and validation tests for space-based scientific and military electro-optical sensing and communications systems. POAM data could also be used to improve forecasts and nowcasts of the state of the middle atmosphere at places and times of special interest, both for scientific purposes and for predicting the re-entry of missiles and space vehicles.

Acknowledgments: Major roles in developing POAM and in analyzing its data were played by Robert Lucke and Karl Hoppel of NRL's Remote Sensing Physics Branch, by Davidson Chen of NRL's Special Projects Staff, by Jerry Lumpe, Steven Krigman, Michael Fromm, and David Debrestian, of Computational Physics Incorporated, by William Glaccum, of Applied Research Corporation, and by Michael Abrams, of Falcon Research, Incorporated. The POAM-II instrument was built by

the Thermo Trex Corporation. The French Centre National D'Etudes Spatiales built and operates the *SPOT-3* spacecraft, and plays a significant role in POAM's operation. Launch and initial operations were sponsored by the Air Force Space Test Program. POAM is operated by Detachment 2 of the Air Force Space and Missile Command.

[Sponsored by BMDO and SERDP]

References

1. R.M. Bevilacqua, E.P. Shettle, J.S. Hornstein, W. Glaccum, J.D. Lumpe, S.S. Krigman, P.R. Schwartz, and D.T. Chen, "Polar Stratospheric Studies with the Polar Ozone and Aerosol Measurement Experiment (POAM II)," *Proc. American Meteorological Society Eighth Conference on Atmospheric Radiation*, 23-28 Jan. 1994.

2. E.P. Shettle, R.M. Bevilacqua, J.S. Hornstein, W.J. Glaccum, D. Debrestian, M. Fromm, S. Krigman, J. Lumpe, J.L. Bertaux, E. Chassefière, F. Dalaudier, C. Deniel, C. Brogniez, J. Lenoble, P. Pruvost, J. Olivero, C. Randall, and D. Rusch, "POAM II: Early Results and Comparisons with the COSPAR International Reference Atmosphere Models," to be published in *Adv. Space Res.*

3. R.M. Bevilacqua, K. Hoppel, J. Hornstein, R. Lucke, E. Shettle, T. Ainsworth, D. Debrestian, M. Fromm, J. Lumpe, S. Krigman, W. Glaccum, J. Olivero, R.T. Clancy, D. Rusch, C. Randall, S. Dalaudier, C. Deniel, E. Chaussefiére, C. Brogniez, and J. Lenoble, "First Results from POAM II: The Dissipation of the 1993 Antarctic Ozone Hole," (1994), submitted to *Geophys. Res. Lett.* ■

Long Time Period Adjustment of the Ocean Climate

G.A. Jacobs
Oceanography Division

The atmospheric forcing variations on the ocean occur at relatively short time scales, on the order of weeks to a year. The ocean circulation and climate driven by these changes in forcing can take years to decades to respond at the large scale. The long time period response is provided through Rossby waves. Research work conducted at the Naval Research Laboratory (NRL) was the first to reveal long time period ocean response through Rossby waves produced by extreme climatic events such as the 1982-83 El Niño. The 1982-83 El Niño Rossby wave was initiated at the American coasts and had reached Japan by 1992. Upon reaching Japan, the wave interacted with the Kuroshio Extension to produce sea-surface temperature anomalies over 1° C extending across the Pacific Ocean. Such temperature anomalies have been shown to have significant impact on weather patterns throughout the world. These results indicate that oceanic climate on the large-scale changes very slowly. Model results indicate that the climate variations produced by these waves are very predictable.

Long Time Period Waves: Rossby waves are theoretical wave solutions to simplified ocean dynamics. The time and space scales of the waves are of the order of several years and 1000 km at midlatitudes. Observations of the waves from in situ data have been attempted with limited success. Direct observation and demonstration of a Rossby wave had never been accomplished until the advent of two tools: accurate altimeter data provided by the Navy's Geosat-Exact Repeat Mission and accurate global ocean models. The vision and development of both tools have occurred side by side in NRL's Ocean Dynamics and Prediction Branch.

Further work through altimeter data from the more recent TOPEX/POSEIDON satellite has revealed Rossby waves produced by El Niño events subsequent to the 1982-83 event. These El Niño events occurred in 1986-87, 1991-92, and 1992-93. These waves are generated by Kelvin waves, which propagate from the west equatorial Pacific eastward (Fig. 4). The reflection of the Kelvin waves at the American coasts produces the much slower-moving Rossby waves. The Rossby waves move with a very distinct propagation speed determined by the ocean's vertical density stratification and the coriolis force.

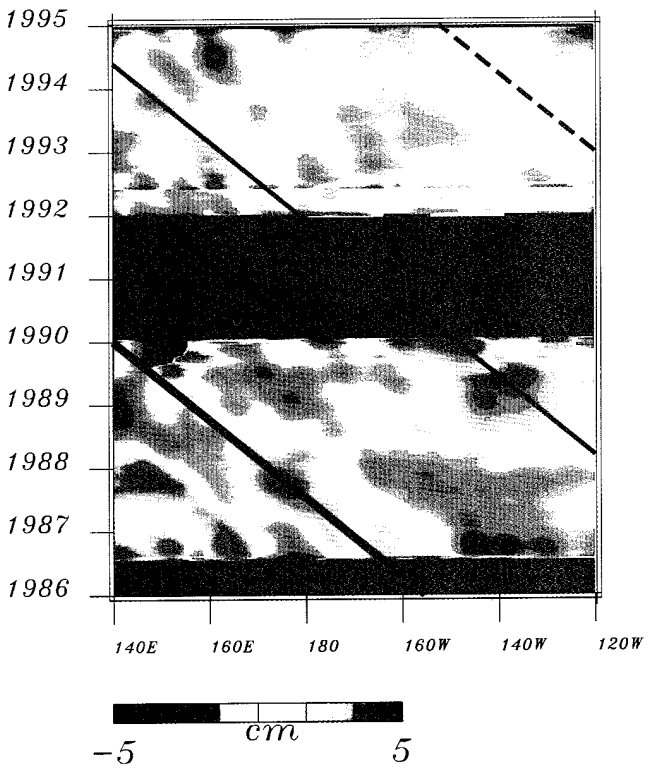

Fig. 6 — Sea-surface height variations along 30°N indicate a distinct westward propagation (moving from right to left as time increases from bottom to top). The lines indicate the Rossby wave signals from the 1982-83 (heavy solid), 1986-87 (solid), and 1991-92 (dashed) El Niño events.

Effects of Rossby Waves: The winds are the main source of momentum input into the oceans. Ocean circulation is directly linked to the wind forcings, and when the wind forcings change, ocean circulation changes. Wind-forcing changes in one area are transferred to circulation changes throughout the world by means of waves. Thus wind changes over the equatorial Pacific Ocean initiating El Niño produce a Kelvin wave, and the Kelvin wave initiates Rossby waves. The Rossby waves propagate a change in ocean circulation through the Pacific Ocean.

Each of these waves induces a geostrophic current perturbation to the ocean circulation. This anomalous current is felt across the Pacific Ocean. Though the induced currents are small, they may produce profound effects, as has been seen by the Rossby wave from the 1982-83 El Niño. This wave was strong enough to influence the Kuroshio Extension, which advects large amounts of warm water and heat into the central North Pacific Ocean. A portion of the Kuroshio Extension was brought further northward, and the warm waters produced an extreme temperature anomaly across the North Pacific Ocean for a time period over 1 year. This remarkable event occurred 9 years after the 1981-82 El Niño.

Numerical Models of Ocean Circulation: A test of the accuracy of an ocean model is its ability to generate and propagate a Rossby wave over a long time period. The NRL global 1/4° global ocean model has demonstrated its capability to do just this. As theoretical Rossby waves require no forcing to propagate, once the wind forcing has generated a Rossby wave, the forcing may be turned off. This test of the NRL global model was conducted, and the model was able to propagate the Rossby wave across the Pacific Ocean at the observed speed for a time period of 10 years without dissipating the wave away (Fig. 7). Figure 7(a) presents the sea surface height variations at 30°N from the Navy's Geosat-Exact Repeat Mission. This particular panel is a subsection of Fig. 6 and shows the Rossby wave from the 1982-83 El Niño event propagating from just north of Hawaii to the southern tip of Japan. The NRL numerical ocean model forced by observed

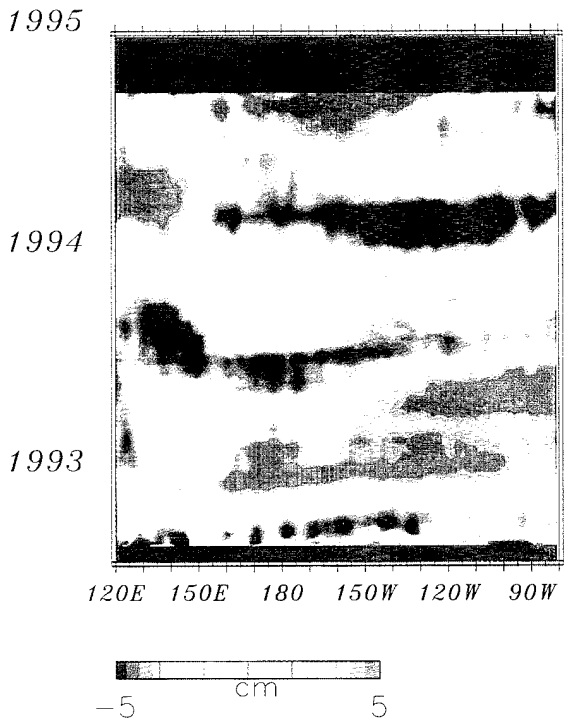

Fig. 4 — Sea surface height variations along the equatorial Pacific indicate Kelvin waves propagating from west to east (from left to right as time increases from bottom to top). These Kelvin waves reflect from the American continents, producing the Rossby waves seen in Figs. 5 and 6.

Rossby waves produced by the El Niño events are evident as ridges spanning the Pacific Ocean in the altimeter data (Fig. 5). The initial shape of each wave is an image of the American continental coastlines. Near the equator, the waves propagate much faster than near the poles, thus the wave shape gradually deforms. As the waves propagate across, they obtain a refracted appearance. At a particular latitude, the propagation speed is fixed. A view of the propagation across the Pacific Ocean at 30°N is presented in Fig. 6. At this latitude, a Rossby wave requires 9 years to cross the Pacific Ocean. To observe such a long time period event, data from three separate altimeter missions must be used. The data are a combination of the U.S. Navy's Geostat-Exact Repeat Mission, the European Remote Sensing satellite (ERS-1), and NASA's TOPEX/POSEIDON altimeter. Within the time period covered by these satellites, three significant El Niño events occurred, and the Rossby waves initiated by the events are present in the observations. El Niño events are an extreme intensification of the normal annual cycle. Indications of weaker Rossby waves also are present in non-El Niño years.

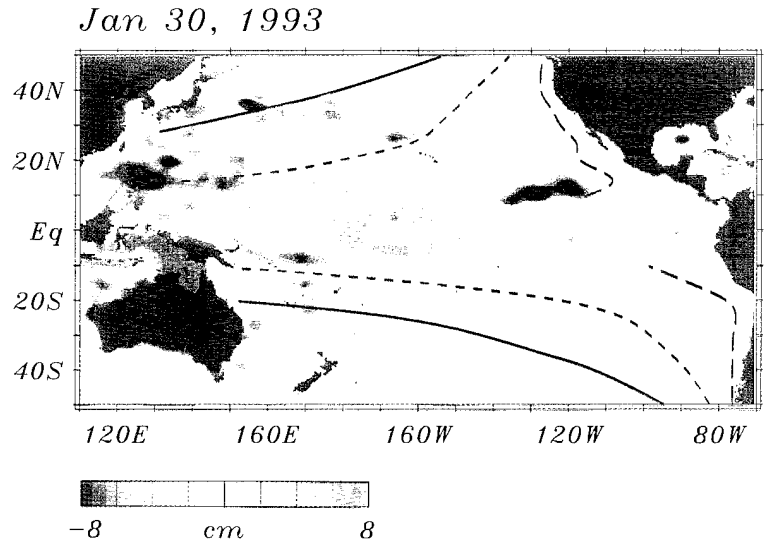

Fig. 5 — Rossby waves created by the three El Niño events during 1986-87 (solid), 1991-92 (dash), and 1992-93 (long dash) are visible in the Pacific Ocean from TOPEX/POSEIDON altimeter data. Lines mark the leading edge of the waves. The plot shows the sea-surface height deviation during January 1, 1992, from its mean over 2 years.

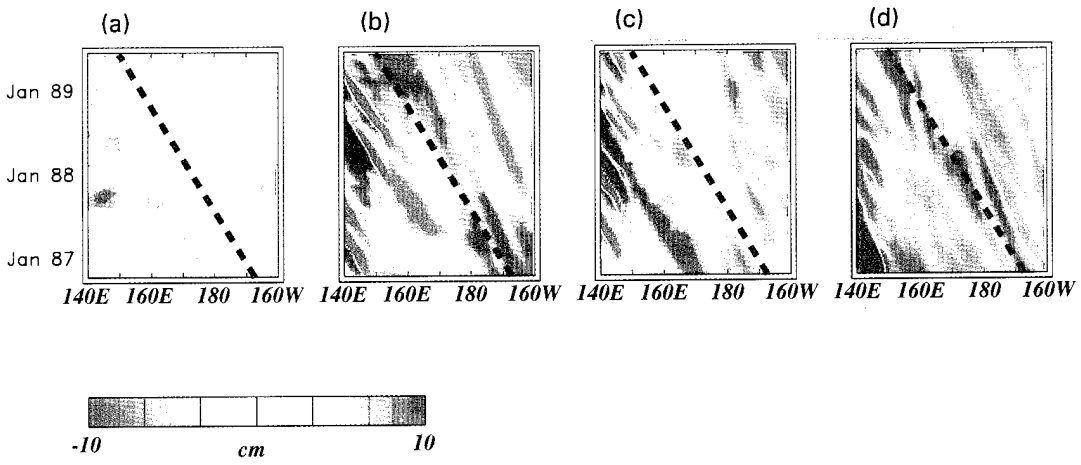

Fig. 7 — Sea-surface height variations along 30°N from (a) the Navy's Geosat-Exact Repeat Mission, (b) the NRL global numerical ocean model forced by observed winds from 1981 to 1993, (c) the NRL model forced by observed winds from 1984 to 1993, (d) the NRL model forced by observed winds from 1981 to 1984.

winds reproduces the wave (Fig. 7(b)). If the model is forced by observed winds beginning in 1984 (after the 1982-83 El Niño event), the Rossby wave is not generated (Fig. 7(c)). If the model is forced by winds that produce the 1982-83 El Niño and the generated Rossby wave is allowed to propagate freely with no wind forcing beyond 1984, the Rossby wave again propagates across the Pacific Ocean, as observed. Most global ocean models must be slowly pushed toward an observed climatological field. This slow push would gradually dissipate away the Rossby wave. However the NRL model has no such requirement and maintained the wave successfully. This is a promising result for climate prediction studies.

[Sponsored by ONR, ARPA, and SERDP] ■

The Modular Ocean Data Assimilation System

R.C. Rhodes, M.R. Carnes, and G.W. Heburn
Oceanography Division

Many naval operations require accurate knowledge of the three-dimensional structure of temperature and salinity in the world's oceans. To support this need, the Fleet Numerical Meteorology and Oceanography Center (FNMOC) produces ocean thermal analyses for the global oceans and performs higher-resolution regional analyses for the Gulf Stream, Kuroshio, and Greenland-Iceland-Norwegian Seas [1]. These "shore-based" analyses are generated using the Optimum Thermal Interpolation System (OTIS), which had its genesis within what is now the Naval Research Laboratory's (NRL) Ocean Dynamics and Prediction Branch. OTIS combines observations, simple models of coherent ocean features, and ocean climatologies to produce each analysis by using objective assimilation techniques. Recent advances in computer technology now make it possible to move these ocean analysis capabilities from the shore sites to shipboard systems on desktop workstations. The Modular Ocean Data Assimilation System (MODAS 1.0) [2] has been developed for this purpose and is also used in several projects by the Navy.

The Office of Naval Research/Space and Naval Warfare Systems Command (SPAWAR)-funded Navy Ocean Modeling Program (NOMP) sponsored the NRL's Ocean Dynamics and Prediction Branch to develop shipboard systems capable of producing ocean nowcast and forecast analyses consistent with those produced by the current state-of-the-art systems at FNMOC and the Naval Oceanographic Office. As part of this effort, MODAS was designed as a highly modular set of software to allow configuration for use in several potential systems.

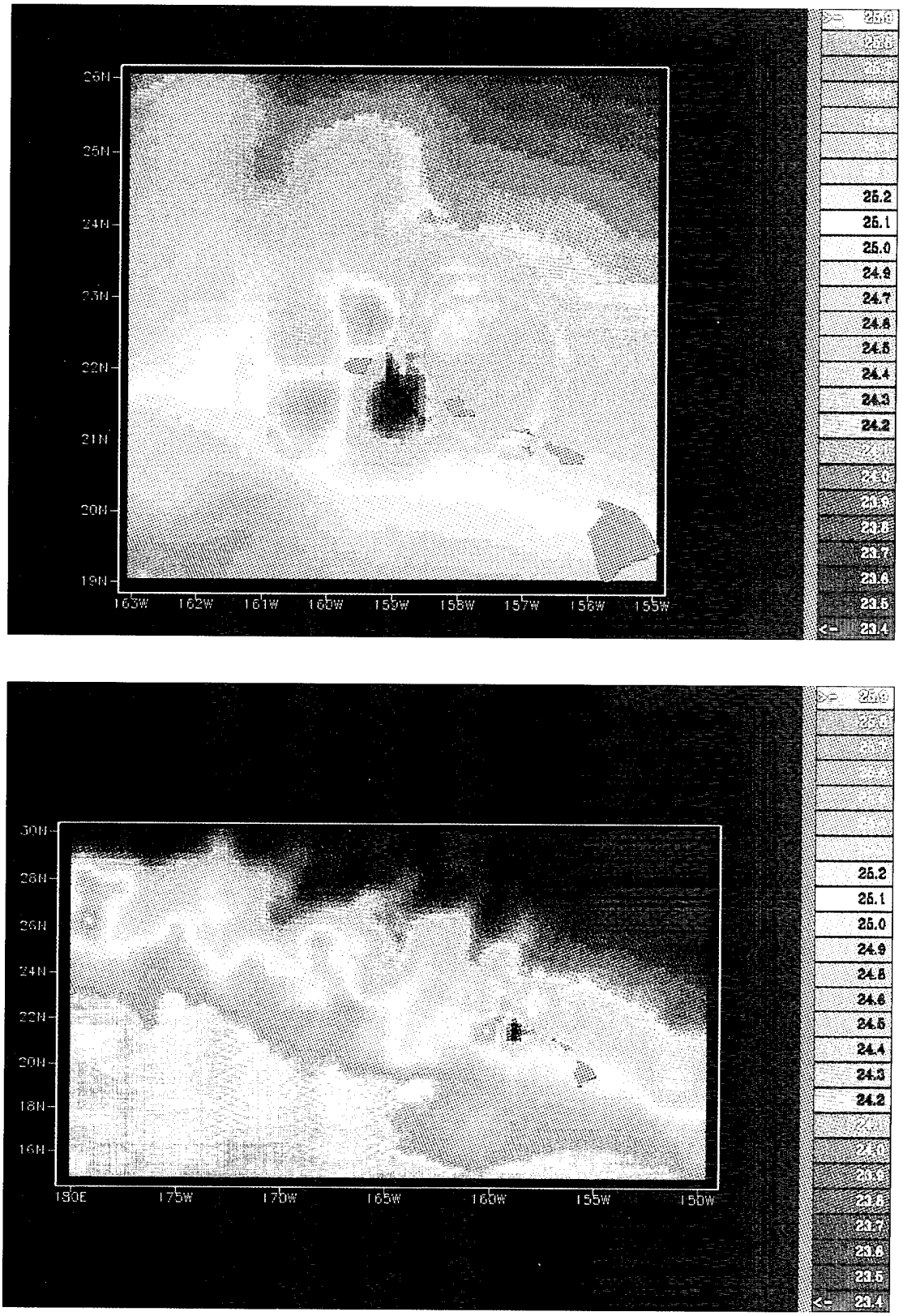

Fig. 8 — Nested MODAS analyses produced at the Naval Pacific Meteorological and Oceanographic Center to support the RIMPAC '94 exercise. The MODAS analysis in the lower panel was on a 0.25° grid and used the FNMOC 1.25° OTIS analysis as the first-guess field. The MODAS analysis in the upper panel was on a 0.1° grid and used the MODAS analysis in the lower panel as the first-guess field.

This versatility also allows MODAS to emulate the OTIS methodology used in its regional analyses (derived from software provided by FNMOC) while supporting many additional capabilities. The first version of MODAS has been accepted into the Navy's Oceanographic and Atmospheric Master Library, which maintains standardized software and databases.

Applications: MODAS is now being implemented into the Tactical Environmental Support System (TESS(3)); here it will assimilate on-scene observations taken at sea, together with satellite-based observations, to produce local ocean thermal nowcasts to increase the effectiveness of tactical decision aids. MODAS is also integrated into the Navy Ocean Models and Assimilation Demonstration System (NOMADS), which was recently implemented by NRL at the Naval Pacific Meteorology and Oceanography Center. There it is used to support exercises in the Hawaii, Kamchatka, and northern and southern California operations areas. Figure 8 shows a surface temperature analysis in the Hawaii area produced to support the RIMPAC '94 exercise. MODAS/NOMADS also supported the Magellan exercises coordinated by SPAWAR and the Sea of Japan maritime simulation sponsored by the Advanced Research Projects Agency. The Naval Oceanographic Office is presently testing MODAS analyses in the Arabian Sea, Sea of Japan, South China Sea, Bay of Bengal, and Philippine Sea for eventual operational use. New methods and applications of MODAS are being explored and tested in the North Pacific Nowcast/Forecast system. The North Pacific system is being developed by the Data Assimilation and Rapid Transition Project funded by NOMP. Figure 9 shows temperature along a vertical section from

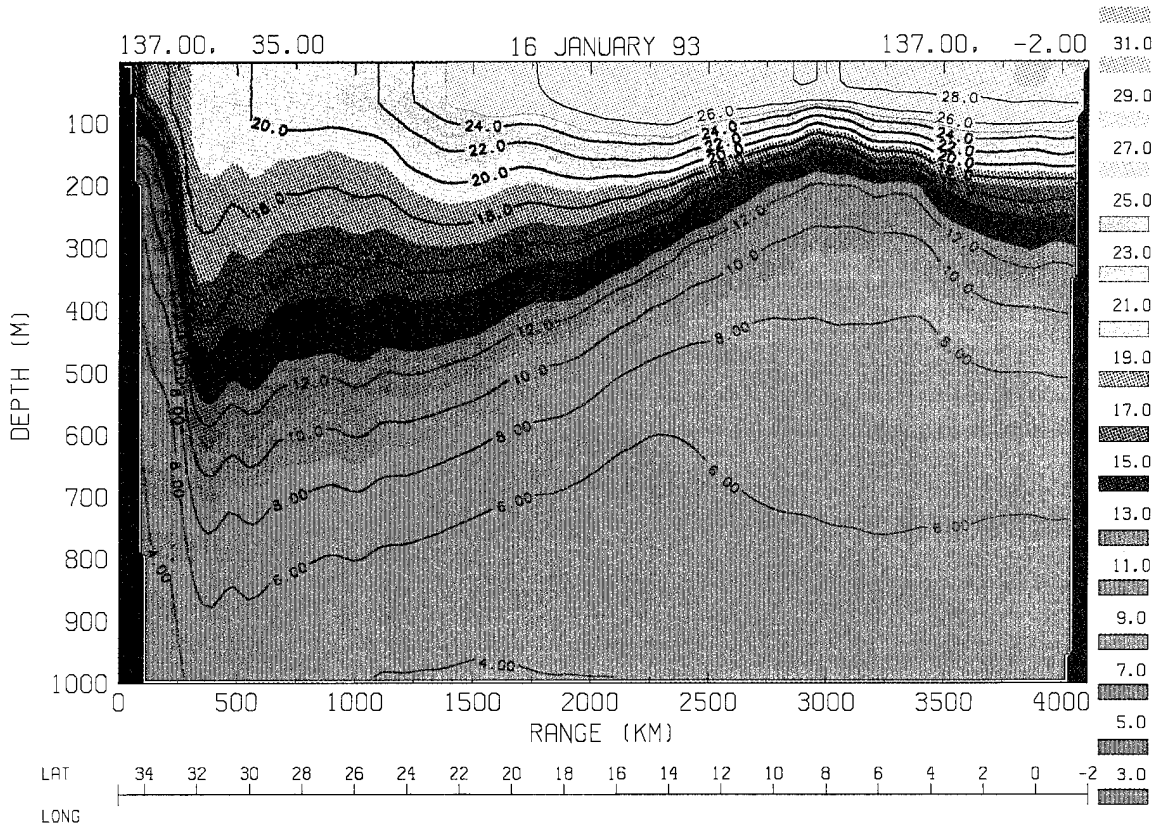

Fig. 9 — Temperature vertical section from Japan (right) to New Guinea (left) produced by MODAS in the North Pacific nowcast/forecast system. The first-guess field is a forecast from a thermodynamic upper-ocean model. Satellite-observed multichannel sea-surface temperatures, XBT profiles, and synthetic temperature profiles generated from the NRL eddy-resolving hydrodynamic layered model fields are assimilated into the first-guess field by optimum interpolation.

Japan to New Guinea for January 16, 1993, produced by MODAS in this system by combining in situ and satellite-based temperature observations with fields from two ocean models.

Summary: MODAS provides a core set of oceanographic data assimilation software, which, due to its modularity, can be modified, expanded, and scripted for many different purposes. It is already finding wide use within the Navy's research and operational communities. Further development is now centered on improving capability in shallow water (less than 200 m) to support scene description and simulation for near-shore naval operations. This new capability will also find immediate application as part of the research and development of near-shore ocean models.

[Sponsored by SPAWAR and ONR]

References

1. M.R. Clancy, "Operational Modeling: Ocean Modeling at the Fleet Numerical Oceanography Center," *Oceanogr.* **5**, 31-35 (1992).

2. R.C. Rhodes, M.R. Carnes, J. Cartmill, and J.W. Crout, "Software Design Document for the Modular Ocean Data Assimilation System (MODAS) Version 1.0," NRL/FR/7322--94-9407, Naval Research Laboratory, in preparation. ■

Coastal Benthic Boundary Layer Program

M.D. Richardson
Marine Geosciences Division

The Naval Research Laboratory manages and is a major participant in the Coastal Benthic Boundary Layer Special Research Program (CBBLSRP). This 5-year (FY93-97) Office of Naval Research (ONR)-sponsored basic research program focuses on modeling the effects of benthic boundary layer processes on sediment structure, properties, and behavior (Fig. 10). The CBBLSRP supports 27 research projects equally divided among various government and university laboratories. Central to the program is the quantitative characterization of sediment structure at micron-to-meter scales. Sediment physical structure provides the common perspective to (a) quantitatively model relationships among sediment physical, acoustic, electrical, and rheological (mechanical) properties, (b) quantify the effects of environmental processes on the spatial and temporal distribution of sediment properties, and (c) model sediment behavior (acoustic, electrical, and mechanical) under direct and remote stress [1].

Experimental Approach: Quantitative physical models, based on the research directions depicted in Fig. 10, are being tested by a

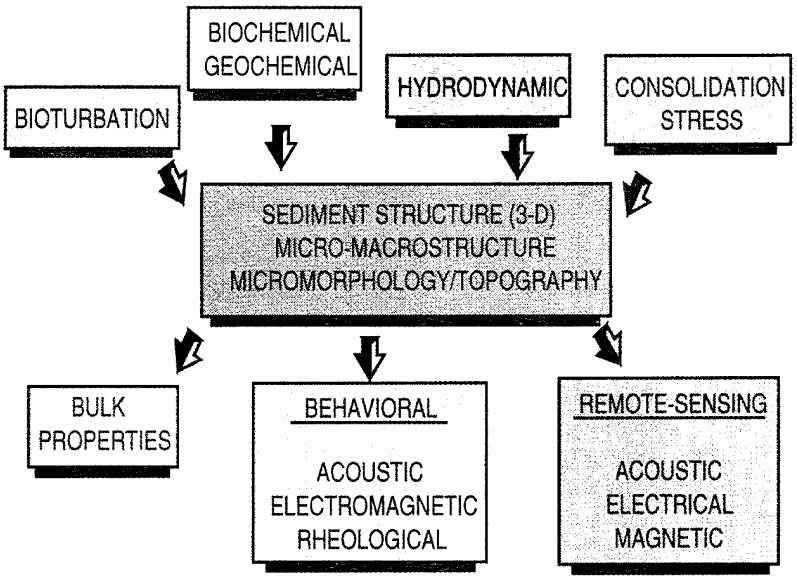

Fig. 10 — The Coastal Benthic Boundary Layer Special Research Programs' scientific direction.

series of field experiments at coastal locations where differing environmental processes determine sediment structure [2]. Experiments have been conducted in the gas-rich muds of Eckernforde Bay, Germany, on the West Florida sand sheet, and in carbonate sediments near the Florida Keys. At the Eckernforde site, biogeochemical processes are responsible for the formation of subsurface methane gas bubbles that significantly affect sediment structure, behavior, and properties. Remote acoustic measurements suggest that methane bubbles are present as shallow as 0.5 to 0.7 m below the sediment-water interface (Fig. 11). The presence, size, and distribution of these gas bubbles are confirmed by computerized X-ray tomography scans of sediments maintained at in situ pressure (Fig. 12). Models are being developed to allow prediction of the distribution of methane bubbles based on rates of biochemical processes, types, and rates of biological reworking, sedimentation rates and organic-loading sediment physical properties, bed stresses related to bottom water movements, and changes in pore water characteristics (salinity, temperature, and pressure). High-frequency acoustic scattering and propagation are greatly affected by the presence of methane bubbles, whereas sediment mechanical (strength) properties are little affected. Sediments of the West Florida sand sheet are a mixture of relict clastic sands and shells. Large-scale seafloor morphology is controlled by hydrodynamic processes, especially major storms, whereas fine-scale sediment structure is dominated by reworking by benthic animals. Spatial and temporal variations of sediment properties and behavior are much greater in this dynamic environment than in the soft muds of Eckernforde Bay. Biogeochemical diagenetic processes such as mineralization, dissolution, and cementation have a major impact on sediment properties and behavior in the carbonate sediments of the Florida Keys. Both hydrodynamic and biological processes, such as bioturbation, exert a major influence on near-surface sediment structure. Sediment strength is higher than predicted from sediment physical properties. High value compressional and shear

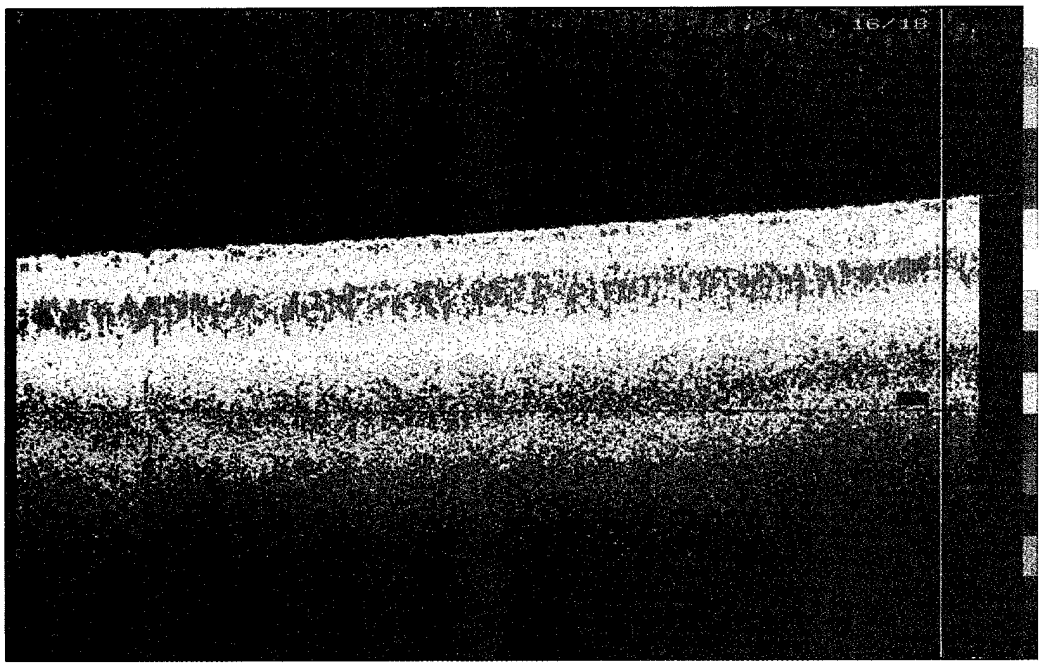

Fig. 11 — Acoustic (30 kHz) subbottom seismic reflectivity profile (1200-m horizontal distance) of sediments at the Eckernforde Bay experimental site. A gas horizon, indicated by red colors, is found 75 cm below the sediment-water interface. Data provided by D.N. Lambert (NRL).

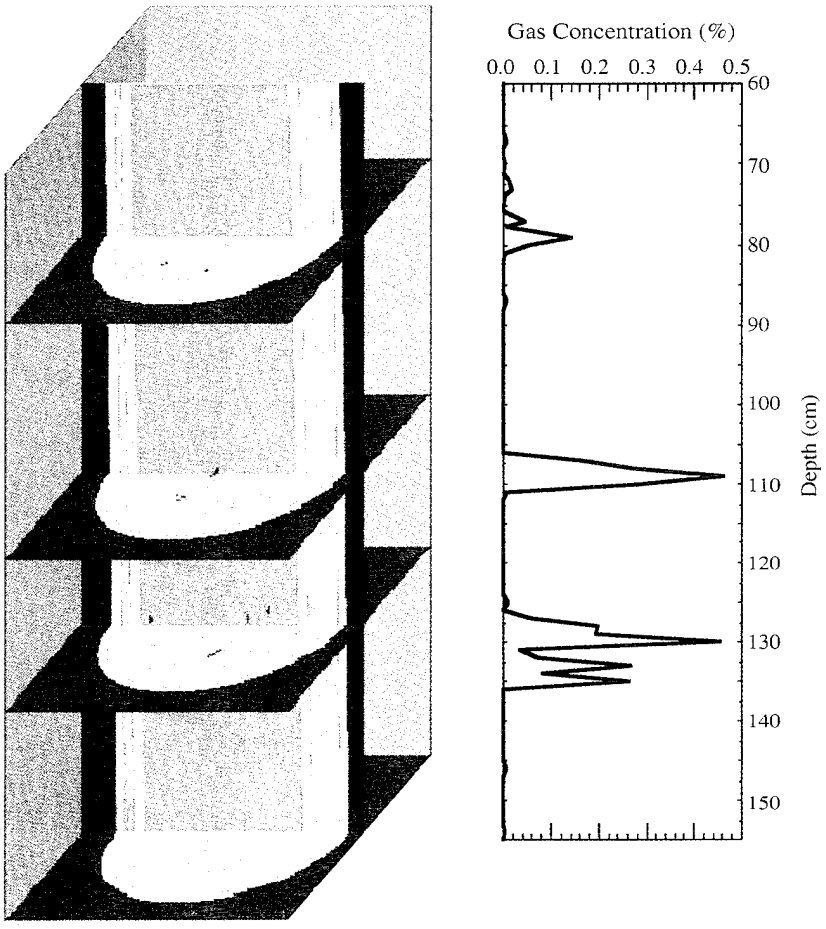

Fig. 12 — X-ray CT scan of Eckernforde Bay sediments showing the distribution and percent volume of free methane bubbles. Data provided by A.L. Anderson (Texas A&M).

wave speeds are related to cementation processes and, together with the abundant shell material, result in high values of acoustic scattering near the sediment-water interface.

Research Relevance: A basic understanding of the physical relationships among processes and properties will contribute to development of realistic models of sediment strength, stability, and transport; sediment stress-strain relationships in cohesive and noncohesive sediments; dynamic seabed-structure interactions; animal-sediment interactions; high-frequency acoustic-scattering phenomena; and propagation of high-frequency acoustic energy into and through poroelastic media. Predictive models developed through this program should enhance mine countermeasures technological capabilities in several important areas, including acoustic and magnetic detection, classification, and neutralization of proud and buried mines; shock-wave propagation; prediction of mine burial; and sediment classification.

Acknowledgments: The CBBLSRP is supported by ONR, with contributing support from NRL and Forschungsanstalt der Bundswehr fur Wasserschall-und Geophysik.

[Sponsored by ONR]

References

1. M.D. Richardson, "The Coastal Benthic Boundary Layer Special Research Program: Workshop Recommendations and Program Direction," Naval Research Laboratory Special Report SP 017:361:92.
2. M.D. Richardson, "The Coastal Benthic Boundary Layer Special Research Program: A Review of the First Year," NRL/MR/7431--94-7099, Naval Research Laboratory.

■

Model Sensitivity Evaluation Using the Adjoint Method

R.H. Langland
Marine Meteorology Division

R.L. Elsberry
Naval Postgraduate School

The adjoint of an atmospheric or oceanic numerical model can be used to identify regions and times for which changes to variables or parameters would have the largest impact on a selected forecast feature. In these regions of high "sensitivity," small perturbations can grow rapidly and strongly influence the growth of forecast error. An adjoint model is the only practical method to determine this sensitivity in a comprehensive manner. In addition to providing estimates of forecast uncertainty and predictability, the adjoint can also be used to interpret the effects of physical processes, such as temperature advection or surface heat fluxes.

Sensitivity Example: We consider the development of an extratropical cyclone from idealized initial conditions that are representative of a midlatitude baroclinic zone with a westerly jet and uniform surface pressure of 1000 hPa. (Reference 1 provides a complete description of the initial state and results.) After 90 h, the surface pressure in the center of the cyclone has decreased to 985.7 hPa, with frontal features typical of observed extratropical cyclones. The 90-h position of the cyclone is identified by $\mathbf{J}_{90}$ in Fig. 13.

The adjoint model provides *gradients* that describe the sensitivity of a selected forecast aspect **J** (here defined as surface pressure at 90 h) to variations of model variables or parameters at earlier times. For example, the adjoint field $\partial \mathbf{J}/\partial T$ in this simulation defines how the pressure in the center of the forecast cyclone will be increased or decreased by changes to the initial (or intermediate time during the forecast) temperature anywhere in the model domain. Even though the adjoint sensitivity is a first-order approximation to the true nonlinear sensitivity, the adjoint error is less than 10% for the most rapidly growing perturbations over 90 h in this simulation.

The largest sensitivity to temperature and wind perturbations is found to be in the lower troposphere (near 750 hPa) during the entire cyclone life cycle. The sensitivity is localized above the developing cyclone (shown in Fig. 13 at 30 h), which is consistent with horizontal thermal advection being the primary forcing for intensification of the cyclone. The adjoint information from this and other studies suggests that forecast skill can be improved most efficiently by improving observational accuracy in the lower troposphere where sensitivity is greatest.

Sea-Surface Temperature: It is also possible to obtain the forecast sensitivity to sea-surface temperature (SST) perturbations maintained over the entire forecast period. As the cyclone moves northeast between 60 h and 90 h, the adjoint sensitivity indicates that storm intensity would be increased by higher sea-surface temperatures to the south and east of the storm track (Fig. 14). A higher SST in that region will suppress heat loss from the atmosphere to the ocean surface and thus increase warm advection in the lower troposphere ahead of the cyclone. This sensitivity pattern agrees well with the tendency of midlatitude storms in the western Atlantic and Pacific Oceans to intensify rapidly while moving north and east along the north walls of the Gulf Stream or Kuroshio currents.

Other Applications: Adjoint methods also provide a basis for next-generation data assimilation systems that will improve the initial conditions provided to numerical forecast models

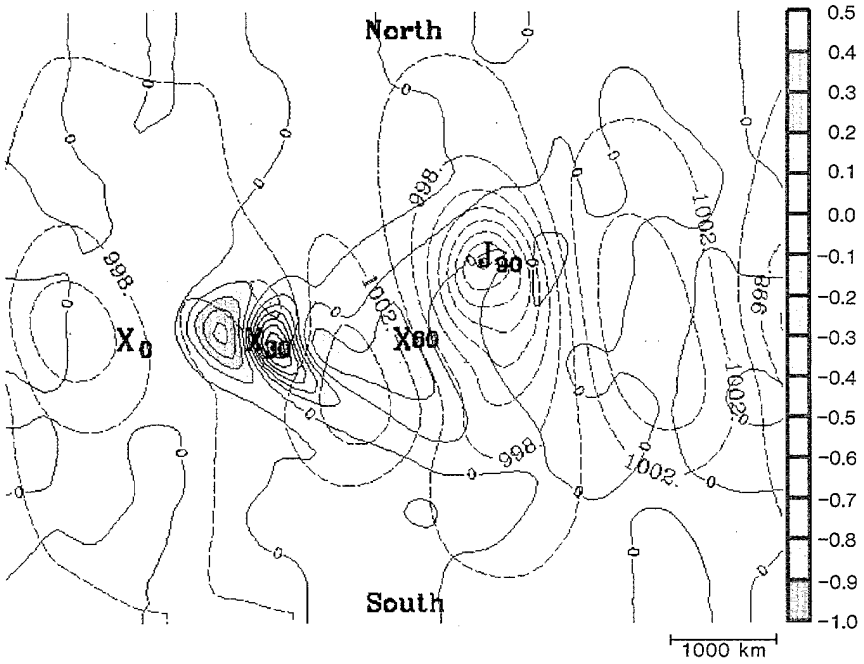

Fig. 13 — Adjoint field $\partial J/\partial T$ near 750 hPa at 30 h (contour interval = 0.01 hPa deg^{-1}, color bar labels scaled to 10x units). Surface pressure at 90 h (dashed, contour interval = 2.0 hPa). Cyclone positions at 0, 30, and 60 h are shown as large X's. Central pressure at 90 h (J) = 985.7 hPa. Warming in the dark green and blue regions at 30 h will *decrease* 90 h surface pressure (J); warming in red region will *increase* 90 h surface pressure at J. Changes to 30 h temperature in light green and yellow regions will have relatively small impact on pressure forecast at J.

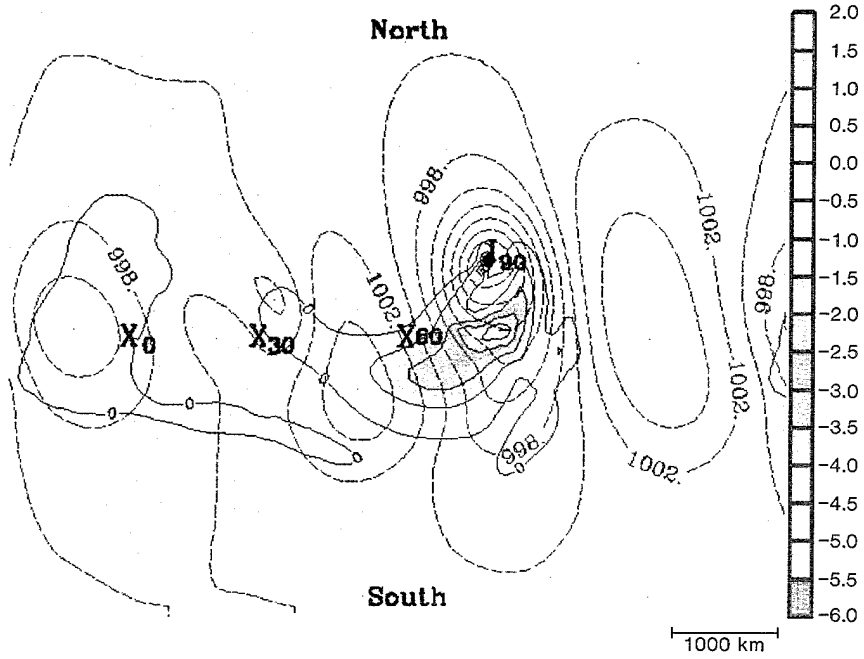

Fig. 14 — Adjoint field $\partial J/\partial T_S$ (contour interval = 0.001 hPa deg^{-1}, color bar labels scaled to 1000x units). Cyclone positions and surface pressure at 90 h, as in Fig. 13. Higher SST in the green and blue regions will *decrease* 90 h surface pressure (J); lower SST in green and blue region will *increase* 90 h surface pressure at J. Changes to SST in other areas will have relatively small impact on pressure forecast at J.

and are being used to provide estimates of possible forecast errors due to initial condition uncertainty. For example, the European Centre for Medium-Range Weather Forecasts has implemented an adjoint-based ensemble forecast system [2] that provides a suite of forecast products, including event-probability estimates and depictions of possible variability in forecast 500 hPa height and other fields.

The adjoint model used in this study was developed at the National Center for Atmospheric Research [3]. A recent upgrade in the adjoint provides the capability to determine sensitivity to moist processes. Development of adjoints for U.S. Navy atmospheric models is currently under way in NRL's Marine Meteorology Division.

[Sponsored by ONR]

References

1. R.H. Langland, R.L. Elsberry, and R.M. Emco, "Evaluation of Physical Processes in an Idealized Extratropical Cyclone Using Adjoint Techniques," accepted by *Quart. J. Roy. Meteor. Soc.*

2. F. Molteni, R. Buizza, T. N. Palmer, and T. Petroliagis, "The ECMWF Ensemble Prediction System: Methodology and Validation," Technical Memorandum No. 202. (Available from ECMWF, Shinfield Park, Reading, Berkshire, U.K., RG2 9AX.)

3. R.M. Errico, K. Raeder, and T. Vukićević, "Mesoscale Adjoint Modeling System Version 1 (MAMSl)," NCAR Technical Note, 1994. (Available from the authors: National Center for Atmospheric Research, P.O. Box 3000, Boulder, CO 80307-3000, USA.)

Fiber-Optic-based Structural Sensor System

A.D. Kersey, M.A. Davis,
and D.G. Bellemore
Optical Sciences Division

Fiber-optic sensors have been developed for a diverse range of application areas over the past 20 years. In many of these applications, fiber-optic-based devices compete with conventional sensor technologies on the basis of performance criteria such as sensitivity and drift or on issues such as size or cost. However it is becoming increasingly apparent that fiber-based sensors offer new and unique capabilities over their electronic counterparts that make them more attractive for certain applications. This is particularly true in the case of structural monitoring where the optical fiber can be embedded directly within structural materials and used to profile a measurand (strain or temperature) over the length of the fiber. In addition, such a "distributed" sensor system can be tailored to respond to a range of measurable parameters (measurands) or to multiple measurands on a single sensing fiber. In addition to having the capability of being embedded directly within the structural material, fiber-optic sensors can also be surface-mounted on new or existing structures, allowing them to be retrofitted to older structures.

For structural health monitoring, the principal parameter of interest is strain. The ability of fiber sensors to "profile" the strain at a number of locations distributed throughout a structure or structural component in real time with very high resolution and wide dynamic range represents a powerful enabling technology for monitoring the integrity of structural components and systems. This technology will find applications in the analysis of load-induced stresses, deterioration or damage on new or existing structures such as aircraft, spacecraft, ships and offshore structures, bridges, buildings, pipelines and storage tanks, for example.

Bragg Grating Sensors: Although a wide variety of sensor types can be used for strain monitoring, the use of fiber-optic Bragg grating sensors has recently attracted the most research interest. Bragg gratings are sensor elements optically written into photosensitive Ge-doped fibers by exposure to a periodic UV interference pattern. These devices can be fabricated by side exposure using holographic-based means or by a diffractive mask. Gratings written into fibers by this process can be highly resonant devices that exhibit a strong reflection peak over a very narrow wavelength range at what is termed the Bragg resonance condition, as illustrated in Fig. 1. When the fiber is subjected to strain, the periodicity of the grating is altered, and the wavelength at which resonance occurs changes. Detection of this shift in resonance wavelength thus allows the strain to be determined. These devices, which are short ($\sim$5 mm) and intrinsic (that is, contained completely within the fiber), represent one of the most attractive forms of fiber sensor for embedded sensing.

The inherently wavelength-encoded nature of the output of fiber Bragg grating (FBG) sensors has a number of distinct advantages over other sensing schemes. One of the most important advantage is that as the sensed information is encoded directly into wavelength, which is an absolute parameter; the output does not depend directly on the total light levels, losses in the connecting fibers and couplers, or source power. In addition, the sensor can easily be operated intermittently without the need for recalibration or reinitialization of the system. The wavelength encoded nature of the output also facilitates wavelength division multiplexing by writing each grating with a different nominal resonance wavelength within the available source spectrum.

Prototype System: The key to a practical sensor system based on FBGs lies in the development of low-cost fabrication techniques and instrumentation capable of determining the relatively small shifts in Bragg wavelength of FBG elements induced by strain changes. Several options exist for making this measurement. An approach we have focused on is based on the use of a micro-Fabry-Perot optical filter, which is used to sweep over the wavelength span of the grating sensors to provide an indication of the Bragg resonance of each element. In

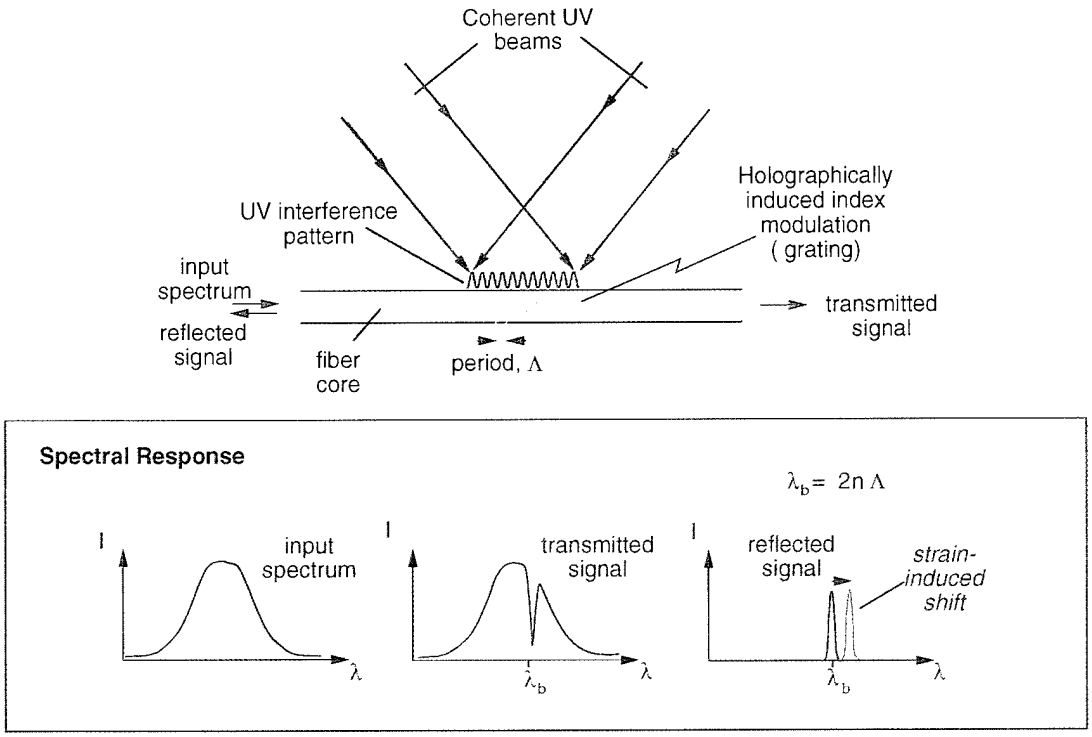

Fig. 1 — Holographic fabrication of fiber-optic Bragg gratings.

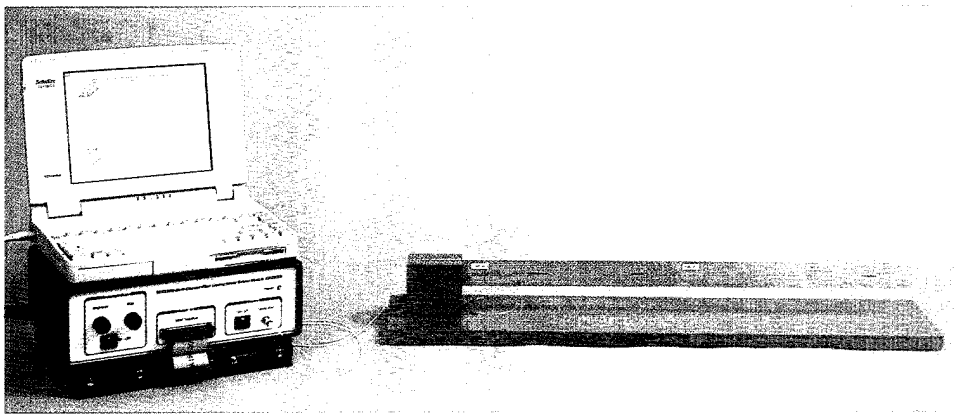

Fig. 2 — Packaged electro-optics unit for structural monitoring.

the system, light from a broadband source, such as an edge-emitting light-emitting diode is coupled into the fiber and fed to a series of FBG sensor elements, each of which is written with a different Bragg wavelength. The optical signals reflected from each sensor are fed to the scanning Fabry-Perot filter, and the wavelength of the signals is assessed. This information is then processed and displayed on a video screen for real-time monitoring of strain. The system developed (shown in Fig. 2) is a compact portable unit that can provide a strain resolution of ~ 1 μstrain (1 part in 10^6) and has been used to address as many as 9 gratings simultaneously but is potentially capable of addressing as many as 32 elements by combining wavelength and time-division-based multiplexing. The outputs of these sensors have been used to provide accurate determination of the shape of a structural component, such as a beam or panel, which is subjected to deflection forces. Figure 3 demonstrates the real-time distributed strain monitoring

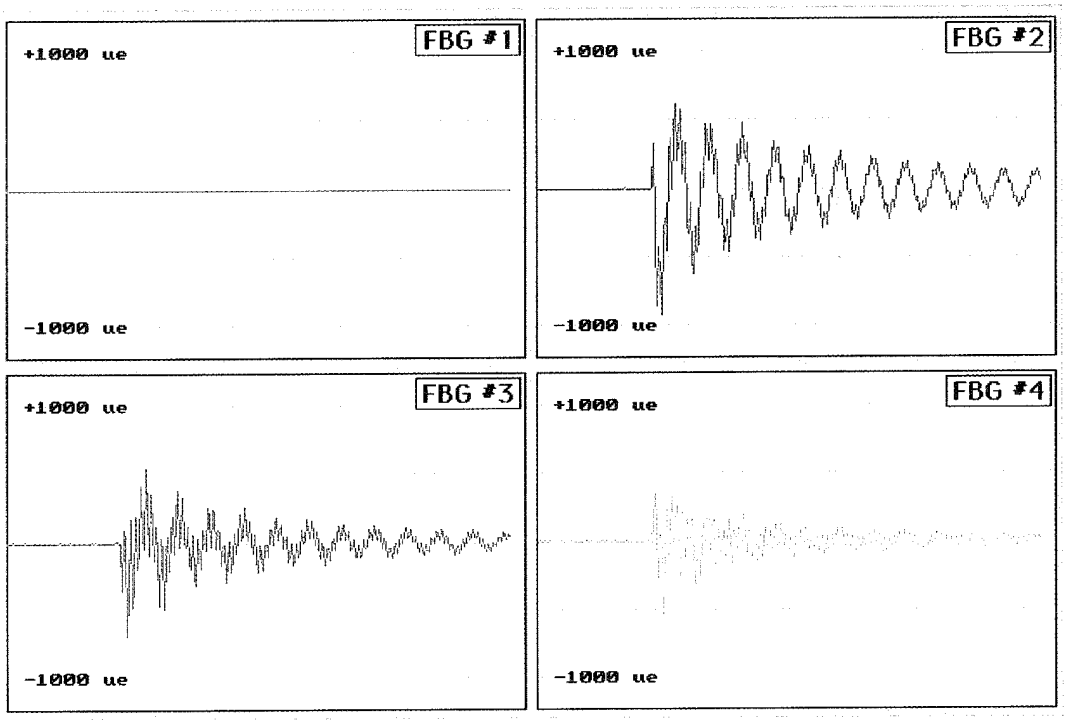

Fig. 3 — Strain responses obtained for four FBG sensors when the tip of a cantilever beam is subjected to a transient force. FBG #1 is an isolated reference sensor while the other three are surface attached at different points along the cantilever beam.

capability of the system. Here the strains along a cantilever beam, which is subjected to a transient force at its tip, are monitored with four multiplexed FBG sensors. FBG sensor #1 is fixed to the rigid mount of the beam and acts as an isolated reference sensor while the other three sensors, surface attached at different points along the beam, indicate the local strains caused by modal vibrations induced by the deflection forces.

With a modified electro-optics system, we believe that it should be possible to multiplex many tens to potentially hundreds of sensors along a single fiber. This will represent a quantum leap forward in the capabilities of sensor technology for distributed sensing and will allow the strain in a structural component or system to be analyzed in detail. The concept represents a very powerful technique with extremely promising potential for widespread application in a range of intelligent structural systems for use in both the military and commercial sectors.

[Sponsored by ONR and FHWA] ■

Fiber-Optic Wideband Array Beamforming

R.D. Esman and M.Y. Frankel
Optical Sciences Division

M.G. Parent
Radar Division

Phased-array antennas incorporate a number of fixed-antenna elements. The individual control of the amplitude and phase of the signals driving each element allows substantial flexibility in the radiation pattern shaping and steering. However the conventional radio-frequency components required to implement individual element feeds result in an antenna that is bulky, heavy, power-hungry, susceptible to electromagnetic interference, and inherently narrowband. The fiber-optic control of phased-array antennas can provide benefits in each one of the above areas. Most importantly, the optical control

systems make possible such desirable array functions as true time-delay beamsteering required for wide instantaneous bandwidth and squint-free operation. Many optical techniques have been suggested for obtaining true time-delay capability. Still their practicality is limited by several drawbacks, including the requirement for a large number of precisely matched optical elements, excessive power losses, instability, or specialized custom component development. A novel and elegant fiber-optic true-time-delay technique has been proposed that alleviates the above constraints [1]. The technique requires only one wavelength-tunable laser for each steering dimension, yet provides feeds to each antenna element or subarray with minimal power losses. The system uses only commercially available components and has potentially high reliability and stability.

Here we describe the implementation and characterization of a true time-delay fiber-optic beamformer feeding a sparsely populated eight-element phased-array transmitter antenna. The true time-delay function is realized in a high-dispersion fiber when the optical carrier wavelength is tuned with the radiation direction determined by a single voltage signal controlling the optical source wavelength. The transmitter has an instantaneous bandwidth of 2 to 12 GHz, limited by the antenna elements. The transmitter shows $>100°$ azimuth-steering characteristics without observable squint and pattern distortion that would normally be associated with conventional phase-steering beamformers.

Phased-Array Antenna Configuration: Figure 4 shows the complete antenna measurement system. The system includes the optical and microwave sources located outside of an anechoic chamber, along with the fiber-optic prism and the antenna located inside the chamber and remotely controlled by a single optical fiber. The optical source is a fiber-optic sigma laser (physically, the laser resembles the Greek letter σ), with an output wavelength-tunable over >50 nm. The output of the laser is amplitude-modulated, amplified in an Er-fiber amplifier, and fed to a fiber-optic 1:8 splitter by a single-mode dispersion-shifted fiber. Figure 4 shows all dispersion-shifted fiber links in dark-blue. The 1:8 splitter feeds an eight-channel fiber-optic dispersive prism. The fiber-optic

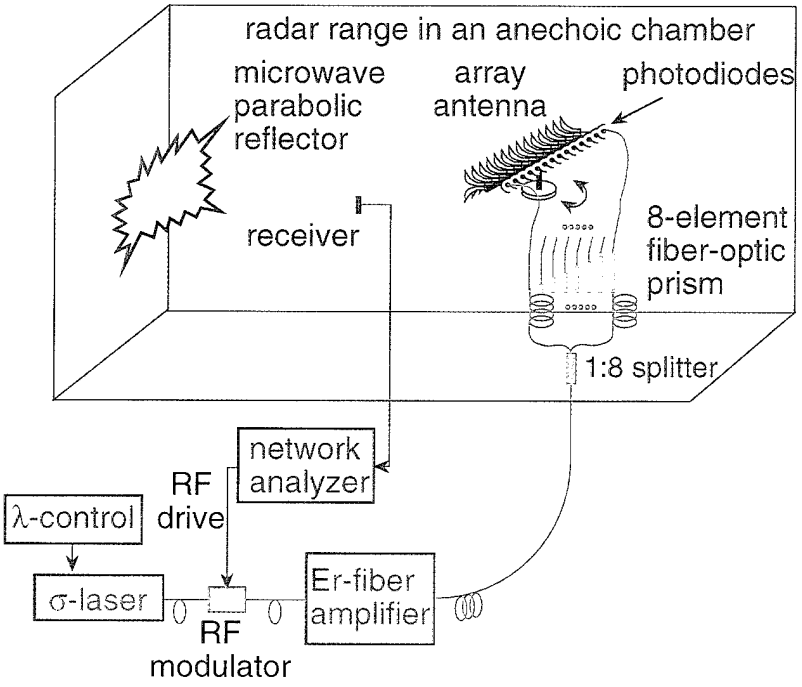

Fig. 4 — Antenna pattern measurement system.

prism includes high-dispersion fiber (seen in red in Fig. 4) in each channel, with lengths proportional to the corresponding antenna element position within the array. Each channel of the prism feeds an individual InGaAs *p-i-n* photodiode connected to a corresponding antenna element.

The antenna was tested in a compact radar range. A network analyzer was used to drive the amplitude modulator and to detect the received signal. The linear array consisted of 50 broadband Vivaldi flares arranged on 2.5-cm centers. The eight actively driven elements were separated by 7.5, 7.5, 7.5, 10, 10, 17.5, and 12.5 cm to form a sparsely populated array with a narrow main lobe and suppressed grating lobes at the expense of increased side-lobe amplitudes. The nominal lengths of 0, 138, 276, 414, 598, 782, 1104, and 1334 m of the high-dispersion fiber ($D \sim -70$ ps/nm km) were used in each channel, with the overall channel lengths equalized with dispersion-shifted fiber at a center wavelength of $\lambda_0 = 1558$ nm.

Antenna Response Characteristics: Array patterns were obtained as a function of the azimuth angle and were normalized by an equivalent single-element pattern. As mentioned above, the steering function is accomplished by the laser wavelength detuning from the nominal center wavelength λ_0. Figure 5 shows the array pattern with the laser wavelength detuned by -10 nm, without any other adjustments. The main lobe steers to $-23°$ off broadside, and the side-lobe level is ~ 10 dB below the main lobe in its vicinity and is 5 dB below far off the main lobe. The top plot of Fig. 5 compares the measured (red) and the calculated (blue) antenna pattern at 6 GHz. Excellent agreement is observed for the main-lobe position and width, as

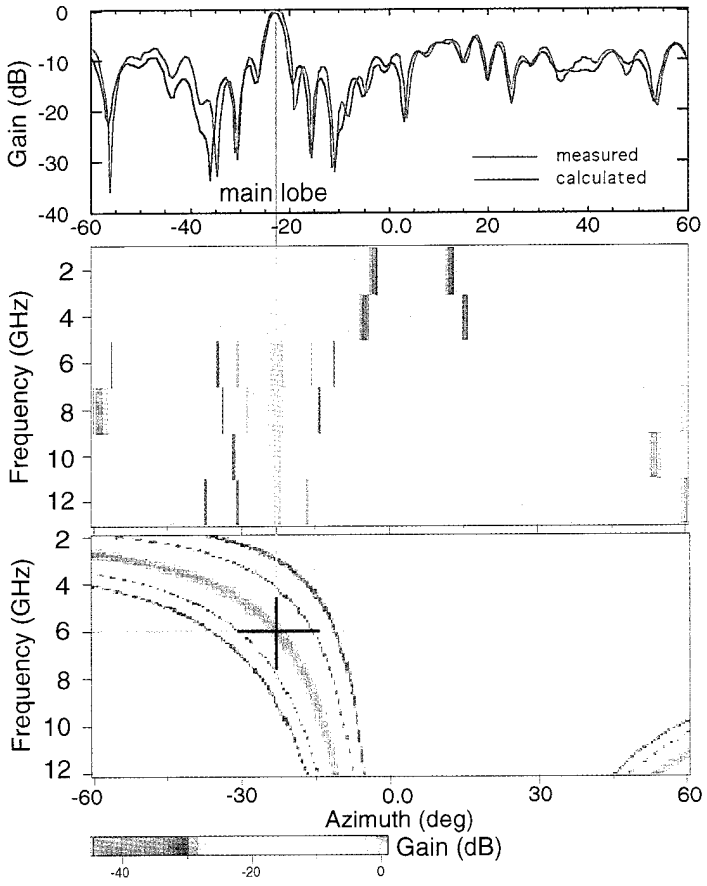

Fig. 5 — Antenna patterns at -10 nm laser detuning showing $-23°$ steering: top—measured and calculated pattern at 6 GHz; middle—intensity plot of the measured true time-delay antenna pattern; bottom—intensity plot of calculated phase-steered array pattern.

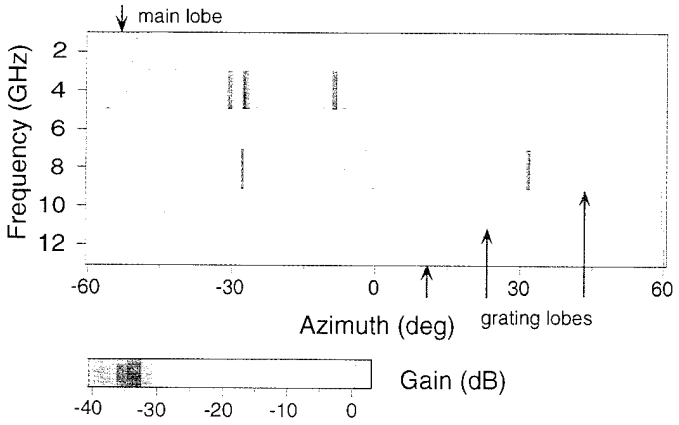

Fig. 6 — Intensity plot of the measured antenna patterns at −20 nm laser detuning showing −53° steering.

well as for the irregular (but predictable) sidelobe levels and positions. We also see that the grating lobes have been effectively suppressed despite the large active element spacing. Similarly good agreement between the measured and calculated patterns was obtained at other frequencies.

The real power of the true time-delay beamsteering technique becomes apparent when the array patterns for all frequencies are viewed simultaneously. The top intensity plot in Fig. 5 shows the array pattern as a function of azimuth angle and frequency. The highest gains, corresponding to the main-lobe peak, are shown in red. From this intensity plot we observe that the main-lobe position stays fixed at −23° independent of frequency in the range of 2 to 12 GHz. The main-lobe width narrows with increasing frequency, as expected. Thus the fiber-optic beamformer implements squint-free steering of the antenna pattern. In contrast to above, the bottom intensity plot of Fig. 5 shows similar data calculated for a conventional phase-steered antenna. The phase angle has been fixed to produce a −23° steering at 6 GHz, as indicated by the marker lines. However as the frequency is changed, the main lobe, which appears as high-intensity red, shows a significant change in the steering angle. This effect is the frequency-dependent squint commonly observed in conventional phased-array antennas.

The limits of the optical array steering can be tested by detuning the laser wavelength by −20 nm. Figure 6 shows the intensity plot of the array pattern from which we observe that the main lobe is steered to −53° for the whole 2 to 12 GHz frequency range. As before, the main lobe also shows the expected narrowing with increasing frequency. The grating lobes, marked by arrows, can now be observed in the 8, 10, and 12 GHz data. Similar results were obtained by detuning the laser to positive wavelengths to produce positive steering angles. This confirmed that the array was indeed capable of being steered over more than ±50° azimuth range.

Summary: We have demonstrated a novel and elegant fiber-optic true-time-delay beamformer. The beamformer is built entirely of commercially available components and potentially has high reliability, high stability, and low cost. The beamformer was used to drive a linear sparse-array antenna with an instantaneous 2 to 12 GHz bandwidth. The measured antenna characteristics agree well with the calculated ones and show excellent squint-free steering over >100° azimuth range.

[Sponsored by ONR]

References

1. R.D. Esman, M.Y. Frankel, J.L. Dexter, L. Goldberg, M.G. Parent, D. Stilwell, and D.G. Cooper, "Fiber-Optic Prism True Time-Delay Antenna Feed," *IEEE Phot. Techn. Lett.* **5**, 1347-1349 (1993). ■

Multilayer Optics for Imaging X Rays

J.F. Seely
Space Science Division

At normal angles of incidence, the reflectance of all materials is quite low in the X-ray wavelength region of the spectrum. Instruments that are used for imaging or spectroscopic studies of X-ray sources typically have mirrors or gratings that operate at grazing angles of incidence where the reflectance is higher. However the collecting area of the optics and the resulting throughput of the instrument are small, and the instruments are difficult to align and are relatively expensive to implement.

Multilayer coatings have long been used in the visible region of the spectrum to enhance reflectance or to define wavelength bandpasses. The coatings are composed of alternating layers of two materials with high and low index of refraction. The layer thicknesses are usually one quarter of the wavelength of the incidence light, and the light reflected from the layer interfaces constructively interferes resulting in high reflectance.

Recent progress in the material technology of thin layers has allowed the extension of normal-incidence multilayer reflection techniques into the X-ray region. Thin layers can now be sputter-deposited with excellent control over the thickness and smoothness of the layers. Materials are chosen that have high contrast in their X-ray optical properties and that form discrete and smooth interfaces. Computational models are used to specify the layer thicknesses to give optimal normal-incidence reflectance at a particular wavelength of interest.

Naval Research Laboratory (NRL) personnel have used normal-incidence multilayer mirrors to image the X-ray emission from hot plasmas at wavelengths as short as 34 Å. The multilayer coating technology was developed in collaboration with Ovonic Synthetic Materials of Troy, Michigan [1]. The wavelength of 34 Å falls in the so-called water-window region where carbon is absorptive and oxygen is relatively transmissive; this wavelength can be used to image biological specimens with high contrast between the organic material and water.

X-ray Images: Figures 7 and 8 show the X-ray images of laser-irradiated targets that were recorded by using a normal-incidence multilayer mirror. In experiments performed jointly with Lawrence Livermore National Laboratory, high-intensity laser radiation was focused onto targets composed of metal and plastic materials, and the resulting X-ray emission was imaged at a wavelength of 34 Å [2]. The images reveal the fine details of the emissions from various regions of the targets. A sketch of the target before laser irradiation is shown at the top of each figure. The spatial scale is indicated in a corner of each image.

Figure 7 is the image of a compound target that was composed of a thin gold foil and a solid plastic cylinder. A laser beam was incident from the left onto the back side of the gold foil, and the X-ray continuum from the resulting plasma indirectly heated the plastic cylinder. Also visible near the bottom of the image are the two glass stalks that supported the gold foil and plastic cylinder. Images of this type were used to study the indirect heating of materials by X rays from laser-produced plasmas. This image won a Second Place Award in the Radiological Centennial Imaging Contest, a worldwide contest to celebrate the discovery of X rays by Roentgen in 1895.

Figure 8 shows two images of a laser-irradiated target. The target was composed of a strip of germanium that was deposited onto a titanium and carbon support. The target was irradiated by a laser beam incident from the right. The laser beam was focused into a line that covered the germanium strip. An alignment mirror was positioned on the long axis of the target. Figure 8(a) is the image recorded by a microscope that viewed the target from a position that was nearly perpendicular to the axis of the target; Fig. 8(b) is the image recorded on the same laser shot by a second microscope that viewed from behind the alignment mirror along the axis. The linear germanium plasma is visible in the side-on image. In the axial image, the conical-shaped features resulting from the expansion of the plasma and the back-illuminated alignment mirror are visible. Images of this type were used to study the expansion and extent of hot laser-produced plasmas.

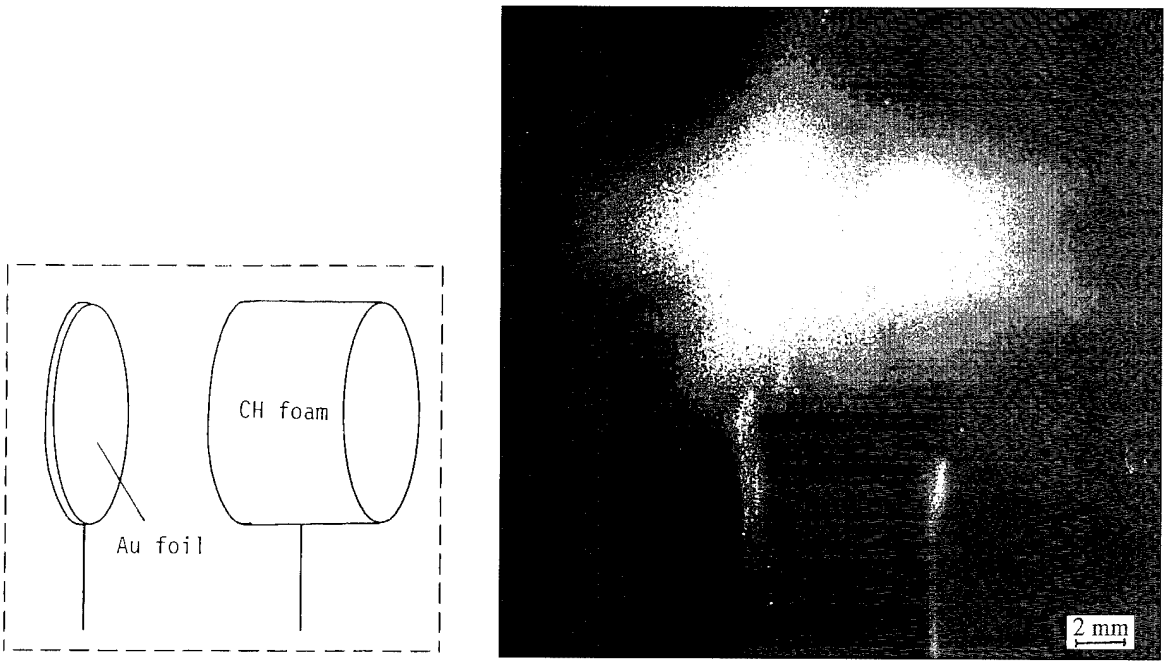

Fig. 7 — The X-ray image of a plastic cylinder that was indirectly heated by the X-ray continuum from a laser-irradiated gold foil.

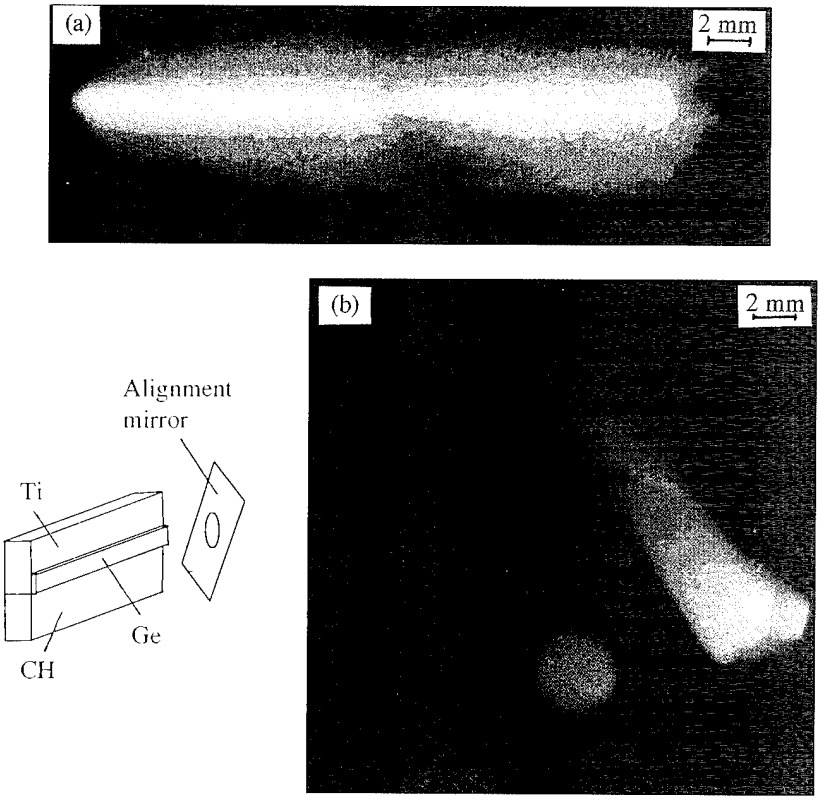

Fig. 8 — X-ray images of the hot plasma expanding from a laser-irradiated germanium target: (a) the image recorded by a microscope that viewed the target from a position that was nearly perpendicular to the axis of the target; and (b) the image recorded on the same laser shot by a second microscope that viewed from behind the alignment mirror along the axis.

Acknowledgment: Glenn Holland and Charles Brown are especially recognized for their contributions to the success of the experiment.

[Sponsored by ONR]

References

1. J.F. Seely, G. Gutman, J. Wood, G.S. Herman, M.P. Kowalski, J.C. Rife, and W.R. Hunter, "Normal-Incidence Reflectance of W/B4C Multilayer Mirrors in the 34-50 Å Wavelength Region," *Appl. Opt.* **32**, 3541 (1993).

2. J.F. Seely, C.M. Brown, G.E. Holland, R. Lee, J. Moreno, B. MacGowan, C. Back, L. DaSilva, and A. Wan, "Imaging of Laser-Irradiated Targets at a Wavelength of 33.8 Å Using a Normal-Incidence Multilayer Mirror," *Phys. Plasmas* **6**, 1997 (1994). ■

Plasma Physics of Solar-Terrestrial Coupling

J. Chen, P.J. Cargill, S.P. Slinker, and J.A. Fedder
Plasma Physics Division

The Earth, with its neutral atmosphere, is embedded inside the plasma-filled ionosphere and magnetosphere. The conditions in these regions (geomagnetic conditions) are referred to as "space weather" and are characterized by electric and magnetic fields and the distribution of charged particles. The driver of space weather is the solar wind, a stream of magnetized plasmas continually emitted by the Sun and impinging on the Earth. The properties of the solar wind are determined by solar activity. As a result, although invisible to the naked eye, the solar wind plasmas provide the coupling between solar activity and Earth's space weather. In particular, solar-wind disturbances induced by eruptive events can have a significant impact on satellite-borne and ground-based systems vital to both Department of Defence (DoD) and commercial needs.

Occasionally the Earth experiences geomagnetic storms lasting several hours to a few days, during which time the electric and magnetic fields around the Earth are highly disturbed. Under such conditions, communications and navigational systems can be disrupted, and anomalies in satellite operations occur, including spurious (phantom) commands and loss of satellite control. In addition, increased degradation of satellite orbits can be a serious problem. On the ground, electric power plants can experience strong surges in electric fields that can cause power distribution grids to fail. For example, the Hydro-Quebec Power Company suffered a massive blackout for nearly 9 h under such conditions during March 1989. With continuing integration of electronic systems and miniaturization of microelectronics, the impact of geomagnetic disturbances will become an increasingly important concern for the Navy's Command, Control, Communication, and Computer Intelligence (C^4I) and Command and Control Warfare (C^2W) systems.

Solar Eruptive Events: Recent research has identified a class of solar phenomena that are particularly effective in producing geomagnetic disturbances. Such phenomena are referred to as "geoeffective" and include eruptions of solar prominences. Prominences are enormous structures, with typical dimensions comparable to the solar radius (7×10^5 km). Figure 1 shows a prominence that has just started to lift up (erupt) from its initial location. A remarkable feature is the apparent organization over large distances; the structure has the appearance of being a section of a large circular torus with a uniform minor radial cross section. The filamentary plasma structures near one footpoint appear helical. These properties have led to the suggestion that their underlying magnetic geometry is a magnetic flux loop with twisted magnetic field lines.

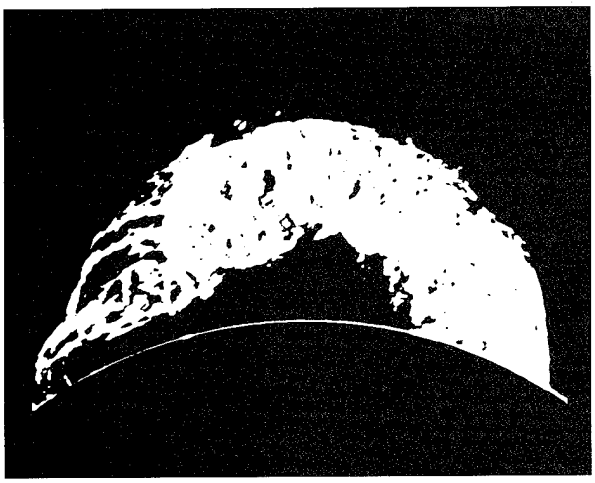

Fig. 1 — A prominence observed in 1946 shortly after the previously quiescent structure started to erupt. The footpoint separation is comparable to the solar radius of 7×10^5 km. Observed in H_α (λ = 6563 Å) (courtesy of High Altitude Observatory).

The ejecta resulting from erupting prominences have estimated mass of $10^{15\text{-}16}$ g and propagate away from the Sun with initial speeds ranging from ~100 km/s to more than 1000 km/s. These eruptions can produce major modifications in the solar wind reaching the Earth, with stronger-than-average magnetic field over distances of several times 10^7 km, encompassing

a significant fraction of 1 astronomical unit (AU)—the distance between the Sun and the Earth. Such structures typically propagate past the Earth with speeds in the range of 400 to 600 km/s, corresponding to time periods of several hours to a few days. If the strong magnetic field turns and remains southward during the Earth passage, the entire magnetosphere can be strongly disturbed; this leads to geomagnetic storms and various adverse terrestrial consequences, as discussed above.

Theoretical Modeling: Thus what causes eruptions, how the resulting ejecta are driven through the interplanetary medium, and how the ejecta interact with the Earth's magnetosphere are major scientific questions with pressing practical concerns. We have developed a program to address these questions. As an initial effort, we have focused our attention on a class of structures referred to as magnetic clouds, which were first discovered behind interplanetary shocks [1]. These are relatively simple structures, having the inferred magnetic topology of flux loops. They constitute approximately one-third of all coronal mass ejections (CMEs) intercepted at 1 AU and are associated with perhaps 50% to 60% of major geomagnetic storms. Thus they are highly geoeffective structures. Empirically they are closely associated with prominence eruptions. In a recent theoretical model [2], we studied the dynamics of a toroidal flux loop, which is initially in equilibrium in the lower solar corona. This corresponds to the observed fact that prominences can remain quiescent for days and sometimes for a few weeks before erupting suddenly. In our model, the initial flux loop expands in response to an increase in its electric current. The initial expansion speed depends on the rate of flux injection and can range from ~ 100 km/s to greater than 1000 km/s in agreement with observations. The model allows one to compute physical observables such as the velocity, size, and average magnetic field strength continuously as the loop expands through the interplanetary medium. The computed properties are quite consistent with those of observed magnetic clouds.

Figure 2 is a three-dimensional rendition of a calculated model loop as it approaches 1 AU. The location of the Earth is indicated by the green asterisk at right, with the Sun located at left. The apex of the loop is approximately 3×10^7 km (0.2 AU) in width and has an average speed of nearly 600 km/s moving toward 1 AU. This model loop has evolved from an initial structure of height 10^5 km and width 5×10^4 km. The color indicates the magnetic field strength, ranging from $\sim 1.7 \times 10^{-4}$ G (dark blue) at 1 AU to ~ 7 G (red) near the Sun. The white line shows a typical magnetic field line calculated from the model.

Geomagnetic Storms: The field profiles inside the model loop of Fig. 2 also closely resemble those of the observed magnetic clouds. We have imposed the calculated magnetic field on the three-dimensional magnetohydrodynamic simulation model of the solar wind-magnetosphere interaction previously developed at NRL. The particular model loop of Fig. 2 propagates past the Earth in about 14 h. In our simulations, this time has been artificially shortened to reduce the required computational time. The qualitative behavior for any size magnetic clouds can be inferred by scaling the time shown. Figure 3 shows the time-sequence of the flux of energy injected into the ionosphere in the auroral cap surrounding the North Pole. The color represents energy flux, increasing from light blue to red. The numbers "00" and "12" denote midnight and noon, respectively, and "6" and "18" indicate dawn and dusk, respectively. These are the magnetic local time relative to the Sun-Earth direction. The magnetic field of the incident cloud is northward initially and rotates smoothly until a southward component begins to develop at time $T = 3{:}00$. At $T = 3{:}00$, the magnetic field has the maximum magnitude and points in the east-west direction. The light blue region at $T = 0{:}00$ indicates the auroral oval under unstressed conditions. The field continues to rotate until it is purely southward at $T = 4{:}30$. At this point, the energy flux into the ionosphere and the expansion of the auroral oval have reached maximum levels. The total energy flux integrated over the polar cap at

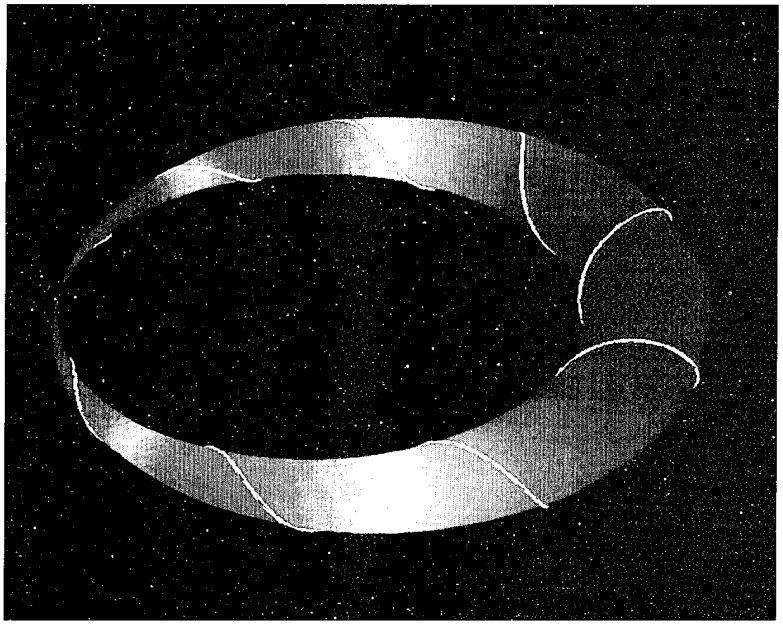

Fig. 2 — A model magnetic cloud approaching the Earth. For comparison, the Earth's diameter ($2R_E$) is approximately 1.3×10^4 km, which is 4×10^{-4} of the width of the loop. The lengths are shown to scale, but the solar rotation is not included. A "magnetic surface" is used to depict the loop: in reality, flux loops do not have sharp boundaries.

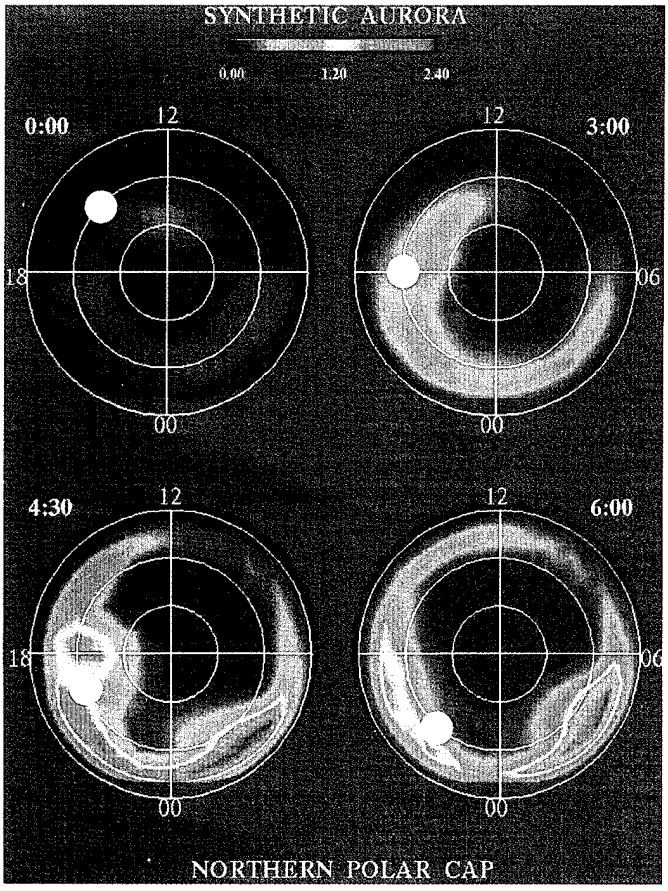

Fig. 3 — An MHD simulation of the magnetosphere's response to the passage of a magnetic cloud. The magnetic field obtained from the model cloud of Fig. 2 is imposed as input on NRL's global MHD model of the magnetosphere. The energy flux into the auroral regions at one time frame is shown for the northern polar cap. The color bar shows the relative intensity of the energy flux. Observationally, the red regions would correspond to dramatic auroral displays. The geomagnetic storm intensity peaks near T = 4:30.

this time is several orders of magnitude greater than that at T = 0:00. At T = 6:00, the cloud has passed the Earth, and the stress on the magnetosphere is declining. Near the South Pole, the auroral oval exhibits similar behaviors in time. It is worth noting that the levels of disturbance are significantly different between the dayside and nightside and that the disturbances are associated with the magnetic local time. As the Earth rotates counterclockwise in these panels, a given geographic region, indicated by the white circle in each panel, experiences different levels of disturbances depending on the magnetic local time.

It is well-established empirically that long periods of southward interplanetary magnetic field (IMF) are associated with major geomagnetic storms and that prominence eruptions/CMEs can produce such IMF structures. We now have developed the first quantitative model of the eruption of prominences and their subsequent coupling to the magnetospheric dynamics, providing a theoretical glimpse of how southward IMF may be related to structures resulting from prominence eruptions. Currently there is a national effort to establish a program to develop space weather forecasting capabilities. A major component of our research effort is to provide a firm scientific basis to properly define the requirements for an operational space weather forecasting system in order to meet these DoD and national needs.

[Sponsored by ONR]

References

1. L.F. Burlaga, E. Sittler, F. Mariani, and R. Schwenn, "Magnetic Loop Behind an Interplanetary Shock: Voyager, Helios, and IMP 8 Observations," *J. Geophys. Res.* **86**, 6673 (1981).

2. J. Chen and D.A. Garren, "Interplanetary Magnetic Clouds: Topology and Driving Mechanism," *Geophys. Res. Lett.* **20**, 2319 (1993). ■

Radio Observations of Comet Crash on Jupiter

R.S. Foster
Remote Sensing Division

Context: Scientists from the Naval Research Laboratory's (NRL) Remote Sensing Division and the National Aeronautics and Space Administration's (NASA) Jet Propulsion Laboratory (JPL) are conducting a long-term study of Jupiter's magnetosphere. The recent collision of Comet Shoemaker-Levy 9 with Jupiter has resulted in an enhancement of the radio synchrotron emission observed from the planet. By using the division's 85-ft diameter radio telescope at Maryland Point in nearby Maryland, researchers have collected data from Jupiter's inner magnetosphere—a magnetic region surrounding the planet filled with energetically charged electrons. The telescope began monitoring the planet in June 1994, just prior to the comet impact (Fig. 4). Data collection stopped 2 months later, as Jupiter moved too near to the Sun to gather meaningful data.

Observations of Jupiter's radio emission began in the 1950s with the identification that Jupiter was a source of radio emission bursts (22 MHz). This discovery provided the initial evidence for the existence of a Jovian magnetic field. By 1960, astronomers separated the Jovian decimeter radiation into a thermal component originating from the atmosphere and a nonthermal component identified as synchrotron emission from Jupiter's strong magnetic field. Routine biweekly monitoring of Jupiter's synchrotron emission by JPL by using NASA's Deep-Space Network of antennas led to the discovery of a multiyear variation correlated with fluctuations in the solar wind. Many early data sets suggested the existence of variations on the order of days to weeks. The NRL Jupiter radio-monitoring program began in June 1994 to investigate short-term variations through daily observations of the planet. This program is preparing for in situ data collection during

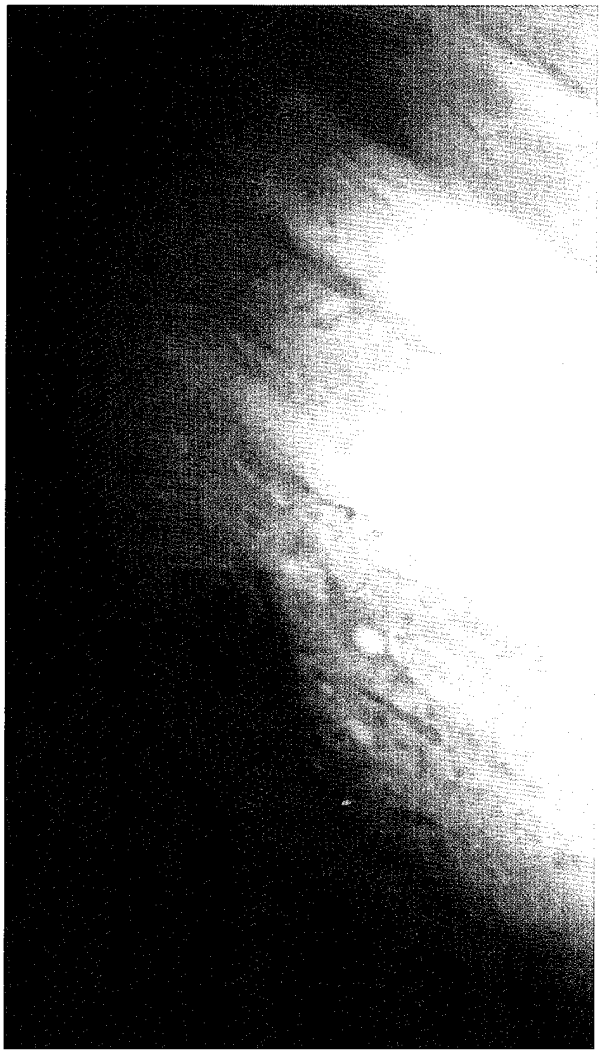

Fig. 4 — An image of the giant planet Jupiter, by NASA's Hubble Space Telescope, revealing the impact sites of fragments "D" and "G" from Comet Shoemaker-Levy 9 (Credit: H. Hammel, MIT and NASA).

NASA's *Galileo* spacecraft mission scheduled to begin a 2-year orbiting tour with Jupiter in December 1995. The impact of the Comet Shoemaker-Levy 9 with Jupiter provided an added bonus to this program, with surprising consequences.

Observations: The Maryland Point telescope (Fig. 5) began collecting data on June 29, 1994. The telescope was operated by remote control. Regular operation of the telescope from a remote site was difficult at first. On many nights, data were lost due to power dropouts that shut down the telescope control computer.

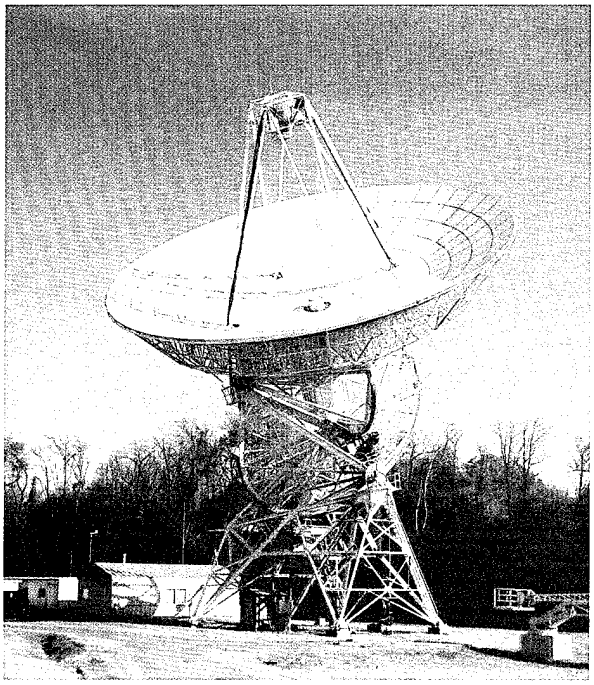

Fig. 5 — NRL's 85-ft radio telescope at Maryland Point used to observe Jupiter at 1665 MHz.

Four radio sources provided primary flux density calibration at the observing frequency of 1665 MHz. The telescope recorded data every 2 s from a single circular polarization over a bandwidth of 50 MHz. The data were scaled to the flux density that would be observed if Jupiter were at a fixed distance of 4.04 AU (1.50×10^{11} m) from the Earth. This allows a direct comparison with observations from the past, as Jupiter's distance from the Earth varies as a function of orbital period. Jupiter was actually at a distance of about 5 AU during these observations. To scale the data to the nominal distance required introducing a 50% correction to the data. By using an atmospheric model, the thermal emission component was subtracted to give an estimate of the total synchrotron flux density. Figure 6 shows the daily average fluxes of Jupiter along with the impact times of comet fragments "A," "G," and "W." The radio flux unit is the Jansky (Jy), where 1 Jy = 10^{-26} W m^{-2} Hz^{-1}.

Scientific Results: To date, the results have been somewhat mystifying. Theoretical models predicted that the Jovian synchrotron emission

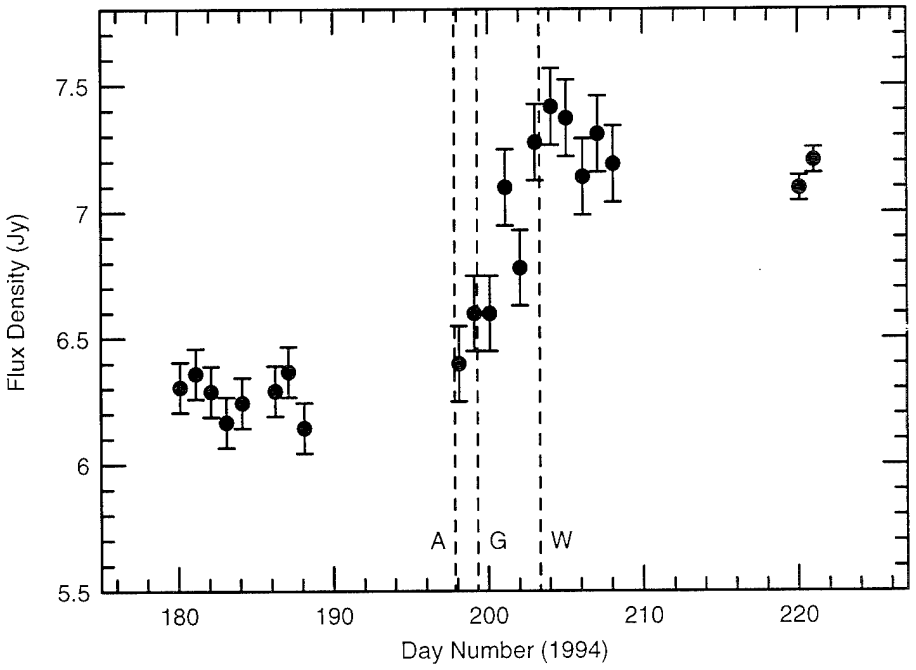

Fig. 6 — A plot of Jupiter's synchrotron radio flux density, normalized to a distance of 4.04 AU, as a function of observation date. The impact times of fragments "A," "G," and "W" from Comet Shoemaker-Levy 9 are drawn as vertical dashed lines.

would decrease after the impact due to the cometary dust-absorbing energy from the high-energy electrons. Alternatively, if the dust were not dense enough, then the synchrotron emission would remain constant. Yet the actual effect of the comet collision has been an increase in the radio emission. Jupiter's flux density rose by approximately 26% at 1665 MHz during the cometary impacts.

A number of mechanisms could account for the enhanced emission, including (1) an increase in the average electron energy triggered by the explosive impacts, (2) a change in the supply of electrons being inserted into the radiation belts, and (3) electromagnetic waves associated with the impact-driving electrons up the field lines toward stronger magnetic fields. Observations of the Jovian atmosphere, continued radio observations of the magnetosphere, and more analyses of available data will help to distinguish among these and other possible explanations. We await Jupiter's emergence from behind the Sun to see what has happened to its magnetosphere in the intervening months. The results may be quite significant understanding what effects a future cometary impact on the Earth might have on the Earth's own Van Allen radiation belts.

[Sponsored by NASA]

Reference

1. S.J. Bolton, S. Gulkis, M.J. Klein, I. de Pater, T.J. Thompson, "Correlation Studies Between Solar Wind Parameters and the Decimetric Radio Emission from Jupiter," *J. Geophys. Res.* **94**, 121-128 (1989).

Vertical Total Electron Content Maps Derived from GPS Ionospheric Measurements

S.B. Gardner
Space Systems Development Department

A new method for mapping the vertical total electron content (VTEC) of the ionosphere using Global Positioning System (GPS) receivers is under development. The new tech-

nique (for which a Navy patent application is pending) differs significantly from previous methods in that both the spatial and temporal behavior of the ionosphere are modeled by means of a space-time polynomial expansion, which includes terms up to second order. Using the method of discrete inverse least squares (ILS), expansion coefficients are calculated with up to 2 h of data from five satellites. Although the GPS L1-L2 differential delay biases can be calculated with the new method, only carrier phase measurements are required to construct the vertical total electron content (TEC) maps. GPS phase data from widely separated receivers are available over the Internet from the National Aeronautics and Space Administration (NASA) and the Jet Propulsion Laboratory (JPL). By using the ILS method and a hierarchical algorithm, wide-area VTEC maps can be constructed. When fully developed, these techniques will be able to compute global VTEC maps in near real time.

GPS Ionospheric Measurements: The GPS is a satellite-based radio navigation system operated by the Department of Defense. When fully operational, the system will consist of 24 satellites in 6 circular orbits—20,200 km above the Earth, at an inclination angle of 55°, with a 12-h period. Since the ionosphere is a dispersive medium with delay effects inversely proportional to the square of the frequency, a dual-frequency GPS receiver can measure TEC along lines-of-sight to GPS satellites. A GPS receiver, with calibration of the L1 (1.57542 GHz) minus L2 (1.2276 GHz) instrument delays can measure TEC by measuring group delay or change in carrier phase between L1 and L2 frequencies. However group delay measurements are noisy and subject to multipath effects. The measurement of carrier phase differences between L1 and L2 is more precise but ambiguous because of the unknown number of carrier cycles.

In the fall of 1992, the Naval Research Laboratory (NRL) began experiments to determine if a calibrated GPS receiver could be used to obtain a local map of vertical TEC. The traditional approach required both group delay and carrier-phase measurements as well as knowledge of receiver and spacecraft delay biases between the L1 and L2 frequencies. Time averages of group delay, corrected for bias, were used to adjust the phase measurements. At that time, measurements of the spacecraft biases by JPL and other laboratories did not agree. NRL proceeded to develop a new method that modeled both the spatial and temporal behavior of the ionosphere. The new method is based on a space-time expansion of the local ionosphere and uses ILS computations. The ILS method is capable of providing measurements of spacecraft (or receiver) biases as well as space-time maps of the local ionosphere. The ILS results for spacecraft biases agree with JPL measurements and indicate that the spacecraft biases are stable in time. However, more importantly, the ILS method does not require group delay measurements to construct a local TEC map [1].

TEC Mapping: The multichannel GPS receiver located at NRL is capable of collecting simultaneous dual-frequency data from up to eight satellites. A typical data set consists of differential group delay (DGD) and differential phase delay (DPD), sampled at 30-s intervals, from five GPS satellites for a period of 2 h. Figure 7 shows ground tracks for a set of five GPS satellites for a 2-h period. The measured data are the sum of bias terms and slant TEC, which is considered a product of two factors. The first factor is the cosecant of the elevation angle at the so-called ionospheric pierce point (IPP) at the height of the F2 layer maximum electron density (approximately 350 km). The second factor is a mapping function called VTEC, which approximates the actual vertical TEC from the ground up to GPS altitude. This VTEC mapping function is expanded as a second-order polynomial in latitude, longitude, and time variables about the receiver location. The inclusion of a time variable as an expansion coefficent is a new feature of the ILS method and a key ingredient. It avoids making specific assumptions about the temporal behavior of the ionosphere. Ten polynomial expansion coefficients and the unknown satellite differential biases are simultaneously determined from an ILS analysis of the DPD data. The VTEC solution enables the direct prediction of slant TEC

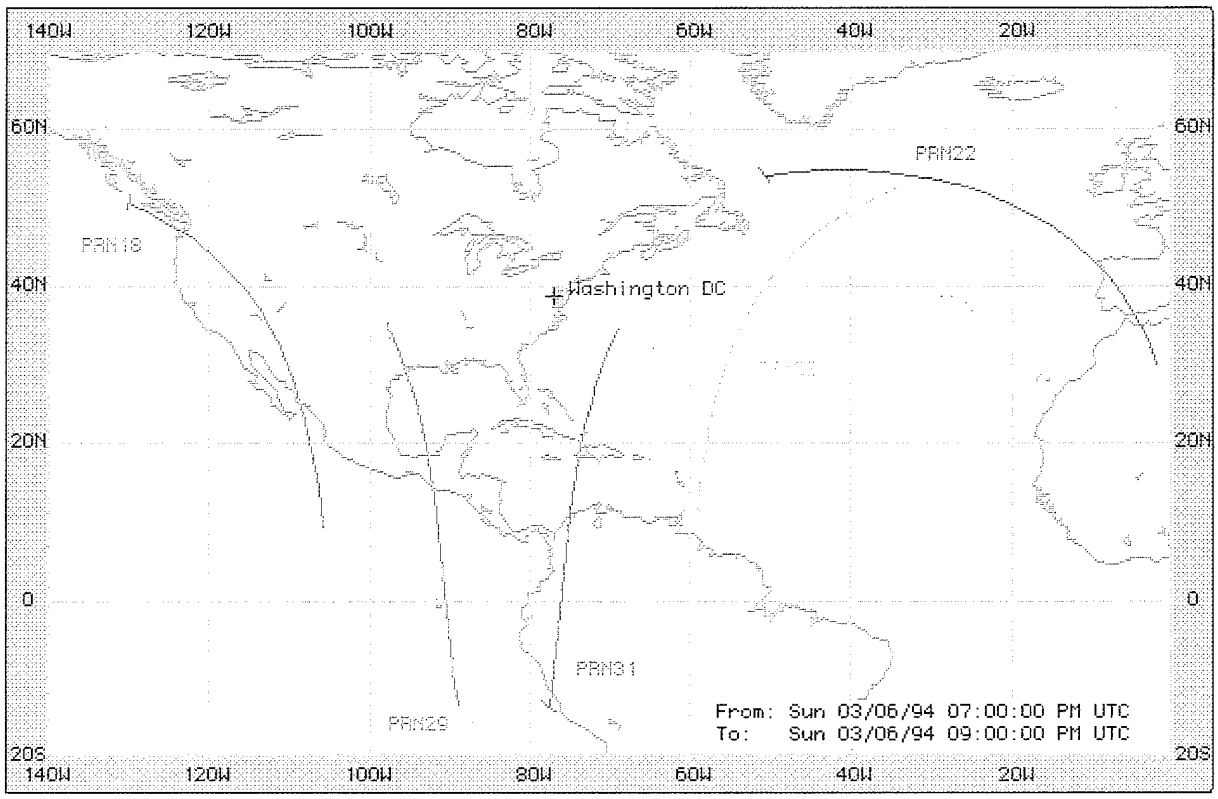

Fig. 7 — Ground tracks for GPS satellites.

over the range of azimuth and elevation angles within the space-time region sampled by the measurements. The prediction is associated with the smoothed background ionosphere since small space-time scales are essentially averaged out. When the ILS method is repeated with data sets from several days, relatively close agreement (within 20% of the mean) is obtained with differential spacecraft L1-L2 biases measured by JPL.

Multisite TEC Mapping: While TEC mapping at a single site is useful, a goal of our work is to develop a method that will provide global TEC maps in near real-time. NASA and JPL provide Internet archives of TEC data from the International GPS Service (IGS) network of about 40 receivers distributed globally [2]. Figure 8 shows geographic coverage for three IGS receiver sites; Goddard Space Flight Center (GSFC) in Maryland, Richmond (RCMD) in south Florida, and Bermuda (BRMU). The dashed map boundary is the approximate range of validity for a composite VTEC map constructed with data from these stations. Figure 9 shows typical slant TEC data from the BRMU site for two GPS satellites—PRN 29 and PRN 30. From the ground tracks shown in Fig. 7, we see that the slant paths for these satellites are approximately opposite. This is confirmed by the shape of both plots. The increase (or decrease) of slant TEC over time is caused by a combination of latitude/longitude gradients and elevation angle changes. The ILS solution unscrambles this variation to produce the VTEC map. Local TEC maps computed for each site were combined using a hierarchical algorithm. Figure 10 shows the contour maps constructed from three-site data for March 6, 1994. Figure 10 only shows the VTEC contours at 1900 UT and 2100 UT, although the combined map has an update interval of 30 s. When viewed as an animation with a 30-s interval, the combined map shows interesting features such as traveling

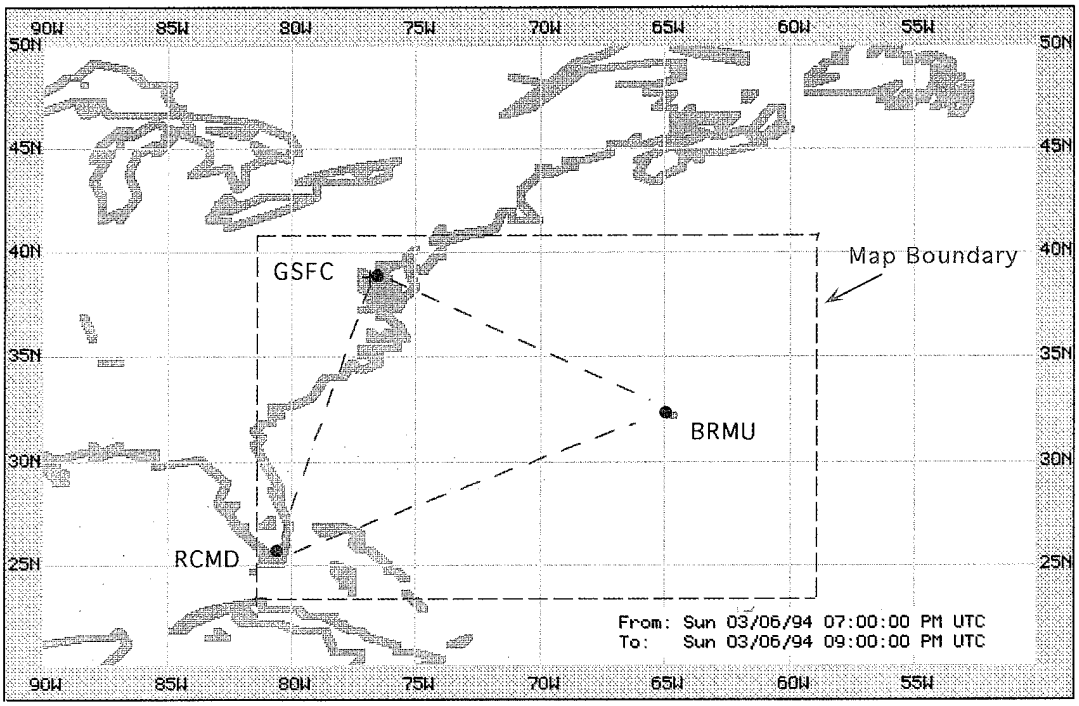

Fig. 8 — Geographic coverage for three GPS receiver sites.

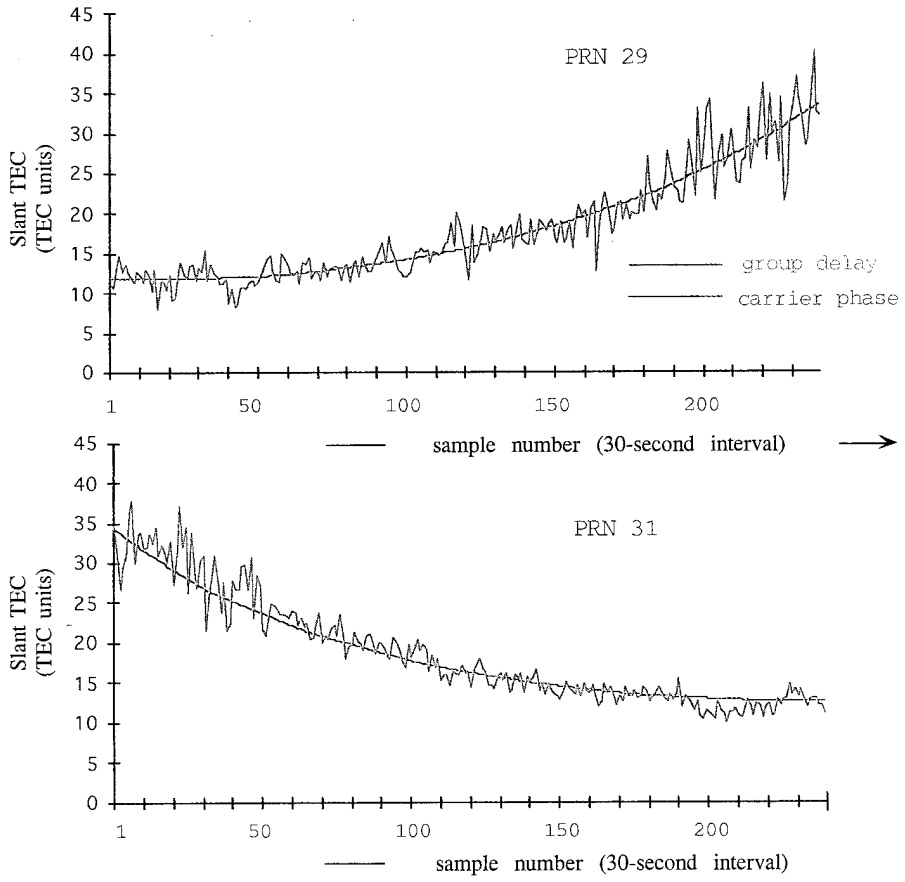

Fig. 9 — Bermuda (BRMU) slant TEC measurements 1900-2100 UT, March 6, 1994.

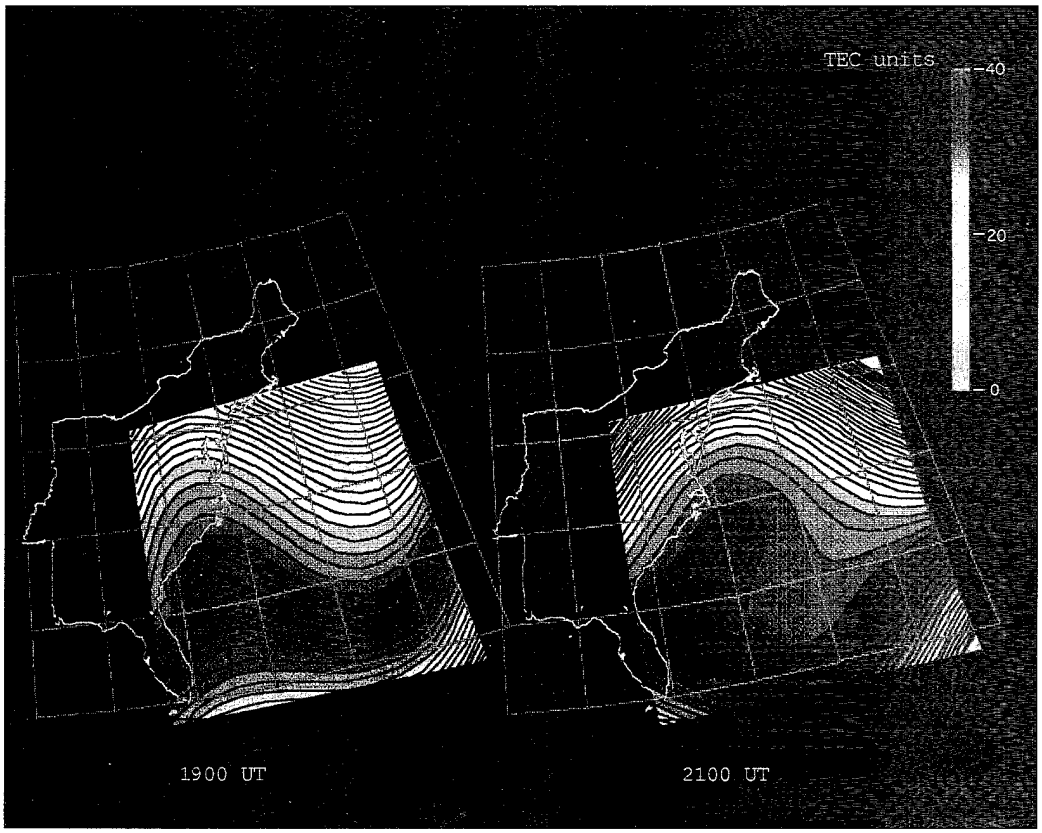

Fig. 10 — VTEC contour maps, three-site coverage, March 6, 1994.

ionospheric disturbances, which are also seen in more detail in the respective local map animations.

Summary: The ILS mapping method has application wherever local or large-scale ionospheric TEC maps are required. The wide range of potential applications covers research for development of global ionospheric and space weather models, through defense applications in geolocation and communications where near-real-time global-ionospheric information is required. We expect the developmental work to continue in this important area.

[Sponsored by NELO]

References

1. U.S.Patent Application: Apparatus and Method for Ionospheric Mapping, S. Gardner, Inventor, Navy Case No.75,950, May 1994.
2. S. Gardner, M. Reilly, and J. Goodman, "Space-Time Maps of Vertical Total Electron Content Derived from GPS Ionospheric Measurements," International Beacon Satellite Symposium, Aberystwyth Wales, UK, July 1994. ■

Structural Control for Enhanced Space-based Sensing

S. Fisher and A. Bosse
Naval Center for Space Technology

Future space-based sensors will require high-performance spacecraft structures that cannot only sense low-level vibrations due to disturbances but also provide control forces to cancel them out. Addressing this need, the Naval Center for Space Technology maintains a structural control laboratory that is being used to study the integration of sensors and actuators

into structures, as well as algorithms for identification and control suitable for on-orbit operation. The development of a smart spacecraft boom can potentially enable consolidation of payloads from two or three conventional spacecraft onto a single platform, resulting in a more capable system that costs less. This technology will not only enhance future Naval spacecraft, but can also benefit health monitoring fields and civil systems, such as dams, buildings, bridges, and automobiles.

Spacecraft Boom Simulator: The structure pictured in Fig. 11—the spacecraft boom simulator—is representative of a support structure that can be deployed from a spacecraft and support multiple sensor packages along its length. The in-line actuators in the base (which have dynamic extension/retraction capability) and the accelerometers are space-realizable sensors, whereas the function of the shakers is only to simulate on-orbit disturbances, including moving parts on the spacecraft, thermal snap, or slewing maneuvers.

The primary technical challenges in building smart structures are (1) precise sensing of the motion of a large number of points on the structure, (2) development of an accurate model of the system which relates the sensor outputs to actuator inputs, and (3) design of an effective control law to be used by the controller. This article is concerned mainly with item (2). Experimental results for the spacecraft boom simulator are presented below.

Identified Models: Figure 12 shows a measured frequency response function (that is, ratio of Fourier transformed output over input) along with synthesized measurements generated from a finite-element model (FEM) and from an identified model of the structure. For frequencies less than 50 Hz, the error in the damped natural frequencies (the frequencies at which peaks occur) from the FEM is less than 5%, however the discrepancies are quite large at high frequencies. On the other hand, when measured frequency response functions are used to "identify" a mathematical model of the system, one obtains a set of model parameters (modes and mode shapes), which almost perfectly match the experimental data over the frequency range of interest.

In the field of experimental modal analysis, there are a number of reliable methods for estimating structural modes and mode shapes using observed input-output data [1]. Using measured data to form the system model yields the best results, especially for spacecraft, since often they cannot be tested on the ground in their fully deployed configuration and because the space environment itself can cause the system to change over time. A technique called modal

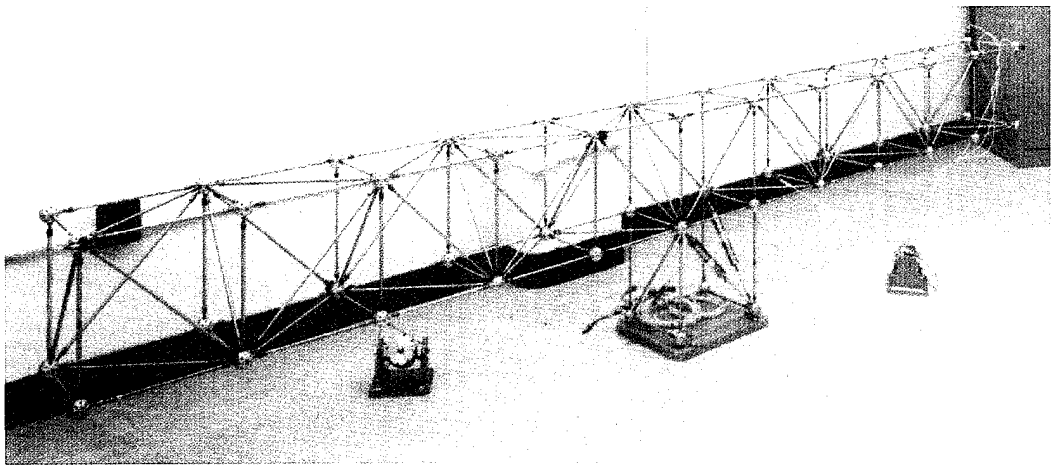

Fig. 11 — The 3.4-m aluminum space truss is instrumented with active struts and accelerometers and shakers for injecting disturbances.

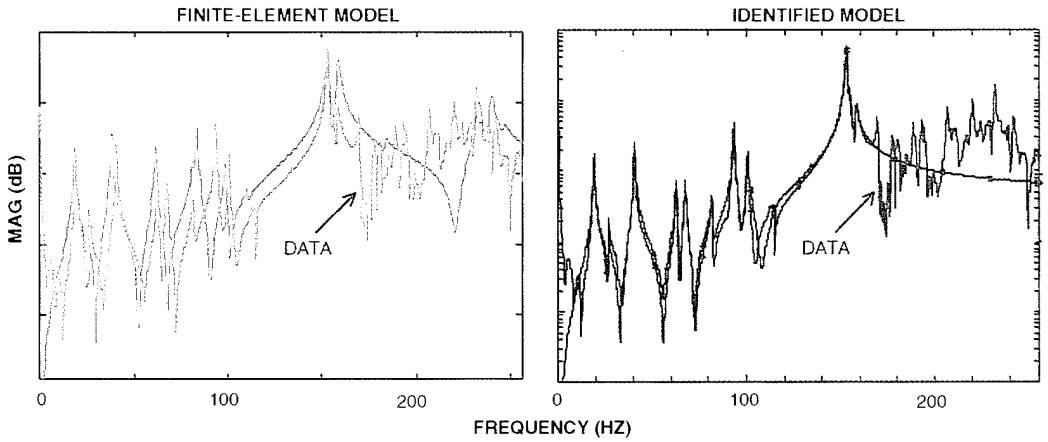

Fig. 12 — Measured vs synthesized frequency response functions indicate significant model mismatch (especially at higher frequencies) for the finite-element model, whereas the identified model captures system behavior extremely well.

filtering, which reduces the structural response to its principal components or modes of vibration is discussed next, and additional experimental results are given.

Modal Filter Test Results: A modal filtering algorithm, called the Modified Reciprocal Modal Vector (MRMV) algorithm [2], was used to extract the first four global modes of the boom (rotation and bending in two planes). To reliably extract modes, a large number of sensors must be used, equal to or greater than the number of modes active in the analysis band. Figure 13 shows the single degree-of-freedom frequency response functions corresponding to lightly damped modes at 12.9, 18.9, 26.5, and 40.3 Hz. Modal filter vectors are used in the time domain as a coordinate transformation to convert multiple sensor measurements (which are complex waveforms consisting of many damped sinusoids) into modal coordinates for the modes of interest (which are individual, damped sinusoids).

To damp vibrations in the truss, the modal coordinates are fed back to compute control forces that oppose the undesired motion. We are currently working to implement a modal filter-based 4-mode controller using 15 accelerometers and 2 active struts. By employing modal coordinate feedback, the design of the feedback gain matrix is simplified, and the control can be carried out one mode at a time.

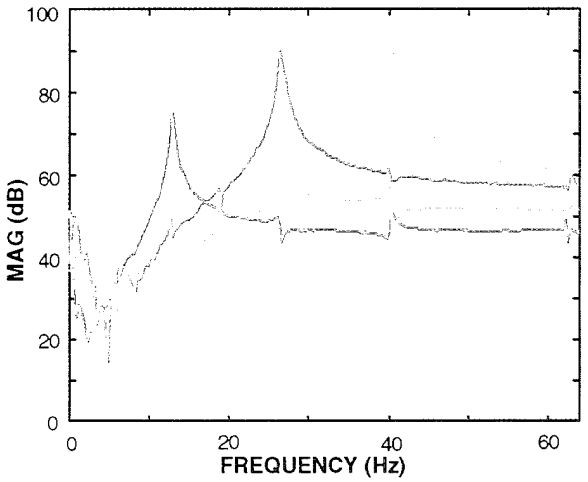

Fig. 13 — Two-hundred and sixteen frequency response functions, corresponding to 6 inputs and 36 outputs, were modally filtered to yield 4 single degree-of-freedom frequency responses.

Although the MRMV algorithm is applicable to systems that are linear and time-invariant, by employing an adaptive pole estimator to get modal frequencies and damping ratios, this control scheme can be reconfigured to automatically update modal filter coefficients and control gains to compensate for a system with time-varying characteristics.

Future Work: Our goal is to implement an adaptive modal filter-based controller on the spacecraft boom simulator and demonstrate a

vibration controller that continues to perform well even though the modal frequencies vary as much as 10% from their nominal values. To control the higher frequency modes, we require 10 times the number of sensors currently used; therefore we plan to evaluate high-density sensor arrays, including multiplexed fiber-optic strain sensors currently under development in the Naval Research Laboratory's Optical Sciences Division. Finally, a deployable version of the actively controlled boom will be developed for use in ground and flight experiments and to serve as a prototype for future hardware development.

Acknowledgments: The authors thank Bob Laskin and Jeff Umland of the Jet Propulsion Lab for their generous loan of equipment, as well as for technical assistance provided during the course of this work. This research was completed while the second author was an NRC/NRL Post-Doctoral Research Associate.

[Sponsored by SPAWAR]

References

1. R.J. Allemang and D.L. Brown, *Experimental Modal Analysis and Dynamic Component Synthesis-Final Report*, AFWAL-TR-87-3069, Flight Dynamics Lab, Wright-Patterson AFB, OH, Vols. 1-6, Dec. 1987.

2. S.J. Shelley, "Investigation of Discrete Modal Filters for Structural Dynamic Applications," Ph.D. Thesis, University of Cincinnati (1991). ■

Special Awards and Recognition

NRL is proud of its many distinguished scientists, engineers, and support staff. A few of these have received exceptional honors for their achievements.

1993 BOWER AWARD AND PRIZE FOR ACHIEVEMENT IN SCIENCE

Dr. Isabella Karle, of NRL's Laboratory for Structure of Matter, received the Franklin Institute's prestigous 1993 Bower Award and Prize for Achievement in Science at a ceremony held on April 7, 1994, at the Institute, in Philadelphia. Dr. Karle received the award for her "pioneering contributions in determining the three-dimensional structure of molecules, making use of both X-ray and electron diffraction and, in particular, for her definitive introduction of a procedure to reveal molecular structure directly from X-ray studies." In this photo, Dr. James L. Powell, president of the Franklin Institute, presents the award to Dr. Karle.

Dr. Frances Ligler
Center for Bio/Molecular Science and Engineering

CHEMICAL SOCIETY OF WASHINGTON'S 1993 HILLEBRAND PRIZE

This prize is awarded annually to one of its members for exceptional achievements in chemistry during the past five years. The nomination reads, "The scientific creativity and leadership of Dr. Ligler is evident in the widespread academic, government, and industrial attention received by two of her biosensor projects [the flow immunosensor and the fiber-optic biosensor]. As a result of her research and scientific leadership, they are now being transitioned to industrial development."

Dr. Anthony Dandridge
Optical Sciences Division

E.O. HULBURT ANNUAL SCIENCE AND ENGINEERING AWARD

According to the award citation, Dr. Dandridge was recognized for his "exceptional scientific and engineering leadership on an international level in the field of fiber-optic sensors and their very current importance to the U.S. Navy and industry. His technical expertise in fiber-optic sensors and related subjects is evidenced by at least 335 publications, over 120 presentations, and 10 patent awards to date." Dr. Dandridge was also cited for his 1993 work on the Lightweight Planar Array and the ongoing Magnetic Array System Program.

Dr. Phillip Sprangle
Plasma Physics Division

SIGMA XI 1994 PURE SCIENCE AWARD

Dr. Sprangle was cited "for his sustained pioneering research, creativity, and originality in the areas of advanced accelerators and advanced radiation source physics. Dr. Sprangle's creativity and ingenuity in conceiving new concepts and physical mechanisms in advanced accelerators and radiation source physics has resulted in numerous theoretical and experimental programs at NRL and throughout the world. These programs include the free electron laser, modified betatron, electron cyclotron maser, quasi-optical gyrotron, and the ultraintense laser physics."

Dr. Robert Brady
Chemistry Division

SIGMA XI 1994 APPLIED SCIENCE AWARD

Dr. Brady was recognized "for his sustained success in applying polymer science to Navy needs. Dr. Brady's knowledge and leadership extend beyond the scope of section interests, encompassing a broad view of materials chemistry....Dr. Brady has been skilled at matching coating properties to Navy mission needs. He has been equally skilled at developing techniques for applying coatings in the naval environment, which is often dirty, always wet, and not conducive to long-lived coatings. These abilities reflect in Dr. Brady an insightful mind with a practical bent, as much an engineer as chemist."

Dr. Donald Horan
Naval Center for Space Technology

NASA'S EXCEPTIONAL ENGINEERING ACHIEVEMENT MEDAL

Dr. Horan was cited "for his inspired leadership of the technical planning of the *Clementine* mission and for his role in mission operations."

Mr. Mark Johnson
Naval Center for Space Technology

NASA'S EXCEPTIONAL ENGINEERING ACHIEVEMENT MEDAL

Mr. Johnson was recognized "for designing, building, and testing *Clementine's* electrical systems, as well as for his leading role in mission operations."

Mr. Paul Regeon
Naval Center for Space Technology

NASA'S EXCEPTIONAL SCIENTIFIC ACHIEVEMENT MEDAL

Mr. Regeon was cited "for his outstanding engineering management of the NRL team who designed, constructed, and tested the complex deep-space *Clementine* satellite within cost and delivered it to the launch pad in less than 22 months."

Dr. David J. Michel
Materials Science and Technology Division

AMERICAN SOCIETY FOR METALS' 1993-94 KIMBALL BURGESS MEMORIAL AWARD

This award recognized Dr. Michel for "his outstanding contributions to research in elevated temperature deformation mechanisms and for his leadership qualities demonstrated...from 1988 to 1993."

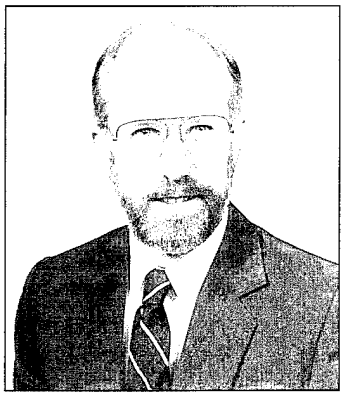

Mr. Lee M. Hammarstrom
Executive Directorate

SENIOR EXECUTIVE SERVICE MERITORIOUS RANK AWARD

Mr. Hammarstrom "has exhibited bold leadership and astute management for a distinguished support team of individual senior-level expert analysts, scientists, and engineers who have made major contributions to major studies, research and development initiatives, and key strategic program planning....He anticipated and fostered major breakthroughs in networking technology and massively parallel computing, which have become known as the 'Global Grid.' Mr. Hammarstrom is a nationally recognized authority on space systems research and development in pursuit of the military defense of the United States."

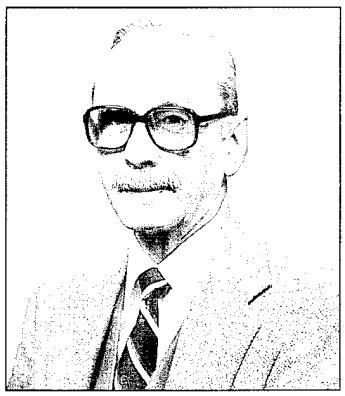

Dr. William Fox
Chemistry Division

NAVY MERITORIOUS CIVILIAN SERVICE AWARD

Dr. Fox was cited "for his [incisive] analysis of many critical Navy/DoD science and technology issues; his development of successful programs to address those issues, with NRL environmental research and safety projects being the most recent examples; and his patient, sage counsel, which enabled so many of his associates to excel at their own tasks."

Mr. Richard W. Smith
Financial Management Division

NAVY MERITORIOUS CIVILIAN SERVICE AWARD

Mr. Smith was recognized for his leadership and financial expertise in managing the close-out of financial operations associated with the merging of the Naval Oceanographic and Atmospheric Laboratory and NRL. He played an important role in converting the SCC accounting system to the Defense Business Operating Fund (DBOF) and acted as an advisor on DBOF to operating managers at NRL SCC.

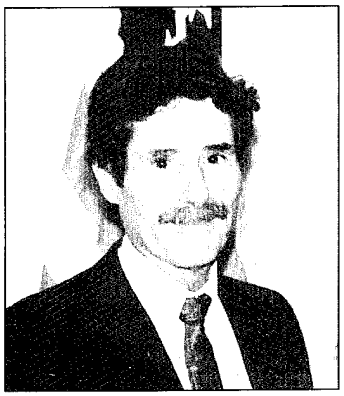

Dr. Joseph W. McCaffrey, Jr.
Oceanography Division

NAVY MERITORIOUS CIVILIAN SERVICE AWARD

Dr. McCaffrey's citation reads as follows: "For exceptionally meritorious performance of his duties as the Head, Ocean Dynamics and Prediction Branch and for significant achievements in the development of ocean-monitoring modeling and prediction systems and remote sensing data assimilation techniques....He led his group to the creation of the world's first eddy-resolving global ocean model, application of satellite altimetry to unlock the secrets of El Niño, establishment of the GEOSAT Exact Repeat Mission, and development of a whole range of coastal and global ocean dynamics tools judged, today, as world standards."

Mr. Donald Del Balzo
Ocean Acoustics and Technical Directorate

NAVY MERITORIOUS CIVILIAN SERVICE AWARD

Mr. Del Balzo's award recognized his service as science advisor to the Commander Sixth Fleet from August 1988 to September 1990. He was cited for producing many significant improvements in Fleet readiness across a broad spectrum of warfare areas, including the Mobile Data-Link Translator, bioluminescence applications, improved HF communications via autolink establishment, long-range UHF communications via multiple relays, laser-warning detectors, and sonobuoy delivery devices.

Dr. John Hovermale
Marine Meteorology Division

NAVY MERITORIOUS CIVILIAN SERVICE AWARD

Dr. Hovermale was cited for "his effective and dedicated leadership as the founding chairman of the Technology Panel for Environmental Sciences of the Project Reliance Joint Planning Process. As chairman, Dr. Hovermale had to garner the support of the individual service R&D laboratories to gather detailed information about the scope, resources, and funding of ongoing and planned projects, while simultaneously preparing recommendations that could lead to consolidation and possible transfer of those research projects between services. The resulting Joint Service Program is a cornerstone for future triservice cooperation in research and development in environmental sciences."

Dr. Hovermale, superintendent of NRL's Marine Meteorology Division, died on July 8, 1994.

Ms. Gwen Van Hoosier
NRL Staff, National Test Facility

NAVY MERITORIOUS CIVILIAN SERVICE AWARD

Ms. Van Hoosier was cited for "her exemplary service to the Department of the Navy, Naval Research Laboratory, from June 1957 through March 1994." Further, "her outstanding contributions in the areas of equal employment, prevention of sexual harassment, and Federally Employed Women set high marks for others to follow. She was instrumental in establishing a joint program office at the National Test Facility and a cornerstone in making it successful."

Dr. Gary A. Prinz
Materials Science and Technology Division

NAVY MERITORIOUS CIVILIAN SERVICE AWARD

Dr. Prinz was recognized for "providing an outstanding example of initiative and innovation in transferring basic research results in magnetism into the technological applications sector. Augmenting his extremely successful role of carrying out and directing world-class basic research in the field of magnetism, by moving into inventing new applications, and actively pursuing their implementation, he has provided both NRL and other Navy programs with a model for rapidly transmitting new basic research accomplishments into new technology."

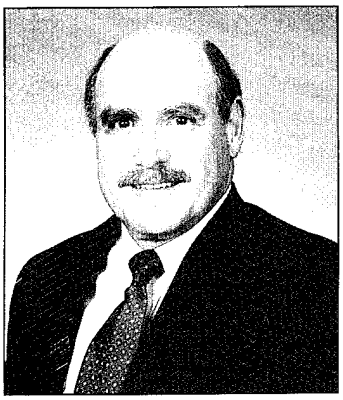

Mr. Jeffrey Knowles
Tactical Electronic Warfare Division

NAVY MERITORIOUS CIVILIAN SERVICE AWARD

In an award presented by the Commander, Surface Warfare Development Group, Mr. Knowles was cited "in recognition and appreciation for outstanding service and contribution to command mission while attached to Surface Warfare Development Group AEGIS/ AAW/EW Programs (N4) Directorate." The Group is responsible for developing tactical doctrine, techniques, and procedures for the Navy's surface weapon systems.

Mr. Italo deGrandi
Tactical Electronic Warfare Division

NAVY MERITORIOUS CIVILIAN SERVICE AWARD

Mr. deGrandi was cited for his "exceptional analytic ability and technical insight, which enabled him to develop high-leverage electronic countermeasures to antiship missile threats." Further, "the survivability of U.S. Navy surface forces has been improved markedly through his determination and innovative efforts."

Ms. Miriam Oliver
Executive Directorate

NAVY MERITORIOUS CIVILIAN SERVICE AWARD

Ms. Oliver was recognized "for the critical role she has played in the formulation, administration, and review of NRL's basic research program. Her outstanding efforts have had a significant impact on the direct annual support of over 500 scientists at NRL. She is also recognized for her outstanding support in permitting the Laboratory to respond to the many urgent demands placed upon it over the years....As a result of her professionalism and dedication, NRL scientists and engineers have been able to focus their time and energy on producing the scientific and technical products for which NRL is so highly regarded."

Ms. Janice Walker
Human Resources Office

NAVY MERITORIOUS CIVIAN SERVICE AWARD

This award was presented to Ms. Walker "for her exemplary service to the Department of the Navy, Naval Research Laboratory, from January 1973 through June 1994. Her outstanding contributions in the areas of labor relations, performance management, incentive awards, employee benefits programs, and prevention of sexual harassment set high marks for others to follow. She has been instrumental in creating and maintaining an employee relations staff of specialists second to none in the Navy. Her wise counsel, dynamic personality, and sage advice inspire a dedicated staff and ensure continuity of programs. Her long and dedicated service to the United States Government reflects great credit upon herself and the United States Navy."

Mr. Richard R. Rojas
Warfare Systems and Sensors Research Directorate

DEPARTMENT OF THE NAVY'S HISPANIC FIVE-POINT PROGRAM RECOGNITION AWARD

Mr. Rojas was recognized "for his tireless efforts in support of NRL's affirmative employment efforts and to the Department of the Navy's Advisory Council on Hispanic Employment (ACHE)." Mr. Rojas was also cited for his personal attention to NRL's recruitment efforts, which include providing subject matter experts to conduct on-site recruitment at technical career fairs and taking advantage of employment techniques to aid in employee retention.

Dr. Randall Shumaker
Information Technology Division

1993 OFFICE OF NAVAL RESEARCH (ONR) AND THE NAVAL RESEARCH LABORATORY (NRL) AWARDS FOR ACHIEVEMENT IN THE FIELD OF EQUAL EMPLOYMENT OPPORTUNITY (SUPERVISORY CATEGORY)

Dr. Shumaker was recognized by ONR and NRL for his "outstanding work in hiring and promoting women, disabled, and minority employees; for setting as a division objective, the development of an open and representative workplace; and for fostering activities among his employees to achieve that end." Dr. Shumaker also "acts upon his convictions that women, handicapped, and members of minority groups may be the best people to fill jobs at any level at NRL."

Ms. Caryn Dampier
Marine Meteorology Division

FIRST ANNUAL AWARD FOR EXCELLENCE IN SECRETARIAL SUPPORT

Ms. Dampier was recognized for her "overall excellence in performing her duties. Especially noteworthy was her support of the Environmental Sciences Panel of the Joint Directors of Laboratories, for which she assumed the major responsibility for setting up the complex and elaborate system of internal procedures vital in maintaining continuity and organization of the project."

Ms. Dorothy Harbour
Spacecraft Engineering Department

FIRST ANNUAL AWARD FOR EXCELLENCE IN SECRETARIAL SUPPORT

Ms. Harbour was cited for "significant contributions during launch-site operations of NRL's *Clementine* spacecraft. Personal initiative, dedication, and organization skills were instrumental in the timely and extremely successful integration and processing of the flight satellite."

Ms. Faye Zidek
Spacecraft Engineering Department

FIRST ANNUAL AWARD FOR EXCELLENCE IN SECRETARIAL SUPPORT

Ms. Zidek was cited for "significant contributions during launch-site operations of NRL's *Clementine* spacecraft. Personal initiative, dedication, and organization skills were instrumental in the timely and extremely successful integration and processing of the flight satellite."

Ms. Denise Quinn
Office of Management and Administration

FIRST ANNUAL AWARD FOR EXCELLENCE IN SECRETARIAL SUPPORT

Ms. Quinn was recognized for her "significant contributions and overall excellence and her consistently outstanding performance and contributions to major Laboratory projects."

Ms. Elsie Reinstein
Electronics Science and Technology Division

FIRST ANNUAL AWARD FOR EXCELLENCE IN SECRETARIAL SUPPORT

Ms. Reinstein was cited for her "outstanding performance personified by her work ethic, keen intellect, thoughtfulness, loyalty, self-motivation, and respect and friendliness, which she shows to all she comes in contact with in the course of her duties."

NAVAL DISTRICT WASHINGTON PERSONAL EXCELLENCE PARTNERSHIP OF THE YEAR AWARD

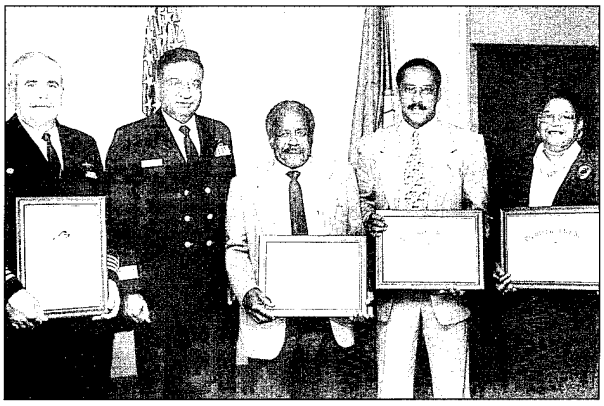

NRL is the recipient of this award for the fourth consecutive year in the collaborative category for exemplary partnership with the following schools: Leckie and Patterson Elementary Schools, Harris Educational Center, and Ballou Senior High School. Through this award, NRL Community Outreach volunteers are recognized for their outstanding performance in support of the four partner schools. Additionally, program volunteers support enrichment programs to both public and private schools in the Washington metropolitan area, on a case-by-case basis. Shown are a few of NRL's volunteers and school representatives and CAPT Cassidy, who accepted the award on behalf of the volunteers.

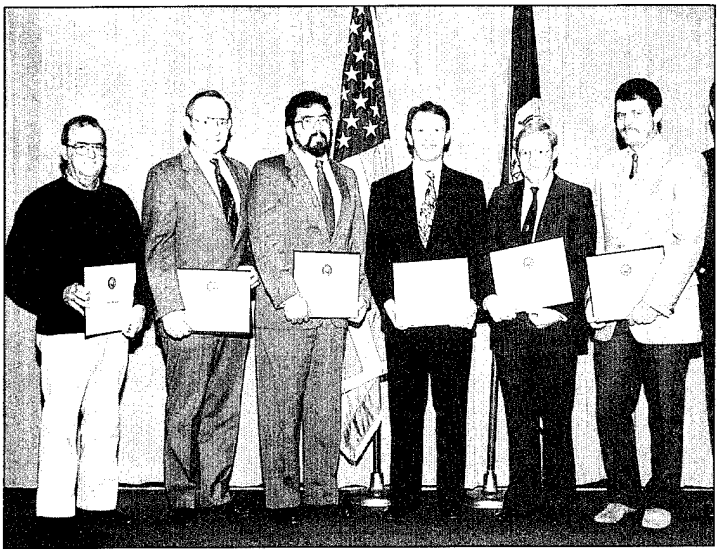

DEPARTMENT OF THE NAVY'S AWARD OF MERIT FOR GROUP ACHIEVEMENT

Employees from NRL's Optical Sciences and Marine Geosciences Divisions were the recipients of this award "for their significant contributions to the Magnetic Array System (MARS) project....The data collected by the MARS array will make a significant contribution to our understanding of electromagnetic activity in the shallow water environment and of our ability to protect that environment." Pictured (left to right) are Mr. Thomas McClelland, Mr. Gary Cogdell, Mr. Carl Villarruel, Dr. Frank Bucholtz, Dr. Anthony Dandridge, and Mr. Daniel Phillips. (Not photographed are Mr. William Avera and Mr. Daniel Fraley.)

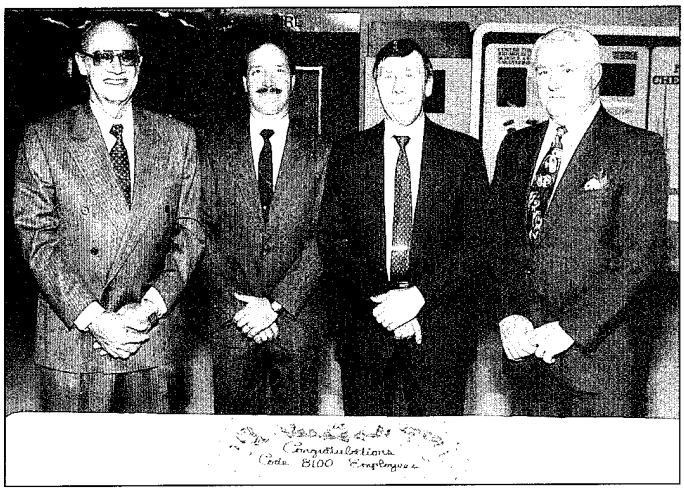

DEPARTMENT OF THE NAVY'S AWARD OF MERIT FOR GROUP ACHIEVEMENT

Four members of the Space Systems Development Department have been given this award for exceptional contributions as the original Midway Research Center (MRC) management team. Mr. Wayne Abernathy transitioned the MRC between development stage and operational status. Mr. John R. Dent II was responsible for major subsystem and system-level design and development, including the timing system, the calibration and verification system, and the broadband antenna feed system. Mr. Roger Eisinger led the MRC planning, development, and operations and for R&D activities and projects for outside sponsors. Mr. Orville (Pete) Jerrell contributed heavily to the Antenna Tracking System development, directing multiyear design, fabrication, and installation effort.

DEPARTMENT OF THE NAVY'S AWARD OF MERIT FOR GROUP ACHIEVEMENT

These individuals, representatives of the Command Support, Technical Information, and Research and Development Services Divisions, have made substantial contributions to producing audio-visual and press materials on *Clementine I* in record time and setting up the *Clementine I* display at the National Academy of Sciences. The recipients are: standing (from left to right) Brenda Turner, Ron Martin, Darlene DeMarr, Richard Bussey, Christopher Morrow, Paul Sweeney, Cathy Johnson, James Smego, Gayle Fullerton, Dick Baturin, Diltricia Montgomery, Donald Ford, Carol Hambric, Janice Schultz, Micheal McMullin, Eugene Smith, Leona Jackson, Leona Sprankel, and Kathy Parrish; and foreground (left to right) Dora Wilbanks, Michael Savell, Linda Greenway, James Marshall, and Sue Moorhouse. (Not photographed are Tazewell Rufty, Beba Zevgolis, William Griffith, and Jonna Atkinson.)

Individual Honors

On June 6, 1994, NRL awarded its second Lifetime Achievement Award to Dr. Homer Carhart, head of NRL's Navy Center for Safety and Survivability, for "his technological achievements, which have contributed benefits far beyond the U.S. Navy. Our NATO allies, worldwide commercial aviation, the maritime industry, and other Federal agencies now employ materials and methods directly attributable to his programs. Dr. Carhart has brought international renown to himself and NRL for his pioneering research and for his technology transfer accomplishments, both of which span his more than five decades of NRL/Navy service....The creation of the Center for Safety and Survivability... was a direct tribute to this outstanding devotion to making naval platforms better prepared to 'to in harm's way'."

Dr. Homer Carhart

Other Laboratory employees also received numerous scientific medals, military service awards, academic honors, and other forms of recognition, including election and appointment to offices in technical societies. The following is an alphabetical list of persons who received such recognition in FY 1994.

Achille, L.B., Newsletter editor of Division 21, American Psychological Association.

Ahn, S., Elected Vice President of the Korean-American Scientist and Engineers Association (KSEA); Elected Counselor in Physics of KSEA.

Ali, H.B., Received Sigma Xi Kaminski Award for best paper published in 1993; initiated and chaired technical session at Oceans '93 Conference in Victoria, British Columbia, Canada; initiated and chaired technical session at Oceans '94 Conference in Brest, France; edited technical paper for *Journal of Underwater Acoustics*.

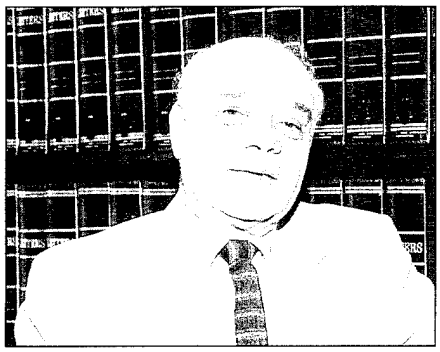

Dr. Jerome Karle, head of the Laboratory for the Structure of Matter at NRL has been awarded the distinction of fellow by the American Association for the Advancement of Science (AAAS). The association, which represents the world's largest federation of scientists, awards the rank of fellow to members "because of their efforts toward advancing science or fostering applications that are deemed scientifically or socially distinguished." Dr. Karle was specifically cited by AAAS for "fundamental advances in the understanding of the nature of atoms and molecules."

Anderson, W.T., Technical Chairman of the GaAs Reliability Workshop; Member, Scientific and Steering Committee of the Workshop on Expert Evaluation and Control of Compound Semiconductor Material and Technologies (EXMATEC); Member, The Technical Program Committee of the European Symposium on Reliability of Electron Devices, Failure Physics, and Analysis; Member, The Technical Program Committee of the European Symposium on Advanced Microelectronics Qualification, Reliability, and Logistics Workshop; Member, the Advisory Board of the NASA MMIC Reliability Assurance Group; and Member, The Technical Program Committee of the International Reliability Physics Symposium.

Antiochos, S.K., Appointed Chair of Science of Working Group of the NASA Mechanism for Solar Variability Program; appointed to the CSSP/CSTR Committee of the National Academy of Science.

Bernhardt, P.A., Fellow of the American Physical Society (Awarded Sept. 1994); Union of Radio Science Commission II Chairman; Member, Arecibo Science Advisory Council Board; Member, American Geophysical Union Books Board (overview and selection of AGU monographs); and Member, COSPAR Program Committee on Active Experiments in Space, Hamberg, Germany.

Boavis, C.S., Appointed to the American Institute of Aeronautics and Astronautics (AIAA) Flight Test Technical Committee.

Boos, J.B., Member, Steering Committee for International Conference on InP and Related Materials.

Broadhead, M.K., Elected to full membership in Sigma XI.

Bultman, J.D., Member, Committee on Creosote and Creosote Solutions and Member, Committee for the Evaluation of Wood Preservatives, both of the American Wood Preservers' Association; Associate Editor, *Biotropica* (published by the Association for Tropical Biology); Associate Sciences Editor (NRL) for *Naval Research Reviews* (published by the Office of Naval Research).

Buot, F.A., Invited review article, *Physics Reports*, November 1993, "Mesocopic Physics and Nanoelectronics: Nanoscience and Nanotechnology."

Campbell, A.B., Guest Editor, *IEEE Transactions on Nuclear Science.*

Cargill, P. Member, Organizing Committee for joint AAS Solar Physics Division/AGU meeting; Member, NASA Review Panel for Solar Physics SR&T Program.

Carhart, H.W., In his honor, the Homer W. Carhart Award for Fire Protection Excellence will be presented annually in Dr. Carhart's name at the Damage Control/ Firefighting Working Group Conference to the Navy Department civilian or military member who most exemplifies his professional standards and concerns for shipboard fire safety. This award will perpetuate his devotion to the fire safety of the Fleet of the United States Navy. (The award was

established by RADM M.S. Firebaugh, USN, Chief Engineer of the Navy.)

Carruthers, G.R., Editor of the *National Technical Association Journal*.

Chen, J., Member, NASA Proposal Review Panel; Member, DOE Basic Energy Science Review Panel.

Cheng, C.C., Appointed as a Member of Advisory Committee, Institute for Astronomy and Astrophysics, Academia Sinica (Taiwan); appointed as a Visiting Professor at the Beijing Astronomical Observatory, Beijing, China, by the Chinese Academy of Sciences.

Cherkis, N., Member and Chairman, U.S. Board on Geographic Names, Advisory Committee on Undersea Features; Member, U.S. Board on Geographic Names, Committee on Diacritical Marks; Scientific Advisor, GEBCO Guiding Committee; Bathymetric Coordinator, International Science Committee (IASC); Bathymetry Advisor, Coordinating Committee for Circum-Atlantic Project (CAP) (IUGS/USGS); Invited Expert, U.S.-Japan Cooperative Program in Natural Resources (UJNR)-Joint Sea Bottom Surveys Panel.

Chin-Bing, S.A., Member, Technical Committee on Underwater Acoustics of the Acoustical Society of America; appointed as National Research Council Postdoctoral Advisor; Member, International Editorial Board of *Mathematical Modelling and Scientific Computing*.

Chow, G.M., Co-organizer for symposium "Molecularly Designed Ultrafine/Nanostructured Materials," Materials Research Society Spring Meeting (1994); Chair, symposium session of the Materials Research Society Spring Meeting (1994); Co-editor of MRS proceedings, *Molecularly Designed Ultrafine/Nanostructured Materials*.

Collins, M.D., Recipient of the A.B. Wood Medal from the Institute of Acoustics.

Colombant, D.G., Advisor for FCAR Research Center, Quebec, Canada (to evaluate funding requests and allocate for university center in Quebec province).

Commisso, R., Chosen as Technical Coordinator for Joint DNA/SNL Jupiter Design Options Study Team.

Cook, B.J., Member of the Scientific Review Panel for the FAA Integrated Terminal Weather System (ITWS), a component of the Aviation Weather Development Program (AWOP).

Cooper, K.P., Past Chairman, Washington, D.C. Chapter of ASM International, 1994-95; appointed member of Chapter Council of ASM International, 1994-97.

Cooperstein, G., Fellow, American Physical Society; Technical Program Chairman, 1995 IEEE International Pulsed Power Conference; Member, International Advisory Committee, 1994 International Conference on High Power Particle Beams.

Dale, C.J., Received "Best Paper" Award at the 1994 IEEE Nuclear and Space Radiation Effects Conference.

Dere, K.P., Appointed to the NASA Space Physics Division Committee for the Next Japanese Solar Mission.

DeVore, C.R., Chair, Presidential Task Force on Membership Information Services, American Physical Society; Executive Committee Member and Newsletter Editor, Division of Computational Physics, American Physical Society.

Mr. Michael J. Monsma, of the Tactical Electronic Warfare Division, receives an award from former CO, CAPT Paul Gaffney at the Annual Publication Awards Ceremony.

Edelstein, A.S., Appointed Divisional Associate Editor of *Physical Review Letters*.

Fischer, J., Member of Management and Operations Working Group for the NASA IR Telescope Facility (IRTF); Member of Time Allocation Committee for the IRTF; appointed to membership on Committee to Select the Near-Infrared Spectrograph for the 8-m Gemini Telescope.

Flippen-Anderson, J.L., Elected Vice-Chair of the U.S. National Committee for Crystallography; appointed Member of Executive Committee for organization of the 17th General Assembly of the International Union of Crystallography to be held in Seattle, Washington, in August 1996; Co-editor, American Crystallographic Association Newletter.

Ford, R.T., Awarded Life Member status in IEEE Electromagnetic Compatibility Society, August 1994.

Friedman, H., Member, Meetings Committee for American Philosophical Society; Member, Committee for the Magellanic Premium Award for American Philosophical Society; Member, Internal Audit Committee for National Academy of Sciences; elected Honorary Fellow of AIAA; Member, Film Committee of the NAS/Production of the Space Age Film.

Froscher, J.N., Member, Program Committee, First NIST/ACSA Workshop on Information Technology Assurance and Trustworthiness; Chair, TTCP XTP-1 Workshop on Research Progress in MLS Relational Database Systems; Evaluation Committee, NSA University Research Program; Member, NSA Technical Evaluation Working Group on Database Security.

Fuller-Mora, W.W., Elected to the Mid-Atlantic Regional Nominating Committee for Sigma Xi; appointed Chairman of the Mid-Atlantic Regional Nominating Committee for Sigma Xi.

Glembocki, O.J., Edited Proceedings of MRS, V**324**, 1994, *Diagnostic Techniques for Semiconductor Materials Processings* and Proceedings, SPIE, V**2141**, 1994, *Spectroscopic Characterization Techniques for Semiconductor Technology V*; invited by the World Scientific Press to write a book on "Optical Properties and Electronic Properties of Semiconductors."

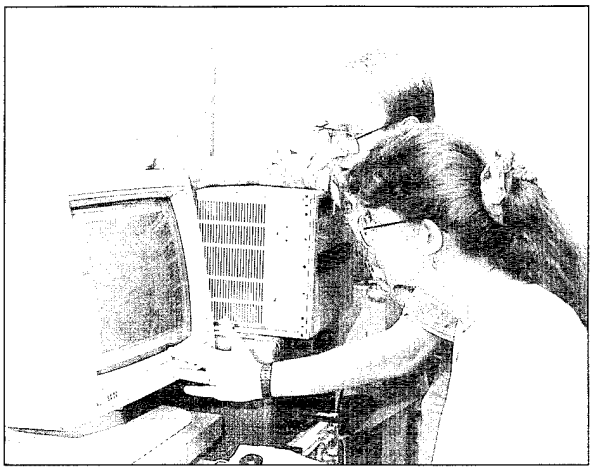

NRL has received the National Security Agency's (NSA's) annaual Frank B. Rowlett Trophy for Organizational Excellency—Honorable Mention—in the field of protecting U.S. information handling systems. NRL's Center for Computer High Assurance Systems, in the Laboratory's Information Technology Division, was cited by NSA for "significant contributions to the improvement of the national information systems security posture by a U.S. government organization."

Gold, S.H., Member of and Secretary to the Executive Committee of the IEEE Plasma Sciences and Applications Committee; Member, Program Committee, 21st IEEE International Conference on Plasma Science, 6-8 June 1994, Santa Fe, New Mexico, and Member, Program Committee, 22nd IEEE International Conference on Plasma Science, to be held on 5-8 June 1995 in Madison, Wisconsin; Associate Editor, *IEEE Transactions on Plasma Science*; Member, Review Committee, Department of Energy Annual Program Review of the Stanford Linear Accelerator Center; Member, Review Committee, Department of Energy annual review of the Next Linear Collider Test Accelerator.

Gossner, J., Navy Meritorious Civilian Services Award, 1994 (awarded by Surface Warfare Development Group).

Gray, H.F., Session Chair of the Chemistry and Physics of Micromachining and the Fabrication of 3-D Nanostructures at the 1993

Meeting of the Electrochemical Society, Miami, Florida, October 9-14, 1994.

Gursky, H., Reappointment to the Advisory Board of the Institute for Computational Sciences and Informatics, George Mason University (through 30 June 1995).

Hale, R.A., Invited Member, Security Directorate of the Internet Engineering Task Force.

Hardy, D., Elected to Steering Committee of International Association for Stability and Handling of Liquid Fuels (IASHLF); elected to Awards Subcommittee of IASHLF.

Hartwig, E.O., Appointed Program Chair to The Oceanographic Society Pacific Basin Meeting, July 1994, and appointed to the Ocean Fellows Nominations Committee and the Cody Award Nominations Committee.

Hawkins, J., Member, SSM/I Algorithm Research and SST Algorithm Research Panels.

Heitmeyer, C.L., Keynote Speaker, 1994 Real Time Applications Workshop; Track Chair, International Workshop on Software Specification and Design; Program Committee, SIGPLAN Workshop on Real-Time Programming Languages and Tools, COMPASS, and CONCUR '95.

Hembree, L.A., Member, Distributed Interactive Simulation (DIS) Steering and Technical Committees; Chair of DIS Atmosphere Subgroup.

Hertz, P., Appointed to NASA X-ray Timing Explorer Users Group (XUG).

Hornstein, J., Elected First Vice President, National Capital Section of the Optical Society of America.

Horan, D.M., Recipient of NASA's Medal for Exceptional Scientific Achievement.

Hoskins, G., Appointed by NASA as member of Global Geoscience WIND Mission Review Panel; served on the Secretary of Navy Steering Committee for Laboratory and Warfare Centers Mission Review.

Hubler, G.H., Edited book on *Pulsed Laser Deposition of Thin Films*, published by Wiley Interscience.

Hurlburt, H.E., Appointment to an international working group: North Pacific Marine Science Organization (PICES) Working Group 7 on Modeling of the Subarctic North Pacific Circulation.

Idzerda, Y.U., Publications Co-chair for the Conference on Magnetism and Magnetic Materials; Member of the MMM '95 Steering Committee.

Johnson, M., Recipient of NASA's Exceptional Engineering Achievement Medal.

Joyce, G.R., Fellow, American Physical Society.

Kabler, M.N., Fellow, American Physical Society; Spokesman for Beamline X24C Participating Research Team, National Synchrotron Light Source, Brookhaven National Laboratory; Program Committee, 1996 International Conference on Defects in Insulating Materials.

Kailasanath, K., Associate Fellow, American Institute of Aeronautics and Astronautics (AIAA); Vice-Chair, AIAA Propellants and Combustion Technical Committee; Papers' Chair, The Combustion Institute (Eastern States Section); Member, Program Advisory Subcommittee, 25th Symposium (International) on Combustion.

Kang, M.H., Member, IFIP Working Group 11.3 Database Security; Invited Receiver, Second ACM Conference on Computer and Communications Security.

Kaplan, C.R., Combustion Institute, Co-chair of Poster Session; Member of Program Advisory Committee.

Karle, I.L., Biography in book *Women in Chemistry and Physics*, by Grinstein, Rose, and Rafailovich; honoree at Symposium at American Chemical Society regional meeting held at University of Michigan in Ann Arbor (also presented plenary lecture); one of three women honored at New York Academy of Sciences (Women's Month); presented "First Penn Women Lecture in Chemistry" at University of Pennsylvania.

Kaufman, B., Deputy Director of Aerospace Sciences Group of American Institute of Aeronautics and Astronautics (AIAA); Member, Astrodynamics Committee of the International Astronautical Federation (IAF).

Sailor of the Year, AD1 James Johnson, receives a Navy Achievement Medal from Flight Support Detachment Officer in Charge, CDR Steven Smith, USN.

Kelner, G., Member, Advisory Committee for International Conference on SiC and Related Materials, to be held September 18-21, 1995, Kyoto, Japan.

Keskinen, M., Member, USAF/Phillips Laboratory Committee on HAARP Program and ONR Space Science Subcommittee on Ionospheric Modification.

Killiany, J.M., Senior Member, IEEE.

Kim, M.W., Member, Program Committee, International Conference on Neural Information Processing, 1994.

Kindle, J.C., Citation for Excellence in refereeing for the *Journal of Geophysical Research - Oceans*.

Knowles, J.P., Awarded Meritorious Civilian Service Medal while temporarily assigned to Commander, Surface Warfare Development Group, NAB, Little Creek, Norfolk, VA.

Korendyke, C.M., Appointed to Mail-in Review Panel for the NASA Supporting Research and Technology Program.

Kowalski, M.P., Served on the NASA review committee for UVG proposals.

Krowne, C., Member, 1994 Technical Program Committee for the Microwave Theory and Techniques International Symposium.

Kub, F., Committee Member, International Solid State Circuits' Conference.

Lampe, M., Member, Program Committee, American Physical Society, Plasma Physics Division Conference.

Lanwehr, C.E., Chairman and U.S. National Leader, TTCP XTP-1 (Trustworthy Computing Technologies); Chairman, Working Group 11.3 (Database Security), International Federation for Information Processing (IFIP); Associate Editor, *Journal of Computer Security*; Associate Editor, *High Integrity Systems Journal*; Vice Chair, 1994 IEEE Symposium on Research in Security and Privacy; Invited Address, IFIP World Computer Congress '94.

Lee, T., Co-chairman, American Meteorological Society's Seventh Conference on Satellite Meteorology and Oceanography, June 1994; selected to be next chairman of the American Meteorological Society Committee on Satellite Meteorology and Oceanography, beginning January 1996.

Ligler, F., Recipient of Hillebrand Award from The Chemical Society; elected Chairman, Gordon Research Conference on Bio/Analytical Sensors, organized and presided over 1994 meeting.

Little, B.J., Secretary, Microbiologically Influenced Corrosion Committee (T3J) of the National Association of Corrosion Engineers; Member, Organizing Committee for the 1995 International Conference on Microbiologically Influenced Corrosion.

Livingston, M.D., Elected to Executive Council of Theta Tau, National Professional Engineering Fraternity.

Marks, C.J., Vice President, Policy and Long Range Planning, Federally Employed Women (2nd term).

Marrian, C.R.K., Program Chair, Third International Conference on Nanometer Scale Science and Technology; Secretary, Nanometer Scale Science and Technology Division of the American Vacuum Society; Program Committee, E-Beam, X-Ray, EUV, and Ion Beam Lithographies for manufacturing.

McCafferty, E., Chairman, Honors and Awards Committee, The Electrochemical Society.

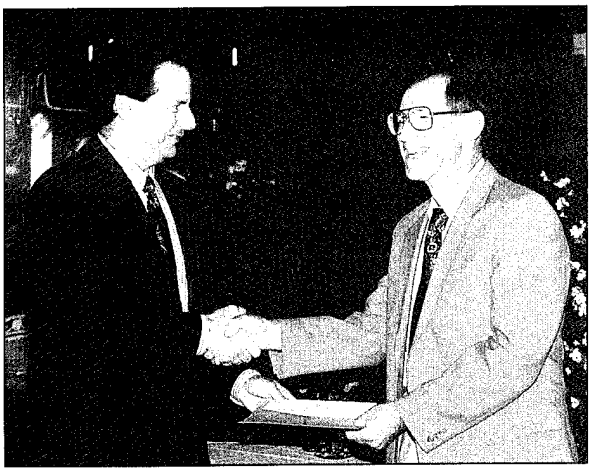

Dr. Richard Gould (left) presents a Support to Research Sigma Xi award (Gulf Coast Chapter) to Mr. Raymond E. Burge. Mr. Burge, an electronics technician with the Oceanography Division, made outstanding contributions to the research of Sigma Xi members.

McCaffrey, J.W., Organizer and Chair, J. Dana Thompson Tribute Sessions at AGU Ocean Sciences Meeting; Organizing Committee and Session Chair, Environmental Simulation '94 Workshop.

McDermott, J.P., Member, IFIP Working Group 11.3 Database Security; Invited Reviewer, 10th Annual Computer Security Applications Conference; Adjunct Faculty, ISSE, George Mason University.

McLean, J.D. Associate Editor, *Journal of Computer Security*; Invited Member, Scientific Advisory Board of 1996 Isaac Newton Institute; Editor, *Security and Privacy*, Vols 3 & 4 (IEEE Press).

Meadows, C.M., Associate Editor, *Journal of Computer Security*; Editor, *SIGSAC Review*; Program Co-chair, IEEE Symposium on Research in Security and Privacy.

Meier, R.R., Corresponding member, International Academy of Astronautics.

Michel, D.J., Fellow, ASM International; recipient of George Kimball Burgess Memorial Award of ASM International.

Middour, J.W., Member, Space Flight Mechanics Committee, American Astronautical Association.

Moore, A.P., Member, NSA Technical Evaluation Working Group on Hardware Verification.

Mosher, D., Fellow, American Physical Society.

Moskowitz, I.S., Contributing Editor, *Computer & Communications Security Review*.

Mowery, R.G., Re-elected Chairman, DoD Instrument Bearing Working Group; Member, Organizing Committee, '94 Rolling Element Bearing Symposium.

Nagel, D.J., North American Vice President, International Radiation Physics Society.

Ngai, K.L., Guest Editor, *Journal of Non-crystalline Solids*; Member, International Advisory Committee, International Conference on Defects in Insulating Materials, Raleigh, North Carolina.

O'Grady, W.E., Appointed to the General User's Oversight Committee National Synchrotron Light Source, Brookhaven National Laboratory, Upton, New York; appointed to the Editorial Board of the Frontiers of Electrochemistry Series, published by VCH.

Oran, E.S., Invited presentation, Zel'Dovich Memorial Symposium, Moscow, 1994; Fellow, American Physical Society; Board of Directors and Vice President of Publications, American Institute of Aeronautics and Astronautics; Program Chair, 25th Symposium (International) on Combustion, August 1994; Associate Editor, *Journal of Computational Physics*; Board of Directors, Combustion Institute.

Ossakow, S.L., Member, U.S. Particle Accelerator School Program Advisory Committee; Member, DOE Screening Panel for 1994 E.O. Lawrence Award in National Security.

Ottinger, P., Fellow, American Physical Society.

Parker, R.K., Fellow, American Physical Society; recepient of the Robert L. Woods Award from the DoD Advisory Group on Electron Devices for leadership in the vacuum electronics community.

Patel, V.L., Fellow, American Physical Society; Member, NSF Interagency Committee on Solar-Terrestrial Research; Board Member, Institute for Advanced Physics Studies, La Jolla, California.

Payne, C.N., Chair, Tools Fair, 9th Annual IEEE Conference on Computer Assurance

(COMPASS '94); Program Committee, 10th Annual Computer Security Applications Conference; Treasurer, 1995 IEEE Symposium on Security and Privacy.

Peckerar, M.C.; Elected Fellow, IEEE, for "Contributions to and Leadership in X Ray and Microlithography."

Preller, R.H. High latitudes physics, mixed layers, and turbulence and marine meteorology editor, *Journal of Geophysical Research. Series C. Oceans*.

Prinz, D.K., Appointed to Technical Peer Review Committee, NASA Space Environment and Effects Program; Technical Review Panel, USDA UVB Monitoring Program; and the Peer Review, NOAA Climate and Global Change Programs.

Prokes, S.M., Trustee, Alpha Sigma Mu, the Materials Sciences Honor Society, for work in the spectroscopy of solids.

Qadri, S., Member, User's Executive Committee, National Synchrotron Light Source, Brookhaven National Laboratory; selected for *Five Thousand Personalities of the World*.

Rajagopal, A.K., Award for Outstanding Achievement from the Washington Academy of Sciences for Achievement in the Field of Engineering Sciences.

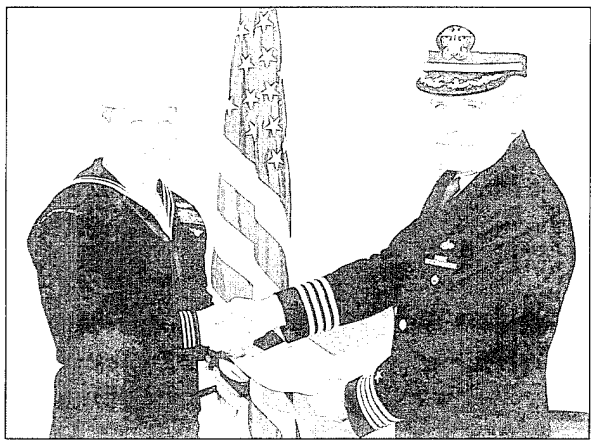

AG1 Gene Crain, of the Military Branch, Marine Meteorology Division, Monterey, California, receives award certificate and gold star in lieu of a fourth award of the Good Conduct Medal from CAPT Richard M. Cassidy, NRL's Commanding Officer.

Regeon, P., Recipient of NASA's Exceptional Engineering Achievement Medal.

Reinecke, T.L., Fellow, American Physical Society; Co-chairman, "Workshop on Advances in the Physics and Technology of Mesoscopic Physics," Moscow, July 1994; Member, Organizing Committee, "Workshop on Surface Dynamics," Knoxville, Tennessee, October 1993.

Ripin, B.H., Chair-Elect and Program Chair, American Physical Society, Division of Plasma Physics; Board of Governors, American Institute of Physics; Chair, APS Publication Oversight Committee; Member, Committee on International Freedom of Scientists, APS; Editorial Board, Laser and Particle Beams, Cambridge University Press.

Rojas, R.R., Recipient of Department of Navy's Hispanic Five-Point Program Recognition Award (1994).

Roleson, D.R., Appointed to the Editorial Board of the *Journal of Electroanalytical Chemistry* for the 1995-1998 term. (Dr. Roleson will be the first woman member of this Editorial Board.)

Rosenbaum, L.J., DoN Special Act Award for achievements as Liaison Scientist, ONR European Office; Elected to Senior Member, IEEE; Elected Chairman, Technical Committee on Computer Graphics, IEEE Computer Society; Editor, J. Virtual Reality Society and IEEE Computer Graphics and Applications; Program Chairman, IEEE Visualization '94 Conference; Program Committee, Workshop for Graphics and Machine Vision, Computer Animation Conference, Frontiers of Research in Virtual Environments, Fifth Eurographics ViSC Workshop.

Saks, N., Appointed to Program Committee, IEEE Semiconductor Interface Specialist.

Saunders, K.D., Chairman, Ocean Instrument Committee, Marine Technology Society; President-Elect, American Society of Civil Engineers, Gulf Coast Branch.

Schmidt-Nielsen, A. Secretary-Treasurer, Division 21 of American Psychological Association.

Seely, J.F., Second place, International Radiology Centennial Imaging Contest.

Shanabrook, B.V., Appointed to the International Advisory Committee, 11th International Conference on the Electronic Properties of Two-Dimensional Systems.

Shashidhar, R.N.S.; Elected Board Member (to represent USA), International Crystal Society; Appointed Chairman, SPIE Symposium on "Liquid Crystal Materials and Devices;" Appointed Chairman, "ACS Conference on Liquid Crystals," by the Colloid and Surface Division of the American Chemical Society.

Sheeley, Jr., N.R., Elected to Editorial Board, *Solar Physics Journal*.

Sheinson, R.S., One of the U.S. Government representatives of the United Nations' Environment Program's Halon Technical Options Committee.

Simpson, C.G., Recipient of Federal Technology Transfer Award for 1994.

Siskind, D.E., Cited for "Excellence in Refereeing," by the *Journal of Geophysical Research - Space Physics*.

Sleger, K., Member, RF Components Subpanel on JDL Reliance Electronics Devices; Navy Deputy Member, Advisory Group on Electron Devices (AGED) Working Group A; Senior Member, Institute of Electrical and Electronics Engineers (IEEE).

Spezio, A., Chairman, TTCP-QTP-20-KTAI; Session Chairman, SPIE Conference, April 1994.

Sprangle, P.A., Fellow, American Physical Society; Member, Sigma Xi; Senior Member, Institute of Electrical and Electronics Engineers (IEEE); Member, Exploratory Working Group to consider joint U.S.-Russia collaboration on FEL research; Chairman, International FEL Prize Committee, 1994; Member, Executive Committee of the 17th International Free Electron Laser Conference, New York, Sept. 1995.

Stahlbush, R., Local Arrangements Chairman, 1994 Semiconductor Interface Specialists Conference.

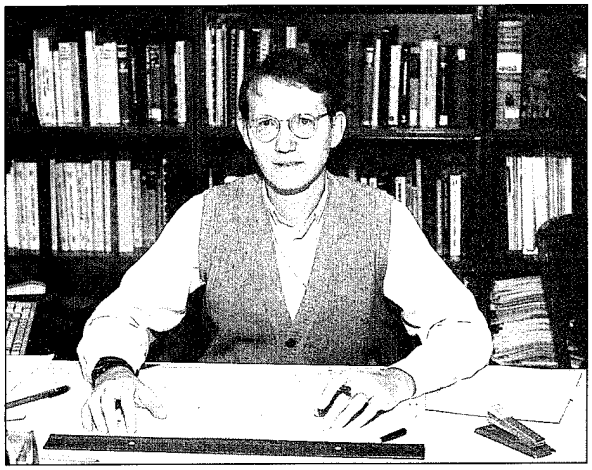

Dr. Arne W. Fliflet, of NRL's Plasma Physics Division, has been elected a fellow of the American Physical Society (APS) "for [his] significant and outstanding contributions to research on electron cyclotron masers, pioneering work in gyrotron and cylotron autoresonance maser theory, and in experimental quasioptical gyrotron research."

Tang, C.M., Fellow, American Physical Society; Program Committee, IEEE Particle Accelerator Conference for 1995; Program Committee, 1994 International Free Electron Laser Conference; Program Committee, 1994 International Conference of Plasma Science and Technology; NIH Work Study Panel on Medical Imaging.

Tatem, P.A., Selected as an Excellence in Government Fellow for 1994-95; Appointed as Committee Member of the National Academy of Sciences/National Research Council/ National Materials Advisory Board Committee, "Improved Fire and Smoke Resistant Materials for Commercial Aircraft Interiors;" Board of Directors, Eastern States Combustion Institute.

Teague, W.J., Best Poster of Session, Satellite Altimetry and Oceanography (JASO) Symposium, 1-3 December 1993, Toulouse, France.

Tolstoy, A., Fellow, Acoustical Society of America (ASA); Senior Member, IEEE; Guest Editor for Special issue of *Journal of Computational Acoustics (JCA)*; second patent approved for Matched-field Tomography Method.

Trunk, G.V., Chairman, KTP-2, a technical exchange panel on radar data processing under the auspices of subgroup K (radar) within The Technical Cooperation Program (TTCP); Member, Technical Papers Committee of the International Radar Symposium.

Turner, N.H., Elected Vice Chairman, Division of Colloid and Surface Chemistry of the American Chemical Society for 1995; Appointed to the Program Committee for the Sixth Topical Conference on Quantitative Surface Analysis.

Vogt, P.R., Associate Editor, *Bulletin of the Geological Society of America*; Co-convener and invited speaker at the "Workshop on Arctic Ridges," Kiel, Germany, 16-20 November 1994.

Wagner, R.J., Program Committee, 1994 Meeting of IRIS Specialty Group on Infrared Material; Member, Organizing Committee for the 1995 International Conference on Narrow Gap Semiconductors.

Waterman, J.R., Proceedings Editor, 1993 Workshop on the Physics and Chemistry of Mercury Cadmium Telluride; Member, Program Committee, 1994 Workshop on the Physics and Chemistry of Mercury Cadmium Telluride.

Webb, D.C., Chairman, Intersocietal Liaison Committee, Vice-Chairman, Technical Coordinating Committee; IEEE-Microwave Theory and Techniques Administrative Committee; Member, Technical Program Committee, 1994 IEEE-Microwave Theory and Techniques International Symposium; Chairman, Technical Committee, ARPA Ferrite Development Consortium.

Wieting, T.J., Program Chairman, Seventh National Conference on High-Power Microwave Technology; Editor, *Proceedings of the Seventh National Conference on High-Power Microwave Technology*; Chairman, OSD System Effects Assessment Team.

Wilsey, N.D., Member, Editorial Board, *Journal of Materials Science: Materials in Electronics*; Appointed Member, Organizing Committee, Gordon Research Conference on Point Defects, Line Defects, and Interfaces.

Zedd, M.F., Named Associate Fellow, American Institute of Aeronautics and Astronautics (AIAA).

Alan Berman Research Publication and Edison Patent Awards

The Annual Research Publications Awards Program was established in 1968 to recognize the authors of the best NRL publications each year. These awards not only honor individuals for superior scientific accomplishments in the field of naval research but also seek to promote continued excellence in research and in its documentation. In 1982, the name of this award was changed to the Alan Berman Research Publications Award in honor of its founder.

There were 296 separate publications submitted by the divisions in 1994 to be considered for recognition. Of those considered, 37 were selected. These selected publications represent 132 authors, each of whom received a publication awards certificate, a bronze paperweight, and a booklet listing the publications that received special recognition. In addition, NRL authors share in their respective division's monetary award.

The winning papers and their respective authors are listed below by their research units. Non-Laboratory coauthors are indicated by an asterisk.

NRL also recognizes patents as part of its annual publication awards program. The NRL Edison Patent Award was established in January 1991 to recognize NRL employees for outstanding patents issued to NRL by the U.S. Patent and Trademark Office during the preceding calendar year. The award recognizes significant NRL contributions to science and engineering as demonstrated by the patent process that are perceived to have the greatest potential benefit to the country. Of the 91 patents considered for 1994, 4 were selected representing 9 winners. They are listed under the NRL Edison Patent Awards.

Radar Division

Unsupervised BCM Projection Pursuit Algorithms for Classification of Simulated Radar Presentations
Charles M. Bachmann, Dong Luong, Abraham Schultz, and Scott A. Musman*

Coherent Detection of Radar Targets in a Non-Gaussian Background
Kevin J. Sangston and Karl Gerlach

Information Technology Division

Speech Analysis and Synthesis Based on Pitch-Synchronous Segmentation of the Speech Waveform
George S. Kang and Lawrence J. Fransen

A General Theory of Composition for Trace Sets Closed Under Selective Interleaving Functions
John McLean

Optical Sciences Division

All-Optical Deployable Systems Architecture and Performance Study
Alan D. Kersey, Aileen M. Yurek, Anthony Dandridge,
Carl Villarruel, and Gary Cogdell

Stepped-Wavelength Optical-Fiber Bragg Grating Arrays Fabricated in Line on a Draw Tower
Charles G. Askins, Martin A. Putnam, E. Joseph Friebele, and Glen M. Williams*

Tactical Electronic Warfare Division

Wideband Surface Acoustic Wave (SAW) Recirculation Loop False Target Generator (FTG) Development
Kimberly A. Hrin, Mitchell H. Kobil, and Jerry Hausner*

Radar Antenna Characterization Using Polarization Measurements
Elaine Chincheck

Underwater Sound Reference Detachment

Direct Measurements of Edge Diffraction from Soft Underwater Acoustic Panels
Jean C. Piquette

Temperature Dependence of the Electromechanical Properties of 0-3 $PbTiO_3$-polymerPiezoelectric Composite Materials
Kurt M. Rittenmyer

Laboratory for the Structure of Matter

Alkynylcubanes as Precursors of Rigid-rod Molecules and Alkynylcycloöctatetraenes
Richard Gilardi, Philip E. Eaton,* and Elena Galoppini*

Chemistry Division

Direct Measurement of the Forces Between Complementary Strands of DNA
Linda A. Chrisey, Richard J. Colton, and Gil U. Lee*

An Elastomeric Ejection System
C. Michael Roland, Il Sup Choi,* and Laurent C. Bissonnette*

Materials Science and Technology Division

The Evolution and Growth Kinetics of Precipitate Plates Growing by the Ledge Mechanism
George A. Spanos, Robert A. Masumura, Roy A. Vandermeer, and M. Enomoto*

Real-Time Parallel Computation and Visualization of Ultrasonic Pulses in Solids
Richard S. Schechter, Henry H. Chaskelis, Richard B. Mignogna, and P. P. Delsanto*

Laboratory for Computational Physics and Fluid Dynamics

Detonation Structures Behind Oblique Shocks
Chiping Li, K. Kailasanath, and Elaine S. Oran

Condensed Matter and Radiation Sciences Division

Direct Observation of Microscopic Inhomogeneities with Energy-Dispersive Diffraction of Synchrotron Produced X-rays
Earl F. Skelton, Andrew R. Drews, Michael S. Osofsky, Syed B. Qadri, J. Z. Hu,* Terrell A. Vanderah,* J. L. Peng,* and Richard L. Greene*

Pulsed Laser Deposition of Thin Films
Douglas B. Chrisey and Graham K. Hubler

Plasma Physics Division

Antiphase Switching in Josephson Junction Arrays
Ira B. Schwartz and Kwok Yeung Tsang*

Thermostructural Response Testing with Ion Beams
David Mosher, John R. Boller, Gerald Cooperstein, Stavros J. Stephanakis, Frank C. Young, Gerry Gurtman,* Joe Sallay,* and Steven H. Richter*

Electronics Science and Technology Division

Role of Interfacial Oxide-Related Defects in the Red-Light Emission in Porous Silicon
S. M. Prokes and O. J. Glembocki

A Nonequilibrium Time-Dependent Functional Theory Based on Liouvillean Quantum Field Dynamics in Condensed Matter Systems
A. K. Rajagopal and F. A. Buot

Center for Biomolecular Science and Engineering

Spatially Controlled Adhesion, Spreading, and Differentiation of Endothelial Cells on Self-Assembled Molecular Monolayers
Barry J. Spargo, Mary A. Testoff, David A. Stenger, Alan S. Rudolph, Thor B. Nielsen,* and James J. Hickman*

Stability of Magnetic Field-Induced Dipolar Order in a Ferroelectric Side-Chain Liquid Crystal Polymer
Jawad Naciri, Banahalli R. Ratna, Ranganathan Shashidhar, S. Sprunt,* and G. Nounesis*

Acoustics Division

Scattering from Flexural Waves on a Ribbed Cylindrical Shell
Douglas M. Photiadis, Joseph A. Bucaro, and Brian H. Houston

The Impulse Response of an Aperture: Numerical Calculations within the Framework of the Wedge Assemblage Method
Richard S. Keiffer, Guy V. Norton, and Jorge C. Novarini*

Remote Sensing Division

Marine Boundary Layer Measurements of New Particle Formation and the Effects Nonprecipitating Clouds Have on Aerosol Size Distribution
W. A. Hoppel, G. M. Frick, J. W. Fitzgerald, and R. E. Larson*

Gulf Stream Surface Convergence Imaged by Synthetic Aperture Radar
G. O. Marmorino, R. W. Jansen, G. R. Valenzuela, C. L. Trump, J. S. Lee, and J. A. C. Kaiser

Oceanography Division

Decade-scale Trans-Pacific Propagation and Warming Effects of an El Niño Anomaly
Gregg A. Jacobs, Harley E. Hurlburt, John C. Kindle, E. Joseph Metzger, William J. Teague, Jimmy L. Mitchell,* and Alan J. Wallcraft*

Marine Geosciences Division

Deep Pleistocene Iceberg Plowmarks on the Yermak Plateau: Sidescan and 3.5 kHz Evidence for Thick Calving Ice Fronts and a Possible Marine Ice Sheet in the Arctic Ocean
Peter Vogt, Kathleen Crane,* and Eirik Sundvor*

Marine Meteorology Division

Potential Application of the SSM/I Cloud Liquid Water Parameter to the Estimation of Marine Aircraft Icing
Thomas F. Lee, James R. Clark, and Steven D. Swadley*

Cloud Classification of AVHRR Imagery in Maritime Regions Using a Probabilistic Neural Network
Richard L. Bankert

Space Science Division

An Algorithm for Forecasting Mountain Wave-Related Turbulence in the Stratosphere
Julio T. Bacmeister, Paul A. Newman,* Bruce L. Gary,* and K. Roland Chan*

Solar Fine-Scale Structures in the Corona, Transition Region, and Lower Atmosphere
Dan J. Moses, John W. Cook, Guenter E. Brueckner, Kenneth P. Dere, John-David F. Bartoe,* David F. Webb,* John M. Davis,* Jack W. Harvey,* Frank Recely,* Sara F. Martin,* and Harold F. Zirin*

Space Systems Development Division

Effect of Broadcast and Precise Ephemerides on Estimates of the Frequency Stability of GPS NAVSTAR Clocks
Thomas B. McCaskill, Wilson G. Reid, James A. Buisson,* and Hugh E. Warren*

Spacecraft Engineering Division

Frozen Orbits for Satellites Close to an Earth-Like Planet
Shannon L. Coffey, Andre Deprit,* and Etienne Deprit*

Advanced Release Technologies Program
William E. Purdy

NRL Edison Patent Awards

Limited Bandwidth Microwave Filter
Christen Rauscher

Microassay on a Card
David A. Kidwell

Lyophilized Ligand-Receptor Complexes for Assays and Sensors
Frances S. Ligler and James P. Whelan*

Carborane-(Silane or Siloxane)-Unsaturated Hydrocarbon Based Thermosetting Polymers
Teddy M. Keller and Leslie J. Henderson*

Awards for *NRL Review* Articles

Awards for *NRL Review* articles were established in 1990 to recognize authors who submit outstanding research articles for this scientific publication. The articles are judged on the relevance of the work to the Navy and DoD, readability to the college-graduate level, and the use of graphics that are interesting and informative. The following awards were presented for articles that appeared in the *1994 NRL Review*.

FEATURED RESEARCH ARTICLE

Computational Materials Science
Larry A. Boyer, Michael J. Mehl, Dimitrios A. Papaconstantopoulos, Warren E. Pickett, and David J. Singh
CONDENSED MATTER AND RADIATION SCIENCES DIVISION

DIRECTORATE AWARDS FOR SCIENTIFIC ARTICLES

Warfare Systems and Sensors Research Directorate

High-Resolution Underwater Acoustic Imaging
Behzad Kamgar-Parsi
INFORMATION TECHNOLOGY DIVISION

Materials Science and Component Technology Directorate

Origins of Magnetic Anisotrophy in Magneto-optical Storage Materials
William T. Elam
CONDENSED MATTER AND RADIATION SCIENCES DIVISION
and
Vincent G. Harris and Norman C. Koon
MATERIALS SCIENCE AND TECHNOLOGY DIVISION

Ocean and Atmospheric Science and Technology Directorate

Numerical Ocean Models
NRL Global Modeling Team
(J. McCaffrey, J. Mitchell, H. Hurlburt, J. Kindle, D. Fox, M. Carnes, R. Rhodes, G. Jacobs, Z. Hallock, W. Teague, T. Townsend, J. Metzger, J. Dastugue, and A. McManus)
OCEANOGRAPHY DIVISION

Naval Center for Space Technology

Impedance Model Study for the Common Pressure Vessel Battery
William E. Baker, Jr., James C. Garner, and Daniel J. Shortt
SPACE SYSTEMS DEVELOPMENT DEPARTMENT

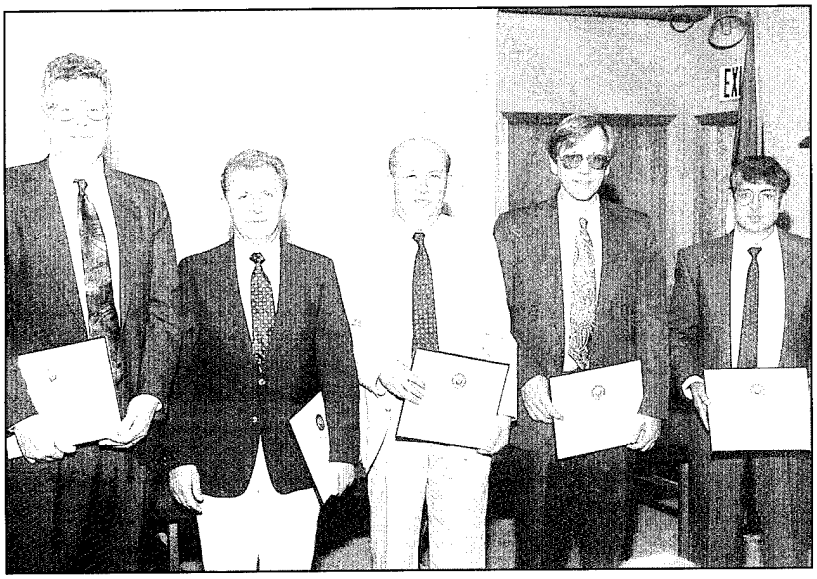

(Left to right) Drs. Mehl, Boyer, Papaconstantopoulos, Pickett, and Singh receive the featured article award

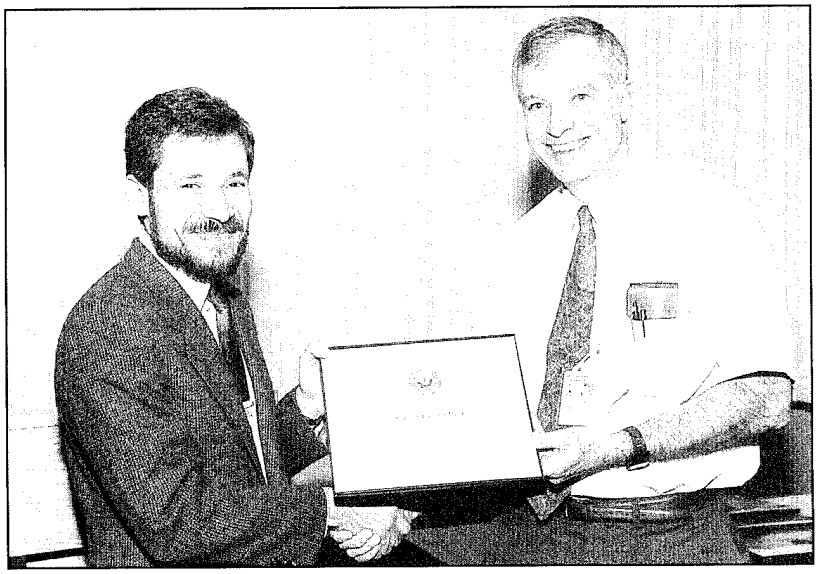

Dr. Kamgar-Parsi (left) receives the award from Dr. T. Coffey, NRL's Director of Research, for the Warfare Systems and Sensors Research Directorate

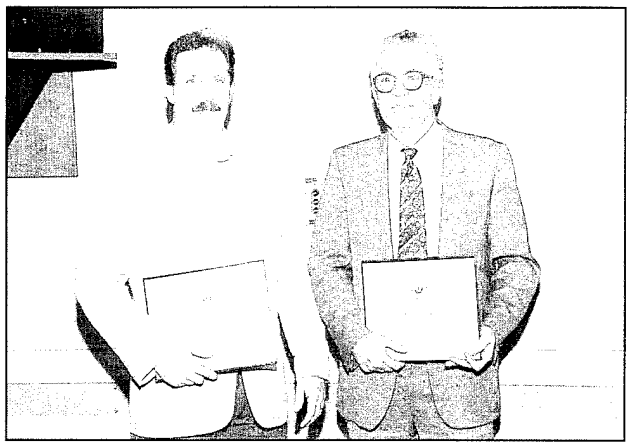

Left to right: Drs. Harris and Koon receive recognition for the Materials Science and Component Technology Directorate. (Missing from this picture is Dr. Elam).

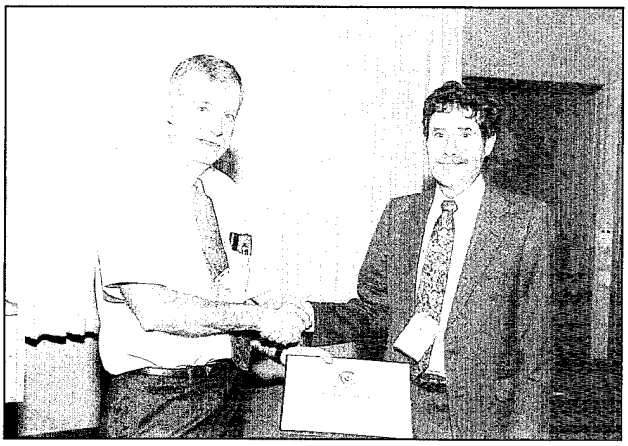

Dr. Coffey (left) presents the award for the Ocean and Atmospheric Science and Technology Directorate to Dr. McCaffrey, who represents the NRL Global Modeling Team

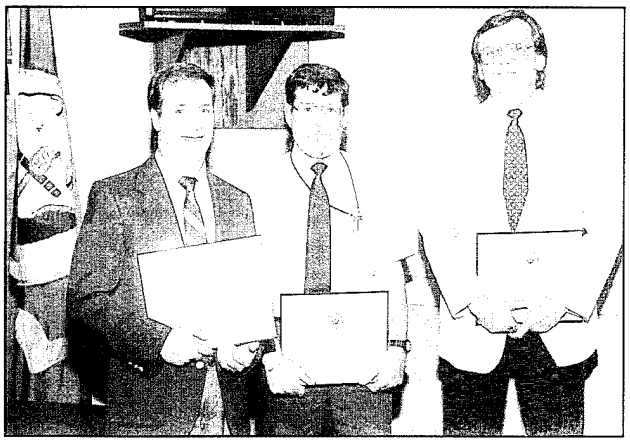

(Left to right) Mr. Garner, Mr. Baker and Dr. Shortt receive the award for the Navy Center for Space Technology

Programs for NRL Employees

During 1994, under the auspices of the Employee Development Branch, NRL employees participated in about 5600 individual training events. Many of these were presented as either videotaped or on-site instructed courses on diverse technical subjects, management techniques, and enhancement of such personal skills as efficient use of time, speed reading, memory improvement, and interpersonal communications. Courses are also available by means of computer-based training (CBT) and live television courses for monitoring nationwide.

One common study procedure is for employees to work full time at the Laboratory while taking job-related scientific courses at universities and schools in the Washington area. The training ranges from a single course to full graduate and postgraduate programs. Tuition for training is paid by NRL. The formal programs offered by NRL are described here.

GRADUATE PROGRAMS

• The **Advanced Graduate Research Program** (formerly the Sabbatical Study Program, which began in 1964) enables selected professional employees to devote full time to research or pursue work in their own or a related field for one year at an institution or research facility of their choice without the loss of regular salary, leave, or fringe benefits. NRL pays all educational costs, travel, and moving expenses for the employee and dependents. Criteria for eligibility include professional stature consistent with the applicant's opportunities and experience, a satisfactory program of study, and acceptance by the facility selected by the applicant. The program is open to paraprofessional (and above) employees who have completed 6 years of Federal Service, 4 of which are at NRL.

• The **Edison Memorial Graduate Training Program** enables employees to pursue advanced studies in their fields at local universities. Participants in this program work 24 hours each workweek and pursue their studies during the other 16 hours. The criteria for eligibility include a minimum of 1 year of service at NRL, a bachelor's or master's degree in an appropriate field, and professional standing in keeping with the candidate's opportunities and experience.

• To be eligible for the **Select Graduate Training Program**, employees must have a college degree in an appropriate field and must have demonstrated ability and aptitude for advanced training. Students accepted in this program devote a full academic year to graduate study. While attending school, they receive one-half of their salary, and NRL pays for tuition, books, and laboratory expenses.

Dr. Wallace Manheimer of the Plasma Physics Division was afforded the opportunity to participate in the Advanced Graduate Research Program. Dr. Manheimer was a visiting physics professor at the Moscow State University.

• The **Naval Postgraduate School** (NPS), located in Monterey, California, provides graduate programs to enhance the technical preparation of Naval officers and civilian employees who serve the Navy in the fields of science, engineering, operations analysis, and management. It awards a master of arts degree in national security affairs and a master of science degree in many technical disciplines. In addition, a doctor of philosophy degree may be earned in select fields of science and engineering.

NRL employees desiring to pursue graduate studies at NPS may apply for a maximum of six quarters away from NRL, with thesis work accomplished at NRL. Specific programs are described in the NPS catalog. Participants will continue to receive full pay and benefits during the period of study.

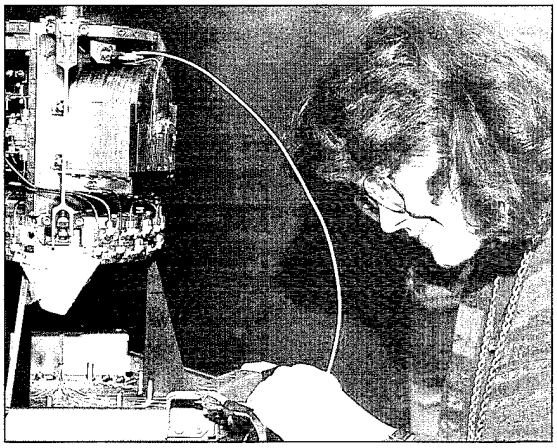

Sheleen Turner of the Spacecraft Engineering Department pursues a master's degree in mechanical engineering at the University of Maryland under the Edison Memorial Graduate Training Program.

• In addition to NRL and university offerings, application may be made to a number of noteworthy programs and fellowships. Examples of such opportunities are the **Alfred P. Sloan Fellows Program**, **Brookings Institute Advanced Study Program**, The **Fellowship in Congressional Operations**, and the **Women's Executive Leadership Program**. These and other programs are announced from time to time as schedules are published.

• Research conducted at NRL may be used as **thesis material for an advanced degree**. This original research is supervised by a qualified employee of NRL who is approved by the graduate school. The candidate should have completed the required course work and should have satisfied the language, residence, and other requirements of the graduate school from which the degree is sought. NRL provides space, research facilities, and supervision but leaves decisions on academic policy to the cooperating schools.

CONTINUING EDUCATION

• Local colleges and universities offer **undergraduate and graduate courses** at NRL for employees interested in improving their skills and keeping abreast of current developments in their fields. These courses are also available at many other DoD installations in the Washington, D.C. area.

• The Employee Development Branch at NRL offers **short courses** to all employees in a number of fields of interest including technical subjects, computer operation, supervisory and management techniques, and clerical/secretarial skills. Laboratory employees may attend these courses at nongovernment facilities as well. Interagency courses in management, personnel, finance, supervisory development, and clerical skills are also available.

For further information on any of the above programs, contact the Employee Development Branch (Code 1840) at (202) 767-2956.

TECHNOLOGY TRANSFER

• The **Office of Research and Technology Applications Program** (ORTA) ensures the full use of the results of the Nation's federal investment in research and development by transferring federally owned or originated technology to state and local governments and the private sector. (Contact Dr. Richard Rein (Code 1004) at (202) 767-3744.)

TECHNOLOGY BASE

• The **Navy Science Assistance Program** (NSAP) establishes an information loop between the Fleet and the R&D shore establishments to expedite technology transfer to the user. The program addresses operational problems, focuses resources to solve specific technical problems, and develops a nucleus of senior scientific personnel familiar with the impact of current research and system performance on military operations. (Contact Dr. Stephen Sacks (Code 4040) at (202) 767-3666.)

• The **Scientist-to-Sea Program** (STSP) provides increased opportunities for Navy R&D laboratory/center personnel to go to sea to gain first-hand insight into operational factors affecting system design, performance, and operations on a variety of ships. (Contact Dr. George Abraham (Code 4040.1) at (202) 767-3521.)

PROFESSIONAL DEVELOPMENT

NRL has several programs, professional society chapters, and informal clubs that enhance the professional growth of employees. Some of these are listed below.

• The **Counseling Referral Service** (C/RS) helps employees to achieve optimal job performance through counseling and resolution of problems such as family, stress and anxiety, behavioral, emotional, and alcohol- or drug-related problems that may adversely impact job performance.

C/RS provides confidential assessments and short-term counseling, training workshops, and referrals to additional resources in the community. (Contact Ms. Helen Loughrey at (202) 767-6857.)

• A chartered chapter of **Women in Science and Engineering** (WISE) was established at NRL in 1983. Informal monthly luncheons and seminars are scheduled to inform scientists and engineers of women's research at NRL and to provide an informal environment for members to practice their presentations. WISE also sponsors a colloquium series to feature outstanding women scientists. (Contact Dr. Wendy Fuller-Mora at (202) 767-2793, Dr. Debra Rolison at (202) 767-3617, or Dr. Cha-Mei Tang at (202) 767-4148.)

• **Sigma Xi**, the Scientific Research Society, encourages and acknowledges original investigation in pure and applied science. As an honor society for research scientists, individuals who have demonstrated the ability to perform original research are elected to membership in local chapters. The NRL Edison chapter, comprised of approximately 600 members, recognizes original research by presenting awards annually in pure and applied science to outstanding NRL staff members. The chapter also sponsors lectures at NRL on a wide range of scientific topics for the entire NRL community. These lectures are delivered by scientists from all over the nation and the world. The highlight of the Sigma Xi lecture series is the Edison Memorial Lecture, traditionally featuring a Nobel laureate. (Contact Dr. Wendy Fuller-Mora at (202) 767-2793 or Dr. Robert Morris at (202) 767-3845.)

• The **NRL Mentor Program** was established to provide an innovative approach to professional and career training and an environment for personal and professional growth. It is open to all permanent NRL employees in all job series and at all sites. Mentorees are matched with successful, experienced colleagues with more technical and/or managerial experience who can provide them with the knowledge and skills needed to maximize their contribution to the success of their immediate organization, to NRL, to the Navy, and to their chosen career fields. The ultimate goal of the program is to increase job productivity, creativity, and satisfaction through better communication, understanding, and training. NRL Instruction 12400.1 established the NRL Mentor Program, and it provides the policy and procedures for the program. (Contact Dr. Susan Numrich (202) 767-3567 or Dr. Pat Tatem at (202) 767-2476.)

• The Charlotte Moore-Sitterly Chapter of **Federally Employed Women, Inc.** (FEW) was

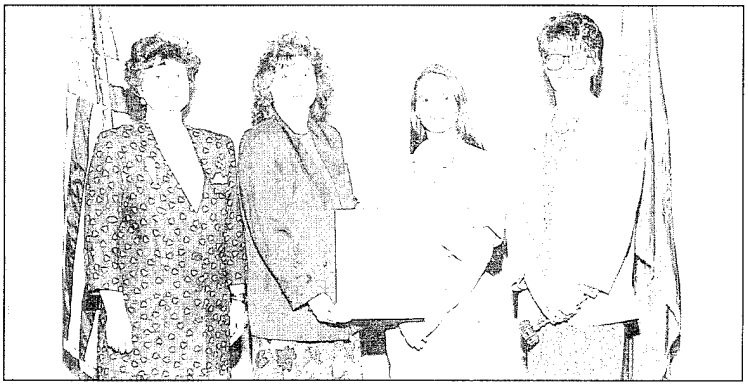

In the fall of 1993, the Charlotte Moore-Sitterly Chapter of Federally Employed Women (FEW) was established at NRL. The founding officers for the new FEW Chapter are (left to right) Doris Marshok, Treasurer; Velma Stiverson, Secretary; Jeannie Osborn, Vice President; and Chris Thorowgood, President.

chartered at NRL in 1993. FEW is an international organization of federally employed women and men whose purpose is to eliminate sex discrimination and sexual harassment and enhance career opportunities for women in government. FEW works closely with other Federal agencies and organizations, including the Office of Personnel Management, Equal Employment Opportunity Commission, and Federal Women's Program subcommittees. (Contact Ms. Chris Thorowgood at (202) 767-3121.)

• Employees interested in developing effective self-expression, listening, thinking, and leadership potential are invited to join either of two NRL chapters of **Toastmasters International**. Members of these clubs, who possess diverse career backgrounds and talents, meet three times a month in an effort to learn to communicate not by rules but by practice in an atmosphere of understanding and helpful fellowship. NRL's commanding officer and the director of research endorse Toastmasters, and the Employee Development Branch pays for membership and educational materials for those NRL employees whose supervisors see a need for their active training in public speaking or communication skills. (Contact Ms. Kathleen Parrish at (202) 767-2782.)

• Through the **Women in Science and Technology Program** (WIST), the NRL Stennis Space Center (NRL SCC) works closely with coordinators from Mississippi Gulf Coast Community College and Pearl River Community College to introduce young high school women to careers in math and science. Conferences held at NRL SCC and college campuses focus on encouraging young women to take those courses that provide the educational background necessary for developing high-technology skills and promoting their entrance into nontraditional careers. The WIST Program began in 1986 as a Mississippi State Department of Education joint effort between the Department of Vocational Education and the Sex Desegregation Office. (Contact Mr. George Stanford at (601) 688-5211.)

• An agreement between NRL SSC and **Mississippi's Alliance for Minority Participation** places students whose background and interests match the Laboratory's field of research with NRL mentors in a 10-week research environment. Together with accomplished senior researchers and faculty advisors, students plan, develop, and conduct a summer research project to include challenging, hands-on experiences with research equipment and principles of modern research. (Contact Mr. George Stanford at (601) 688-5211.)

EQUAL EMPLOYMENT OPPORTUNITY (EEO) PROGRAMS

Equal employment opportunity is a fundamental NRL policy for all persons, regardless of race, color, sex, religion, national origin, age, or physical/mental handicap. The EEO Office's major functions include affirmative action in employment, discrimination complaint process, EEO training, advice and guidance to management on EEO policy, and the following special emphasis programs:

• The **Federal Women's Program** (FWP) supports and enhances employment and advancement opportunities for women and addresses issues that affect women in the workplace. It provides counseling and referral services and sponsors a chapter of Women in Science and Engineering to recognize outstanding female scientists and engineers. Distinguished women scientists are guest lecturers at quarterly presentations.

• The **Hispanic Employment Program** (HEP) focuses on working with supervisors, managers, and subcommittees to recruit and place qualified Hispanics. The program is involved with Hispanic community organizations and local schools and provides activities specifically designed to offer employment opportunities to Hispanics. "El Ingeniero" (The Engineer), which encourages Hispanic youth to pursue a career in engineering, is one such program.

The **Black Employment Program** (BEP) concentrates on recruiting, placing, developing, and advancing African-American employees throughout NRL. It also encourages them to achieve their maximum potential.

• The **Individuals with Disabilities Program** (IDP) assists management to improve employment and advancement opportunities for qualified handicapped and disabled veteran employees. It also advises on accommodations necessary for handicapped persons. It recruits handicapped summer students from colleges and universities for technical positions in engineering and science and paraprofessional positions in accounting and administration; it also seeks Cooperative Education Program (Co-op) candidates who are pursuing degrees in engineering, computer sciences, or the physical sciences.

• The **Asian-American/Pacific-Islander Program** (API) identifies areas of concern regarding the recruitment, selection, advancement, and retention of API employees throughout NRL. The program interacts with API professional/community organizations to address employment concerns.

• The **American-Indian/Alaskan-Native Employment Program** (AI/ANEP) focuses on the employment concerns of AI/ANEP employees. The program provides counseling and referral services on recruitment, hiring, placement, promotion, retention, and other areas of employee interest.

• The **Federal Employment Opportunity Recruitment Program** (FEORP) is designed to establish, maintain, and update targeted recruitment programs to reduce the conspicuous absence or manifest imbalance categories of NRL employment through innovative internal and external recruitment. In addition, it fosters relationships with minority and women's institutions and organizations.

Group members of Danza Del Rio perform the Flaminco dance during the National Hispanic Heritage Month Program

Special programs are held during the year to promote an awareness of the contributions and capabilities of women and minorities. (Contact the EEO Office at (202) 767-2486 for all EEO programs.)

OTHER ACTIVITIES

• The **Community Outreach Program** traditionally has used its extensive resources to foster programs that provide benefits to students and other community citizens. Volunteer employees assist with and judge science fairs, give lectures, tutor, mentor, coach, and serve as classroom resource teachers. The program also sponsors Black History Month art and essay contests for local schools, student tours of NRL, a student Toastmasters Youth Leadership Program, an annual holiday party for neighborhood children, an annual collection for Children's Hospital, and other programs that support the local community. Also through this program, NRL has active partnerships with four District of Columbia public schools. (Contact the Public Affairs Office at (202) 767-2541.)

The NRL Community Outreach Program holds an annual art and essay contest for nearby schools. Here Outreach volunteer Levi Daniels is shown with the Honorable Mention Art winners from Leckie Elementary School.

• Other programs that enhance the development of NRL employees include four computer user groups (**IBM PC**, **Mac**, **NeXT**, and **Sun**), the **Microcomputer Software Support Center**, and the **Amateur Radio Club**. The **Recreation Club** accommodates the varied interests of NRL's employees with its numerous facilities, such as a refurbished 25-yard, 6-lane indoor swimming pool; basketball and volleyball courts; a weight room and exercise area; table tennis; meeting room; softball and basketball leagues; jacuzzi whirlpool; saunas; classes in five different types of martial arts; aerobics exercise; swimming and water walking; and specialized sports clubs (running, skiing, biking, and golfing). The **Showboaters**, a nonprofit drama group that presents live theater for the enjoyment of NRL and the community, performs two major productions each year in addition to occasional performances at Laboratory functions and benefits for local charities. The most recent productions were "The Pajama Game" and "Nunsense." Though based at NRL, membership in Showboaters is not limited to NRL employees.

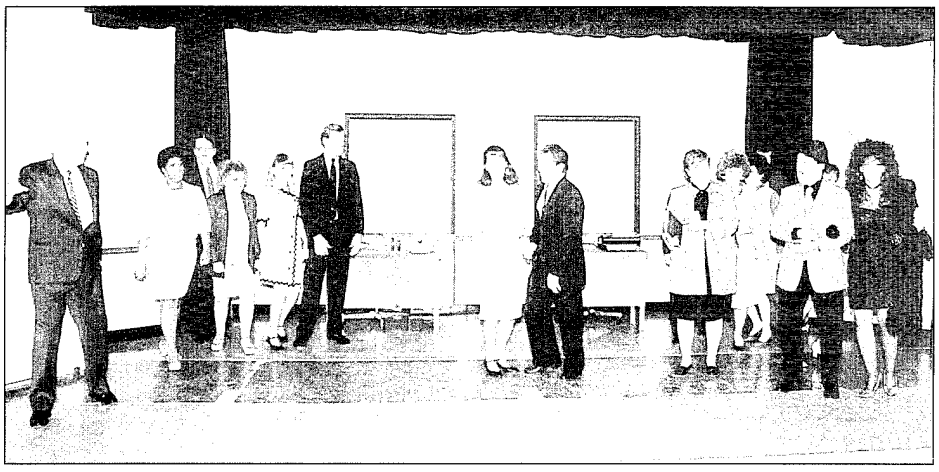

Shown are the NRL Showboaters' cast from their recent production of "The Pajama Game"

Programs for Non-NRL Employees

Several programs have been established for non-NRL professionals. These programs encourage and support the participation of visiting scientists and engineers in research of interest to the Laboratory. Some of the programs may serve as stepping-stones to federal careers in science and technology. Their objective is to enhance the quality of the Laboratory's research activities through working associations and interchanges with highly capable scientists and engineers and to provide opportunities for outside scientists and engineers to work in the Navy laboratory environment. Along with enhancing the Laboratory's research, these programs acquaint participants with Navy capabilities and concerns.

RECENT PH.D., FACULTY MEMBER, AND COLLEGE GRADUATE PROGRAMS

• The **National Research Council (NRC)/ NRL Cooperative Research Associateship Program** selects associates who conduct research at NRL in their chosen fields in collaboration with NRL scientists and engineers. The tenure period is 2 years. The Office of Naval Research offers the associate post-tenure research grants tenable at an academic institution.

• The American Society for Engineering Education (ASEE) administers the **Office of Naval Research (ONR) Postdoctoral Fellowship Program** that aims to increase the involvement of highly trained scientists and engineers in disciplines necessary to meet the evolving needs of naval technology. Appointments are for 1 year (renewable for a second and sometimes a third year). These competitive appointments are made jointly by ONR and ASEE.

• The American Society for Engineering Education also administers the Navy/ASEE **Summer Faculty Research Program** for university faculty members to work for 10 weeks with professional peers in participating Navy laboratories on research of mutual interest.

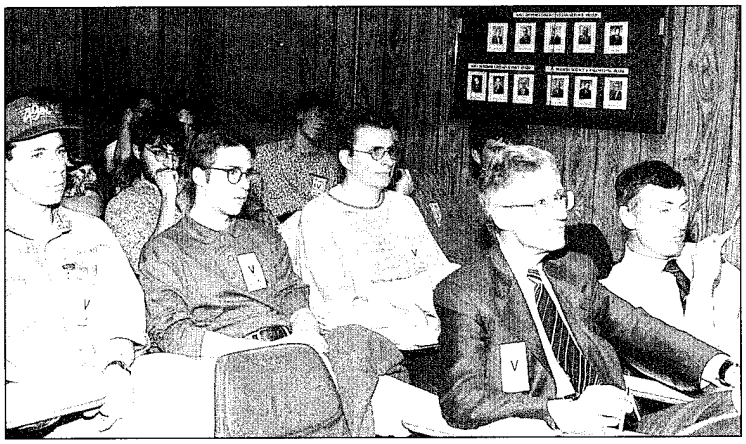

A group of 19 physics students and 2 professors from the University of Lausanne in Switzerland visited NRL to hear speakers discuss the environments that research physicists work in and to visit work areas and laboratories.

• The **NRL/United States Naval Academy (USNA) Cooperative Program for Scientific Interchange** allows faculty members of the U.S. Naval Academy to participate in NRL research. This collaboration benefits the Academy by providing the opportunity for USNA faculty members to work on research of a more practical or applied nature. In turn, NRL's research program is strengthened by the available scientific and engineering expertise of the USNA faculty.

• The **Office of Naval Research Graduate Fellowship Program** helps U.S. citizens obtain advanced training in disciplines of science and engineering critical to the U.S. Navy. The 3-year program awards fellowships to recent outstanding graduates to support their study and research leading to doctoral degrees in specified disciplines such as electrical engineering, computer sciences, material sciences, applied physics, and ocean engineering. Award recipients are encouraged to continue their study and research in a Navy laboratory during the summer.

For further information about the above five programs, please contact Mrs. Jessica Hileman at (202) 767-3865.

• The **Professional Development Program for Ensigns** assigns newly commissioned Ensigns who are awaiting future training to NRL to work in areas of their own choosing commensurate with their academic qualifications. These young officers provide a fruitful summer of research assistance while gaining valuable experience in the Navy's R&D program. For more information, contact the Military Administrative Office at (202) 767-2103.

PROFESSIONAL APPOINTMENTS

• **Faculty Member Appointments** use the special skills and abilities of faculty members for short periods to fill positions of a scientific, engineering, professional, or analytical nature.

• **Consultants and experts** are employed because they are outstanding in their fields of specialization or because they possess ability of a rare nature and could not normally be employed as regular civil servants.

• **Intergovernmental Personnel Act Appointments** temporarily assign personnel from the state or local government or educational institution to the federal government (or vice versa) to improve public services rendered by all levels of government.

UNDERGRADUATE COLLEGE STUDENT PROGRAMS

Several programs are tailored to the undergraduate that provide employment and work experience in naval research. These are designed to attract applicants for student and full professional employment in the Laboratory's shortage category positions, such as engineers, physicists, mathematicians, and computer scientists. The student employment programs build an understanding of NRL job opportunities among students and educational personnel so that educators can provide students who will meet NRL's occupational needs. The employment programs for college students include the following:

• The **Cooperative Education Program** alternates periods of work and study for students pursuing bachelor degrees in engineering, computer science, or the physical sciences. Several universities participate in this program.

• The **Clerical Cooperative Education Program** employs students interested in pursuing careers in the clerical occupation. Students work part time during the school year and full time during school breaks.

• The **Federal Junior Fellowship Program** hires needy students entering college to be assistants to scientific, professional, or technical employees.

• The **Summer Employment Program** employs students for the summer in paraprofessional and technician positions in engineering, physical sciences, and computer sciences.

• The **Student Volunteer Program** helps students gain valuable experience by allowing them to voluntarily perform educationally related work at NRL.

• The **1040-Hour Appointment** employs students on a half-time basis to assist in scientific work related to their academic program.

For additional information on these undergraduate college student programs, contact Cindy Stiles at (202) 767-3030.

HIGH SCHOOL PROGRAMS

• The **DoD Science & Engineering Apprentice Program** (SEAP) employs high school juniors and seniors to serve for 8 weeks as junior research associates. Under the direction of a mentor, students gain a better understanding of research, its challenges, and its opportunities through participation in scientific programs. Criteria for eligibility are based on science and mathematics courses completed and grades achieved; scientific motivation, curiosity, and capacity for sustained hard work; a desire for a technical career; teacher recommendations; and achievement test scores. The NRL Program is the lead program and the largest in DoD.

For additional information, contact the Employee Development Branch (Code 1840) at (202) 767-2956.

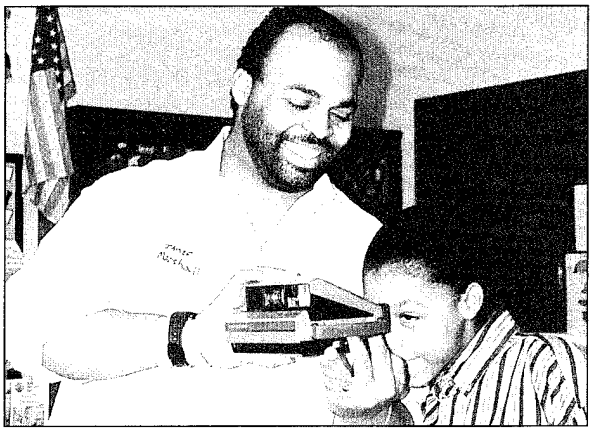

NRL photographer James Marshall shows a student how to operate a Polaroid camera during Career Awareness Day at one of NRL's partnership schools, Patterson Elementary. This activity is sponsored annually by NRL's Community Outreach Program.

Technical Output

The Navy continues to be a pioneer in initiating new developments and a leader in applying these advancements to military requirements. The primary method of informing the scientific and engineering community of the advances made at NRL is through the Laboratory's technical output—reports, articles in scientific journals, contributions to books, papers presented to scientific societies and topical conferences, patents, and inventions.

The figures for Calendar Year 1994 presented below represent the output of NRL facilities in Washington, D.C.; Orlando, Florida; Bay St. Louis, Mississippi; and Monterey, California.

In addition to the output listed, NRL scientists made more than 1467 oral presentations during 1994.

A complete listing of the publications by NRL authors appears in the *Bibliography of NRL Publications*, a separate annual publication.

Type of Contribution	Unclass.	Class.	Total
Articles in periodicals, chapters in books, and papers in published proceedings	1140	1	1141*
NRL Formal Reports	36	19	55
NRL Memorandum Reports	126	27	153
Other NRL Reports and NRL Publications	38	19	57
Books	1		1
Patents granted			91
Statutory Invention Registrations (SIRs)			4

*This is a provisional total based on information available to the Ruth H. Hooker Research Library and Technical Information Center on January 13, 1995. Additional publications carrying a 1994 publication date are anticipated.

Technology Transfer at NRL

There are many ways for private companies to benefit from the technical resources of the Naval Research Laboratory (NRL). Some of these include: (1) entering into Cooperative Research and Development Agreements (CRADAs), (2) obtaining licenses for Navy-owned patents, and (3) consulting with NRL scientists and engineers.

Entering into a CRADA is an excellent way for U.S. companies to gain access to commercially important NRL research and development (R&D) technology. Authorized under the Federal Technology Transfer Act of 1986, a CRADA is an agreement between one or more federal laboratories and one or more nonfederal parties, such as private companies. Designed to encourage and facilitate cooperative R&D, CRADAs can involve research in any area that is consistent with NRL's mission.

Additionally, the Federal government can license its own inventions. NRL has developed many new technologies and processes in areas as diverse as advanced materials, chemistry, biotechnology, optics, ocean and atmospheric sciences, and electronics. NRL currently has over 450 patents available for license in these fields.

As the Navy's corporate laboratory, NRL draws on the powerful resources of an interdisciplinary combination of scientific expertise and modern facilities. NRL's technical staff is recruited from all disciplines of engineering and the physical sciences and is available to work with private companies to help them solve their technical problems. Many of the staff have received the Award for Excellence in Technology Transfer from the Federal Laboratory Consortium (FLC). This award recognizes employees who have accomplished outstanding work in the process of transferring laboratory-developed technology.

During 1994, new products have been introduced from NRL technology by the private sector. For instance, NRL has developed new nuclear quadrupole resonance (NQR) technology that has resulted in smaller, more sensitive, and more selective explosive detection units (Fig. 1).

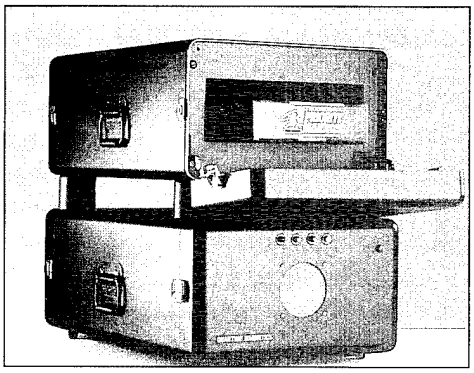

Fig. 1 — Explosive detector

The flow immunosensor, which is used in drug detection, was also introduced in 1994 (Fig. 2). The immunosensor capitalizes on the ability of antibodies to recognize specific molecules at high sensitivity. It can analyze hundreds of discrete samples rapidly and can be integrated into an automatic sampling system.

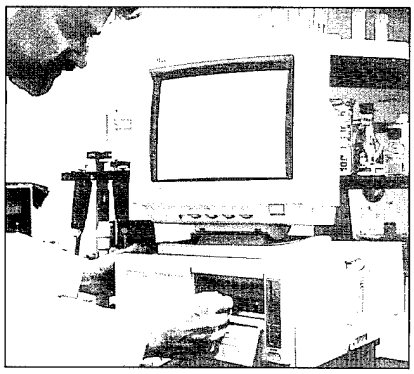

Fig. 2 — Drug detector

For additional information on the Technology Transfer Program, contact NRL's Technology Transfer Office, 4555 Overlook Ave., S.W., Washington, D.C. 20375-5320, or call (202) 404-8411 or fax (202) 404-7920.

Key Personnel

Personnel Locator - 767-3200
DSN-297 or 354
Area Code (202) unless otherwise listed

Code	Office		Phone Number
	EXECUTIVE DIRECTORATE		
1000	Commanding Officer	CAPT R.M. Cassidy, USN	767-3403
1001	Director of Research	Dr. T. Coffey	767-3301
1000.1	Scientific Staff Assistant	Mr. K.W. Lackie	767-2880
1002	Chief Staff Officer/Inspector General	CAPT R.E. Leonard, USN*	767-3621
1004	Head, Technology Transfer	Dr. R. Rein	767-3744
1005	Head, Office of Management and Administration	Ms. M. Oliver	767-3086
1010	Deputy for Space Systems	Dr. R. LeFande*	767-3324
1200	Head, Command Support Division	CAPT R.E. Leonard, USN	767-3621
1220	Head, Security	Mr. J.C. Payne	767-3048
1230	Public Affairs Officer	Mr. J.W. Gately, Jr.*	767-2541
1240	Head, Safety Branch	Mr. K.J. King*	767-2232
1280	Officer in Charge, Pax River Flight Support Detachment	CDR S.S. Smith, USN	301-863-3751
1800	Director, Human Resources Office	Ms. B. Duffield	767-3421
1803	Deputy EEO Officer	Ms. D. Erwin*	767-2486
	BUSINESS OPERATIONS DIRECTORATE		
3000	Associate Director of Research	Mr. R.E. Doak	767-2371
3008	Legal Counsel	Ms. H. Halper*	767-2244
3030	Head, Management Information Systems Staff	Mr. R.L. Guest	767-2030
3200	Head, Contracting Division	Mr. J.C. Ely	767-5227
3300	Comptroller, Financial Management Division	Mr. D.T. Green	767-3405
3400	Supply Officer, Supply Division	Ms. C. Hartman	767-3446
3500	Director, Research and Development Services Division	Mr. D.K. Woodington	767-3371
	GENERAL SCIENCE AND TECHNOLOGY DIRECTORATE		
4000	Associate Director of Research	Dr. R.A. LeFande*	767-3324
4003	Consultant for Critical Technology Assessment	Mr. L.M. Winslow	767-2887
4040	Technology Base Manager/BMDO-POC	Dr. S. Sacks	767-3666
4050	Signature Technology Office	Dr. D.W. Forester	767-3116
	WARFARE SYSTEMS AND SENSORS RESEARCH DIRECTORATE		
5000	Associate Director of Research	Dr. R.A. LeFande	767-3324
5200	Head, Technical Information Division	Mr. P.H. Imhof	767-3388
5300	Superintendent, Radar Division	Dr. M.I. Skolnik	767-2936
5500	Superintendent, Information Technology Division	Dr. R.P. Shumaker	767-2903
5600	Superintendent, Optical Sciences Division	Dr. T.G. Giallorenzi	767-3171
5700	Superintendent, Tactical Electronic Warfare Division	Dr. J.A. Montgomery	767-6278
5900	Superintendent, Underwater Sound Reference Detachment	Dr. J.E. Blue	407-857-5230
	MATERIALS SCIENCE AND COMPONENT TECHNOLOGY DIRECTORATE		
6000	Associate Director of Research	Dr. B.B. Rath	767-3566
6030	Head, Laboratory for Structure of Matter	Dr. J. Karle	767-2665
6100	Superintendent, Chemistry Division	Dr. J.S. Murday	767-3026
6300	Superintendent, Materials Science & Technology Division	Dr. D.U. Gubser	767-2926
6400	Director, Lab. for Computational Physics and Fluid Dynamics	Dr. J.P. Boris	767-3055
6600	Superintendent, Condensed Matter & Radiation Sciences Division	Dr. D.J. Nagel	767-2931
6700	Superintendent, Plasma Physics Division	Dr. S. Ossakow	767-2723
6800	Superintendent, Electronics Science & Technology Division	Dr. G.M. Borsuk	767-3525
6900	Center for Bio/Molecular Sciences and Engineering	Dr. J. Schnur	404-6000
	OCEAN AND ATMOSPHERIC SCIENCE AND TECHNOLOGY DIRECTORATE		
7000	Associate Director of Research	Dr. E.O. Hartwig	404-8690
7030	Head, Systems Support and Requirements	Dr. R.M. Root	601-688-4010
7100	Superintendent, Acoustics Division	Dr. E.R. Franchi (Acting)	767-3482
7200	Superintendent, Remote Sensing Division	Dr. P. Schwartz (Acting)	767-2351
7300	Superintendent, Oceanography Division	Dr. W.B. Moseley	601-688-4670
7400	Superintendent, Marine Geosciences Division	Dr. H.C. Eppert, Jr.	601-688-4650
7500	Superintendent, Marine Meteorology Division	Dr. S.W. Payne (Acting)	408-656-4721
7600	Superintendent, Space Science Division	Dr. H. Gursky	767-6343
	NAVAL CENTER FOR SPACE TECHNOLOGY		
8000	Director	Mr. P.G. Wilhelm	767-6547
8100	Superintendent, Space Systems Development Department	Mr. R.E. Eisenhauer	767-0410
8200	Superintendent, Spacecraft Engineering Department	Mr. H.E. Senasack, Jr. (Acting)	767-6407

*Additional Duty

ORGANIZATIONAL CHART
EXECUTIVE DIRECTORATE

COMMANDING OFFICER
Code 1000
CAPT R.M. Cassidy, USN

DIRECTOR OF RESEARCH
Code 1001
Dr. T. Coffey

ASSOCIATE DIRECTORS OF RESEARCH

BUSINESS OPERATIONS DIRECTORATE
Code 3000
R.E. Doak

GENERAL SCIENCE AND TECHNOLOGY DIRECTORATE
Code 4000
Dr. R.A. LeFande†

WARFARE SYSTEMS AND SENSORS RESEARCH DIRECTORATE
Code 5000
Dr. R.A. LeFande

MATERIALS SCIENCE AND COMPONENT TECHNOLOGY DIRECTORATE
Code 6000
Dr. B.B. Rath

OCEAN AND ATMOSPHERIC SCIENCE AND TECHNOLOGY DIRECTORATE
Code 7000
Dr. E.O. Hartwig

NAVAL CENTER FOR SPACE TECHNOLOGY
Code 8000
P.G. Wilhelm

† Additional duty

ORGANIZATIONAL CHART (Continued)
EXECUTIVE DIRECTORATE

EXECUTIVE COUNCIL (DIVISION DIRECTORS)

COMMANDING OFFICER
Code 1000
CAPT R.M. Cassidy, USN

RESEARCH ADVISORY COMMITTEE

DIRECTOR OF RESEARCH
Code 1001
Dr. T. Coffey

CHIEF STAFF OFFICER/ INSPECTOR GENERAL
Code 1002
CAPT R.E. Leonard, USN

HUMAN RESOURCES OFFICER
Code 1800
B. Duffield
- Staffing & Classification
- Employee Development
- Employee Relations
- ONR Satellite Human Resources Office
- NRL-SSC Satellite Human Resources Office
- Manpower Management & Systems Technology

PUBLIC AFFAIRS OFFICER
Code 1230
J.W. Gately, Jr.

SAFETY OFFICER
Code 1240
K. King

OFFICE OF TECHNOLOGY TRANSFER
Code 1004
Dr. R.H. Rein

DEPUTY EQUAL EMPLOYMENT OFFICER
Code 1803
D. Erwin

LEGAL COUNSEL
Code 3008
H. Halper

OFFICE OF MANAGEMENT AND ADMINISTRATION
Code 1005
M. Oliver

COMMAND SUPPORT DIVISION
Code 1200
CAPT R.E. Leonard, USN
- Military Operations
- Security
- Public Affairs
- Safety

FLIGHT SUPPORT DETACHMENT
Code 1280
CDR S.S. Smith, USN

— — — Additional duty

BUSINESS OPERATIONS DIRECTORATE
Code 3000
R.E. Doak

CONTRACTING DIVISION
Code 3200
J. Ely
- Policy & Analysis
- Contract Negotiations
- Acquisition Strategies/Training
- Advance Acquisition Planning
- Contractual Execution
- Contract Administration
- Acquisition Policy Interpretations & Implementation

FINANCIAL MANAGEMENT DIVISION
Code 3300
D.T. Green
- Budget
- Systems Operations
- Accounting
- Financial
- Disbursing

SUPPLY DIVISION
Code 3400
C. Hartman
- Purchasing
- Technical
- Customer Liaison
- Credit Card
- Material Control
- Supply Stores
- Delivery & Storage

RESEARCH AND DEVELOPMENT SERVICES DIVISION
Code 3500
D.K. Woodington
- Project Management
- Chesapeake Bay Detachment
- Operations
- Services
- Administrative
- Engineering

GENERAL SCIENCE AND TECHNOLOGY DIRECTORATE/ DEPUTY FOR SPACE SYSTEMS
Code 4000/1010
Dr. R.A. LeFande†

CRITICAL TECHNOLOGY ASSESSMENT
Code 4003
L.M. Winslow

TECH BASE/BMDO-POC
Code 4040
Dr. S. Sacks

SIGNATURE TECHNOLOGY OFFICE
Code 4050
Dr. D.W. Forester

WARFARE SYS AND SENSORS RESEARCH DIRECTORATE
Code 5000
Dr. R.A. LeFanc

TECH DIVIS
Code
P. In
- Tech
- Publi
- Grap
- Syst

RADA
Code
Dr. M
- Rada
- Adva
- Sear
- Targ
- Ident
- Airbo

INFOI
Code
Dr. R
- Navy in
- Comn
- Huma
- Cente As

OPTIC
Code
Dr. T.
- Advan
- Appli
- Laser
- Electr
- Optic

TACTI
Code
Dr. J.
- Off-Bo
- EW S
- Airbor
- Ships
- Integr

UNDE DETAC
Code
Dr. J.
- Acous
- Acous
- Techn
- Meas

1053

ORGANIZATIONAL CHART (Continued)

WARFARE SYSTEMS AND SENSORS RESEARCH DIRECTORATE
Code 5000
Dr. R.A. LeFande

TECHNICAL INFORMATION DIVISION
Code 5200
P. Imhof
- Technical Library/Software Support
- Publications
- Graphic Design Services
- Systems/Photographic

RADAR DIVISION
Code 5300
Dr. M.I. Skolnik
- Radar Analysis
- Advanced Radar Systems
- Search Radar
- Target Characteristics
- Identification Systems
- Airborne Radar

INFORMATION TECHNOLOGY DIVISION
Code 5500
Dr. R.P. Shumaker
- Navy Center for Applied Research in Artificial Intelligence
- Communication Systems
- Human-Computer Interaction
- Center for Computer High Assurance Systems
- Transmission Technology
- Advanced Information Technology
- Center for Computational Science

OPTICAL SCIENCES DIVISION
Code 5600
Dr. T.G. Giallorenzi
- Advanced Concepts
- Applied Optics
- Laser Physics
- Electro-optical Technology
- Optical Techniques

TACTICAL ELECTRONIC WARFARE DIVISION
Code 5700
Dr. J.A. Montgomery
- Off-Board Countermeasures
- EW Support Measures
- Airborne EW Systems
- Ships EW Systems
- Integrated EW Simulation

UNDERWATER SOUND REFERENCE DETACHMENT
Code 5900/NRL-ORL
Dr. J.E. Blue
- Acoustical Materials & Transduction
- Acoustical Systems
- Technical Services
- Measurements

MATERIALS SCIENCE AND COMPONENT TECHNOLOGY DIRECTORATE
Code 6000
Dr. B.B. Rath

LABORATORY FOR THE STRUCTURE OF MATTER
Code 6030
Dr. J. Karle

CHEMISTRY DIVISION
Code 6100
Dr. J.S. Murday
- Chemical Dynamics & Diagnostics
- Materials Chemistry
- Surface Chemistry
- Navy Technology Center for Safety & Survivability

MATERIALS SCIENCE AND TECHNOLOGY DIVISION
Code 6300
Dr. D.U. Gubser
- Physical Metallurgy
- Materials Physics
- Composites & Ceramics
- Mechanics of Materials

LABORATORY FOR COMPUTATIONAL PHYSICS AND FLUID DYNAMICS
Code 6400
Dr. J.P. Boris
- Center for Reactive Flow & Dynamical Systems
- Center for Computational Physics Developments
- Reactive Flow Physics

CONDENSED MATTER AND RADIATION SCIENCES DIVISION
Code 6600
Dr. D.J. Nagel
- Radiation Effects
- Directed Energy Effects
- Surface Modification
- Dynamics of Solids
- Complex Systems Theory

PLASMA PHYSICS DIVISION
Code 6700
Dr. S. Ossakow
- Radiation Hydrodynamics
- Laser Plasma
- Charged Particle Physics
- Pulsed Power Physics
- Space Plasma
- Beam Physics

ELECTRONICS SCIENCE AND TECHNOLOGY DIVISION
Code 6800
Dr. G.M. Borsuk
- Nanoelectronics
- Solid State Devices
- Vacuum Electronics
- Microwave Technology
- Surface & Interface Sciences
- Electronic Materials

CENTER FOR BIO/MOLECULAR SCIENCE AND ENGINEERING
Code 6900
Dr. J. Schnur
- Molecular Architectures
- Biomaterials
- Biological & Environmental Systems
- Advanced Programs

OCEAN A ATMOSPH AND TEC DIRECTO
Code 700
Dr. E.O.

2003

OCEAN AND ATMOSPHERIC SCIENCE AND TECHNOLOGY DIRECTORATE
Code 7000
Dr. E.O. Hartwig

SYSTEMS SUPPORT AND REQUIREMENTS
Code 7030/NRL-SSC
Dr. R.M. Root

ACOUSTICS DIVISION
Code 7100
Dr. E.R. Franchi (Acting)
- Center for Environmental Acoustics
- Acoustic Signal Processing
- Physical Acoustics
- Acoustic Systems
- Ocean Acoustics
- Acoustic Simulation & Tactics

REMOTE SENSING DIVISION
Code 7200
Dr. P. Schwartz (Acting)
- Special Projects Office
- Radio/IR Optical Sensors
- Remote Sensing Physics
- Imaging Systems & Research
- Remote Sensing Applications
- Remote Sensing Hydrodynamics

OCEANOGRAPHY DIVISION
Code 7300/NRL-SSC
Dr. W.B. Moseley
- Ocean Dynamics & Prediction
- Ocean Sciences

MARINE GEOSCIENCES DIVISION
Code 7400/NRL-SSC
Dr. H.C. Eppert, Jr.
- Tactical Oceanography Warfare Support
- Marine Physics
- Seafloor Sciences
- Mapping, Charting, and Geodesy

MARINE METEOROLOGY DIVISION
Code 7500/NRL-MRY
Dr. S.W. Payne (Acting)
- Prediction Systems
- Forecast Support

SPACE SCIENCE DIVISION
Code 7600
Dr. H. Gursky
- Office of Strategic Phenomena
- Engineering Management
- Ultraviolet Measurements
- X-Ray Astronomy
- Upper Atmosphere Physics
- Gamma & Cosmic Ray Astrophysics
- Solar Physics
- Solar Terrestrial Relationships
- E.O. Hulburt Center for Space Research

NAVAL CENTER FOR SPACE TECHNOLOGY
Code 8000
P.G. Wilhelm

SPACE SYSTEMS DEVELOPMENT DEPARTMENT
Code 8100
R.E. Eisenhauer
- BMD Office
- Mission Development
- Advanced Systems Technology
- Space Electronic Systems Development
- Command, Control, Communications, Computers, & Intelligence
- Space Applications

SPACECRAFT ENGINEERING DEPARTMENT
Code 8200
H.E. Senasack, Jr. (Acting)
- Design, Test, & Processing
- Systems Analysis
- Control Systems

† Additional duty

3063

Contributions by Divisions, Laboratories, and Departments

Space Science Division

Space Systems Development Department

Spacecraft Engineering Department

Employment Opportunities for Entry-Level and Experienced Personnel

The *NRL Review* illustrates some of the exciting science and engineering carried out at the Naval Research Laboratory as well as the potential for new personnel.

NRL offers a wide variety of challenging positions that involve the full range of work from basic and applied research to equipment development. The nature of the research and development conducted at NRL requires professionals with experience. Typically there is a continuing need for electronics, mechanical, aerospace, ceramic, and materials engineers, metallurgists, and oceanographers with bachelor's and/or advanced degrees, and physical and computer scientists with Ph.D. degrees. Opportunities exist in the areas described below.

Ceramic Engineers and Materials Scientists/ Engineers. These employees are recruited to work on materials, microstructure characterization, electronic ceramics, solid-state physics, fiber optics, electro-optics, microelectronics, fracture mechanics, vacuum science, laser physics technology, and radio frequency/microwave/ millimeter wave/infrared technology.

Electronics Engineers and Computer Scientists. These employees may work in the areas of communications systems, electromagnetic scattering, electronics instrumentation, electronic warfare systems, radio frequency/ microwave/millimeter wave/infrared technology, radar systems, laser physics technology, radio-wave propagation, electron device technology, spacecraft design, artificial intelligence, information processing, signal processing, plasma physics, vacuum science, microelectronics, electro-optics, fiber optics, solid state, software engineering, computer design/architecture, ocean acoustics, stress analysis, and expert systems.

Mechanical Engineers. These employees may be assigned to spacecraft design, remote sensing, propulsion, experimental fluid mechanics, experimental structural mechanics, solid mechanics, elastic/plastic fracture mechanics, materials, finite-element methods, nondestructive evaluation, characterization of fracture resistance of structural alloys, combustion, and CAD/CAM.

Chemists. Chemists are recruited to work in the areas of combustion, polymer science, bioengineering and molecular engineering, surface science, materials, fiber optics, electro-optics, microelectronics, electron-device technology, and laser physics.

Physicists. Physics graduates may concentrate on such fields as materials, solid-state physics, fiber optics, electro-optics, microelectronics, vacuum science, plasma physics, fluid mechanics, signal processing, ocean acoustics, information processing, artificial intelligence, electron device technology, radiowave propagation, laser physics, ultraviolet/X-ray/gamma-ray technology, electronic warfare, electromagnetic interaction, communications systems, radio frequency/ microwave/millimeter wave/infrared technology, and computational physics.

Oceanographers, Meteorologists, and Marine Geophysicists. These employees work in the areas of ocean dynamics, air-sea interaction, upper-ocean dynamics, oceanographic bio-optical modeling, oceanic and atmospheric numerical modeling and prediction, artificial intelligence applications for satellite analyses, benthic processes, aerogeophysics, marine sedimentary processes, and advanced mapping techniques. Oceanographers and marine geophysicists are located in Washington, D.C., and the Stennis Space Center, Bay St. Louis, Mississippi.

Meteorologists are located in Washington, D.C., and Monterey, California.

FOREIGN NATIONALS

U.S. citizenship is required for employment with NRL.

APPLICATION AND INFORMATION

Interested applicants should submit an Application for Federal Employment (SF-171), which can be obtained from local offices of the Office of Personnel Management and personnel offices of federal agencies.

Direct inquiries to:

Naval Research Laboratory
Human Resources Office, Code 1813 RV 95
Washington, DC 20375-5324
(202) 767-3030

Location of NRL in the Capital Area

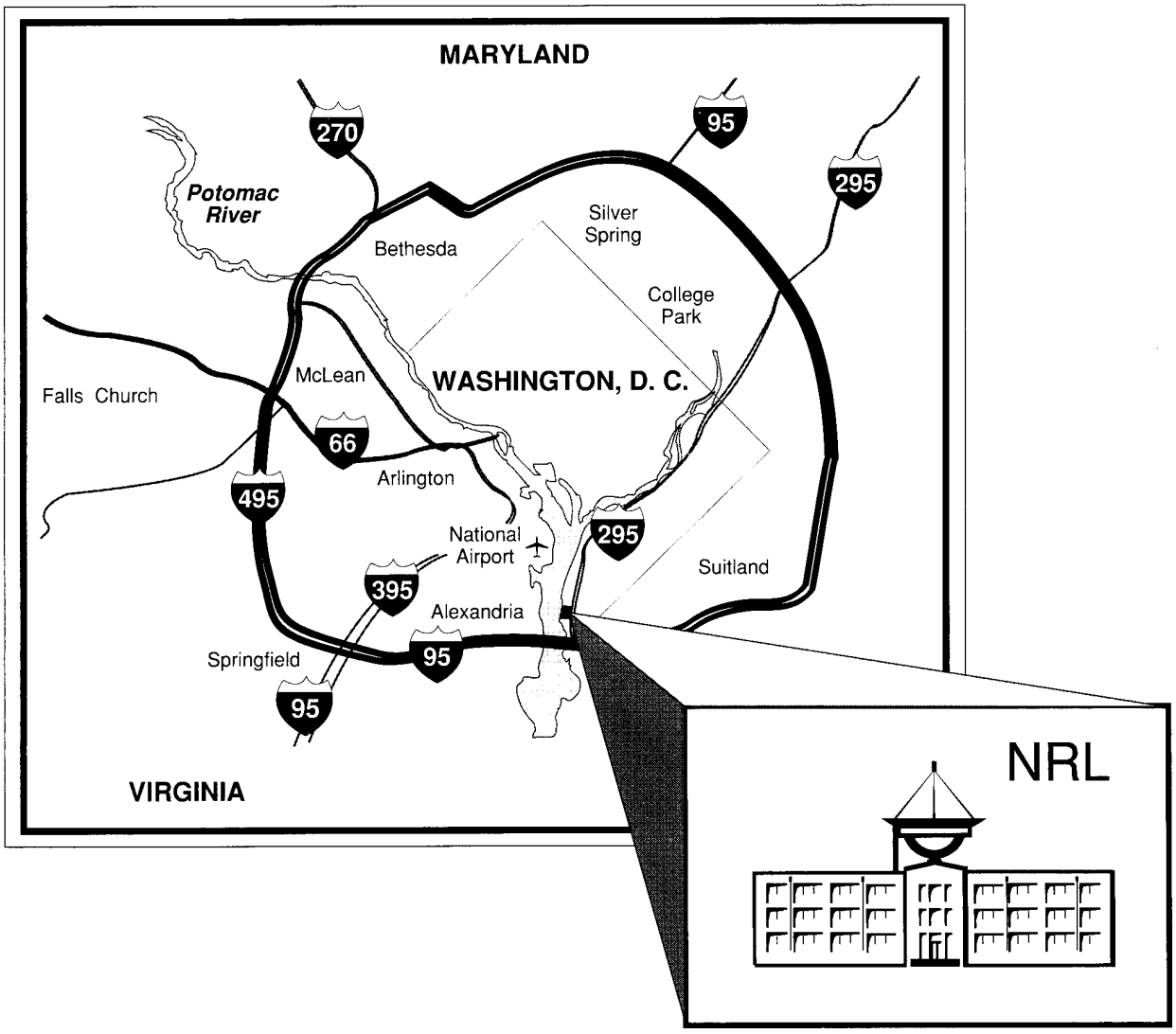

Subject Index

Author Index

NRL Review Staff

Senior Science Editor: John D. Bultman
Senior TID Editor: Patricia Staffieri
TID Consultants: Kathleen Parrish and Timothy Calderwood

Clementine cover design: Micheal McMullen

Cover graphics: Carol Hambric and Tazewell Rufty

Graphic support: Jan Morrow

Computerized composition and design production: Donna Gloystein, Judy Kogok, and Marsha Bray

Historical update: David van Keuren

Editorial assistance: Maureen Long and Saul Oresky

Photographic production: Richard Bussey, Gayle Fullerton, William Griffith, James Marshall, Chris Morrow, Barbara Padgett, and Michael Savell

Production assistance: Rosie Bankert, Diltricia Montgomery, Leona Sprankel, and Paul Sweeney

Distribution: Joyce Harris and Barbara Jolliffe

Head, Technical Information Division: Peter H. Imhof

General information on the research described in this *NRL Review* may be obtained from the Public Affairs Office, Code 1230, (202) 767-2541. Information concerning Technology Transfer is available from Dr. Richard Rein, head of the Technology Transfer Office, Code 1004, (202) 767-3744. The sources of information on the various nonresearch programs at NRL are listed in the chapter entitled "Programs for Professional Development."

The NRL *Fact Book* lists the organization, key personnel, and major facilities for each division. Further, it contains information about Laboratory funding, programs, and field sites. A copy of the *Fact Book* may be obtained by contacting the Technical Information Division, Publications Branch, Code 5231, (202) 767-2782.

REVIEWED AND APPROVED
NRL/PU/5230–95-274
March 1995

R M. Cassidy

Richard M. Cassidy, Jr.
Captain, USN
Commanding Officer